

Magnitude and Spatio-Temporal Variability of Methane Emissions from a Eutrophic Freshwater Lake

by

Charuleka Varadharajan

Bachelor of Technology, Civil Engineering (2001)
Indian Institute of Technology, Madras

Master of Science (2004)
Massachusetts Institute of Technology

Submitted to the Department of Civil and Environmental Engineering
in partial fulfillment of the requirements for the degree of

**Doctor of Philosophy
in Environmental Engineering**

at the

**Massachusetts Institute of Technology
September 2009**

© 2009 Massachusetts Institute of Technology. All rights reserved.

Signature of Author _____

Department of Civil and Environmental Engineering
September 5, 2009

Certified by _____

Harold F. Hemond
William E. Leonhard Professor of Civil and Environmental Engineering
Thesis Supervisor

Accepted by _____

Daniele Veneziano
Chairman, Departmental Committee for Graduate Students

Magnitude and Spatio-Temporal Variability of Methane Emissions from a Eutrophic Freshwater Lake

by

Charuleka Varadharajan

Submitted to the Department of Civil and Environmental Engineering
on September 5, 2009 in partial fulfillment of the requirements for
the degree of Doctor of Philosophy in Environmental Engineering

ABSTRACT

Methane is the second most important greenhouse gas after carbon dioxide, and it can significantly impact global climate change. Considerable amounts of methane can be released to the atmosphere from freshwater lakes, particularly through bubbling. However, spatial and temporal heterogeneity in ebullition has complicated efforts to accurately measure such methane emissions. This thesis presents the results from a two-year study of methane biogeochemistry conducted at the eutrophic, stratified, Upper Mystic Lake located in eastern Massachusetts, US.

Field sampling was done between June and November 2007, and between April and November 2008. In both years, ebullition at the lake was strongly episodic, and the amount and composition of bubbled gas varied considerably between sites. In 2008, under-water bubble traps were equipped with pressure sensors that measured the gas collected every 5 minutes for 4-6 months. The high-temporal resolution data showed that synchronized lake-wide bubbling episodes were triggered when hydrostatic pressures fell below a site-dependent threshold.

Twice as much bubbling was observed in 2007 than in 2008. In both years, approximately 70% of the total methane export from the lake occurred through ebullition, and 30% through diffusion across the air-water interface at the lake surface. About 6-11 kg CH₄/d was emitted to the atmosphere from the Upper Mystic Lake during the sampling periods of 2007 and 2008.

The results from this research indicate that freshwater lakes should be considered as important natural sources in the global methane budget. Other contributions include the development a low-cost, low-power bubble trap for automated measurement of ebullition. The electronics in this device can also be used to measure other phenomena where a pressure differential is of interest, such as lake water level. To our knowledge, there has been no previous study that has measured bubbling fluxes over a comparable period of time with such high temporal resolution. Finally, the wavelet transform is presented as a new tool for identification of bubbling events from sensor data at multiple time scales.

Thesis Supervisor: Harold F. Hemond

Title: William E. Leonhard Professor of Civil and Environmental Engineering

*To my loving family
Amma, Appa, Vini and Prasanna*

ACKNOWLEDGEMENTS

I am immensely grateful to Harry Hemond, for his knowledge, encouragement and patience in guiding me through this research. Working with him has been an amazing experience, both from a scientific and personal standpoint, and I have learnt some invaluable life skills from his understanding of how most things work in the world, and ability to fix almost anything.

The other members of my committee have been very supportive of my work. Phil Gschwend's energy and enthusiasm were always infectious, and his feedback has helped strengthen this dissertation considerably. Steve Lerman's advice and guidance over the last several years have helped shape my life at MIT.

None of the field work conducted for this research would have been possible if it were not for the commitment of the undergraduates involved in this project – Patricia Tcaciuc, Emanuel Borja and Richard Hermosillo. Patricia and Manny helped with the field and laboratory work in 2007 and 2008, which included some very cold and wet days, while Richard was responsible for designing the circuit used in the automated bubble traps. Patricia also assisted with much of the data entry from the gas chromatograph experiments.

I have had some awesome labmates, who have always been ready to lend a helping hand – Amy Mueller, Sarah Jane White, Matt Orosz and Schulyer Senft-Grupp. For this project, Amy helped with circuit design and troubleshooting the electronics, Sarah Jane provided input into some of the methods used for wet-lab chemistry and Matt helped with the machine shop.

There were several other field partners who filled in when needed – Amy Mueller, Sarah Jane White, Loretta Fernandez, Rebecca Neumann, Vinithra Varadharajan (a.k.a my sister), Anirudhan Conjeevaram (i.e. my cousin), and former roommates Karin Lemkau and Catarina Reis. Ed Udas from the Chemistry machine shop and Mark Belanger in the Edgerton machine shop were incredibly helpful in designing and fabricating the hardware for the bubble traps. Aaron Chow and Eric Adams provided the use of the Houdini tank for bubble chamber testing. Ken Legler from Tufts University allowed us to use the Tufts dock for fieldwork and hosted the atmospheric pressure sensor in their boathouse. The seismic survey in June 2009 was conducted with Carolyn Ruppel and Chuck Worley from the USGS.

I was lucky to be around for the formation of the Supergroup, and all its members - John MacFarlane, Desiree Plata, Loretta Fernandez, Dave Kuo, Dave Griffith, Xanat Flores, Rebecca Neumann, Hanan Karam – have listened to an excessive number of my presentations, and have provided invaluable input over the last few years.

Parsons has been a wonderful place to work at, and the Parsons community has always made the lab feel like home! In particular, I have to thank Sheila Frankel who keeps things running in the building, Vicki Murphy who handled the finances for the project.

There are many other members of the MIT community, whom I have to thank for their support during this long journey. In particular, the 1.00 TA staff from 2005-2008, especially David Wang, and the course instructors Dr. Jud Harward, Prof. George Kocur and Prof. Steve Lerman

were very accommodating of my field schedule for several terms. It was great to work with Kirky and Meg, and others from the CECI and the iLabs team in the early years of my life at MIT. The CEE support staff – Kris Kipp, Jeanette Marchocki, Patty Glidden, Cynthia Stewart and Patricia Dixon – have been a pillar of support for the department’s graduate students.

Life at MIT wouldn’t have been fun if it weren’t for all the friends that I have made over the years - Aarthi, Karthik, Hye-sun, Lucy and other friends from the MIT Graduate Student News and Graduate Student Council, Rupa and the rest of mafia. I have particularly enjoyed dancing with the MIT Natya group, especially Gayathri, Chandni, Radha and Soumya.

I owe so much to my family – my mom, dad and sister - without whose support this would not have been possible, and my wonderful husband Prasanna, who has been so patient with our long-distance commute for all these years. Finally I would like to acknowledge my huge, loving, extended family, including Archana, Prasanna’s parents, Rukmini and Vijaykumar, and Dr. Seshadri who has been a source of motivation for all in our family.

This work was supported by NSF Doctoral Dissertation Research Grant 0726806, NSF EAR 0330272, a GSA Graduate Student Research Grant and MIT Martin, Linden and Ippen fellowships. Preliminary field work for summer 2006 was possible due to the support of the Department of Civil and Environmental Engineering, MIT. Emanuel Borja and Alexandra Patricia Tcaciuc were funded by the MIT and Martin UROP programs.

TABLE OF CONTENTS

CHAPTER 1: INTRODUCTION	13
1. MOTIVATION	13
2. BACKGROUND	14
2.1 Methane biogeochemistry in stratified lakes	14
2.2 Measuring methane	17
3. RESEARCH OBJECTIVES	18
4. THESIS OUTLINE	19
CHAPTER 2: A LOW-COST AUTOMATED TRAP TO MEASURE BUBBLING GAS FLUXES	24
1. INTRODUCTION	24
2. MATERIALS AND PROCEDURE	27
2.1 Trap design	27
2.2 Circuit design	29
2.3 Waterproof Housing	31
2.4 Field deployment and sampling	32
2.5 Modifications made for measuring water level	32
2.6 Calculations and Circuit Calibration	33
3. ASSESSMENT	36
3.1 Results	36
3.2 Error budget terms for volumes measured in the automated traps	37
3.3 Effects of large changes in temperature	42
3.4 Effect of wind and waves	43
3.5 Other bubble trap tests	43
4. DISCUSSION	43
5. TABLES	46
6. FIGURES	47
CHAPTER 3: TIME-SERIES ANALYSIS OF HIGH-RESOLUTION EBULLITION FLUXES FROM A STRATIFIED, FRESHWATER LAKE	57
1. INTRODUCTION	57
2. BACKGROUND – TIME SERIES DATA PROCESSING	60
2.1 Statistical and Fourier analysis	60
2.2 Wavelets for time-series analysis	61

3. METHODS	63
3.1 Study site	63
3.2 Data collection and preprocessing	64
3.3 Time series analysis with statistical and Fourier methods	65
3.4 Wavelet analysis	67
4. RESULTS	70
4.1 Statistical properties of site fluxes	70
4.2 Correlation analysis	70
4.3 Auto and cross correlations	71
4.4 Power spectrum analysis	72
4.5 Wavelet analysis	72
4.6 Comparison of wavelet details with hydrostatic pressure	74
4.7 Wavelet variance	74
5. DISCUSSION	75
5.1 Temporal variability of bubbling episodes	75
5.2 Ebullition control mechanisms	75
5.3 Spatial variation in bubbling fluxes	78
5.4 Selection of sampling interval	78
6. TABLES	80
7. FIGURES	83
CHAPTER 4: METHANE EXPORT FROM A EUTROPHIC, TEMPERATE, FRESHWATER LAKE	118
1. INTRODUCTION	118
2. METHODS	119
2.1 Study site	119
2.2 Ebullition flux measurements	120
2.3 Bubble gas concentration measurements	121
2.4 Dissolved gas concentration measurements	122
2.5 Surface air-water gas exchange calculations	124
2.6 Other measurements	125
3. RESULTS	126
4. DISCUSSION	129
4.1 Temporal variability in ebullition fluxes	129
4.2 Spatial variation in ebullition fluxes	131
4.3 Variations in bubble gas content	132
4.4 Diffusive air-water exchange from the lake surface during fall and spring turnover	134
5. SUMMARY AND CONCLUSIONS	135
6. TABLES	137
7. FIGURES	144

CHAPTER 5: A MASS BALANCE OF THE METHANE CYCLE IN THE UPPER MYSTIC LAKE	178
1. INTRODUCTION	178
2. BACKGROUND	179
2.1 Methane production	179
2.2 Methane release to the atmosphere	180
2.3 Aerobic methane oxidation	180
2.4 Anaerobic methane oxidation	181
3. METHODS	182
3.1 Water quality parameters	182
3.2 Ebullition, air-water exchange and dissolved gas concentrations	183
3.3 Oxidation tests	183
3.4 Sediment porewater methane measurements	185
3.5 Other measurements	186
4. RESULTS	187
4.1 Lake stratification	187
4.2 Methane loss to the atmosphere	188
4.3 Methane oxidation tests	188
4.4 Sediment core results	189
5. COMPONENTS OF THE MASS BALANCE MODEL	189
5.1 Overview	189
5.2 Methane buildup in the water column	191
5.3 Ebullition and diffusive air-water exchange to the atmosphere	191
5.4 Dissolution from bubbles	192
5.5 Eddy diffusion	193
5.6 Methane oxidation incubations	195
5.7 Diffusion from sediments	196
6. MASS BALANCE DISCUSSION	198
6.1 Upper mixed layer mass balance	198
6.2 Transition zone mass balance	200
6.3 Hypolimnion mass balance	201
6.4 Sediment mass balance	202
7. SUMMARY AND CONCLUSIONS	204
8. TABLES	206
9. FIGURES	214
CHAPTER 6: SUMMARY AND FUTURE WORK	236
1. SUMMARY	236
2. FUTURE WORK	238
3. BROADER IMPACTS	241

Chapter 1: Introduction

1. MOTIVATION

Methane plays a significant role in global climate change, and is also important from other perspectives such as ecosystem energetics and fuel supply. It is the second most important greenhouse gas after carbon dioxide (Houghton et al. 2001), and its concentration in the atmosphere, based on measurements in 2007 and 2008, is 1.8 ppm (AGAGE 2008, NOAA 2007). Although this seems small when compared to 386 ppm of atmospheric carbon dioxide, each methane molecule absorbs roughly 20 times more longwave radiation than a carbon dioxide molecule; thus methane contributes about 18% of the radiative forcing caused by long-lived green house gases (Forster et al. 2007). Methane concentrations in the atmosphere increased in 2007 and 2008, after stabilizing for about 8 years (Rigby et al. 2008); prior to 1999 concentrations had been increasing at a rate of 1% annually (Houghton et al. 2001).

Recent studies (e.g. Walter et al. 2007) have shown that previous methane measurements (e.g. Ehhalt 1974, Smith and Lewis 1992) seriously underestimate emissions through bubbling from freshwater lakes, which consequently implies that the methane-driven component of global warming based on past estimates of natural sources could be inaccurate and in need of revision. Based on extensive ebullition measurements in North Siberian lakes, Walter et al. (2006) estimated that lakes can account for as much as 6-8% (30 ± 15 Tg/yr) of methane emissions from natural sources. Methane is also an important component of the energy and carbon budget in lakes, and is absorbed into the food web through methanotrophic bacteria (Bastviken et al. 2008, Kankaala et al. 2006).

The purpose of this study was to examine and compare the processes and rates by which methane is lost from a freshwater ecosystem either to the atmosphere (through bubbling and air-water gas exchange from surface waters) or within the water column (in-situ oxidation by microorganisms). In particular, this study focuses on bubbling, which is the main pathway for methane loss from lakes (e.g. Walter et al. 2006). The field work for this project was conducted from June-December 2007, and April-December 2008 at the Upper Mystic Lake (UML) in Woburn, Massachusetts.

2. BACKGROUND

2.1 Methane biogeochemistry in stratified lakes

Methane is an important component of the carbon cycle in aquatic systems. It is produced within the sediment bed through microbially-mediated anaerobic decomposition of organic matter. Some of this methane sporadically escapes into the atmosphere through ebullition (bubbling). Part of the remaining methane slowly diffuses out of the sediments into the water column, eventually reaching the atmosphere or being transformed by methanotrophic bacteria into carbon dioxide (Figure 1) (Rudd and Taylor 1980). In some cases, methane diffusing to oxic zones can quickly reach the atmosphere through the stems of vascular plants present in shallow regions, though this process is more dominant in shallow wetlands than in lakes (e.g. Sebacher et al. 1985).

Many studies have identified bubbling to be the most important sink of methane in freshwater lakes (e.g. Crill et al. 1988, Walter et al. 2006). Bubbles are formed when supersaturation occurs, i.e., when the total pressure of all dissolved gases exceeds the hydrostatic pressure (the difference is referred to as overpressure). The ebullition in lakes likely originates

from the gas-saturated sediments, rather than from the water column where dissolved gas concentrations are lower. Preexisting bubbles or gas cavities in the sediments can serve as sites for bubble formation and nucleation, whereas very high overpressures are required for spontaneous bubble formation within the water column (Jones et al. 1999).

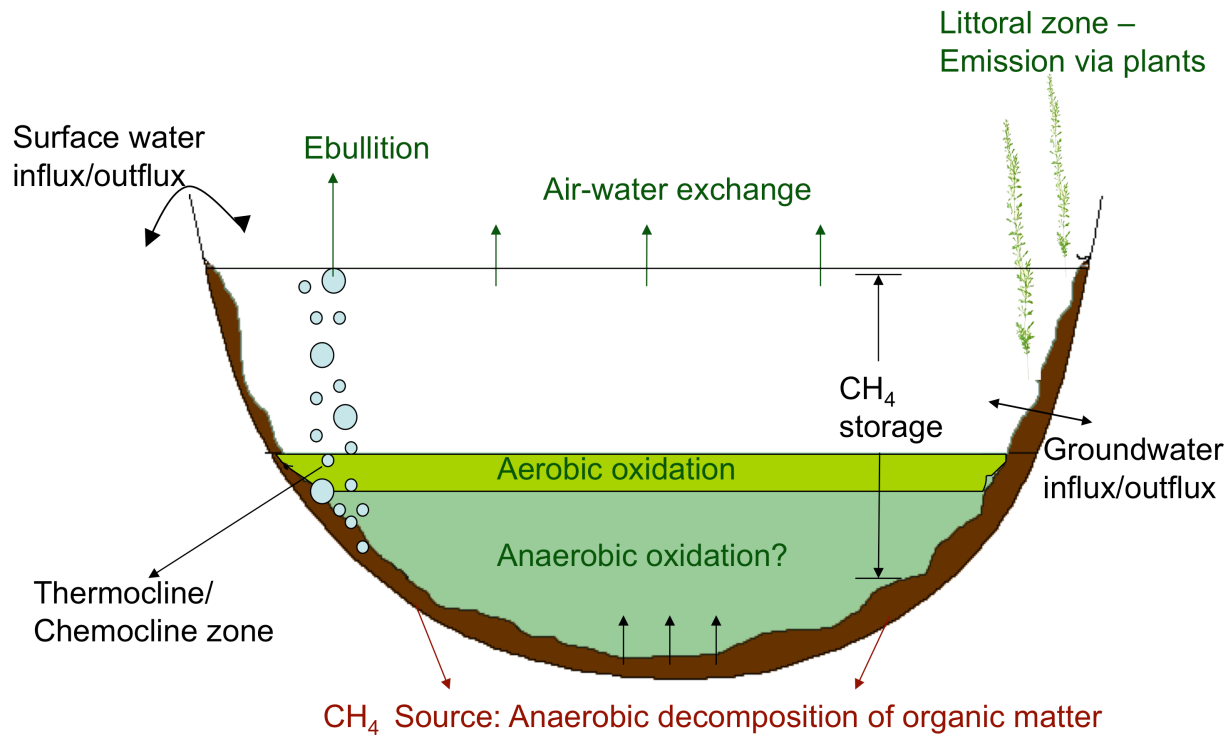


Figure 1 Potential methane source and sink processes in a stratified lake

The other means of methane release to the atmosphere is air-water exchange from the lake surface, which occurs throughout the open-water season and is dependent on the surface concentrations of dissolved methane, on water temperatures, and on wind velocities. Methane loss by surface air-water exchange can be especially important during the turnover periods either in fall or in spring following winter-ice melt in some temperate and boreal lakes. (Michmerhuizen et al. 1996, Rudd and Hamilton 1978).

Aerobic oxidation is considered to be another important sink of methane in the water column. It has been observed in many freshwater lakes in the oxycline region, where methane diffusing upwards from the bottom encounters a sudden increase in oxygen levels (Rudd and Taylor 1980). Microbially mediated anaerobic oxidation using sulfate as an electron acceptor is known to be a significant methane consumer in marine environments (Barnes and Goldberg 1976, Reeburgh 1976), but has been observed to date in very few freshwater lakes (Eller et al. 2005, Zehnder and Brock 1980). Anaerobic oxidation is also thermodynamically favorable with nitrate as an electron acceptor. Such a process has not been demonstrated to exist in any lake or ocean waters, though a recent study has found the existence of organisms that can oxidize methane with nitrate (Raghoebarsing et al. 2006). Methane present in escaping bubbles is almost completely transferred to the atmosphere, resulting in a net energy loss for the aquatic system. In contrast, microbial oxidation of dissolved methane preserves the energy and carbon within the ecosystem.

Methane buildup in the hypolimnion of stratified lakes mainly occurs during summer and fall, where concentrations can be on the order of 100-1000 μ M (e.g. Eckert and Conrad 2007, Rudd and Hamilton 1978). Concentrations in the upper mixed layer are typically about two orders of magnitude lower than in the hypolimnion. Methane is lost from the hypolimnion due to mixing during the fall and spring turnovers; high oxidation and air-water exchange rates have been observed during the turnover periods (e.g. Kankaala et al. 2007, Michmerhuizen et al. 1996, Utsumi 1998). At the Upper Mystic Lake, an earlier study found that dissolved methane concentrations in the hypolimnion gradually increased over the summer and fall (Peterson 2005).

The methane cycle is inseparably linked with carbon dioxide, which is a co-product of methanogenesis (methane production from carbohydrates) as well as a product of methane

oxidation. Previous mass-balance studies have found 20-40% excess carbon dioxide accumulation in some lakes relative to the consumption of known electron acceptors (Kelly et al. 1988, Mattson and Likens 1992, Peterson 2005). One possible explanation for the extra carbon dioxide is the underestimation of the amount of methane produced in the lake, due to its loss by ebullition. Thus the study of methane fate and transport is also relevant for other redox cycles in lakes.

2.2 Measuring methane

Accurately measuring methane processes in lakes is a challenging proposition because of the nature of its production, emission and consumption. These processes are spatially and temporally heterogeneous, and need to be understood in greater detail in order to calculate methane fluxes from the lake, as well as to understand the dynamics of the ecosystem. This becomes additionally important when estimates from individual lakes are extrapolated to a global scale.

It is problematic to quantify methane concentrations and fluxes using conventional measurement techniques that rely on infrequent and spatially incomplete sampling. Bubbling, in particular, is a difficult process to measure, since it is highly episodic and patchy (e.g. Leifer et al. 2004, Ostrovsky 2003). There are large uncertainties in current bubble flux assessments, which have been estimated to range from 50-98% of total lake emissions (e.g. Crill et al. 1988, Keller and Stallard 1994, Mattson 1989). The studies also report different percentages of methane present in the bubbles, varying from 44%-88%. A recent study has shown that altering spatial choices of bubble sampling stations can increase flux estimates by as much as 80% (Walter et al. 2006). Ebullition measurements are further complicated by other factors that can influence bubble release such as air pressure, water level, temperature and wind velocities (e.g.

Chanton et al. 1989, Mattson and Likens 1990). Bubbling has also been observed to vary seasonally, with higher lake-wide release occurring during late summer and early fall, as well as with the time of day (more release during the day than the night) (Casper et al. 2000, Keller and Stallard 1994).

Most bubble experiments involve manually-tended flux chambers (e.g. Bastviken et al. 2004, Casper et al. 2000), with which it is difficult to provide the spatial coverage and temporal continuity that the study of ebullition demands. Some of the above problems can be tackled with the use of sensors that have provided the opportunity to monitor the environment much more closely.

3. RESEARCH OBJECTIVES

The primary goal of this project was to quantify the dominant biogeochemical processes that control methane release from temperate freshwater lakes, using the Upper Mystic Lake as a case study. An emphasis was placed on bubbling, which was hypothesized to be the dominant mechanism of methane release from the lake and whose study is particularly complicated by temporal and spatial heterogeneity. Thus the research involved several components:

- 1) An estimation of the magnitude and timing of bubbling fluxes using automated sensor-based techniques, and a comparison of the results obtained with traditional measurements.
- 2) Understanding the controls that drive ebullition in the Upper Mystic Lake.
- 3) An estimation of the magnitude and timing of methane loss from the surface through diffusive air-water exchange

- 4) A quantification of the extent of seasonal methane buildup in the lake by measuring dissolved methane concentrations in the epilimnion and hypolimnion, as well as transport within the water column.
- 5) An assessment of methane oxidation rates in the water column.
- 6) An assessment of methane concentrations and fluxes in the sediments

4. THESIS OUTLINE

This thesis is organized as follows. Chapter 2 describes the design of an automated trap that was used to collect high temporal resolution ebullition data in the Upper Mystic Lake (UML) from June to December 2008. Chapter 3 discusses the time-series analysis of the automated trap data using statistical and wavelet based techniques. The results show that most of the ebullition during the season occurred as synchronous lake-wide bubbling episodes, which were triggered by falling hydrostatic pressures. Chapter 4 discusses the contribution of the UML and other similar lakes to the atmospheric methane budget through the processes of bubbling and surface air-water gas exchange. Ebullition data collected during 2007 and 2008 are summarized here, and an estimate of the magnitude and spatial variability of bubbling fluxes over the two years is presented. Chapter 5 contains a mass balance of the methane cycle in the UML. Apart from ebullition, the processes considered include diffusion of methane from the sediments into the overlying water, transport and oxidation within the water column, and methane release to the atmosphere through surface air-water exchange. Chapter 6 provides a summary of the major findings from this research, and contains suggestions for future work.

REFERENCES

1. AGAGE. 2008. Advanced Global Atmospheric Gases Experiment. <http://agage.eas.gatech.edu/index.htm>. 2009.
2. Barnes, R. O. and E. D. Goldberg. 1976. Methane production and consumption in anoxic marine sediments. *Geology*. **4**: 297-300.
3. Bastviken, D., J. J. Cole, M. L. Pace and Van de Bogert, M. C. 2008. Fates of methane from different lake habitats: Connecting whole-lake budgets and CH₄ emissions. *J. Geophys. Res.* **113**: , doi:10.1029/2007JG000608.
4. Bastviken, D., J. Cole, M. Pace and L. Tranvik. 2004. Methane emissions from lakes: Dependence of lake characteristics, two regional assessments, and a global estimate. *Global Biogeochem. Cycles*. **18**: B4009.
5. Casper, P., S. C. Maberly, G. H. Hall and B. J. Finlay. 2000. Fluxes of methane and carbon dioxide from a small productive lake to the atmosphere. *Biogeochemistry*. **49**: 1-19.
6. Chanton, J. P., C. S. Martens and C. A. Kelley. 1989. Gas transport from methane-saturated, tidal freshwater and wetland sediments. *Limnol. Oceanogr.* **34**: 807-819.
7. Crill, P. M., K. B. Bartlett, J. O. Wilson, D. I. Sebacher, R. C. Harriss, J. M. Melack, S. MacIntyre, L. Lesack and L. Smith-Morrill. 1988. Tropospheric methane from an Amazonian floodplain lake. *J. Geophys. Res.* **93**: 1564-1570, doi:10.1029/JD093iD02p01564.
8. Eckert, W. and R. Conrad. 2007. Sulfide and methane evolution in the hypolimnion of a subtropical lake: a three-year study. *Biogeochemistry*. **82**: 67-76.
9. Ehhalt, D. H. 1974. The atmospheric cycle of methane. *Tellus*. **26**: .
10. Eller, G., L. Känel and M. Krüger. 2005. Cooccurrence of Aerobic and Anaerobic Methane Oxidation in the Water Column of Lake Plußsee. *Appl. Environ. Microbiol.* **71**: 8925-8928.
11. Forster, P., V. Ramaswamy, P. Artaxo, T. Berntsen, R. Betts, D. W. Fahey, J. Haywood, J. Lean, D. C. Lowe, G. Myhre, J. Nganga, R. Prinn, G. Raga, M. Schulz, R. van Dorland, G. Bodeker, O. Boucher, W. D. Collins, T. J. Conway, E. Dlugokencky, J. W. Elkins, D. Etheridge, P. Foukal, P. Fraser, M. Geller, F. Joos, C. D. Keeling, S. Kinne, K. Lassey, U. Lohmann, A. C. Manning, S. Montzka, D. Oram, K. O'Shaughnessy, S. Piper, G. - Plattner, M. Ponater, N. Ramankutty, G. Reid, D. Rind, K. Rosenlof, R. Sausen, D. Schwarzkopf, S. K. Solanki, G. Stenchikov, N. Stuber, T. Takemura, C. Textor, R. Wang, R. Weiss, and T. Whorf. 2007. Changes in Atmospheric Constituents and in Radiative Forcing. *Climate Change 2007: The Physical Science Basis*. 131-234.
12. Houghton, J. T., Y. Ding, D. J. Griggs, M. Noguer, P. J. van der Linden, X. Dai, K. Maskell and C. A. Johnson. 2001. IPCC, 2001: Climate Change 2001: The Scientific Basis. Contribution of Working Group I to the Third Assessment Report of the Intergovernmental Panel on Climate Change.
13. Jones, S. F., G. M. Evans and K. P. Galvin. 1999. Bubble nucleation from gas cavities—a review. *Adv. Colloid Interface Sci.* **80**: 27-50.
14. Kankaala, P., J. Huotari, E. Peltomaa, T. Saloranta and A. Ojala. 2006. Methanotrophic activity in relation to methane efflux and total heterotrophic bacterial production in a stratified, humic, boreal lake. *Limnol. Oceanogr.* **51**: 1195-1204.
15. Kankaala, P., S. Taipale, H. Nykänen and R. I. Jones. 2007. Oxidation, efflux, and isotopic fractionation of methane during autumnal turnover in a polyhumic, boreal lake. *J. Geophys. Res.* **112**: .

16. Keller, M. and R. F. Stallard. 1994. Methane emission by bubbling from Gatun Lake, Panama. *J. Geophys. Res.* **99 (D4)**: 8307-8319.
17. Kelly, C. A., J. W. M. Rudd and D. W. Schindler. 1988. Carbon and electron flow via methanogenesis, SO_4^{2-} , NO_3^- , Fe^{3+} , and Mn^{4+} reduction in the anoxic hypolimnia of three lakes. *Arch. Hydrobiol.* **31**: 333-344.
18. Leifer, I., J. R. Boles, B. P. Luyendyk and J. F. Clark. 2004. Transient discharges from marine hydrocarbon seeps: spatial and temporal variability. *Environ. Geol.* **46**: 1038-1052, doi:10.1007/s00254-004-1091-3.
19. Mattson, M. D. 1989. An electron budget for aerobic and anaerobic decomposition in oligotrophic lake sediments. Ph.D. thesis. Cornell University.
20. Mattson, M. D. and G. E. Likens. 1990. Air pressure and methane fluxes. *Nature*. **347**: 718-719.
21. Mattson, M. D. and G. E. Likens. 1992. Redox reactions of organic matter decomposition in a soft water lake. *Biogeochemistry*. **19**: 149-172.
22. Michmerhuizen, C. M., R. G. Striegl and M. E. McDonald. 1996. Potential methane emission from north-temperate lakes following ice melt. *Limnol. Oceanogr.* **41**: 985-991.
23. NOAA. 2007. NOAA Annual Greenhouse Gas Index. <http://www.esrl.noaa.gov/gmd/aggi/>. 2009.
24. Ostrovsky, I. 2003. Methane bubbles in Lake Kinneret: Quantification and temporal and spatial heterogeneity. *Limnol. Oceanogr.* **48**: 1030-1036.
25. Peterson, E. J. R. 2005. Carbon and electron flow via methanogenesis, SO_4^{2-} , NO_3^- and Fe^{3+} reduction in the anoxic hypolimnia of Upper Mystic Lake. Master of Science thesis. Massachusetts Institute of Technology.
26. Raghoebarsing, A. A., A. Pol, K. T. van de Pas-Schoonhen, A. J. P. Smolders, K. F. Ettwig, W. I. C. Rijpstra, S. Schouten, J. S. S. Damste, H. Camp and M. S. M. Jetten. 2006. A microbial consortium couples anaerobic methane oxidation to denitrification. *Nature*. **440**: 918-921.
27. Reeburgh, W. S. 1976. Methane consumption in Cariaco Trench waters and sediments. *Earth Planet. Sci. Lett.* **28**:
28. Rigby, M., R. G. Prinn, P. J. Fraser, P. G. Simmonds, R. L. Langenfelds, J. Huang, D. M. Cunnold, L. P. Steele, P. B. Krummel, R. F. Weiss, S. O'Doherty, P. K. Salameh, H. J. Wang, C. M. Harth, J. Mühle and L. W. Porter. 2008. Renewed growth of atmospheric methane. *Geophys. Res. Lett.* **35**:
29. Rudd, J. W. M. and R. D. Hamilton. 1978. Methane Cycling in a Eutrophic Shield Lake and its Effects on Whole Lake Metabolism. *Limnol. Oceanogr.* **23**: 337-348.
30. Rudd, J. W. M., and C. D. Taylor. 1980. Methane cycling in aquatic environments, p. 77-150. In M. R. Droop, Jannasch, H.W. [ed.], *Advances in Aquatic Microbiology*. Academic Press.
31. Sebacher, D. I., R. C. Harriss and K. B. Bartlett. 1985. Methane emissions to the atmosphere through aquatic plants. *J. Environ. Qual.* **14**: 40.
32. Smith, L. K. and W. M. Lewis. 1992. Seasonality of Methane Emissions From Five Lakes and Associated Wetlands of the Colorado Rockies. *Global Biogeochem. Cycles*. **6**: 323-338.
33. Utsumi, M. 1998. Dynamics of dissolved methane and methane oxidation in dimictic Lake Nojiri during winter. *Limnol. Oceanogr.* **43**: 10-17.

34. Walter, K. M., S. A. Zimov, J. P. Chanton, D. Verbyla and F. S. Chapin III. 2006. Methane bubbling from Siberian thaw lakes as a positive feedback to climate warming. *Nature*. **443**: 71-75, doi:10.1038/nature05040.
35. Zehnder, A. J. B. and T. D. Brock. 1980. Anaerobic Methane Oxidation: Occurrence and Ecology. *Appl. Environ. Microbiol.* **39**: 194-204.

A low-cost automated trap to measure bubbling gas fluxes

Charuleka Varadharajan¹, Richard Hermosillo², Harold F. Hemond¹

¹ Department of Civil and Environmental Engineering, Building 48,
Massachusetts Institute of Technology, Cambridge MA 02139

² Texas Instruments, 50 Phillippe Cote St., Manchester, NH 03101

Running Head: Measuring methane ebullition

A revised version of this chapter will be submitted to Limnology and Oceanography: Methods

Chapter 2: A low-cost automated trap to measure bubbling gas fluxes

ABSTRACT

We describe a trap that can be used for automated, high temporal resolution measurement of ebullition fluxes in aquatic environments. The trap comprises a submerged cone connected to a transparent PVC pipe that serves as a collection chamber. A differential pressure sensor at the top of the pipe measures the pressure caused by gas accumulation in the chamber. The sensor circuit consists of low-power electronics and can function for over six months on two high-capacity AA lithium batteries. The circuit, batteries and a commercial data logger that records the measurements are enclosed in a custom-made, 10 cm diameter waterproof housing. The trap is designed to be fabricated economically and easily so that many units can be deployed for greater spatial coverage. We have used several of these automated traps to measure bubbling fluxes at a lake, and have collected data at a resolution of 5-10 minutes over 6 months.

1. INTRODUCTION

Bubbling is an important mechanism for the release of gases to the atmosphere from both freshwater and marine ecosystems. In particular, significant quantities of methane, a powerful greenhouse gas, can be released from sediments to the atmosphere through ebullition (e.g. Hornafius et al. 1999, Glaser et al. 2004, Walter et al. 2007). Ebullition can also serve as a transport mechanism for other volatile species such as nitrogen, hydrogen, carbon dioxide, radon and hydrogen sulfide (e.g. Martens and Chanton 1989, Chanton and Whiting 1995, Higgins et al. 2008).

Ebullition is a difficult process to quantify, since it is highly variable at several temporal and spatial scales (Fechner-Levy and Hemond 1996, Ostrovsky 2003, Leifer et al. 2004, Walter et al. 2006). Considerable amounts of gas are often emitted during occasional, short-lived bubbling episodes. For example, large, rare emission events lasting for about 30 seconds have been observed in Siberian lakes (Walter et al. 2006), while bubbling events in hydrocarbon seeps have been identified to occur on the scale of a few minutes (Greinert 2008). At the Upper Mystic Lake in Massachusetts, U.S., we have observed bubble patches at the lake surface having lifetimes between 1 and 10 minutes. Ebullition has also been observed to vary seasonally, with higher release occurring during early spring, late summer and early fall (e.g. Wilson et al. 1989, Casper et al. 2000). In some ecosystems, bubbling fluxes tend to increase when there is a decrease in atmospheric pressure (Mattson and Likens 1990, Fechner-Levy and Hemond 1996, Kellner et al. 2006) or a lowering of water level (Chanton et al. 1989, Boles et al. 2001), but the sequence of events that leads to increased ebullition is not well understood.

Bubbling fluxes are typically measured using one of two types of collection chambers (Chanton and Whiting 1995). One method uses chambers filled with air that float on the water surface, and fluxes are calculated by measuring the change in concentration of a gas within the chamber over a period of time. Automated versions of this type of device continuously pump the air from the chamber through an infra-red analyzer to obtain methane concentrations, and have been used in several ebullition studies in wetlands (Sebacher and Harriss 1982, Crill et al. 1988, Bäckstrand et al. 2008, Mastepanov et al. 2008). However, such chambers measure the sum of diffusive and ebullitive fluxes, which then need to be separated by other analyses, and also may prove problematic in energetic surface water environments. A second type of flux chamber consists of a submerged, inverted funnel that traps bubbles and delivers the gas to a collection

chamber (e.g. Casper et al. 2000, Huttunen et al. 2001). In such devices, ebullition fluxes are calculated from the volume of gas that accumulates in the chamber, while bubble composition is typically determined by gas chromatographic analysis after withdrawing the gas from the chamber via syringes.

Most reported ebullition measurements are based on manually-tended funnel-type traps that were deployed either for relatively short periods of time and sampled with relatively high frequency (e.g. Martens and Klump 1980, Bartlett et al. 1988, Keller and Stallard 1994), or for long periods with low sampling frequency (e.g. Mattson and Likens 1990, Huttunen et al. 2001). In the former case, major episodes of bubbling may be missed entirely, leading to inaccurate estimates of long-term fluxes. In the latter case, the timing of bubbling events remains unknown within each sampling period. Ultimately, long-term measurement with high sampling frequency, as well as adequate spatial density, is necessary to test hypotheses regarding the magnitude, spatiotemporal variability, and mechanisms of bubbling. However, the collection of such data is not practical over long deployment periods without automation. Automation can also help in monitoring fluxes during periods of time or at locations where site conditions render manual field measurements difficult.

An automated funnel-type trap equipped with a differential pressure sensor has previously been used to measure the volume of gas emitted from a marine hydrocarbon seep (Washburn et al. 2001), although we are unaware of any long-term or extensive deployments of this type of trap, and the device appears to be expensive to build. More recently acoustic techniques have been used for automated measurement of ebullition (e.g. Greinert and Nutzel 2004, Ostrovsky 2008). While these methods have spatial resolutions in the order of tens to hundreds of meters, they are expensive in terms of cost and power to deploy at several sites.

Furthermore the gas content of bubbles is unknown and additional data processing has to be done to estimate methane fluxes to the atmosphere because not all bubbles reach the water surface (McGinnis et al. 2006).

In this paper, we present a design for an inexpensive, but sufficiently accurate, low-power, automated instrument that uses a differential pressure sensor to measure the volume of bubbled gas and accumulating in a flux chamber. The design emphasizes not only high sampling frequency but also low cost and ease of construction, in order that a sufficient number of units can be deployed to characterize both temporal and spatial variation in bubbling.

The device can also be readily adapted to monitor other situations where a pressure differential is of interest. For example, at our field site, we adapted one unit to continuously measure the water level of the lake by repackaging the same electronics in a slightly different enclosure.

2. MATERIALS AND PROCEDURE

2.1 Trap design

The trap consists of a cone attached to a transparent PVC pipe that functions as a collection chamber in which bubbled gas can accumulate (Figures 1(a) and (b)). The bubble collection funnel is made by rolling a sheet of 28-gage galvanized steel, cut from a pattern, into a cone of diameter 0.5m and an approximate height of 0.16m. The cone is painted using a hard enamel paint to keep the surface smooth and to minimize corrosion. The seam of the cone is either pop-riveted or spot welded, and sealed with epoxy adhesive and silicone sealant to prevent gas leakage as well as to create a smooth edge on the inside of the cone.

The gas collection chamber is a length of transparent, nominal $\frac{1}{2}$ inch (1.27 cm) or $\frac{3}{4}$ inch (1.9 cm) schedule 40 PVC pipe. Narrow pipe diameters are chosen to limit the area of the gas-water interface, and hence the amount of methane potentially lost through diffusion to the water column, as well as to increase the sensitivity of the device. Pipe lengths varied from 30 cm to 1 m, and can be chosen according to the flux expected at the deployment location. The pipe is marked in 1cm intervals, so the height of bubbled gas accumulating in the chamber can be read manually, providing a means for in-field calibration checks.

The collection chamber is connected to the cone through a fitting made from a 5 cm slice of a $2\frac{3}{4}$ inch (8.25cm) diameter PVC rod. A hole (of diameter 2.14 cm (27/32 inch) for the nominal $\frac{1}{2}$ inch pipe; 2.7 cm (1 1/16 inch) for the nominal $\frac{3}{4}$ inch pipe) is drilled through the center to accept the pipe, which is attached using standard PVC cement. The opposite face of the fitting is machined to an angle of 34° to fit the top of the cone, to which it is fastened using flat head screws, epoxy adhesive, and silicone sealant.

The collection chamber is capped with a nominal $\frac{1}{4}$ inch (0.63 cm) 3-way brass ball valve via a PVC pipe connector of the appropriate size. A second port of the 3-way valve is connected to the pressure sensor housing, while the third port is sealed with a rubber septum, through which gas can be withdrawn for analysis.

The chambers can hold between 200 and 300 ml of gas, depending on the PVC pipe dimensions, before the gas begins to overflow into the collection funnel. It is undesirable to have gas fill up in the funnel because it then becomes difficult to accurately measure the volume of gas and because the rapidly increasing area of the interface between trapped gas and the water column likely enhances gas exchange.

Three nominal $\frac{1}{4}$ inch (0.63cm) PVC pipes, attached to the cone on one end, and to a 0.63 cm by 30 cm by 30 cm polypropylene panel on the other end, provide structural stiffness to the assembly. The pipes are arranged to form a cross bracing that limits flexing caused by wave action.

The trap is suspended at a depth of 1 m below the water surface using three 1.5 m long ropes connecting the polypropylene board to a polyform A0-series buoy such as is commonly used for marking boat moorings. Buoys are moored to a concrete block anchor using $\frac{1}{4}$ inch (0.63 cm) three-strand nylon rope. Since the traps were to be used in a lake in an urban setting that sees a high volume of recreational use, the entire setup is designed to be unobtrusive, but visible to boat operators. The total cost of materials for a trap, including the buoy but excluding the electronics, was approximately \$85.

2.2 Circuit design

The circuit measures the difference in fluid pressure between the top of the gas collection chamber and the outside water column. This pressure is proportional to the height of the gas collected in the chamber and can be converted to a gas volume given knowledge of the chamber cross-section area. We used a wet-wet, temperature compensated differential pressure sensor (26PCAFA6D, Honeywell Inc.) that has a manufacturer specified range of ± 1 psi (± 6900 Pa), approximately equivalent to ± 70 cm of water. A commercial data logger with an inbuilt temperature sensor (H08-002-02, Onset systems) was used to store the final voltage readings from the circuit.

The millivolt pressure sensor output was buffered and amplified to the 0 to 2.5 V data logger range using the circuit shown schematically in Figure 2. Output from the pressure sensor was applied to an instrumentation amplifier (INA126, Texas Instruments), which provided a gain

of 5 and also presented a high impedance load to the sensor bridge to minimize voltage measurement error. The instrumentation amplifier is followed by an operational amplifier (Op Amp D) set to a gain of 270 by means of resistors R8 and R7.

The pressure sensor itself comprises a bridge, which is driven by a pair of op-amps that divide the 5V supply voltage (3V from Op Amp A and 2V from Op Amp B), and provide the difference between their outputs as excitation. The 2V output from Op Amp B is also used as a signal reference for the data logger. The excitation voltage for the pressure sensor is thus 1V, as opposed to the manufacturer's suggested value of 10V, to keep the power drawn by the sensor to a minimum. Op Amp C buffers the 2.1V reference provided via the resistor divider (R5 and R6) for the instrumentation amplifier. The 2.1V reference creates an offset, which results in a slightly positive input to the data logger when the pressure sensor output is zero, biasing it into its allowable input range. The null offsets generated by the circuits range from 0.04V to 0.35V; this variation primarily arises from the instrumentation amplifier. The circuit shown in the diagram only uses the 0 to 1 psi range of the pressure sensor; this can be modified to use the entire ± 1 psi sensor range by changing resistors R5 and R6 to alter the signal reference voltage. The four op-amps are all contained in a single IC device (TLV2404, Texas Instruments).

All electronics other than the self-contained data logger are powered using two 3.6 V, 2.4 A-H AA lithium batteries. A 5V voltage regulator (LP2952, National Semiconductor) is used to ensure that the supply to the circuit remains constant. Low power circuit elements are selected to keep power consumption to a minimum; the total current drawn from the AA batteries was measured to be 0.41 mA. The circuit can be powered for about 8 months without battery replacement, while the data logger is powered by its own battery that lasts for about a year. Data from the logger can be accessed using a cable connected from a 3.5 mm stereo jack on the logger

to the serial port of a PC. The manufacturers' specifications, cost and power consumption of the electronics are further described in Table 1.

2.3 Waterproof Housing

The electronic circuitry is enclosed in a housing built from a nominal 4 inch (10.16 cm) schedule 40 PVC pipe cap. Two 2.18 cm (55/64 inch) holes are drilled on opposite ends of the wall, and nominal 1/4 inch (0.63 cm) schedule 80 PVC threaded, female adapters are cemented into the holes to provide access to the pressure ports of the sensor. The edges around the adapters are sealed to be watertight with epoxy and silicone sealant. The 3-way valve on top of the collection chamber is attached via a nominal quarter inch (0.63cm) brass nipple to one of the adapters, while the second adapter is left open to the water column. Interior ends of the adapters are connected to the pressure sensor ports with short lengths of 3/16 inch (0.476 cm) flexible plastic tubing. The directionality of the pressure sensor is important; the high-pressure port should be connected to the collection chamber end, while the low-pressure port is to be exposed to the water.

The housing is closed with a nominal 4 inch schedule 40 PVC pipe plug, cut to a length of 2.5 cm. An o-ring groove, 0.282 cm (0.111 inch) deep and 0.475 cm (0.187 inch) wide, is machined into the plug and fitted with an EPDM o-ring (dash size 244). The plug and groove are chamfered at the edges to create smooth surfaces, and the o-ring should be greased before sealing the housing.

The enclosure can be tested for leaks in the laboratory using a vacuum test, in which connections to the sensor are removed and one of the adapters in the housing is plugged to be airtight. The second adapter is attached to a vacuum pump via a tee fitting having a vacuum pressure gage on one end and a ball valve on the other so that vacuum can be retained in the

housing once the pump is turned off. In tests, approximately 3700 Pa (28 inches of mercury) vacuum was applied; a leaky housing could be easily detected within a few seconds, whereas a good seal would allow only a minor pressure increase (order of 100 Pa, or 1 inch mercury) over a 30-minute period.

In addition, the circuit was assembled in the housing and left overnight in a water bath before deployment; this served as a secondary leak test as well as to ensure that the circuit was working correctly. The o-rings had to be replaced in the field about once every two to three weeks, in order to ensure a watertight seal. Indicating silica gel desiccant packs were inserted into the housing before deployment in the field.

2.4 Field deployment and sampling

Gas was collected from the traps for analysis typically every 4-13 days. The height of the bubbled gas column (herein referred to as pipe waterline) was measured before sampling using the markings on the transparent collection chamber. Gas was then withdrawn from the collection chamber into syringes, thus filling the chamber with water. Finally, pressure data were downloaded and the data logger was reset in order to clear its memory. The data logger can store data for 13.5 days at a measurement interval of 5 minutes, or proportionally longer with larger measurement intervals.

2.5 Modifications made for measuring water level

The circuit described above can also be used, for example, to monitor the water level of a lake, by measuring the pressure difference between the water column at a fixed point in the lake, and the atmosphere. The assembly was modified for this purpose by venting one pressure port to the atmosphere. This can be done, for example, with a 75cm long nominal quarter inch (0.63cm)

schedule 40 PVC pipe having a 90° elbow, with a mesh blocking its open end, cemented to the top of the pipe to prevent the entry of rainwater, insects, and debris. Also, the pressure sensor direction must be reversed, such that the low-pressure port connects to the atmosphere, and the high-pressure port connects to the water column.

2.6 Calculations and Circuit Calibration

The sensor measures the difference in pressure between the top of the collection chamber and the water column at that depth. Since the gas pressure at the top of the chamber is equal to the water column pressure at the depth of the pipe waterline (neglecting gas density), the resulting pressure differential (ΔP) is:

$$\Delta P = \rho_{\text{water}} g h_g \quad (1)$$

where ρ_{water} is the density of water, $g = 9.8 \text{ m/s}^2$, h_g = Height of gas in the collection chamber, i.e. pipe waterline.

Voltage output from the circuit is converted to a height measurement (h_g) using calibration curves that are determined in the laboratory for each individual circuit. The calibration setup involves connecting the tip of a burette to one of the pressure sensor ports through a short length of tubing, while the second sensor port is open to atmospheric pressure. Water is added to the burette at approximately 4 cm height intervals and the corresponding voltages recorded by the data logger are noted, in a process adapted from the calibration procedure used by Gardner et al. 2009.

Measured circuit responses were linear within the 0 to 2.5 V output range, with Pearson correlation coefficients (R^2) greater than 0.999. An inverse linear regression on the calibration data gave slope and offset values that can be used to convert the circuit output voltage to height, h_g in cm.

Each circuit was calibrated thrice – first before deployment in the field, second at the end of the field season to check for slope and offset drift, and finally in a cold room at approximately 5°C to estimate the effect of temperature change. Slope values varied among calibrations from 27.1 to 29.2 cm/Volt across circuit units, and were within the range expected from Honeywell's specifications.

Offset values obtained from laboratory calibrations ranged from 1.95 to 12.6 cm among the different circuits from the start to the end of the ~ 6 month deployment period. Variations in offset were caused due to a combination of sensor and amplifier drift, temperature effects and random measurement errors. Thus in order to achieve accurate data reduction, lab offsets are replaced with field offsets that are based on “zero” voltage readings obtained every time the collection chamber was refilled with water during gas collection. The zero voltage at a sample point is calculated by averaging a set of circuit voltages obtained in the first hour or two following gas collection. Field offsets used in calculations are the average of zero voltages measured at the two nearest points of sampling to account for drift between gas collections.

The equation for the gas height in the collection chamber, h_g , is:

$$h_g = \bar{m}(V_{out} - \bar{V}_{zero}) \quad (2)$$

where \bar{m} = Average slope from laboratory calibrations (cm/Volt)

V_{out} = Voltage output recorded on the data logger (Volt)

\bar{V}_{zero} = Average of two nearest zero voltages measured in the field (Volt).

The gas height, h_g , is multiplied by the cross sectional area of the collection chamber (1.88 cm² for nominal ½ inch schedule 40 pipes and 3.32 cm² for nominal ¾ inch schedule 40 pipes) to determine the volume of gas present in the trap. It should be noted that actual PVC pipe dimensions can differ from published values, and that using the latter can potentially lead to

significant errors in volume calculations. Volumes measured at the 1 m deployment depth of the traps are normalized to 1 atmosphere and 20°C, assuming ideal gas behavior.

The formula for calculating the volume of gas present in a trap at 1 atm and 20°C, using the height h_g from equation 2 is:

$$Vol \text{ (in ml)} = (1 + \frac{\rho_{water} g}{P_{atm}} * (1 + 0.01 * h_g)) A_c h_g * \frac{293K}{T_{trap}} \quad (3)$$

where ρ_{water} is 998 kg/m³ at 20°C

$P_{atm} = 101 \text{ kPa}$

A_c = Cross section area of the collection chamber (cm²)

T_{trap} = Temperature recorded by the datalogger

Temperature differences between the water at 1 m depth and the surface, as well as day-to-day barometric pressure and temperature variations, are neglected for purposes of this calculation. Any buoyancy effect caused due to gas accumulating in the collection chamber is also considered to be negligible.

A dead volume correction was applied to automated measurements obtained from traps that use a ¾ inch PVC pipe as the collection chamber. An opaque reducing pipe adapter is cemented to the top of the collection chamber, and multiplying the height of the adapter by the chamber cross-section area leads to a volume overestimation of about 9 ml. No correction is applied to automated data from traps with ½ inch pipes since the effective diameter of the pipe adapter is nearly the same as the collection chamber diameter, and amounts to a volume difference of ~1 ml.

The volumes obtained using the pressure sensor data were compared to manual gas measurements to verify circuit behavior. Manual volumes were measured in two ways:

- (i) By recording the volume of gas collected in syringes while emptying the collection

chamber.

- (ii) By multiplying the gas height obtained from reading the waterline in the transparent PVC pipe with the collection chamber cross-section area. Since the height markings on the transparent pipe start below the opaque pipe adapter attached to the top of the collection chamber, the adapter volume (6.5 to 9.5 ml for the $\frac{1}{2}$ inch pipe and 12 to 13 ml for the $\frac{3}{4}$ inch pipe) has to be added to obtain a final value for the manual volume reading.

The manual volume measurements were, whenever possible, an average of values obtained using both methods. Exceptions were made for instances when no syringe samples were taken or when the pipe waterline was hidden by the opaque pipe adapter. The standard deviation (1σ) of readings obtained using the two methods was used as an estimate of error in the manual measurements. Its value was typically around 1 to 3 ml, depending on the collection chamber dimensions.

3. ASSESSMENT

3.1 Results

Traps built in this design were continuously deployed from June to November 2008, at as many as 7 stations at any given time. Data was collected at a resolution of 5 to 10 minutes. Figure 4 shows a 3-week sample of gas volume data collected from the automated traps. Gas volumes measured by properly functioning automated traps were deviant from manual readings by 2 ± 2 ml (1σ) for a total of 130 readings (Figure 5).

3.2 Error budget terms for volumes measured in the automated traps

The error estimate for volumes calculated using data obtained from the automated traps includes the effects of sensor drift and temperature on circuit electronics, calibration errors, and “dead volume” errors caused by irretrievable gas trapped in the fittings at the top of the collection chamber. In some circuits, zero voltages (i.e. field offsets) stabilized after drifting by as much as 0.1V during the first week of field deployment. The following error calculations are applicable to data collected after the traps were deployed for a week.

A control trap that constantly measured a “zero” voltage was deployed for four weeks at a location that had no bubbling. Data obtained at 5-minute resolution from this trap was additionally used to estimate the effects of circuit drift, temperature and wind on output voltage as shown below.

A root sum squared (R.S.S.) propagation of uncertainty can be applied to equation 3 to obtain the error in estimated gas volume. The error in collection chamber cross-sectional area is neglected in the following error budget because the diameters along the length of representative pipe samples were measured to be uniform. The error caused due to the normalization of gas volume to 1 atm and 20°C is also insignificant. However, an additional term was included to account for dead volume errors, which were on the order of 1-2 ml.

The “ Δ ” in the following equations denotes the standard deviation (1σ) of a term. The final error in volume, ΔVol , is approximately:

$$\Delta Vol \approx Vol * \frac{\Delta h_g}{h_g} \pm \text{Dead volume error} \quad (4)$$

Applying R.S.S. propagation of uncertainty to equation 2, the error in height, Δh_g , can be calculated as shown in equation 5. The height error includes a slope component (Δm), an offset error (ΔV_{zero}), and electronic noise (ΔV_{out}).

$$\Delta h_g = \sqrt{\Delta m^2 [V_{out}^{-2} + \bar{V}_{zero}^2] + \bar{m}^2 [\Delta V_{out}^{-2} + \Delta V_{zero}^2]} \quad (5)$$

Slope Error (Δm)

Slope errors can arise from the following terms (Honeywell technical note):

- i. Calibration error
- ii. Long-term slope stability of the sensor (aging)
- iii. Temperature coefficient
- iv. Linearity and repeatability

The standard deviation of slopes obtained from all the laboratory calibrations for a sensor unit was used as an estimate of slope error. Since calibrations were done at the start and end of the season, and at room and cold room temperatures that were each subject to a 2-3°C variation, it was assumed that all the above effects from the sensor as well as errors from the amplifiers were included in the standard deviation. Slope variability between circuits was not considered since each unit was calibrated independently for subsequent data conversion. Standard deviation values varied from 0.02 (0.02%) to 0.58 (2%) among different units.

For comparison, a theoretical expected error can be calculated using the pressure sensor manufacturer specifications. The Honeywell datasheet lists slope error terms as a percentage of the full operating pressure range of the sensor (denoted as %Span), since net slope errors are directly proportional to applied pressure.

The pressure sensor stability value represents the maximum deviation that the sensor can exhibit over a year when operating within a normal pressure and temperature range, and is specified by the manufacturer as $\pm 0.5\%$ Span. The temperature coefficient of the pressure sensor slope is specified in the Honeywell datasheet as $\pm 1\%$ Span over a compensated temperature range of 0 to 50°C or $\pm 0.02\%\text{Span}/^{\circ}\text{C}$. Typical linearity and repeatability errors are listed as $\pm 0.25\%$ Span. Linearity error reflects the deviation of the pressure sensor from expected straight-line behavior, while repeatability is a measure of the precision with which the sensor can output a certain voltage when cycled through its full pressure range.

Thus a theoretical R.S.S. slope error, assuming a typical slope value of 28 cm/Volt, and a temperature variation of $\pm 3^{\circ}\text{C}$ in the field is 0.16 (0.56%), which is within the error range calculated using the standard deviation of calibration slopes.

$$\Delta m = \frac{m}{100} * \sqrt{\underbrace{(0.5\%)^2}_{\text{Stability}} + \underbrace{(0.02\%/\text{ }^{\circ}\text{C} * 3^{\circ}\text{C})^2}_{\text{Temperature Coefficient}} + \underbrace{(0.25\%)^2}_{\text{Linearity}}} = \pm 0.16 \quad (6)$$

Offset Error (ΔV_{zero})

The offset error determined from field measurements includes the effects of short-term voltage drift and temperature fluctuations. It also includes random volume errors caused either due to incomplete flushing of gas from the collection chamber, or due to possible unknown, irretrievable gas quantities remaining in the trap after gas sampling.

The offset error at any point in time is calculated as the standard deviation of the two nearest zero voltages. Zero voltages recorded over the season for a sample set of circuits is shown in Figure 6. Standard deviations (1σ) varied from 0 to 30 mV across all traps for the entire

season. Zero voltages that deviated by more than 30 mV from the average value (e.g. circuit 1 on Oct 2nd) were considered as outliers and excluded from all calculations. These occurred 10 times out of a total of 125 points, and could typically be attributed to excessive residual gas left due to incomplete sampling of the trap or to bubbling that occurred between the time of sampling and the start of data collection. In some circuits (e.g. circuits 1 and 4) voltages stabilize after drifting by as much as 0.1V during the first week of deployment.

Laboratory tests indicate that the pressure sensor can drift rapidly for a short period of time immediately after the applied pressure on a port is removed. This effect is especially apparent when rapid gas accumulation causes the pressure sensor to go out of range for more than a few hours. The circuit zero voltage in this situation decreases rapidly and has a recovery period of approximately an hour; thus readings from the first hour were dropped from zero voltage calculations in instances where such behavior was suspected.

For comparison, a theoretical error can also be calculated using the published sensor specifications. The pressure sensor stability over a year of $\pm 0.5\%$ Span, i.e. $\pm 12.4\text{mV}$ can be used as an estimate for drift. The maximum null shift for the sensor using an applied excitation voltage of 10V over a compensated temperature range of 0 to 50°C is specified as $\pm 1\text{mV}$. Hence, the temperature coefficient of the circuits for an excitation of 1V and gain of 1350 should be less than $\pm 2.7\text{mV}/^\circ\text{C}$, if there are no temperature effects on any other part of the circuit. The R.S.S. estimated offset error is 15mV, which is within the 30mV error range calculated using field observations:

$$\Delta V_{zero} = \sqrt{\underbrace{(2.7 \frac{\text{mV}}{^\circ\text{C}} * 3^\circ\text{C})^2}_{\text{Temperature Coefficient}} + \underbrace{(12.4\text{mV})^2}_{\text{Short term offset stability}}} \approx \pm 15\text{mV} \quad (7)$$

Electronic noise (ΔV_{out})

Variations of up to $\pm 12\text{mV}$ were observed between adjacent logged values of some circuits when the pressure difference across the ports and the ambient temperature were constant. The data logger has a manufacturer specified 10mV precision error; some data logger units exhibit this amount of noise when connected to a constant voltage source. The various circuit elements (voltage regulator, amplifiers and pressure sensor) can also contribute to noise. Increasing the sampling frequency and averaging a larger number of measurements over the sampling period can greatly reduce the effects of electronic noise. For example, if the sampling frequency is set to 5 minutes, the data can be smoothed on an hourly basis by taking a moving average of 12 values, reducing the noise, ΔV_{out} to 3.5mV .

Total volume error calculations

The estimated slope, electronic noise and field offset error terms can be inserted into equation 5 to calculate the error in gas height. The calculation shown below uses typical values of slope ($28 \pm 0.5\text{cm/V}$), zero voltage (0.15V), offset error (15mV), and smoothed electronic noise (3mV). The error in height occurring at the maximum output voltage of 2.485V (i.e. 70cm) is $1.25\text{ cm} (\sim 2\%)$.

$$\Delta h_g = \sqrt{(0.5)^2 [2.485^2 + 0.15^2] + (28)^2 [(0.015 \text{ Volt})^2 + (0.003 \text{ Volt})^2]} = \pm 1.25\text{cm} \quad (8)$$

The error in volume is calculated using equation 4, and assumes an error of 2ml for random dead volume effects. The final volume error is on the order of 3 to 5 ml for the nominal $\frac{1}{2}$ inch PVC pipe and 4 to 6ml for the nominal $\frac{3}{4}$ inch PVC pipe, depending on the volume of the gas accumulated.

3.3 Effects of large changes in temperature

Several tests were done to observe the actual effects of a varying range of temperatures on zero voltages. First the temperature coefficient was determined as the shift in zero voltage when a circuit at room temperature (20-25°C) is moved to a cold room (~5°C). Zero voltages of five circuits were measured at room temperatures in the laboratory for 2 days, followed by two days in the cold room, and finally for a day back at room temperature (Figure 7). Zero voltages were strongly correlated with temperatures during the transition from room temperature to 5°C and vice versa, which occurred within less than half an hour. Temperature coefficients ranged from -1mV/°C to -3.4mV/°C in all but one circuit, which had a coefficient of -11mV/°C. Independent lab tests confirmed that the data loggers were not significantly affected by changes in temperature.

However, zero voltages repeatedly had poor correlations with temperature when the circuits were only at ambient room temperatures in various tests. Smoothed in-field zero voltages obtained from the control trap also did not correspond well with temperature, except during one week where the observed temperature coefficient was -3.6mV/°C. Hence although the effect of temperature is in concept a systematic error, it was ignored in data reduction and was treated as a random error whose magnitude was included in the standard deviation of field offsets observed over a week.

Keeping the electronics underwater in the field greatly helps minimize temperature variations; the average change in temperature over a week was ~3°C. The temperature sensor in the data logger has a published accuracy of $\pm 0.8^\circ\text{C}$, and resolution of $\pm 0.4^\circ\text{C}$ under ambient conditions. The circuits were also tested in a refrigerator (-5 to 5°C) to mimic winter conditions

and measured temperature coefficients varied between $\pm 2.5\text{mV}^{\circ}\text{C}$, which is within the range obtained from previous tests.

3.4 Effect of wind and waves

Noise caused by wind and associated wave action was estimated by comparing voltages recorded at the control trap against wind speeds obtained from an anemometer installed on a buoy in the middle of the lake (Figure 8). Almost no noise was observed during periods when the wind speed was below 3 km/h; the typical noise was on the order of $\pm 10\text{ mV}$, which corresponds to a height of $\sim 3\text{ mm}$, during moderate wind conditions. A simple moving average filter can be used to smooth the automated trap data to eliminate wind effects.

3.5 Other bubble trap tests

Possible extent of methane loss due to dissolution during trap deployment was tested by injecting 50ml of pure methane gas into a trap. The trap was left for two days at the field site. 45ml of gas was recovered, which contained 93% methane and approximately 0.1% oxygen.

4. DISCUSSION

Bubbling at the Upper Mystic Lake is an episodic process, where high flux periods, with gas release rates on the order of hundreds to thousands of $\text{ml}/(\text{m}^2\text{-day})$ are interspersed with low flux conditions where rates average only tens of $\text{ml of gas}/(\text{m}^2\text{-day})$. The automated bubble trap described in this paper can identify bubble events on the scale of minutes while monitoring fluxes on a long-term basis. The cumulative volumes logged by these traps over a 4 to 6 month deployment interval matched the cumulative sum of manual gas volume measurements within

4%. Deployed in a water level recording mode, the modified device matched readings from a commercial water level sensor (Model 3001 Levelogger Gold, Solinst) within 1%.

The trap can be easily adapted to measure a varying range of fluxes, by altering the diameter and length of the collection chamber. Since the design proposed in this paper relies on the height of the gas in the collection chamber as an indicator of gas flux, it is advantageous to have a high aspect ratio in order to maximize sensitivity and minimize the errors in volume measurement. For higher volume measurements, a larger diameter PVC pipe could be inserted into the collection chamber near the bottom by means of reducing adapters. This would both increase the gas capacity of the chamber, and maximize the sensitivity of the circuit under low-flux conditions. At locations where extremely large volumes of ebullition need to be measured, an electronic valve could be fitted at the top of the collection chamber to automatically release gas when it crosses a threshold, as implemented in Washburn et al. 2001. For situations where greater sensitivity is desired, an auto-zeroing technique that completely eliminates offset errors using a 3-way solenoid valve could be used as shown in Gardner et al. 2009.

In situations where the trap can only be partially submerged due to logistical reasons, air from the collection chamber can be easily removed by applying a mild suction, for example using syringes. The trap and circuit design described above can be used without modifications, as long as some part of the cone is always underwater. However, these circuits will probably be subject to greater variations in temperature than an underwater unit, and a temperature correction might have to be applied to the data.

To our knowledge, there has been no previous study that has measured bubbling fluxes over a comparable period of time with such high temporal resolution. The data obtained from the

automated traps, combined with air pressure and water level data of similar resolution can lead to a better understanding of the processes that trigger bubbling episodes.

5. TABLES

Table 1 Details of electronics used in the circuit

Circuit component	Manufacturer	Model	Current Consumption	Approximate Unit Price
Differential pressure sensor	Honeywell	26PCAFA6D	~ 0.13 mA	\$15-20
Data logger	Onset Systems	HOBO H08-002-02	Temperature/ External logger	\$45-65
Quad Op-amp chip	Texas Instruments	TLV2404	1 µA	\$3
Instrumentation amplifier	Texas Instruments	INA126	175 µA	\$3
Voltage regulator	National Semiconductor	LP2952	130 µA for a 1mA load	\$2
2 high capacity 3.6V lithium batteries	Tadiran	TL-5903		\$7
PC Board	ExpressPCB			\$20

6. FIGURES

Figure 1 – Bubble chamber assembly

Figure 2 – Circuit diagram

Figure 3 – Picture of circuit and packaging

Figure 4 – Automated data from August 15-September 5, 2008

Figure 5 – Comparison of volumes obtained from automated and manual measurements

Figure 6 – Variations in zero voltages of sample circuits over the season

Figure 7 – Temperature coefficients of circuits

Figure 8 – Effect of wind and wave action on circuit output voltage

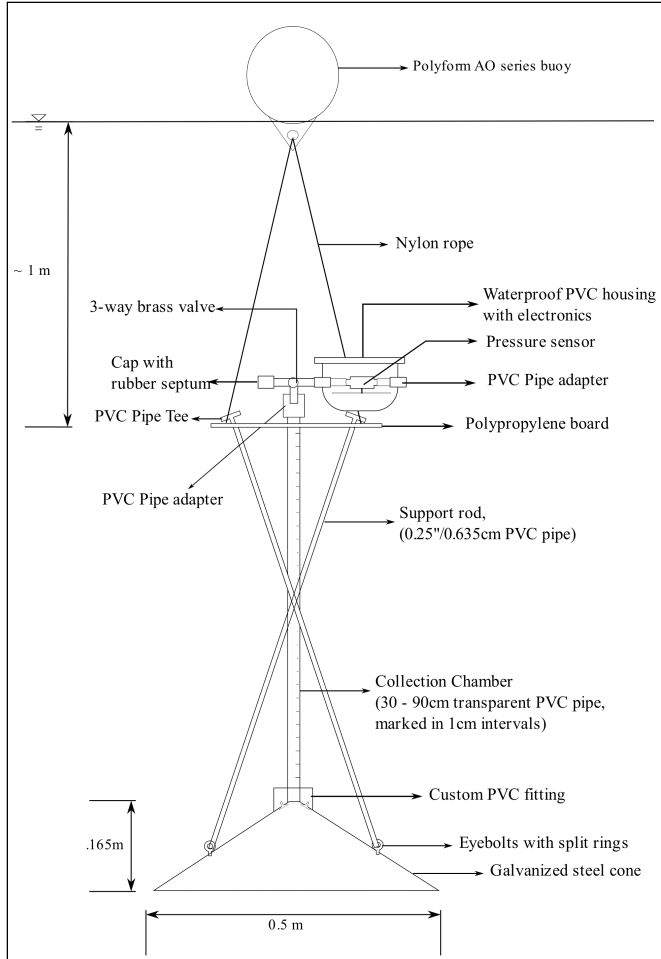


Figure 1 (a) & (b) Bubble Chamber Assembly

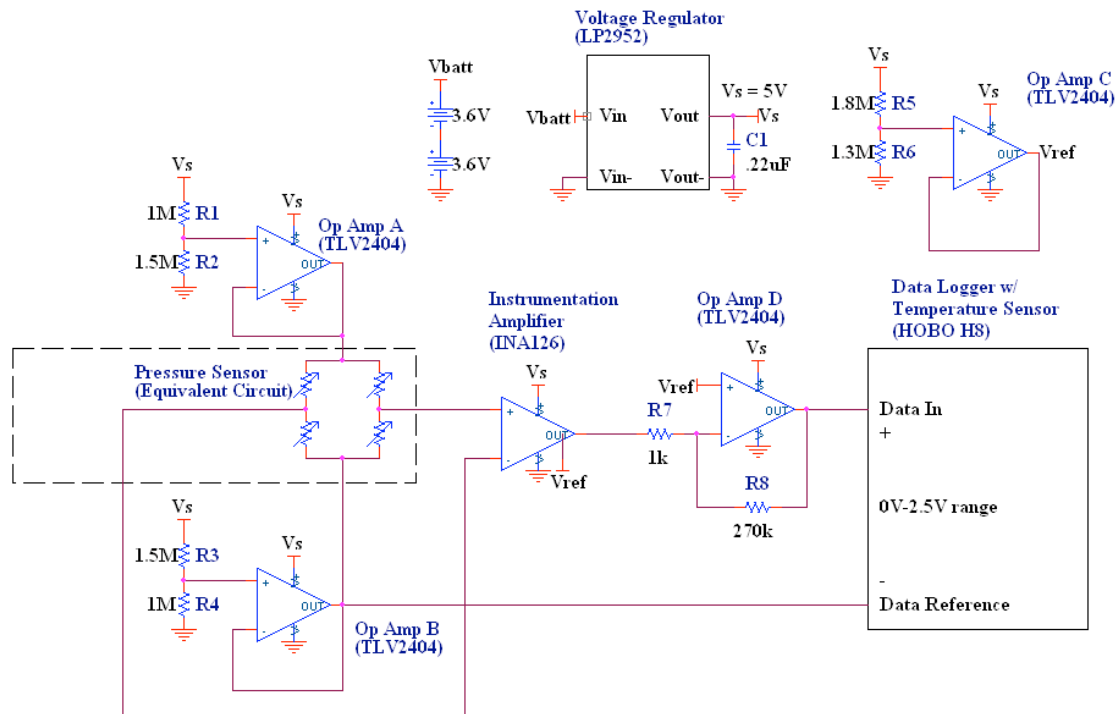


Figure 2

Circuit Diagram

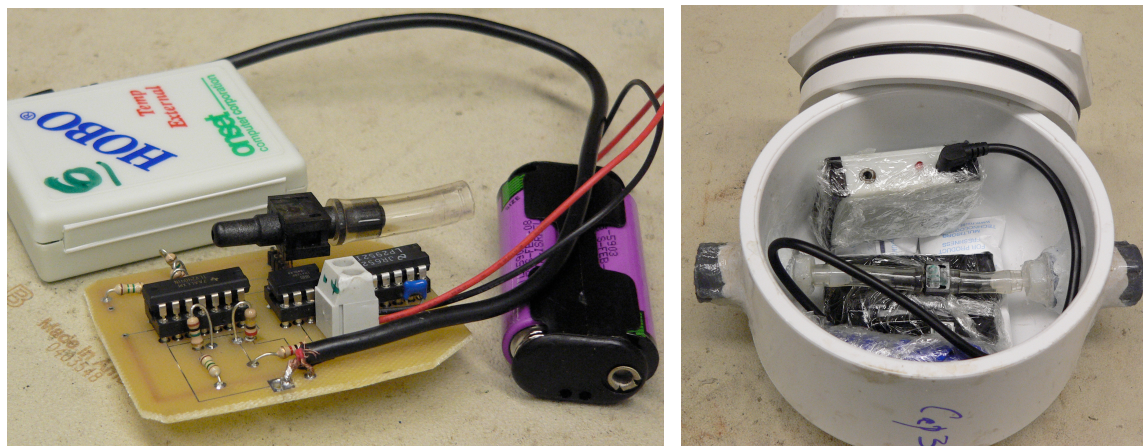


Figure 3 Pictures of circuit (left) and waterproof housing with packaged electronics (right)

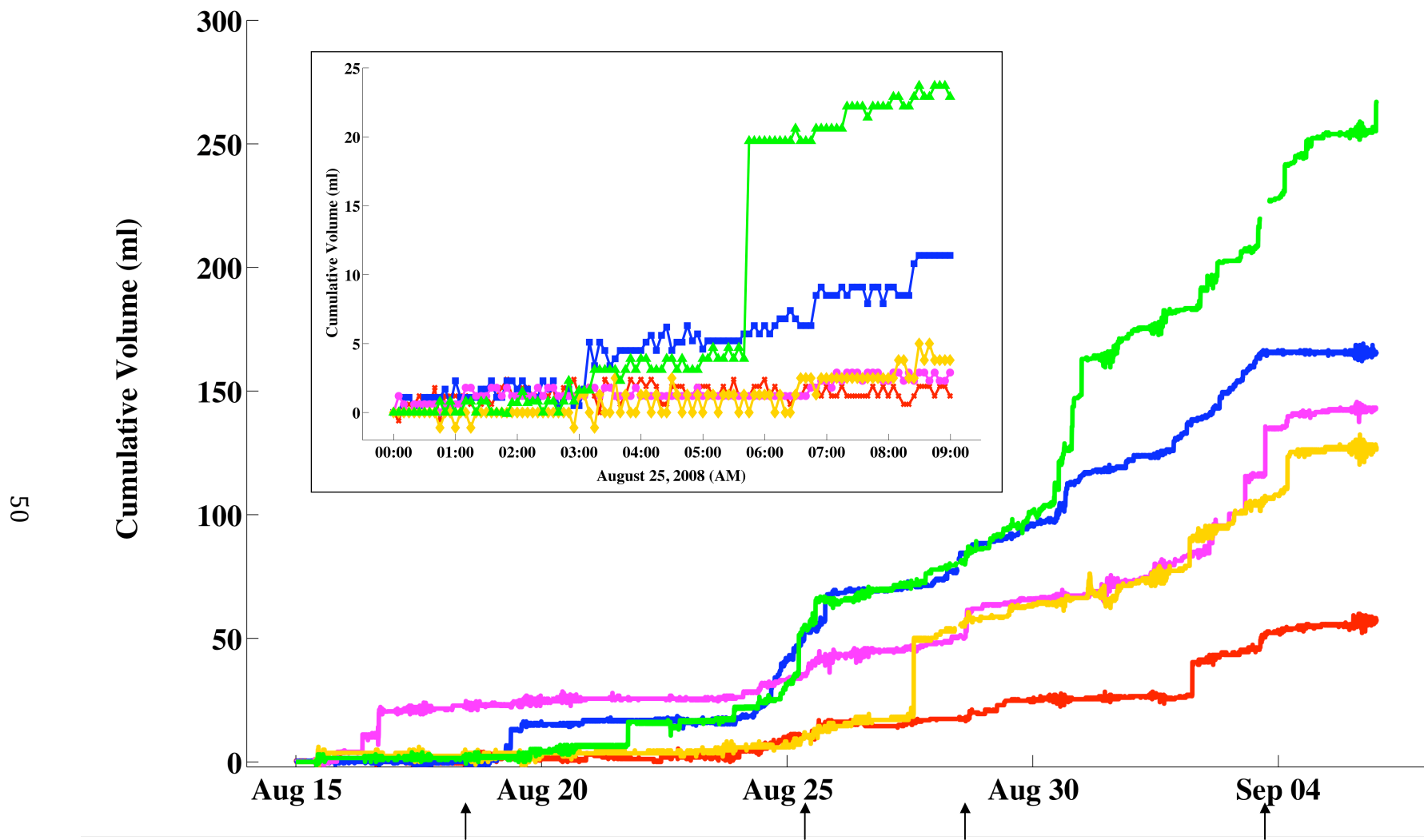


Figure 4 Bubbled gas measured at 5-minute resolution in five automated traps from Aug 15 to Sep 5, 2008. The arrows below the x-axis indicate manual sampling dates. (Inset: Close up of data collected between 12AM and 9AM on Aug 25, 2008). Cumulative volumes shown are initialized to zero for purposes of comparison.

LS

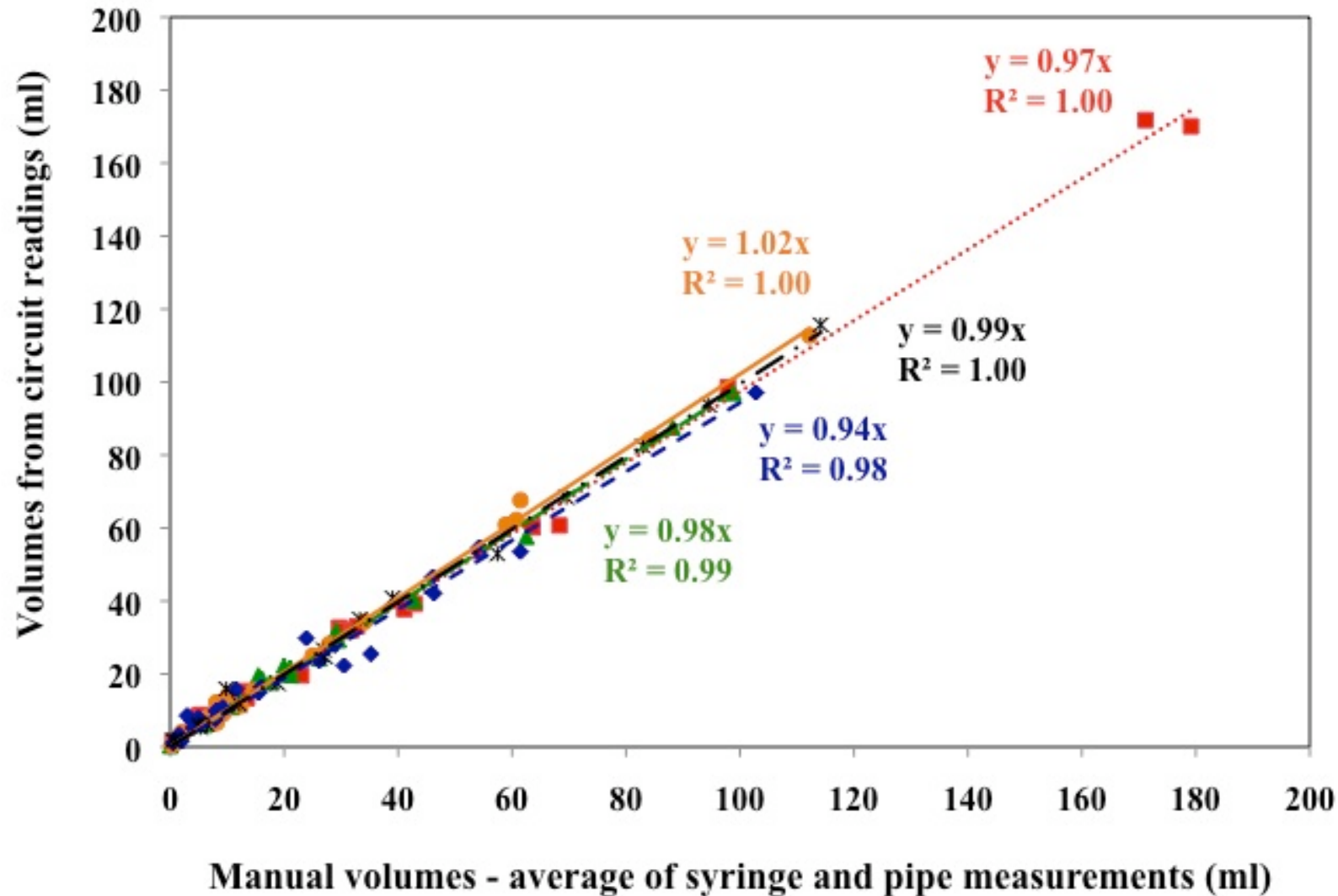


Figure 5 Comparison of volumes obtained from five automated traps with a hundred manual observations collected over 6 months. Volumes shown above are normalized to 1atm and 20 C.

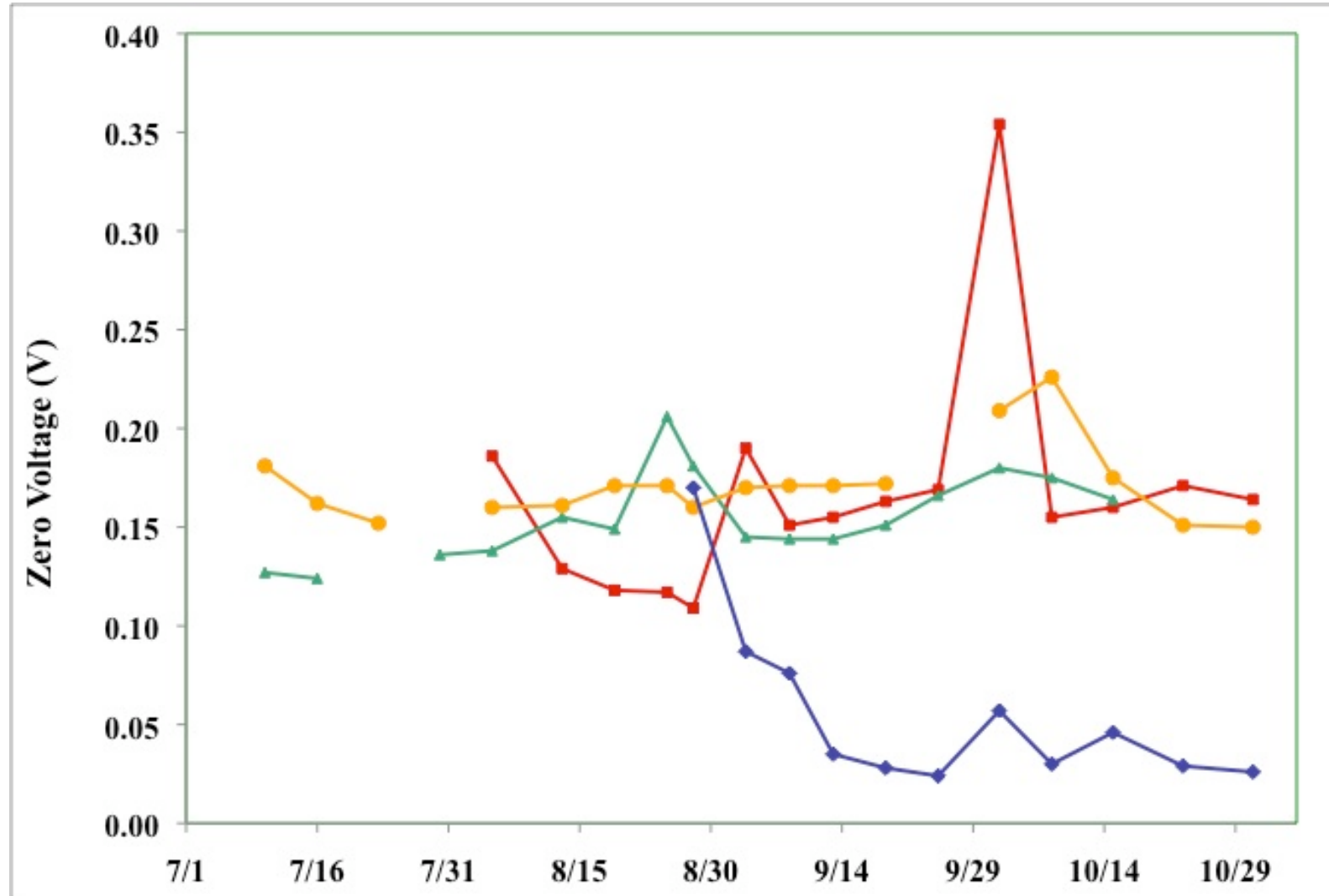


Figure 6 Zero voltages for a sample set of circuits recorded after the traps were manually sampled once every 4-13 days

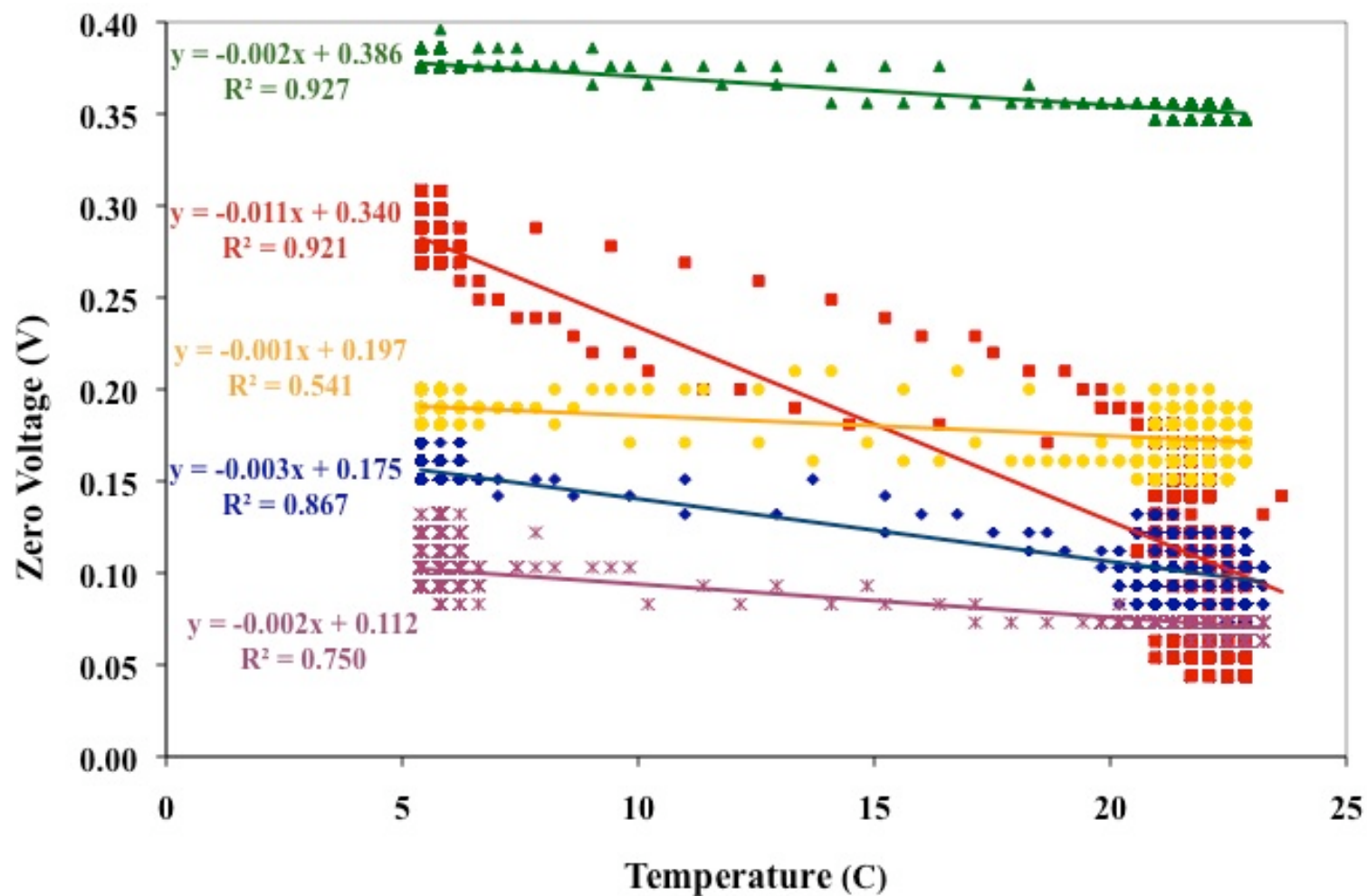


Figure 7 Temperature coefficients of five sample circuits. The circuits were placed in the laboratory at 20-25 C for 2 days, then moved to a cold room at 5 C for 2 days, and finally brought back to the laboratory for a day. Data was recorded at an interval of 2 minutes.

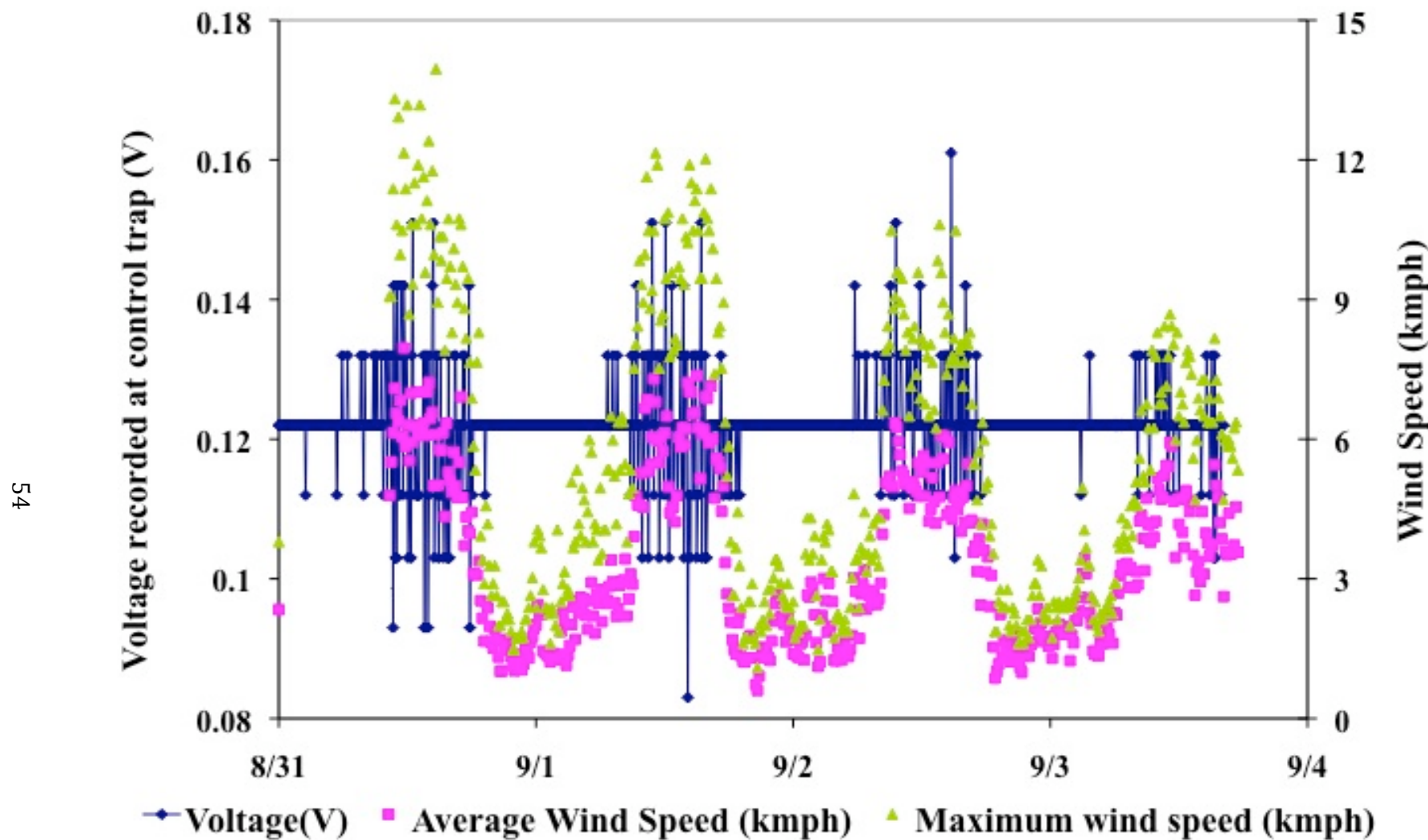


Figure 8 Effect of wind/wave action on circuit output voltage at a control trap for a sample 4 day period. Voltage measured by the circuit at a resolution of 5 minutes was compared against 10-minute wind speed data obtained from an anemometer located close to the control trap.

REFERENCES

1. Bäckstrand, K., P. M. Crill, M. Mastepanov, T. R. Christensen and D. Bastviken. 2008. Total hydrocarbon flux dynamics at a subarctic mire in northern Sweden. *J. Geophys. Res.* **113**: G03026, doi:10.1029/2008JG000703.
2. Bartlett, K. B., P. M. Crill, D. I. Sebacher, R. C. Harriss, J. O. Wilson and J. M. Melack. 1988. Methane flux from the central Amazonian floodplain. *J. Geophys. Res.* **93 (D2)**: 1571-1582.
3. Boles, J. R., J. F. Clark, I. Leifer and L. Washburn. 2001. Temporal variation in natural methane seep rate due to tides. Coal Oil Point area, California. *J. Geophys. Res.* **106 (C11)**: 27,077-27,086, doi:10.1029/2000JC000774.
4. Casper, P., S. C. Maberly, G. H. Hall and B. J. Finlay. 2000. Fluxes of methane and carbon dioxide from a small productive lake to the atmosphere. *Biogeochemistry*. **49**: 1-19.
5. Chanton, J. P., C. S. Martens and C. A. Kelley. 1989. Gas transport from methane-saturated, tidal freshwater and wetland sediments. *Limnol. Oceanogr.* **34**: 807-819.
6. Chanton, J. P., and G. J. Whiting. 1995. Trace gas exchange in freshwater and coastal marine environments: ebullition and transport by plants, p. 98-125. In P. A. Matson and R. C. Harriss [eds.], *Biogenic Trace Gases: Measuring Emissions from Soil and Water*. Blackwell Science.
7. Crill, P. M., K. B. Bartlett, J. O. Wilson, D. I. Sebacher, R. C. Harriss, J. M. Melack, S. MacIntyre, L. Lesack and L. Smith-Morrill. 1988. Tropospheric methane from an Amazonian floodplain lake. *J. Geophys. Res.* **93**: 1564-1570, doi:10.1029/JD093iD02p01564.
8. Fechner-Levy, E. J. and H. F. Hemond. 1996. Trapped methane volume and potential effects on methane ebullition in a northern peatland. *Limnol. Oceanogr.* **41**: 1375-1383.
9. Gardner, A. T., H. N. Karam, A. E. Mulligan, C. F. Harvey, T. R. Hammar and H. F. Hemond. 2009. A differential pressure instrument with wireless telemetry for in-situ measurement of fluid flow across sediment-water boundaries. *Sensors*. **9**: 404-429, doi:10.3390/s90100404.
10. Glaser, P. H., J. P. Chanton, P. Morin, D. O. Rosenberry, D. I. Siegel, O. Ruud, L. I. Chasar and A. S. Reeve. 2004. Surface deformations as indicators of deep ebullition fluxes in a large northern peatland. *Global Biogeochem. Cycles*. **18**: GB1003, doi:10.1029/2003GB002069.
11. Greinert, J. 2008. Monitoring temporal variability of bubble release at seeps: The hydroacoustic swath system GasQuant. *J. Geophys. Res.* **113**: C07048, doi:10.1029/2007JC004704 ER.
12. Greinert, J. and B. Nützel. 2004. Hydroacoustic experiments to establish a method for the determination of methane bubble fluxes at cold seeps. *Geo-Mar. Lett.* **24**: 75-85, doi:10.1007/s00367-003-0165-7.
13. Higgins, T., J. McCutchan and W. Lewis. 2008. Nitrogen ebullition in a Colorado plains river. *Biogeochemistry*. **89**: 367-377, doi:10.1007/s10533-008-9225-4.
14. Honeywell Sensing and Control. Pressure transducer accuracy in application: Technical Note. 1-9.
15. Hornafius, J. S., D. Quigley and B. P. Luyendyk. 1999. The world's most spectacular marine hydrocarbon seeps (Coal Oil Point, Santa Barbara Channel, California) - Quantification of emissions. *J. Geophys. Res.* **104 (C9)**: 20,703-20,711.
16. Huttunen, J. T., K. M. Lappalainen, E. Saarijärvi, T. Väisänen and P. J. Martikainen. 2001. A novel sediment gas sampler and a subsurface gas collector used for measurement of the

- ebullition of methane and carbon dioxide from a eutrophied lake. *Sci. Total Environ.* **266**: 153-158, doi:10.1016/S0048-9697(00)00749-X.
17. Keller, M. and R. F. Stallard. 1994. Methane emission by bubbling from Gatun Lake, Panama. *J. Geophys. Res.* **99 (D4)**: 8307-8319.
 18. Kellner, E., A. J. Baird, M. Oosterwoud, K. Harrison and J. M. Waddington. 2006. Effect of temperature and atmospheric pressure on methane (CH₄) ebullition from near-surface peats. *Geophys. Res. Lett.* **33**: L18405, doi:10.1029/2006GL027509.
 19. Leifer, I., J. R. Boles, B. P. Luyendyk and J. F. Clark. 2004. Transient discharges from marine hydrocarbon seeps: spatial and temporal variability. *Environ. Geol.* **46**: 1038-1052, doi:10.1007/s00254-004-1091-3.
 20. Martens, C. S. and J. P. Chanton. 1989. Radon as a Tracer of Biogenic Gas Equilibration and Transport From Methane-Saturated Sediments. *J. Geophys. Res.* **94 (D3)**: 3451-3459.
 21. Martens, C. S. and J. V. Klump. 1980. Biogeochemical cycling in an organic-rich coastal marine basin-I. Methane sediment-water exchange processes. *Geochim. Cosmochim. Acta.* **44**: 471-490.
 22. Mastepanov, M., C. Sigsgaard, E. J. Dlugokencky, S. Houweling, L. Ström, M. P. Tamstorf and T. R. Christensen. 2008. Large tundra methane burst during onset of freezing. *Nature.* **456**: 628-630, doi:10.1038/nature07464.
 23. Mattson, M. D. and G. E. Likens. 1990. Air pressure and methane fluxes. *Nature.* **347**: 718-719.
 24. McGinnis, D. F., J. Greinert, Y. Artemov, S. E. Beaubien and A. Wüest. 2006. Fate of rising methane bubbles in stratified waters: How much methane reaches the atmosphere? *J. Geophys. Res.* **111**: C09007, doi:10.1029/2005JC003183.
 25. Ostrovsky, I. 2003. Methane bubbles in Lake Kinneret: Quantification and temporal and spatial heterogeneity. *Limnol. Oceanogr.* **48**: 1030-1036.
 26. Ostrovsky, I., D. F. McGinnis, L. Lapidus and W. Eckert. 2008. Quantifying gas ebullition with echosounder: The role of methane transport by bubbles in a medium-sized lake. *Limnol. Oceanogr. - Methods.* **6**: 105-118.
 27. Sebacher, D. I. and R. C. Harriss. 1982. A system for measuring methane fluxes from inland and coastal wetland environments. *J. Environ. Qual.* **11**: 34-37.
 28. Walter, K. M., L. C. Smith and F. S. Chapin III. 2007. Methane bubbling from northern lakes: present and future contributions to the global methane budget. *Philos. Trans. R. Soc. A.* **365**: 1657-1676, doi:10.1098/rsta.2007.2036.
 29. Walter, K. M., S. A. Zimov, J. P. Chanton, D. Verbyla and F. S. Chapin III. 2006. Methane bubbling from Siberian thaw lakes as a positive feedback to climate warming. *Nature.* **443**: 71-75, doi:10.1038/nature05040.
 30. Washburn, L., C. Johnson, C. C. Gotschalk and E. T. Egland. 2001. A gas-capture buoy for measuring bubbling gas flux in oceans and lakes. *J. Atmos. Ocean. Technol.* **18**: 1411-1420.
 31. Wilson, J. O., P. M. Crill, K. B. Bartlett, D. I. Sebacher, R. C. Harriss and R. L. Sass. 1989. Seasonal variation of methane emissions from a temperate swamp. *Biogeochemistry.* **8**: 55-71, doi:10.1007/BF02180167.

Chapter 3: Time-series analysis of high-resolution ebullition fluxes from a stratified, freshwater lake

1. INTRODUCTION

Lakes are important sources of natural methane emissions to the atmosphere (Bastviken et al. 2004, Walter et al. 2007). Methane produced biogenically in lake sediments can subsequently be released to the atmosphere through several pathways such as ebullition, diffusive air-water exchange from the lake surface, and transport through vascular plants (Rudd and Taylor 1980).

Bubbling is usually the dominant pathway for atmospheric methane export from lakes (e.g. Casper et al. 2000, Crill et al. 1988, Walter et al. 2006). However, the episodic and heterogeneous nature of ebullition has complicated efforts to measure it accurately. Currently large uncertainties exist in estimates of the magnitude, timing and controls of bubbling episodes because of inadequate sampling mostly based on manual measurements. Prior efforts to obtain high-resolution data of bubbling fluxes in different aquatic environments have yielded valuable information on the nature of ebullition. For example, acoustic measurements in marine and freshwater settings (e.g. Greinert and Nützel 2004, Ostrovsky et al. 2008) have estimated bubble sizes and rise velocities, and have observed spatial and temporal variability in ebullition over the period of measurement (order of a few hours to days). A study that used automated flow-meters to measure the gas captured in large tents near the sea floor of a hydrocarbon seep on an hourly basis over 9 months (Boles et al. 2001, Leifer et al. 2004) found that ebullition was primarily controlled by variations in water level caused due to tidal forcing. In peatlands, automated chambers measuring total (diffusive and ebullitive) surface fluxes (e.g. Bäckstrand et al. 2008, Mastepanov et al. 2008), and GPS-based measurements of surface deflections (Glaser et al.

2004) have been used to observe the effect of environmental variables such as temperature and water level on methane emissions. However, to our knowledge, there have been no long-term automated measurements of ebullition in deep, non-tidal aquatic environments, such as freshwater lakes.

Ebullition can be triggered by several mechanisms that include changes in atmospheric pressure (Fechner-Levy and Hemond 1996, Mattson and Likens 1990), water level (Engle and Melack 2000, Martens and Klump 1980), rate of methanogenesis as determined by sediment temperatures, oxygen levels and organic matter input (Christensen et al. 2003, Kelly and Chynoweth 1981, Liikanen et al. 2002), wind (Keller and Stallard 1994) and physical sediment disturbance (Joyce and Jewell 2003). In particular, ebullition has been observed during periods of low hydrostatic pressure at several sites (e.g. Boles et al. 2001, Chanton and Martens 1988). Drops in hydrostatic pressure lead to bubble expansion, and bubble rise occurs as a result of the increased buoyancy. Chanton et al. (1989) found that 5-7% fluctuations in tidal height could cause bubbling, while Mattson and Likens (1990) reported an 18% increase in ebullition per millibar drop in atmospheric pressure.

We propose that ebullition may be triggered when the total hydrostatic pressure at the lake bottom falls below a critical value, which is determined by the gas content and gas storage potential of the sediments. Conditions for bubble breakout from sediments should either involve a drop in hydrostatic pressure or/and an increase in the sediment gas phase, with ebullition continuing until hydrostatic pressure rises or sediments are depleted of gas.

Since variations in hydrostatic pressure affect the whole lake simultaneously, any ebullition so triggered should be more or less synchronous across sites within a small lake. Moreover, bubbling fluxes should exhibit an inverse relationship with hydrostatic pressure. If the

above hypothesis were correct, it would also mean that the volume of gas released through ebullition during any particular time period would not necessarily be dependent on hydrostatic pressure alone, due to the effects of sediment gas storage. Excessive sediment gas buildup might cause bubble release to be initiated during periods of higher hydrostatic pressure, and conversely bubbling might not occur during low hydrostatic pressure conditions if sufficient gas is not present in the sediments.

Weekly observations of ebullition fluxes in 2007 at the eutrophic Upper Mystic Lake (UML) in Massachusetts, US indicated that bubbling occurred simultaneously at several sites during periods of low water levels. This was consistent with previous reports of synchronized bubbling episodes, where fluxes were correlated with low pressure storm systems or water levels (Casper et al. 2000, Eckert and Conrad 2007, Mattson and Likens 1990). However the temporal resolution of the 2007 data was inadequate to test the proposed hypothesis, since hydrostatic pressures can vary significantly over a week due to precipitation and fluctuations in atmospheric pressure.

In this paper, we investigate ebullition with long-term, high-temporal resolution data collected using a combination of sensors. In 2008, several automated bubble traps were deployed at the UML and gas collected in the traps was measured every 5 to 10 minutes for 4 to 6 months. Total hydrostatic pressure, lake water level and atmospheric pressure were monitored at similar resolutions. Bubbling events were then identified from the trap data using wavelet analysis, a relatively recent signal-processing approach, in combination with conventional statistical methods. We were thus able to precisely determine the timing of bubbling episodes at different sites around the lake, and correlate them with environmental variables.

2. BACKGROUND – TIME SERIES DATA PROCESSING

2.1 Statistical and Fourier analysis

Traditional approaches for event detection use statistical techniques such as clustering (e.g. Guralnik and Srivastava 1999), likelihood methods (e.g. Ogata 1988), or selection of data using thresholds (Kettunen et al. 2000, Smith 1989). Signal processing techniques based on the short-term Fourier transform can also be used for detecting events of interest (Priestley 1992). Fourier based spectral analyses have been extensively used to identify periodicity in geophysical processes, including in some high temporal resolution studies of methane ebullition (Greinert 2008, Boles et al. 2001). The time scales of variability in a process are typically identified using the frequency peaks exhibiting the highest power in the power spectral density plot (periodogram) of a signal.

However, in many conventional methods, it is commonly assumed that the data are stationary; i.e. the statistical properties and frequencies of the signal do not change with time, which might not be true for a sporadic natural process such as ebullition. Furthermore, the short term Fourier transform cannot resolve signals with high resolution in the time and frequency domains, which means that it is not possible to precisely identify when bubbling episodes occur.

Relationships between methane bubbling and environmental factors that can potentially influence the process have also been traditionally examined using linear regression and correlation analysis (e.g. Dise et al. 1993, Treat et al. 2007). The main problem with this approach is that it does not include any temporal information, and hence it is not possible to identify if there are specific time periods when certain factors have greater influence over the other. Such information is especially desirable for an analysis of methane bubbling, where it is expected that the correlation with hydrostatic pressure is not likely to be linear.

2.2 Wavelets for time-series analysis

Some of the above problems can be overcome with wavelets, a technique that can simultaneously analyze signals in the time and frequency domains, and can be used to identify local variations in non-stationary time series data. In the wavelet analysis of one-dimensional time-series data, the signal is multiplied with a wavelet function (i.e. a small wave that integrates to zero over its length), which can be scaled to analyze the signal at different resolutions as well as shifted along the time axis. Unlike the short-term Fourier transform, where a constant window length is used for all frequencies, the wavelet transform uses smaller windows at higher frequencies and larger windows at lower frequencies. A multi-resolution wavelet analysis can be used to detect events of interest over several different time scales (Hajj et al. 1995).

Wavelets were first used to analyze seismic signals (Grossmann and Morlet 1984, Torrence and Compo 1998), but have since burgeoned in popularity as a tool for event detection and time-series analysis in various fields including other geoscientific studies (Kumar and Foufoula-Georgiou 1997). The mathematical background, concepts and implementation of wavelets for various applications are described in several texts and papers (e.g. Addison 2002, Graps 1995, Mallat 1999).

A continuous wavelet transform (CWT) based methodology for time-series analysis was outlined in Torrence and Compo (1998), and has been used in identifying the time-scales of several geoscientific processes (e.g. Wanner et al. 2001), including a study of methane ebullition in a peatland (Glaser et al. 2004). While the CWT is a good tool to determine time scales of related data, the non-orthogonal wavelets used in the CWT (e.g. Morlet and Mexican hat) were not suitable for identification of the small-step like events that occur in the cumulative bubbling data observed at UML. The CWT is also highly redundant, since wavelet coefficients are

calculated for all possible scales and times, which makes it complicated to derive relationships between time-series processes.

A discrete version of the continuous transform (DWT) using orthogonal wavelet bases and dyadic (powers of 2) time scales can be used to remove redundancies, thus de-correlating the wavelet coefficients. The DWT decomposes a signal into two parts; the first is a smoothed version obtained using a low-pass filter and the second represents signal variations as the output from a high-pass filter. Half of the coefficients so obtained are discarded through downsampling to eliminate redundancies, and the process is subsequently repeated to obtain coefficients at different time scales (i.e. frequency bands). The DWT only computes the wavelet coefficients at dyadic time scales, which simplifies the process of identifying events. A detailed comparison of the CWT and DWT, as well as cross-wavelet analyses of temporal variability of rainfall rates and runoff are presented in Labat et al. (2000).

However the classical DWT is not shift-invariant, in the sense that the magnitudes of the wavelet coefficients are dependent on the choice of the start point for analysis in a signal. A stationary wavelet transform that overcomes this deficiency has been developed, and is presented in literature under several names such as MODWT, undecimated wavelet transform or translation-invariant DWT (e.g. Nason and Silverman 1995, Percival and Walden 2000). This transform generates a redundant set of wavelet coefficients by considering all possible start points at each time scale. This representation allows for accurate identification of events, and direct comparison of wavelet coefficients with the original time-series.

This paper uses the stationary wavelet transform to identify bubbling events from the automated trap data at several dyadic time-scales ranging from 5 minutes to several days. The

results from the wavelet analyses are compared to those obtained from conventional statistical methods.

3. METHODS

3.1 Study site

The Upper Mystic Lake (UML) is a eutrophic, dimictic, kettlehole lake situated in eastern Massachusetts, north of Boston (Figure 1(a)). It has a total surface area of 0.58 km^2 , and a total volume of 6.8 million m^3 . It is 25 m deep at its lowest point, but has sharp gradations in depth near the edges. A spillway at the southern end limits the maximum water level of the lake.

The lake typically stratifies in late spring or early summer, and this effect intensifies through the summer and fall. Mixing occurs around November or December, which typically results in a uniformly oxygenated isothermal water column (Aurilio et al. 1994, Spliethoff 1995). The lake freezes during the winter, when it stratifies again. Ice melt followed by spring overturn generally occurs between mid and late March.

During the period of this study, the temperature measured near the sediments was constant at 4°C throughout the year, and the water column was anoxic below 15 m from April to December (based on the methods and results described in Chapters 4 and 5). The organic matter content of the top meter of the sediment was between 20 and 25% of dry weight. The lake is also nitrogen rich; nitrate concentrations of up to $150 \mu\text{M}$ and ammonium concentrations of up to $400 \mu\text{M}$ in the hypolimnion have been previously reported (Peterson 2005, Senn 2001).

The Upper Mystic Lake contains elevated levels of methane in the sediments and water column. The concentration of methane in the upper mixed layer is less than $1 \mu\text{M}$; however the dissolved methane increases steadily to a $100\text{-}800 \mu\text{M}$ range in the anoxic hypolimnion between

May and November (Chapters 4 and 5, Peterson 2005). Total methane concentrations in the porewater, as measured in a 1 m-long freeze core taken in September 2008 were almost uniform below 25 cm sediment depth, and at ~70% saturation for the temperature and pressure conditions at the site. Bubble patches lasting between 1 and 10 minutes have been observed at the surface on several occasions.

3.2 Data collection and preprocessing

Bubbling fluxes were measured using automated traps submerged at ~ 1 m below the water surface. The construction of the traps, calculations for converting the recorded data into bubble fluxes, and preliminary data were presented in detail in Chapter 2. Briefly, these traps were inverted funnels with an attached collection chamber in which bubbled gas rising through the water column could accumulate. A differential pressure sensor measured the height of the gas in the trap, which was converted to a gas volume using the chamber cross-section area. Gas volume data from the traps were normalized to 1 atm and 20 C. The estimated error in the measured volumes was between 3-7 ml, depending on collection chamber dimensions and gas volume.

The traps were deployed across the lake at various locations that had different water column depths (Figure 1(b)). The periods of automated data collection for all sites are listed in Table 1. The traps however had been in service since April 2008, and manual measurements of fluxes were also conducted roughly once or twice a week from April to December. A control trap was deployed at a location with no bubbling (6m site), based on ebullition flux measurements from 2007.

Total hydrostatic pressure and atmospheric pressure were measured at 10-minute resolutions using commercial sensors (Model 3001 Levelogger Gold, Solinst). Automated water

level data were obtained using an adapted version of the electronics on the bubble traps and were calibrated manually using a staff gage. The error in water level readings was approximately 0.5 cm due to sensor drift and noise caused by wave action. The standard deviation in water level measured over the entire period of measurement was 10.5 cm. The hydrostatic pressure sensor was deployed from August 5, 2008 to December 4, 2008. Hydrostatic pressures are the sum of relative water levels at the sensor site and atmospheric pressure (both measured in cm of water; 1000 cm of water \sim 1 atm).

Volume data obtained from the bubble traps were corrected for effects of sensor drift and temperature variation as outlined in Chapter 2. Volumes for short periods containing bad or missing data caused due to leaks and loose connections were linearly interpolated. Water level and atmospheric pressure data were linearly interpolated to 5-minute resolution for comparison with the trap data.

3.3 Time series analysis with statistical and Fourier methods

Cumulative volumes obtained from the traps were converted into fluxes using 24-hour time bins starting from the first data point of each signal. 24 hours was considered an appropriate time window for analysis based on manual observations of ebullition fluxes, and for purposes of comparison with previous studies. Also variations in meteorological phenomena such as atmospheric pressure predominantly occur on diurnal or semi-diurnal time frames (e.g. Baldocchi et al. 2001, Mass et al. 1991). Results from the wavelet analysis confirm that 24 hours is good window for identifying important events over the deployment period.

Trap volume data were smoothed with a 1-hour moving average filter prior to downsampling to the 24-hour time-bins. A 1-hour filter was selected, as it was the minimum length that achieved adequate noise reduction in the control trap data. Large bubbling episodes

were identified as the times when fluxes were greater than the mean plus one standard deviation of fluxes at each site.

Correlations between site fluxes were computed using the pairwise intersection of their data records. Since the traps were put out on different dates during the season, the 24-hour flux bins were calculated from the first data point of the trap that was deployed later. Correlations with hydrostatic pressure were similarly obtained from the pairwise intersection of trap fluxes with hydrostatic pressure. This effectively resulted in a common start time for analysis, since the hydrostatic pressure sensor was deployed after all the traps, except the 9m(B) site. Hydrostatic pressure data were pre-smoothed using a 1-hour moving average filter and resampled to a 24-hour period. Correlations were considered significant if the p-value was lower than 0.05. Correlations were not significantly affected by changes in binning start times.

Autocorrelations were used to determine the memory in a signal, i.e. the effect that a data point has on future values of a signal. Cross-correlations were used to determine the phase lag between time series, i.e. the delayed effect that one process has over the other (Kettunen et al. 1996). The cross correlation of signal ‘ x ’ and ‘ y ’ at lag ‘ m ’ is computed as (Mathworks , Orfanidis 1995):

$$c_{xy}(m) = \begin{cases} \sum_{n=0}^{N-|m|-1} \left(x(n+m) - \frac{1}{N} \sum_{i=0}^{N-1} x_i \right) \left(y_n^* - \frac{1}{N} \sum_{i=0}^{N-1} y_i^* \right) & m \geq 0 \\ c_{yx}^*(-m) & m < 0 \end{cases}$$

where the autocorrelation coefficients at zero lag are normalized to 1. The autocorrelation was obtained by substituting y with x in the above formula.

Spectral analysis of fluxes was done using both raw and filtered trap volumes. Raw cumulative volume data cannot be used as a signal for Fourier analysis, since the “trend” corresponding to the volume increase with time will generate a large peak at zero frequency,

which dominates other peaks. Analysis was done for fluxes computed with several time-bins (5 min to 24 hours for unfiltered data; 1 to 24 hours for filtered data), since the periodicity with which bubbling occurred was not known *a priori*.

Periodograms were generated by the Welch method using different windows (rectangular, Hamming and Hann) with varying degrees of overlap. It is preferable to use the short-term Fourier transform with overlapping windows to generate an averaged periodogram in order to reduce the noise in the spectrum (Stearns 2002). Window sizes were selected according to the length of each signal; different sizes were chosen to optimize the visual trade-off between frequency peak resolution and peak detection. 95% confidence intervals were used to identify significant peaks.

3.4 Wavelet analysis

The wavelet analysis in this paper is based on the stationary wavelet transform, and uses the WMTSA toolkit developed at the University of Washington (<http://www.atmos.washington.edu/~wmtsa/>). The software implements the MODWT, which is described in detail in Percival and Walden 2000, and has been used in previous geoscientific analyses (e.g. Kallache et al. 2005, Percival 2008, Whitcher et al. 2000).

The MODWT generates two sets of decompositions. The first yields a set of *wavelet* and *scaling* coefficients, which are effectively the coefficients obtained from a classical DWT, but are computed for all data points in a signal without any downsampling. This redundant set of coefficients can however be used to calculate a scale-based variance (analogous to the power spectrum density). The sum of the variances equals the total energy in the time-series; thus the scales with the highest variance can be identified as the dominant time-scales in a process.

The second decomposition is a multi-resolution analysis (MRA), which generates *details* and *smooths* at different time-scales (i.e. frequency bands). These are calculated by averaging the wavelet and scaling coefficients for all possible start point shifts at each time scale, and are effectively computed by performing an inverse transform on the MODWT. Thus they represent an additive decomposition of the signal and can be summed up to perfectly reconstruct the original signal.

The multi-resolution analysis is a useful tool for event identification. The wavelet details and smooths correspond to outputs from a zero-phase high-pass and low-pass filter, and can thus be used to precisely identify events of interest across time scales. Events can be detected by analyzing the details, which are properly aligned with features in the original time-series, and represent the variations caused by successively smoothing the signal.

In this paper, “events of interest” are defined as periods where there is a high likelihood of bubbling. Events are identified for each time-scale in the MRA and include parts of the signal that meet a scale-dependent selection criterion, such as a threshold. An episode of bubbling is then defined as a common period where events occur on multiple time-scales (Figure 2). These definitions are based on the notion that an episode of bubbling can last for several hours to days (as observed from the manual measurements), but in reality, will likely comprise several bubble bursts of shorter durations. Thus, bubbling episodes that are important from a long-term seasonal perspective can be identified from events that occur at time-scales on the order of 1-2 days, while the evolution of these episodes can be subsequently studied by examining events from the minute to hour time-scales. Events identified from the bubble trap data at the different time-scales can then be compared directly with the hydrostatic pressure signal, by matching their horizontal time-axes.

The stationary wavelet transform was done using the Haar wavelet for 10 dyadic time scales. The boxcar filter (i.e. Haar wavelet) was chosen since the predominant step edges in cumulative gas volume data from the traps indicated that the signal could be approximated as a piecewise constant function. The details at the 10th scale correspond to a physical time period of ~2 days (42.5 hours), beyond which the scale is effectively the same as the manual sampling interval. Since the transform is done using the Haar wavelet, the wavelet coefficients obtained from the MODWT are effectively proportional to fluxes computed at each signal data point using time bins corresponding to the scale of analysis.

The transform was directly performed on the cumulative volumes without prior filtering, which is not required for wavelet analysis. Signals were padded at the beginning with zeroes corresponding to the length of the filter at each scale to handle initial boundary effects. Signals were also reflected at the end, and the MODWT coefficients were subsequently truncated to the original signal length.

Events of interest were identified as the times when the absolute modulus of the detail coefficients exceeded a scale-dependent de-noising threshold. The threshold used in this analysis is based on the Stein's Unbiased Risk Estimate (SURE), and is a conservative estimate that is calculated by minimizing the “risk”, i.e. the mean squared error associated with the selection of thresholds (Coifman and Donoho 1995, Donoho et al. 1995). The thresholding assumes that oscillations in the recorded data due to wind and wave effects, as well as small random bubble bursts can be represented as Gaussian white noise at each scale. Two other common de-noising thresholds, i.e. the minimax and universal thresholds (Donoho 1995, Jansen 2001) were found to be too selective and missed significant events, as identified by a visual inspection of the data.

The wavelet power spectrum was used to detect the dominant time scales of variability in ebullition. Wavelet variance was calculated for the sum of all details obtained from a 12 level MODWT decomposition (corresponding to a 170 hour scale). Cumulative volumes cannot be used as a signal for wavelet variance analysis, since the “trend” corresponding to the volume increase with time will cause the larger time scales to have higher energies.

4. RESULTS

4.1 Statistical properties of site fluxes

A considerable amount of spatial and temporal variation in ebullition was observed in the UML (Figure 3). Both the average and standard deviations of daily fluxes varied significantly from site to site (Table 1). About 30-70% of ebullition for the entire deployment period was released during bubbling episodes that occurred about 5-10% of the time at the different sites (Figure 4, Table 1). Small negative fluxes, which appear due to the 3-7 ml error in recorded volumes, were ignored for statistical calculations.

4.2 Correlation analysis

Peak 24-hour fluxes at different sites overlap to an extent, visually indicating that there exist time periods on the scale of day where synchronized bubbling episodes occur throughout the lake (Figure 5). The pair-wise correlation coefficients of the logarithms of site fluxes were significantly related ($p \leq 0.05$) for 17 of the 20 trap combinations (Figure 6). A log scale was used because the daily flux values had a large range (0 to $\sim 700 \text{ ml.m}^{-2}.\text{d}^{-1}$). However, the low correlation coefficients ($R^2 = 0.1$ to 0.5) indicate that the pair-wise trap relationships were not linear.

Significant negative correlations were observed between daily trap fluxes and hydrostatic pressure (Figure 7), though the low R values indicate that the relationships were not linear, or that other factors might possibly influence bubbling. In fact, there appears to be a site dependent hydrostatic pressure threshold below which most of the bubbling occurs (\sim 65 to 85 cm of water at the site of the pressure sensor); this concept is examined further in the wavelet analysis below. The 19m site was the only exception where no significant correlation was observed; however this location had very low fluxes for most of the season. No significant relationship was found between the fluxes and 24-hour gradients of hydrostatic pressure, except at the 9m(A) ($R=-0.25$) and 13m ($R=-0.27$) sites.

4.3 Auto and cross correlations

Autocorrelations were first computed using 24-hour fluxes over 10 days. No significant correlations were found for periods longer than a day at all sites. The analysis was then performed using 2, 6 and 12-hour unfiltered fluxes over 48 hours to study the immediate effects of an ebullition event (Figure 8). Autocorrelations were also performed on the control trap data; this analysis showed that correlations for fluxes computed using time bins smaller than 2 hours were affected by wind noise.

All trap autocorrelations decayed rapidly, except at the 13 m site, with most significant coefficients occurring within 30 hours. These results indicate that the highest probability of gas release following a bubble burst occurs within the first day.

The autocorrelation of hydrostatic pressure slowly decayed to zero over approximately 100 hours; atmospheric pressure and water level signals were similarly autoregressive indicating that the effects of their variations were persistent for about four days (Figure 9). Cross correlations for 24-hour fluxes against hydrostatic pressure peaked at zero lag for all sites except

the control and 19m (not shown); however it is difficult to distinguish if fluxes were affected by changes in hydrostatic pressure within the last 24 hours, or a few hours earlier because of the autoregressive nature of the hydrostatic pressure signal.

4.4 Power spectrum analysis

No significant peaks could be distinguished from the noise in the power spectra of unfiltered fluxes; this is because of the effects of wind on the traps, which occur at relatively high frequencies (corresponding to 1-2 hour time scales or less). Significant peaks were also not present in the spectra of filtered fluxes for all window variations. The results indicate that bubbling at the UML is not periodic at any particular frequency.

4.5 Wavelet analysis

The wavelet multi-resolution analysis (MRA) illustrates that bubbling events occur at several different time scales (Figure 10). The term ‘time scale’ or ‘scale’ refers to the different frequency bands in the wavelet analysis. The relative magnitudes of the wavelet detail coefficients at each scale are indicative of the extent of changes in the signal at that time-scale. The alignment of the details in the MRA enables us to track how bubbling episodes develop.

Some bubbling episodes that comprise one large event on a daily (21.3 hour) or two day (42.6 hour) time scale are found to occur in bursts on the minute to hour scales (refer Figure 10, MRA for 25m trap for following examples). For example, 65% of the gas bubbled between Jul 16th-21st (Event 1 in Figure 10), was released in two short bursts from 12:50-12:55 am on Jul 19th and 9:55-10:15 am on Jul 20th. Another example of such a sharp burst occurs from 6:10-6:15pm on Oct 16th, when 33% of the gas collected between Oct 15th-23rd was bubbled (Event 2).

The MRA can be used to identify if bubble bursts on the minute to hour time scales will eventually evolve into a bubbling episode (e.g. Event 3 from Aug 30th - Sep 5th). The progressive smoothing in the wavelet transform ensures that noise due to wind (e.g. Event 4, Sep 18th-29th) or spurious “events” (e.g. Event 5 in Figure 11, a spike on Jul 23rd at the 13m site) do not propagate up to the 1-2 day time scales. This avoids the need to preprocess the signal using filters that can potentially eliminate events of interest on smaller scales.

The MRA can help distinguish between episodes that involve gradual gas release versus those that comprise bursts where a significant volume of gas is released in the matter of a few minutes. A comparison of details in Figures 10 and 11 show that bubbling occurred in a more temporally diffused manner at the 13m site than at the 25m site. For example, the gradual gas release from Nov. 14th-15th at the 13m site turned out to be a significant episode for the season (Event 6, Figure 11). Such diffused episodes can be recognized as events at higher time scales (2.7 hours and higher in this example), even if they are not identified as events at the 5-10 minute scales.

The MRA of the remaining traps are included in the Appendix. An examination of the wavelet details of all traps reveal that most of the big bubbling episodes involved at least one or two significant bursts at the 5 (0.1 hour)-10 minute scale. It is also evident that time-scales of 10.6 to 21.3 hours are appropriate for identifying events of interest for the entire deployment period. Larger time-scales such as 42.5 hours, show almost the entire signal to be significant in some cases (e.g. 9m(A) and 9m(B)). Events at time-scales less than 10.6 hours mostly comprise sporadic bursts that actually belong to the same episode.

4.6 Comparison of wavelet details with hydrostatic pressure

Events identified at the 10.6 hour and 1.3 hour scales from the MRA were then compared against the hydrostatic pressure signal (Figures 12 and 13). The onset and cease points of bubbling episodes were calculated using the negative (for onset) or positive (cease point) wavelet details that were separated by a period equal to or greater than twice the length of the corresponding time-scale (i.e. 21.2 hours or 2.6 hours).

About 70% of the total gas collected by the 9m(A) automated trap occurred during 7% of the deployment period, while 20% of the total gas measured by the 25m trap was bubbled in 1% of the time (Table 2). Most of the bubbling was triggered when the hydrostatic pressure dropped below a site-dependent threshold and ceased when the hydrostatic rose above the threshold (Figures 12 and 13, Table 3). There were instances when a drop in hydrostatic pressure had a delayed response in bubbling (e.g. Event 7 in Figure 12(a), Oct 21st-22nd and Nov 9th at the 9m(A) site), or when ebullition continued despite rising hydrostatic pressure following a bubbling episode (Event 8 in Figure 12(b), Sep 5th-6th and Oct 25th-29th at the 25m site). A few isolated instances of bubbling were observed at high hydrostatic pressures (e.g. Event 9 in Figure 12(b), Aug 21st at the 25m site). The plots of 10.6 and 1.3 hour details against hydrostatic pressure for the remaining traps are included in the Appendix.

4.7 Wavelet variance

The wavelet variance for was computed for time scales ranging from 5 minutes to 28 days; all sites exhibited similar trends, where most of the energy was concentrated at the higher scales (e.g. Figure 14). This indicates that no particular time scale for variability can be identified for ebullition at the Upper Mystic Lake for the deployment period.

5. DISCUSSION

5.1 Temporal variability of bubbling episodes

The statistical and wavelet analysis show that sporadic bubbling episodes, which occurred less than 10% of the time, were the dominant periods of methane release in the Upper Mystic Lake. About 50% of the total gas bubbled from July to November, the peak period for ebullition in 2008 (as observed from manual measurements), was emitted during these episodes. These episodes also did not occur with any periodicity, as is indicated by the results (or lack thereof) from the Fourier and wavelet variance analyses. This is different from marine systems where ebullition fluxes contained diurnal components, related to tidal variations (Boles et al. 2001).

Bubbling has been previously observed to occur at time scales ranging from minutes to hours during episodes (e.g. Greinert 2008, Leifer et al. 2004). The wavelet analysis shows similar times scales for ebullition at the Upper Mystic Lake, where bubbling episodes could comprise (less than) 5-minute bubble bursts, or at the other extreme, more temporally diffused release that took place over hours. However, no characteristic duration of ebullition could be identified; episode lengths could range anywhere between a few hours and several days. The temporal variability observed in the automated trap data illustrates the need for continuous, long-term monitoring in order to adequately characterize bubbling in aquatic ecosystems.

5.2 Ebullition control mechanisms

Synchronous bubbling episodes were triggered across the Upper Mystic Lake when the hydrostatic pressures fell below a site-dependent threshold. The wavelet analyses at the 1.3 hour scale (Figures 12(b) and 13(b), Table 2) reveal that the largest bubble bursts mostly occurred at times when the hydrostatic pressure was decreasing, or was at its nadir. However, there were

times when ebullition occurred while the hydrostatic pressure was rising as indicated by the negative pressure changes in Table 2; these instances usually followed a drop in pressure and indicate the presence of delayed bubbling. The 21.3 hour wavelet analyses indicate that once an event was triggered, subsequent bubbling could continue during hydrostatic pressure rise until the point when it reached the onset pressure (Table 3). Large increases in hydrostatic pressure caused bubbling to cease immediately.

The thresholds at which bubbling started and stopped were probably related to the sediment gas storage. In the 1.3 hour analysis, cessation pressures were typically lower than the onset pressures (Table 2), which indicates that some of the gas in the sediment reservoir had been exhausted. However the difference between onset and cessation pressures were small (1-10 cm); such a pressure drop would only result in an ~0.1-0.5% change in sediment storage, assuming that the gas concentrations in the porewater were at saturation (Table 2). The thresholds at each site were not constant for the season, which could possibly be a result of changes in sediment storage or structure with time.

Fluxes of gas released during an episode were not correlated with the magnitude of the corresponding hydrostatic pressure drops (not shown, computed from Table 2). It thus appears as though that the amount of gas released at the UML, once bubbling was initiated, was dependent on the sediment gas storage. If this hypothesis were true, it might also explain the large scatter observed in the pairwise trap correlations, which were a result of the inconsistent variations in site fluxes through the season. The relative volumes of gas released during an episode should have been similar for the different sites, if site fluxes had been related to the magnitude of hydrostatic pressure changes. There are also several instances when little or no ebullition was observed even though hydrostatic pressure was below the site threshold. These could have been

the result of insufficient sediment gas (e.g. Event 10 in Figure 12(a), Sep 14th at 9m(A), which followed a bubbling episode). As a caveat, it is possible that the traps might have failed to capture some of the bubbles, due to movement around their watch circles, at some of the times of low hydrostatic pressure. Another possibility is that bubble release from the sediments was triggered; but that some of the bubbles may not have reached the surface waters (as shown in McGinnis et al. 2006).

A mechanistic explanation for the above observations is that bubbles escape through fractures or “bubble tubes” in the sediment (Boudreau et al. 2005, Martens and Klump 1980). When the hydrostatic pressure drops, large bubbles can break out creating preferential flow channels in the sediments. Once these fractures are formed, smaller bubbles that would otherwise have not been able to escape can now follow in the train of the larger bubbles. This would explain why the volume of gas released during an episode is not correlated with the hydrostatic pressure drop. Bubbles can also continue to escape through these fractures even when the hydrostatic pressure rises. In addition to the wavelet analysis, this theory is also supported by the flux autocorrelations that indicate that bubbling is most likely to occur within the first 30 hours of the onset of an ebullition event.

The contributions of variations in atmospheric pressure and water level to the magnitude of total hydrostatic pressure at the UML are similar; the standard deviations of both variables were approximately 10 cm of water through the season (Figure 15). Ebullition episodes were usually triggered by drops in atmospheric pressure that occurred when the lake water level was low.

5.3 Spatial variation in bubbling fluxes

The conclusions that can be drawn about spatial variability, based on a small set of traps, are limited. It is apparent from the range of means and standard deviations of daily bubbling fluxes that the spatial variation in gas collected at different traps is large. Some locations bubble in a more temporally diffused manner (e.g. 13m, 19m) than others that release a lot of gas as short bursts (e.g. 9m(A), 9m(B) and 22m). Even very close traps situated less than 15-30 m apart (e.g. 9m(A) and 9m(B)) are considerably different, both in terms of the magnitude and timing of bubbling episodes. However, the location where the 9m traps were situated bubbled much more than the lake average both in 2007 and 2008.

There was no strong correlation between site depth and gas fluxes; however the onset pressures of bubbling episodes were slightly higher at shallow sites than at deep sites (Table 3), indicating that shallow locations might start to bubble earlier when hydrostatic pressures drop. The 19m site was the only location that did not exhibit significant correlations with hydrostatic pressure; however bubbling fluxes at this site were very low during the period of automated measurement.

5.4 Selection of sampling interval

In any sensor based measurement scheme, the choice of an appropriate sampling interval is critical. Under sampling can lead to important events being missed, whereas over sampling leads to large volumes of data that are difficult to store and process.

At the UML, we chose intervals of 5 to 10 minutes, as a trade-off between the 1-10 minute time scales at which bubbling events were thought to occur (Walter et al. 2006, personal observations) and storage limitations of the commercial data logger (HOBO H8, Onset Systems). This lead to a data record of approximately 30000 samples over the entire deployment period for

each site. However for post-processing, the effects of the wind signal on the trap data had to be eliminated by smoothing the signal using a moving average filter of about 12 sample points, which consequently meant that the minimum time scale for computing fluxes was an hour, thus shrinking the data set to ~2500-3000 samples.

Furthermore, unfiltered data used in the wavelet analysis shows that significant bubbling episodes can occur over intervals of 5 minutes or less. Thus in hindsight, a 5 to 10 minute sampling interval was an appropriate choice for automated trap-based measurement of ebullition fluxes.

6. TABLES

Table 1 – Summary of bubbling at different sites

Table 2 – Bubbling onset and cessation points for 9m(A) and 25m traps at 1.3 hour resolution

Table 3 – Hydrostatic pressure thresholds for different sites at 11.6 hour resolution

Table 1 Summary of bubbling at the different sites where the automated traps were deployed.

Trap	Period of data collection (2008)	Data length (hours)	Average daily flux ($\text{ml.m}^{-2}.\text{d}^{-1}$)	Standard deviation ($\text{ml.m}^{-2}.\text{d}^{-1}$)	% Time bubbling episodes ($\mu+1\sigma$)	% Gas bubbled during episodes
9m(A)	5 Aug - 1 Dec	2832	44	107	9	66
9m (B)	9 Oct – 20 Nov	1013	80	96	19	58
13m	12 Jun – 29 Oct, 14 Nov – 20 Nov	3482	24	38	9	47
19m	2-Jul – 25 Aug, 13 Sep – 8 Oct	1881	9	17	12	63
22m	10 Jul – 1 Dec	3448	20	38	10	56
23m	30 May – 12 Jun, 10 Jul - 1 Dec	3758	19	31	10	52
25m	16 Jul – 1 Dec	3313	28	50	11	58
6m (Control)	5 Aug – 3 Sep	693	1	3		

Table 2(a) Events identified at the 1.3 hour scale at the 9m(A) site (see Figure 12(b)). The total volume of gas collected by the 9m(A) automated trap over the deployment period was 997 ml; thus ~70% of the total gas released occurred in ~7% of the deployment time. The percent storage calculation assumes that the porewater is saturated with gas and is the difference between the onset and cessation hydrostatic pressures divided by the sediment saturation pressure (2 atm). It is not calculated for times when gas release occurs at the time of hydrostatic pressure rises.

Event onset time	Event cessation time	Event length (hours)	Onset hydrostatic pressure (cm of water)	Cessation pressure (cm of water)	Hydrostatic pressure change (atm)	Volume gas released during event (ml)	Percent of sediment storage
9/2/08 4:20 AM	9/2/08 7:34 AM	3.2	61.8	62.6	-7.7E-04	13.20	
9/12/08 4:25 PM	9/12/08 11:15 PM	6.8	71	68.5	2.4E-03	35.20	0.12
9/20/08 8:44 PM	9/21/08 3:00 PM	18.3	69.5	67.55	1.9E-03	39.70	0.09
9/24/08 10:20 AM	9/24/08 1:00 PM	2.7	76.65	76.45	1.9E-04	7.20	0.01
9/29/08 3:49 PM	9/29/08 7:45 PM	3.9	80.35	79.5	8.2E-04	27.60	0.04
9/30/08 3:04 AM	9/30/08 7:00 AM	3.9	76.8	76.2	5.8E-04	30.00	0.03
9/30/08 12:49 PM	9/30/08 7:25 PM	6.6	74.65	70.6	3.9E-03	116.30	0.20
10/1/08 10:14 AM	10/1/08 1:25 PM	3.2	63.2	63.2	0.0E+00	14.60	0.00
10/1/08 3:24 PM	10/1/08 7:14 PM	3.8	62.6	63.2	-5.8E-04	32.69	
10/8/08 6:09 PM	10/8/08 9:09 PM	3.0	67.6	66.8	8.2E-04	11.70	0.04
10/9/08 5:05 AM	10/9/08 11:44 AM	6.7	61.7	61.2	4.8E-04	28.80	0.02
10/13/08 9:15 PM	10/16/08 1:14 AM	52.0	75.1	63.1	1.2E-02	24.10	0.58
10/25/08 6:35 PM	10/25/08 11:15 PM	4.7	60.4	55.1	5.1E-03	110.25	0.26
10/26/08 2:39 AM	10/28/08 11:55 PM	69.3	52.35	51.9	4.4E-04	46.35	0.02
11/9/08 4:30 PM	11/9/08 7:05 PM	2.6	64.25	66.3	-2.0E-03	8.00	
11/14/08 12:15 PM	11/14/08 5:50 PM	5.6	67.2	60.5	6.5E-03	28.70	0.33
11/15/08 10:59 AM	11/15/08 6:45 PM	7.8	55.55	49.8	5.6E-03	99.20	0.28
11/16/08 6:40 AM	11/16/08 10:39 AM	4.0	42.45	45.0	-2.4E-03	19.90	
TOTAL		208.0				693.5	

Table 2(b) Events identified at the 1.3 hour scale at the 25m site (see Figure 13(b)). The total volume of gas collected by the 25m automated trap over the deployment period was 755 ml; thus ~22% of the total gas released occurred in ~1% of the total deployment period. The sediment saturation pressure was assumed to be 3.5 atm for the percent storage calculation.

Event onset time	Event cessation time	Event length (hours)	Onset hydrostatic pressure (cm of water)	Cessation pressure (cm of water)	Hydrostatic pressure change (atm)	Volume gas released during event (ml)	Percent of sediment storage
8/25/08 4:20	8/25/08 7:05 AM	2.8	64	63.4	5.8E-04	17.50	0.02
8/30/08 17:35	8/31/08 1:20 AM	7.7	61.2	62.3	-1.1E-03	36.60	
9/4/08 1:59	9/4/08 4:14 AM	2.3	55.6	55.8	-1.9E-04	11.10	
9/5/08 22:30	9/6/08 12:54 AM	2.4	74.3	73.8	4.8E-04	10.20	0.01
10/2/08 4:14	10/2/08 6:24 AM	2.2	58.7	57.9	7.7E-04	13.00	0.02
10/16/08 13:54	10/16/08 7:45 PM	5.8	55.3	58.5	-3.1E-03	42.90	
10/21/08 11:50	10/21/08 1:59 PM	2.2	54.8	52.7	2.0E-03	12.80	0.06
10/21/08 20:50	10/21/08 11:19 PM	2.5	53.25	53.95	-6.8E-04	11.80	
10/29/08 9:54	10/29/08 12:35 PM	2.7	62.7	63.5	-7.7E-04	12.65	
TOTAL		30.5				168.6	

82

Table 3 Relative hydrostatic pressure (cm of water at sensor site) mean and standard deviations at different sites during the onset and cessation of bubbling events at the 11.6 hour scale. Mean hydrostatic pressure for the entire deployment period = 73.8 cm and standard deviation= 10.2 cm.

Trap Name	Mean hydrostatic pressure at onset of episodes	Standard deviation of onset pressures	Mean hydrostatic pressure when bubbling ceases	Standard deviation of cessation pressures
9m(A)	72	7.2	66	4.6
13m	69	6.7	63	9.4
22m	66	10	69	9.1
23m	61	5.3	62	3.8
25m	67	7.5	67	7.3

7. FIGURES

Figure 1 – UML bathymetry and trap deployment

Figure 2 – Bubbling episodes identified by wavelet multi-resolution analysis (MRA)

Figure 3 – Automated trap data from June to November 2008

Figure 4 – Histograms of daily trap fluxes

Figure 5 – Plot of daily trap fluxes showing synchronized ebullition

Figure 6 – Pairwise correlation plots between fluxes at different sites

Figure 7 – Correlation plots of ebullition fluxes with hydrostatic pressure

Figure 8 – Autocorrelations of site fluxes computed using 2, 6 and 12 hour time bins.

Figure 9 – Autocorrelations of hydrostatic pressure, water level and atmospheric pressure

Figure 10 – MRA of the 25m site data using the Haar wavelet at time scales ranging from 5 minutes to 42.5 hours

Figure 11 – MRA of the 13m site data using the Haar wavelet at time scales ranging from 5 minutes to 42.5 hours

Figure 12 – Comparison of wavelet details at scales 11.6 and 1.3 hours with hydrostatic pressure at the 9m(A) site

Figure 13 – Comparison of wavelet details at scales 11.6 and 1.3 hours with hydrostatic pressure at the 25m site

Figure 14 – Wavelet variance of the 25m site data

Figure 15 – Water level, atmospheric pressure and hydrostatic pressure at the UML

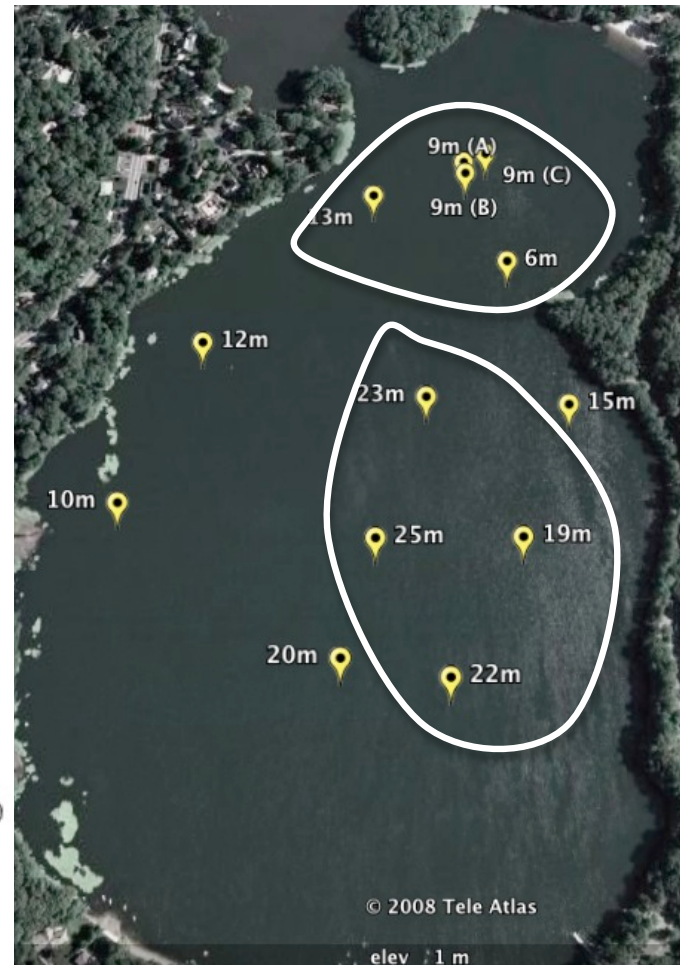
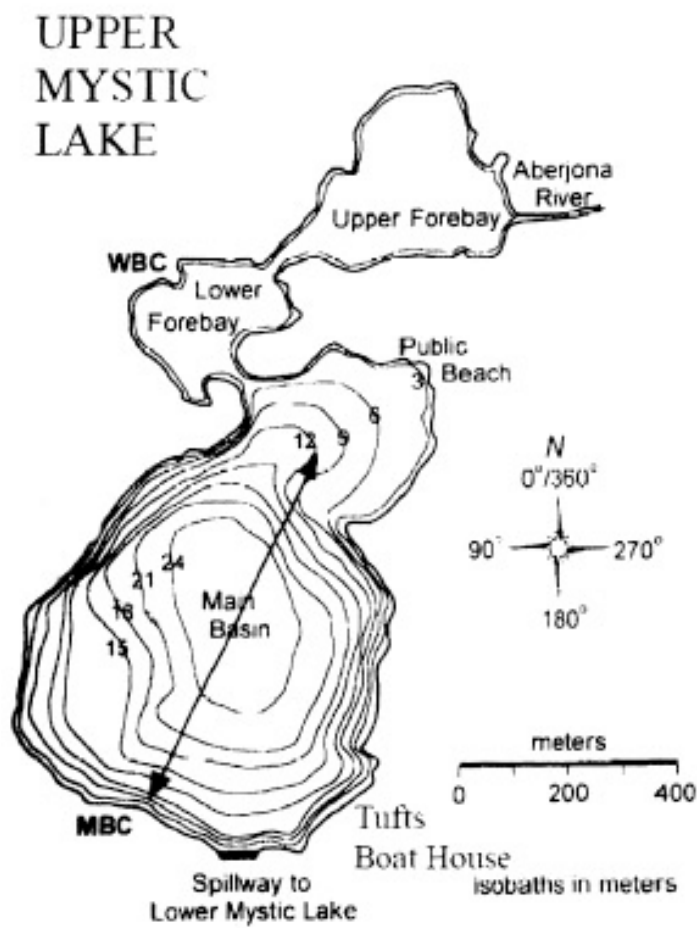


Figure 1 Upper Mystic Lake (a) bathymetry (b) location of all traps. The traps within the white circles were automated. Trap names reflect the approximate depth at their location of deployment. The 6m trap was used as a control, since it was located at a site which did not have much bubbling (based on the 2007 manual data).

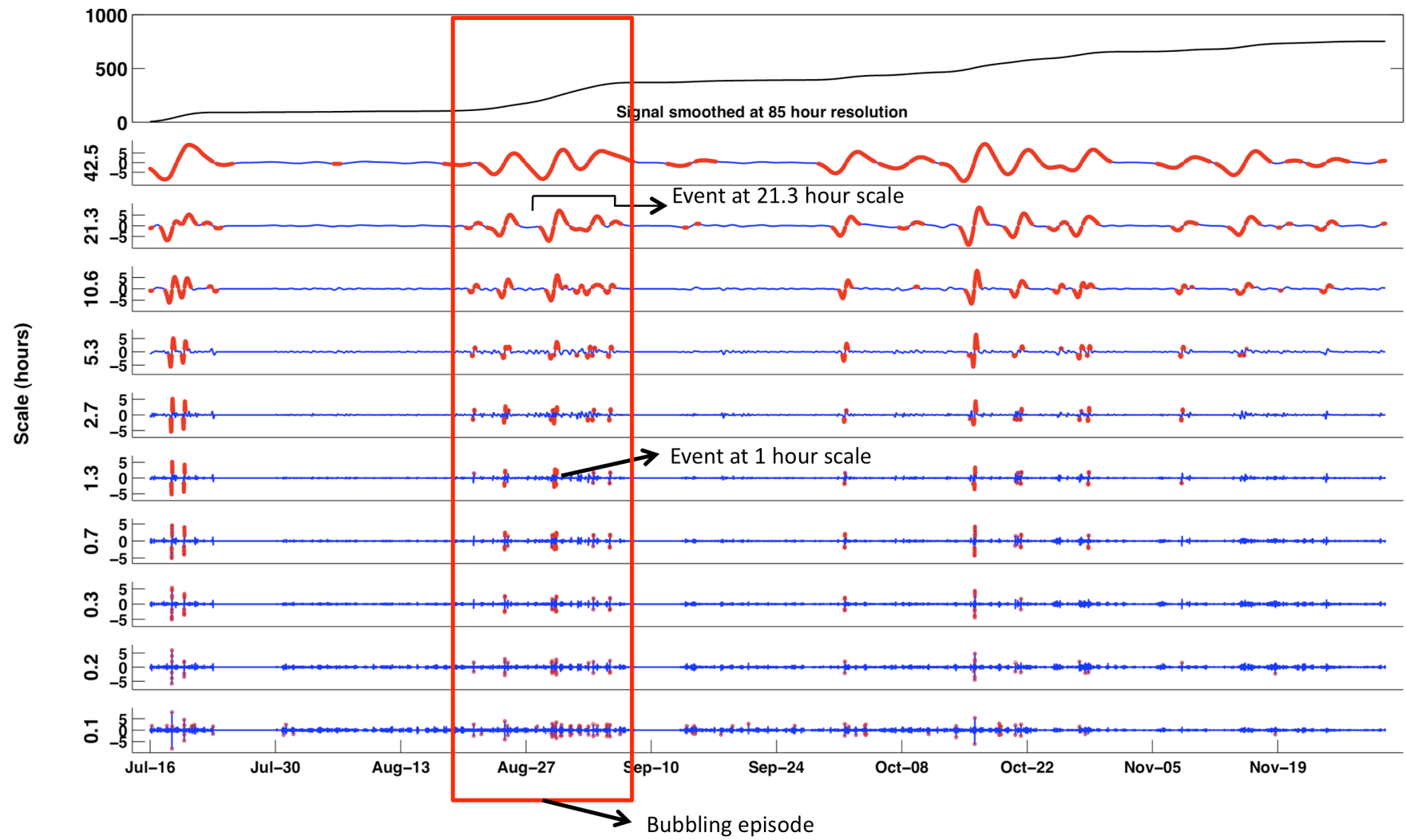


Figure 2 Wavelet multi-resolution analysis of bubbling data from an automated trap for 10 time-scales (5 minutes to 42.5 hours). Events can be identified for each time scale using a selection criterion (e.g. thresholding). Bubbling episodes comprise events that propagate across several time-scales.

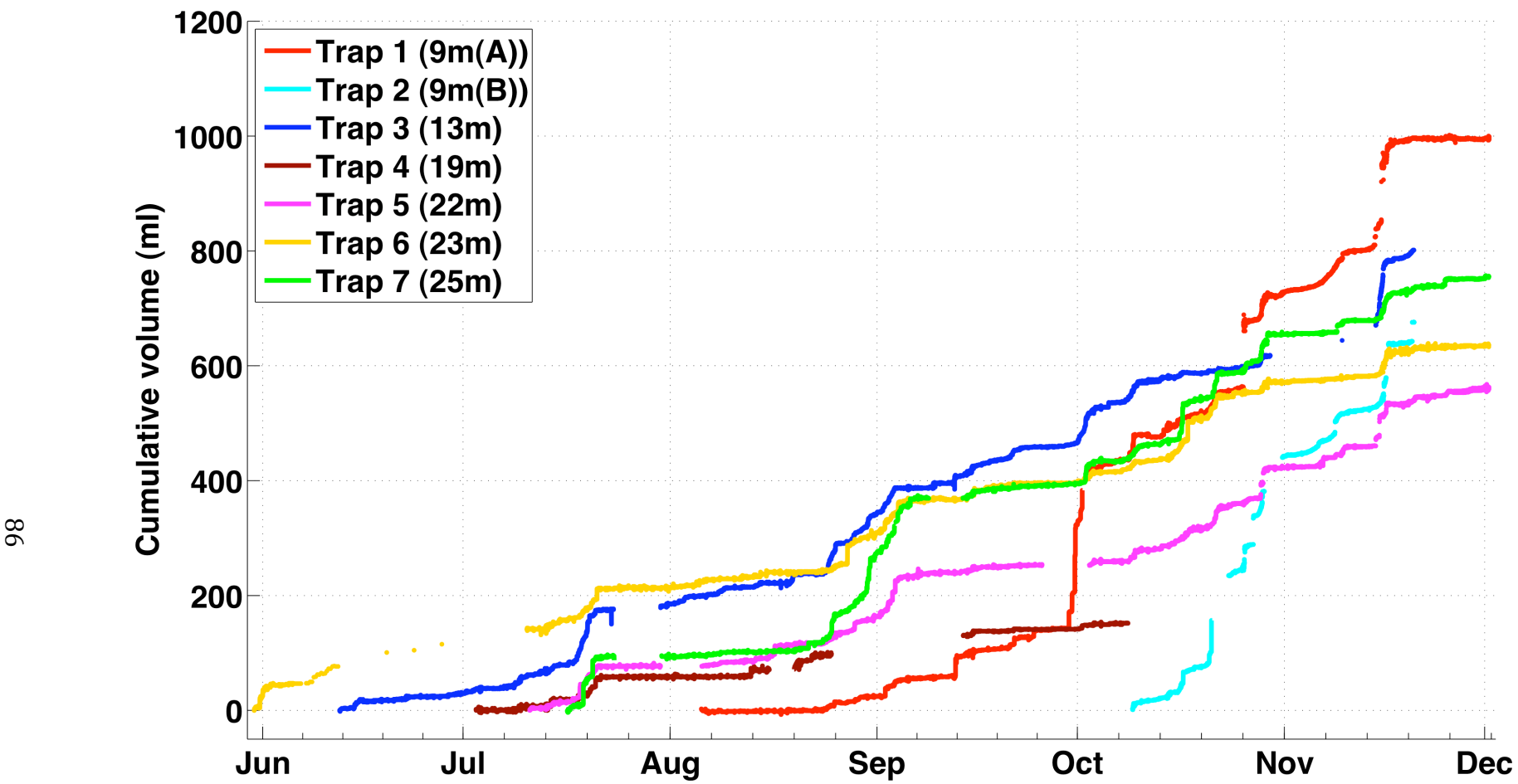


Figure 3 Cumulative gas volumes measured in automated traps between June and December 2008. Data was measured at 5-10 minute resolutions. “0” indicates the start of gas measurement using automated traps, and not cumulative flux at a location for the season.

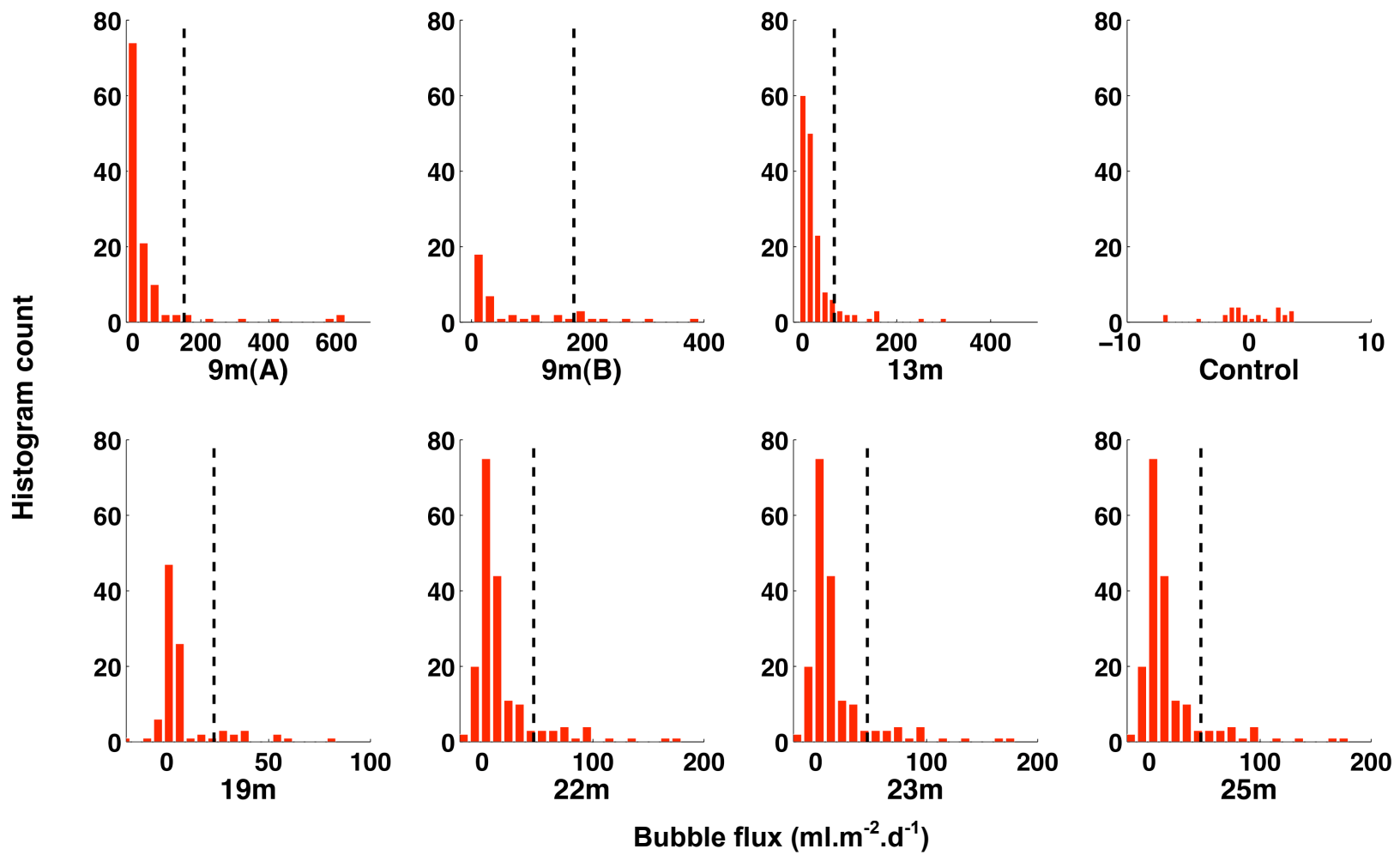


Figure 4 Histogram of trap fluxes computed using 24-hour time bins. The dashed black line indicates the threshold for large bubbling episodes (mean plus one standard deviation)

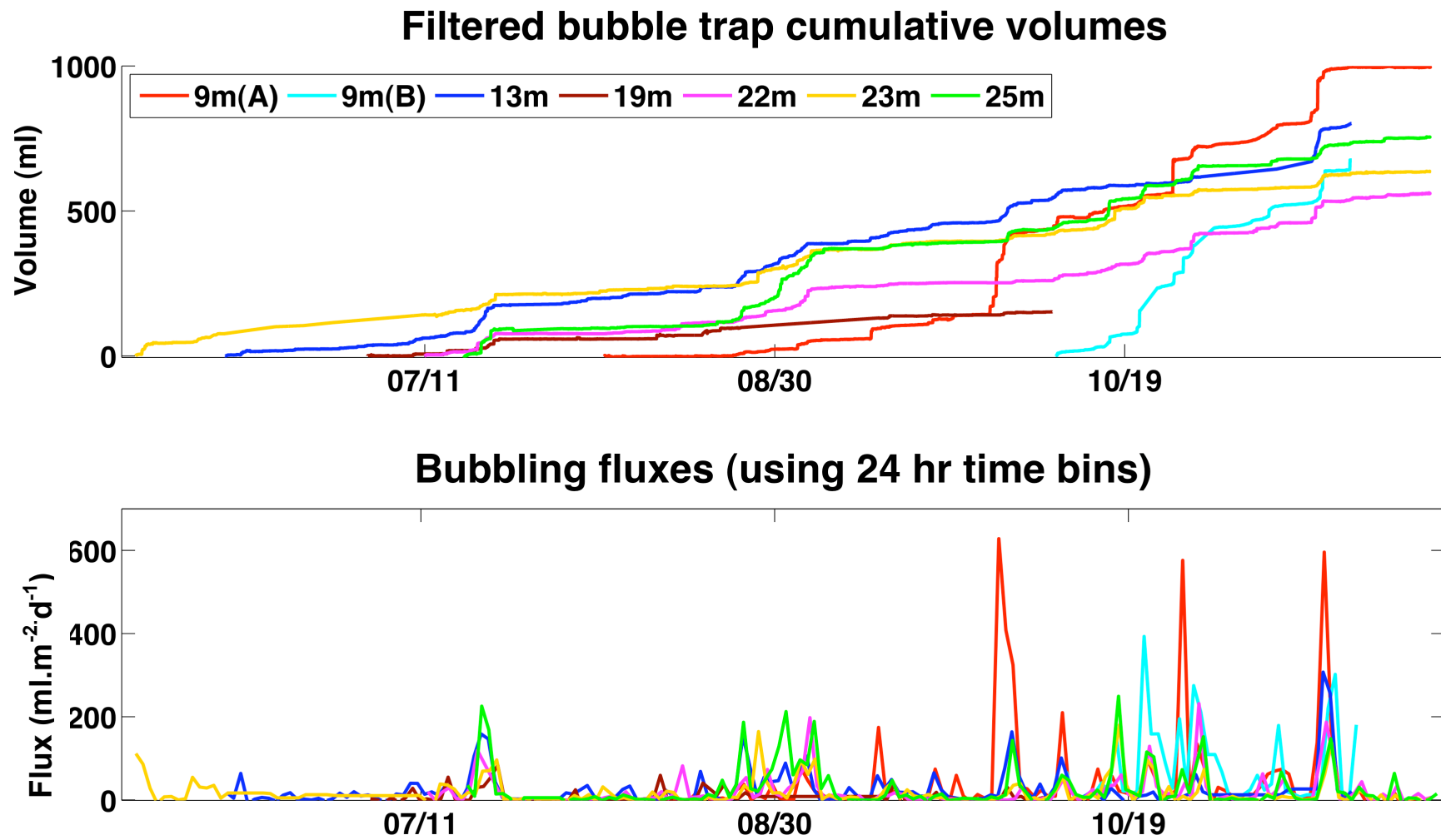


Figure 5 Daily fluxes for all traps. Periods of overlapping fluxes indicate synchronized bubbling throughout the lake.

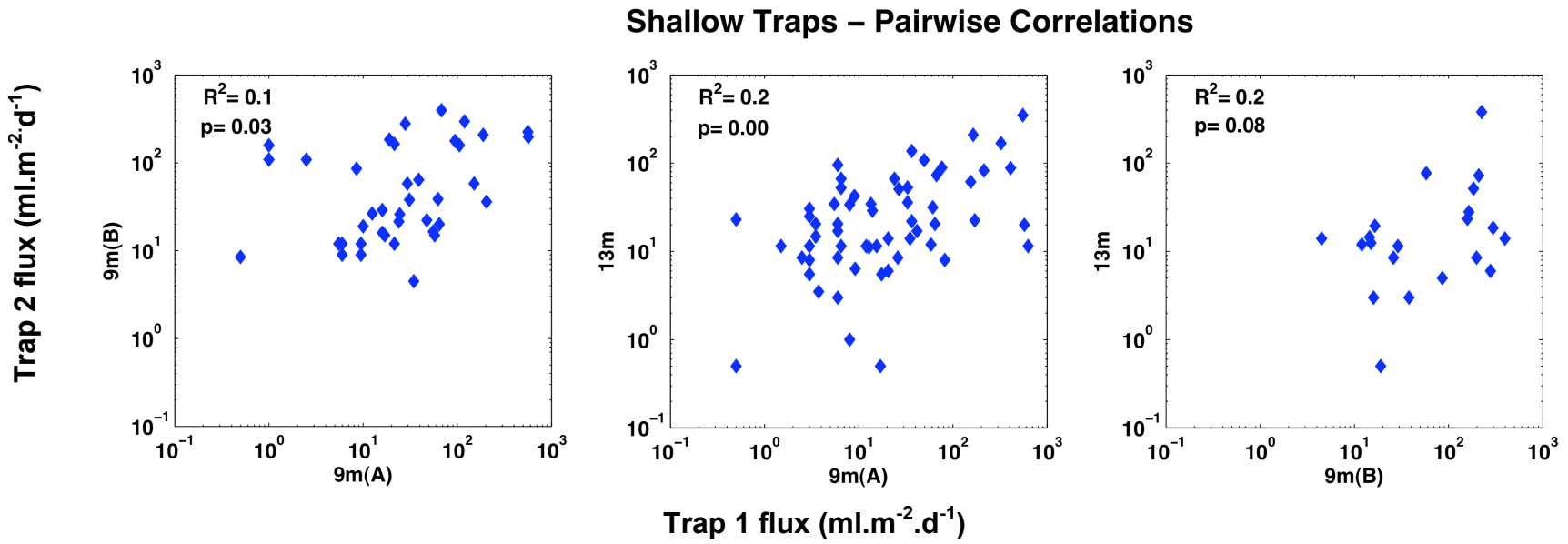


Figure 6 (a) Correlation plots between \log_{10} daily fluxes ($\text{ml} \cdot \text{m}^{-2} \cdot \text{d}^{-1}$) for shallow sites (9m(A), 9m(B) and 13m). R^2 and p values are shown for log-log fits; similar correlation coefficient and significance level values were obtained for linear fits.

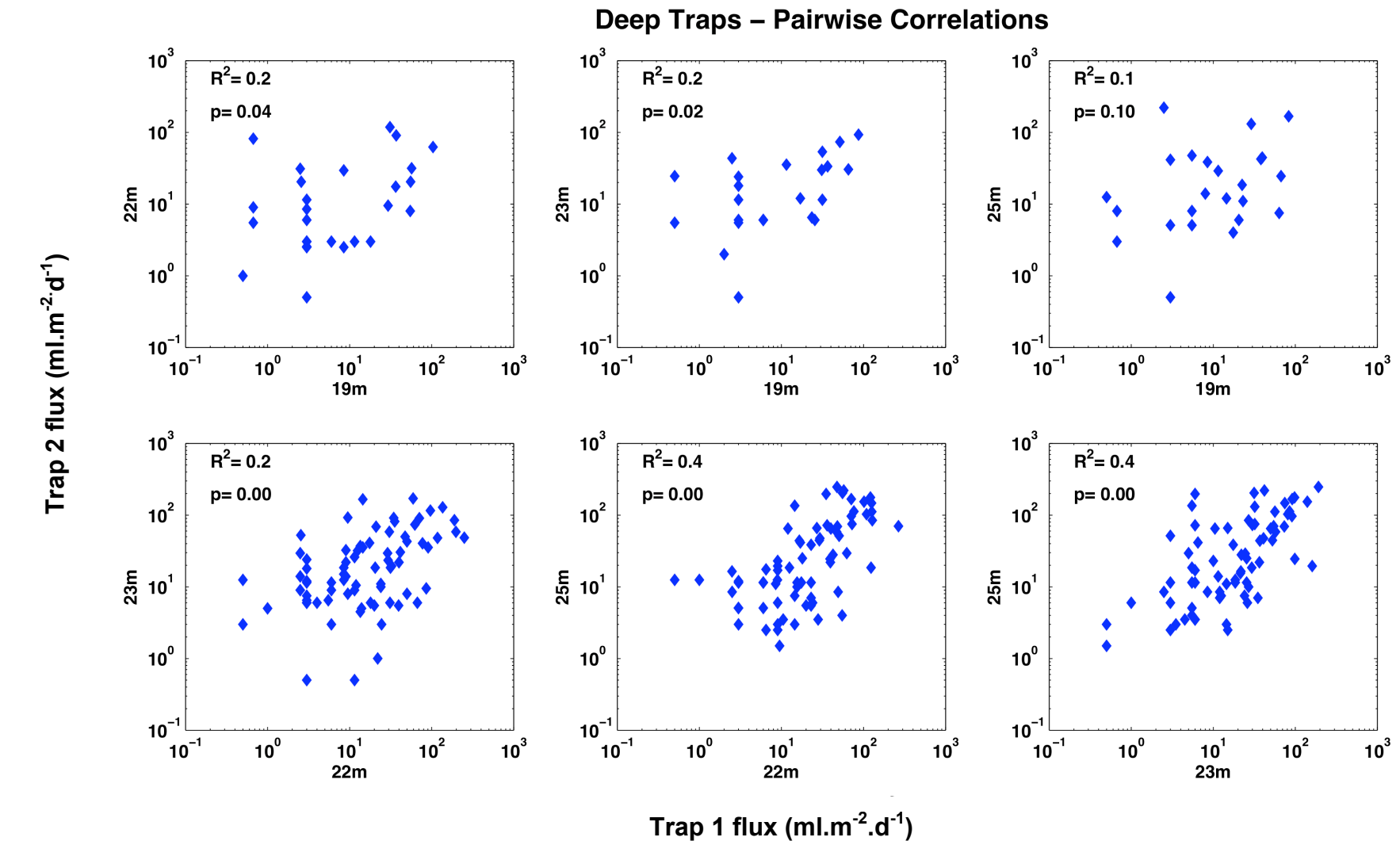


Figure 6 (b) Correlation plots between \log_{10} daily fluxes ($\text{ml.m}^{-2}.\text{d}^{-1}$) for deep sites (19m, 22m, 23m and 25m). R^2 and p values are shown for log-log fits; similar correlation coefficient and significance level values were obtained for linear fits.

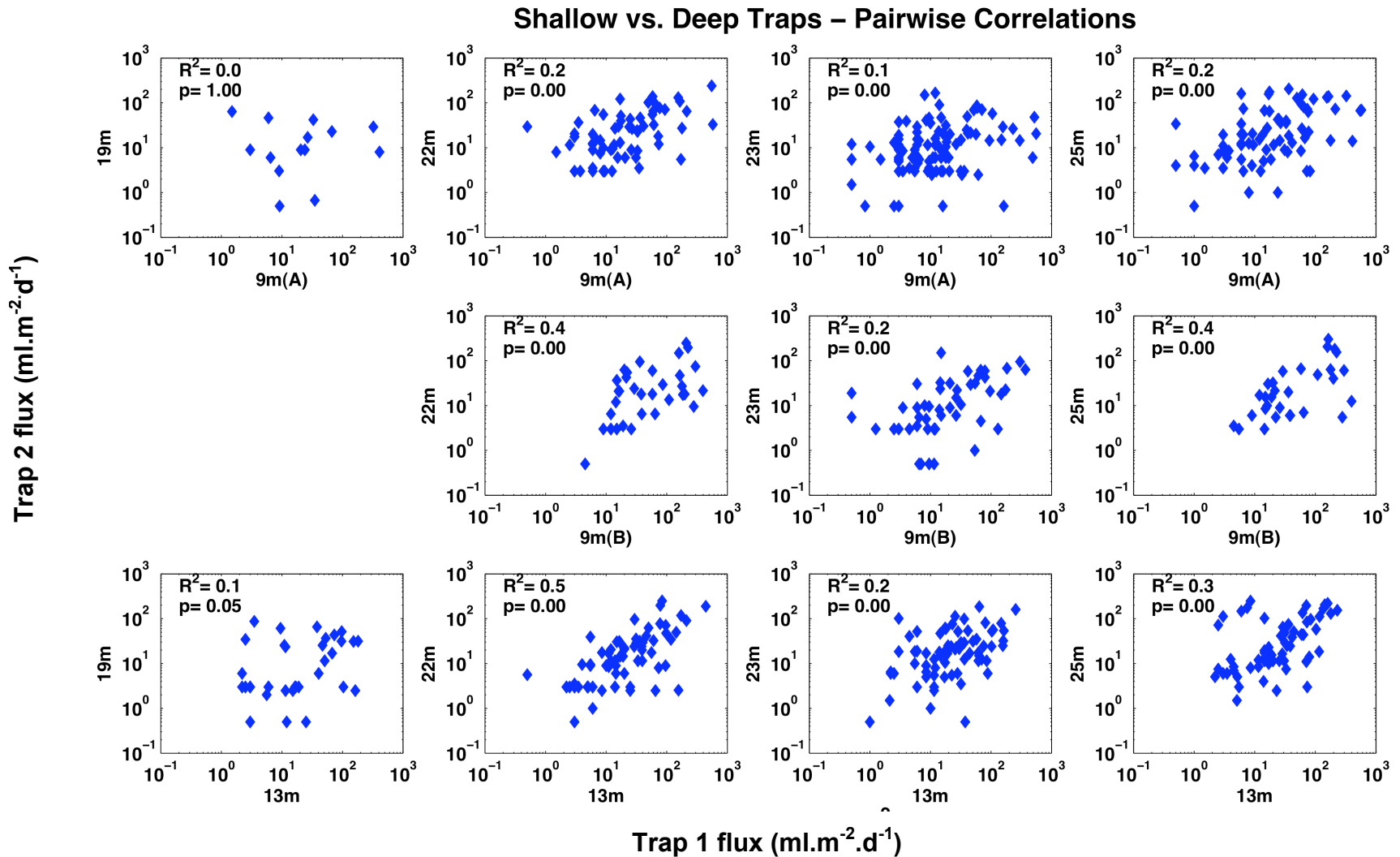


Figure 6 (c) Correlation plots between \log_{10} daily fluxes ($\text{ml.m}^{-2} \cdot \text{d}^{-1}$) at shallow and deep locations. R^2 and p values are shown for log-log fits; similar correlation coefficient and significance level values were obtained for linear fits.

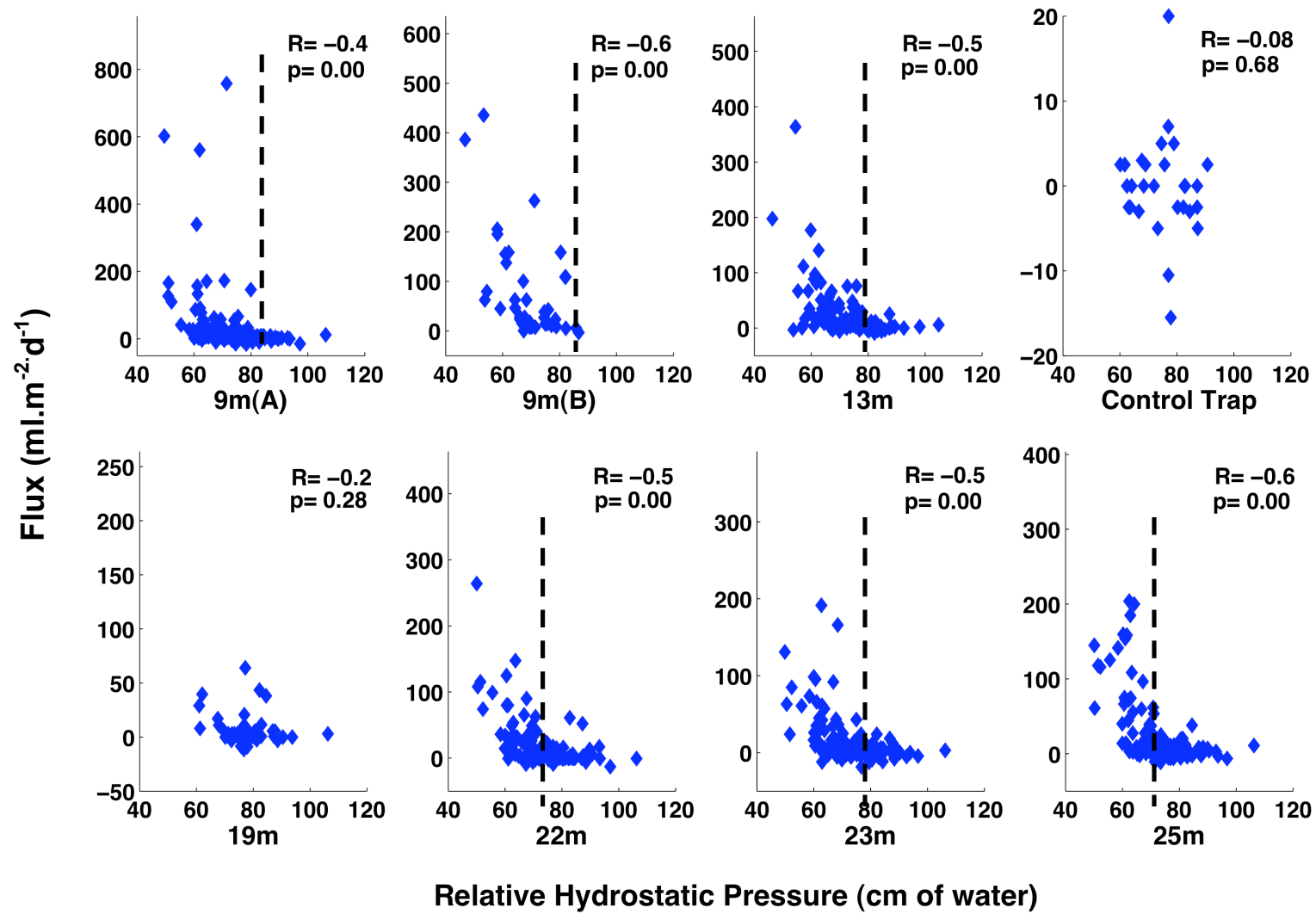


Figure 7 Correlations between daily trap fluxes ($\text{ml.m}^{-2} \cdot \text{d}^{-1}$) and relative hydrostatic pressure (cm of water). Correlation coefficients (R) and statistical significance levels (p) are indicated in the plots. The dashed black line indicates a visually identified hydrostatic pressure threshold, below which most of the bubbling occurs.

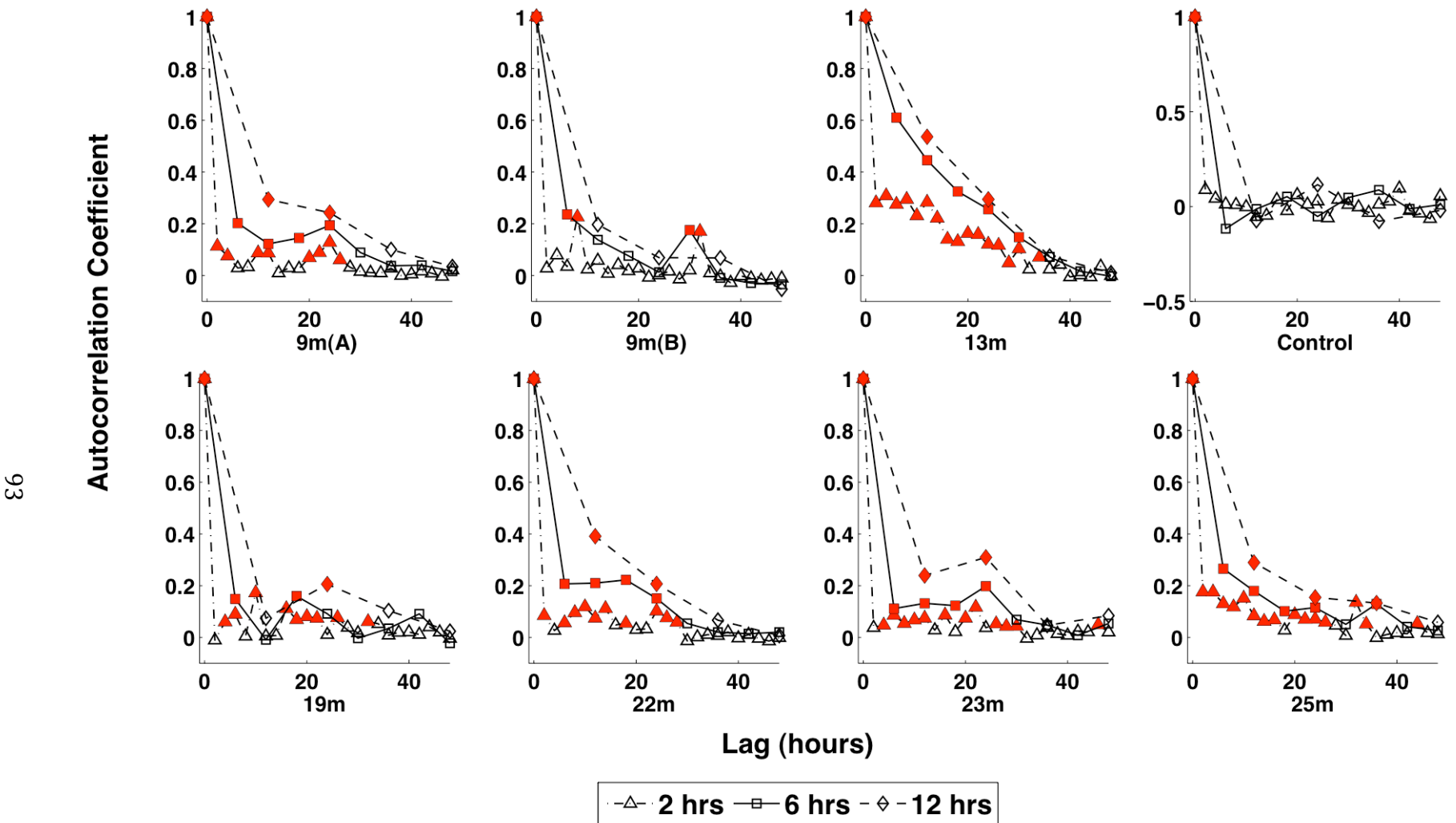


Figure 8 Autocorrelations of 2,6 and 12 hour fluxes over 48 hours. The red, filled-in markers represent significant coefficients ($p < 0.05$).

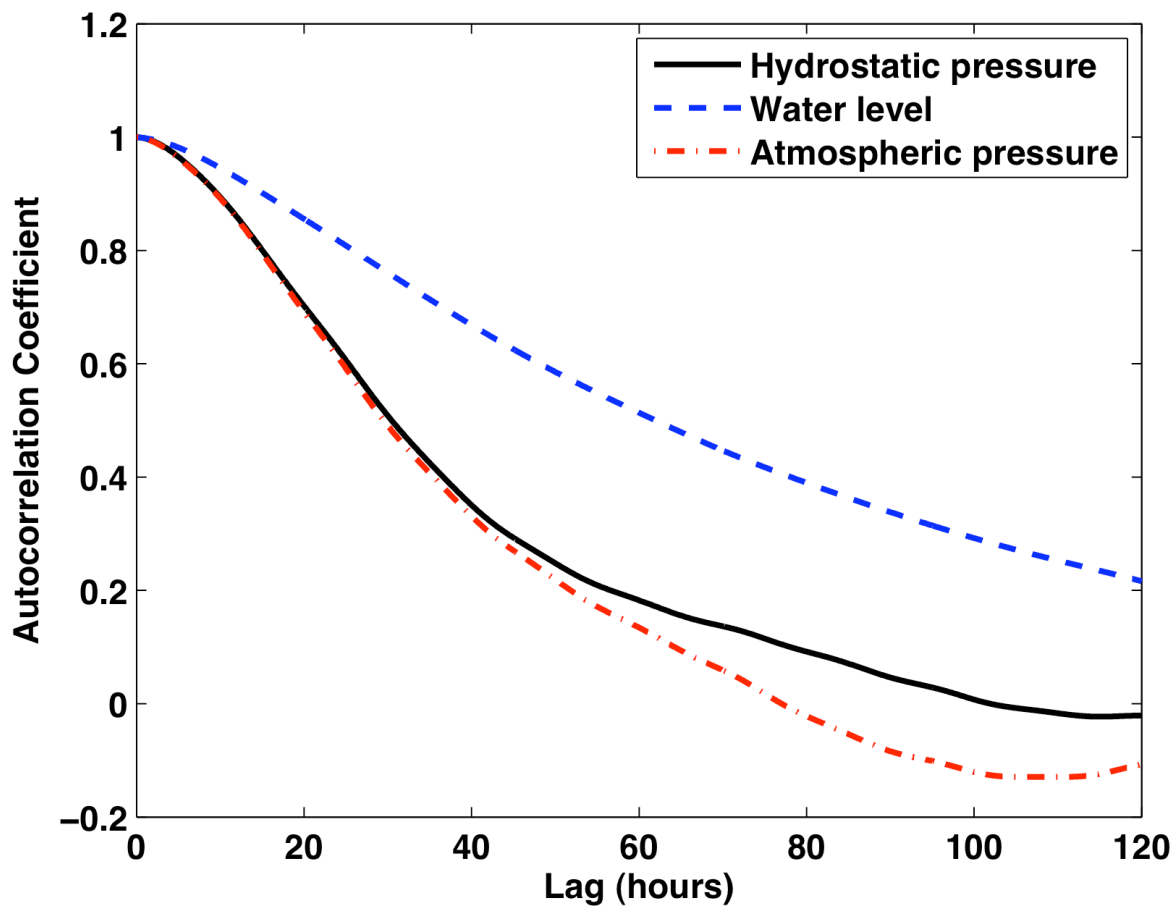


Figure 9 Hydrostatic pressure, water level and atmospheric pressure were strongly autoregressive over a period of 48 hours.

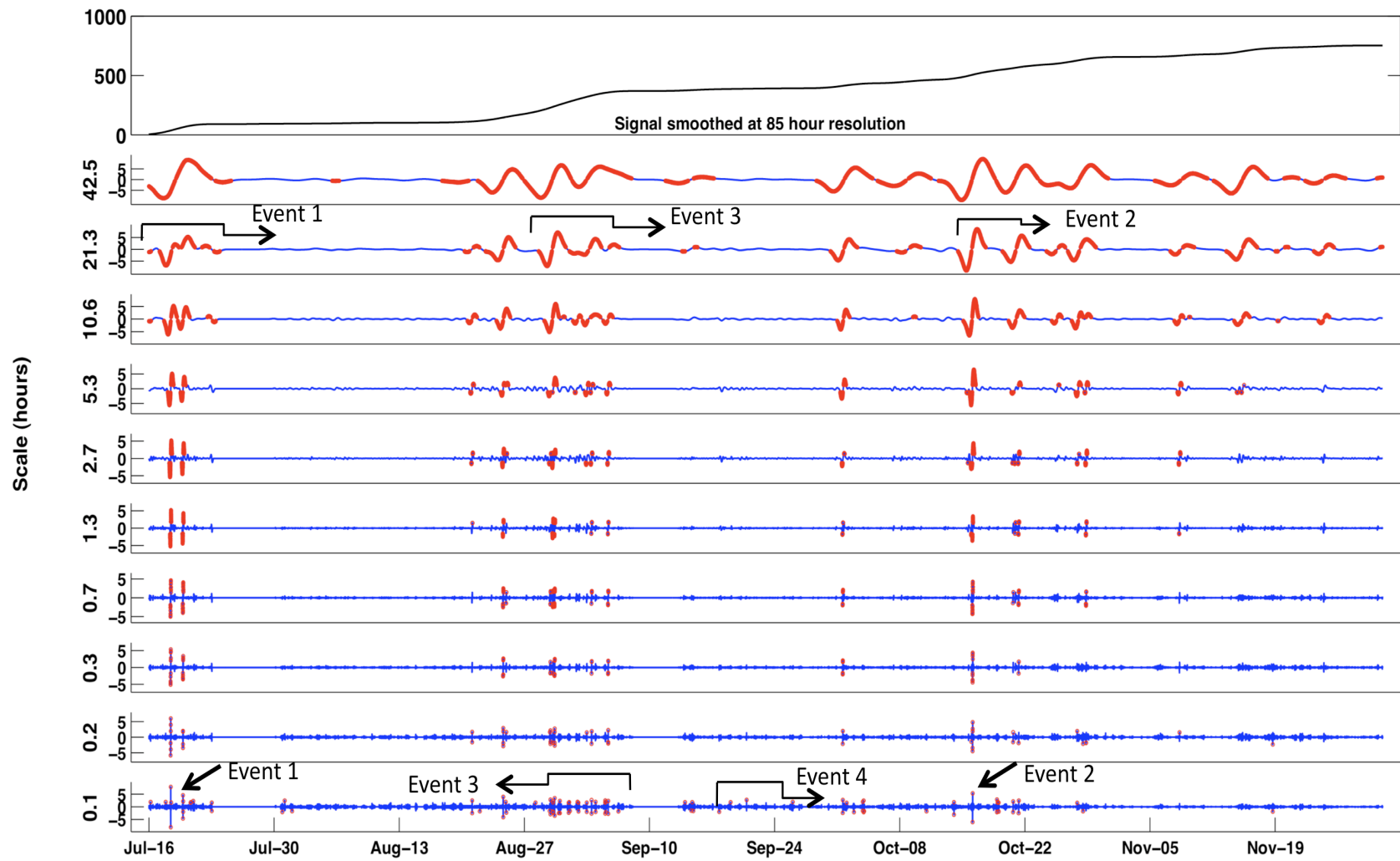


Figure 10 Multiresolution analysis of 25m trap data using the Haar wavelet. The thick red lines/ dots indicate significant events at each scale. The sum of details at all scales with the smoothed signal at 85 hours add up to the original signal.

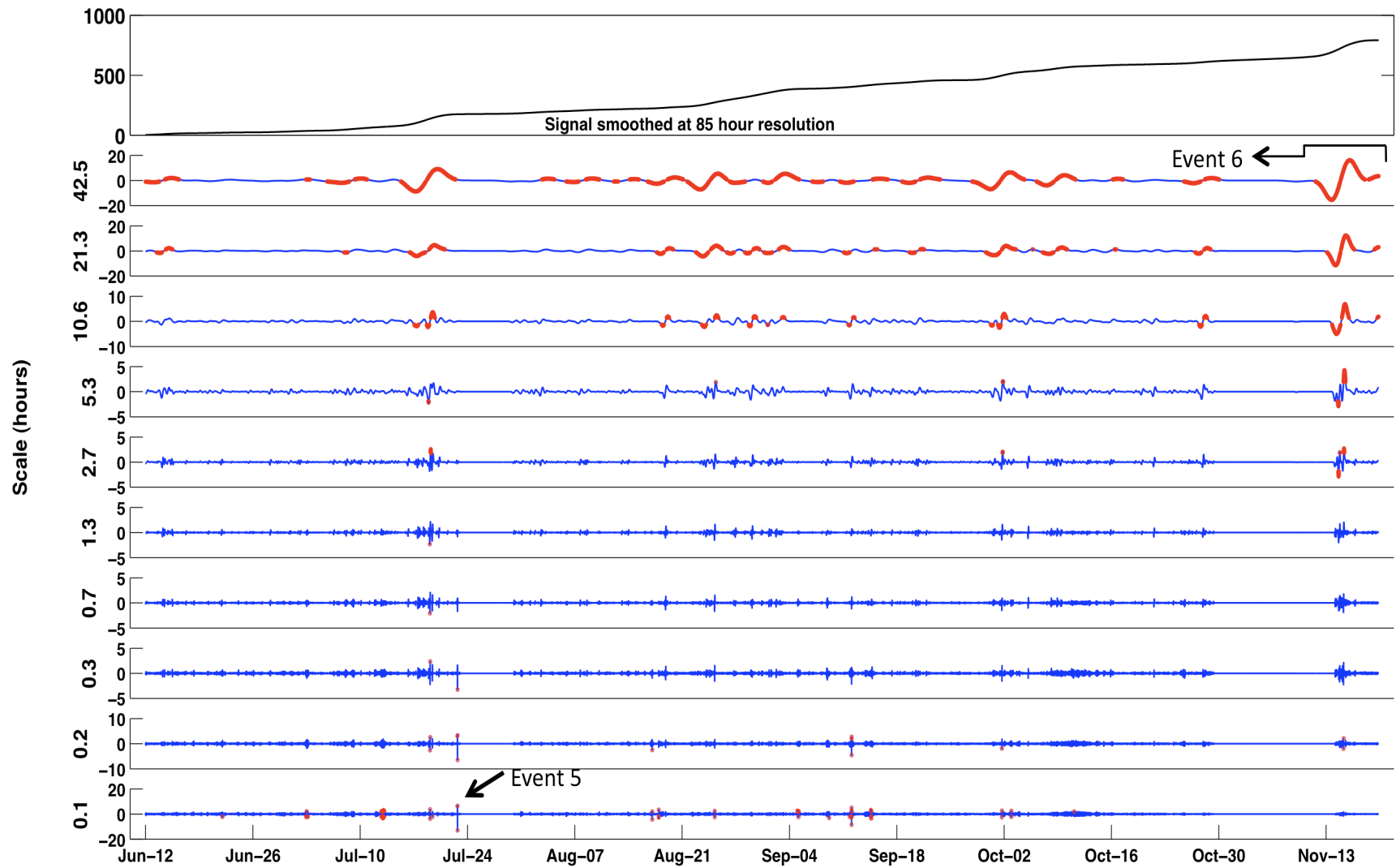


Figure 11 Multiresolution analysis of 13m trap data using the Haar wavelet. The thick red lines/red dots indicate significant events at each scale. The 13m trap was not functioning between Oct 31st-November 9th.

Wavelet details for 9m(A) trap (at 11.6 hour scale) and corresponding hydrostatic pressures

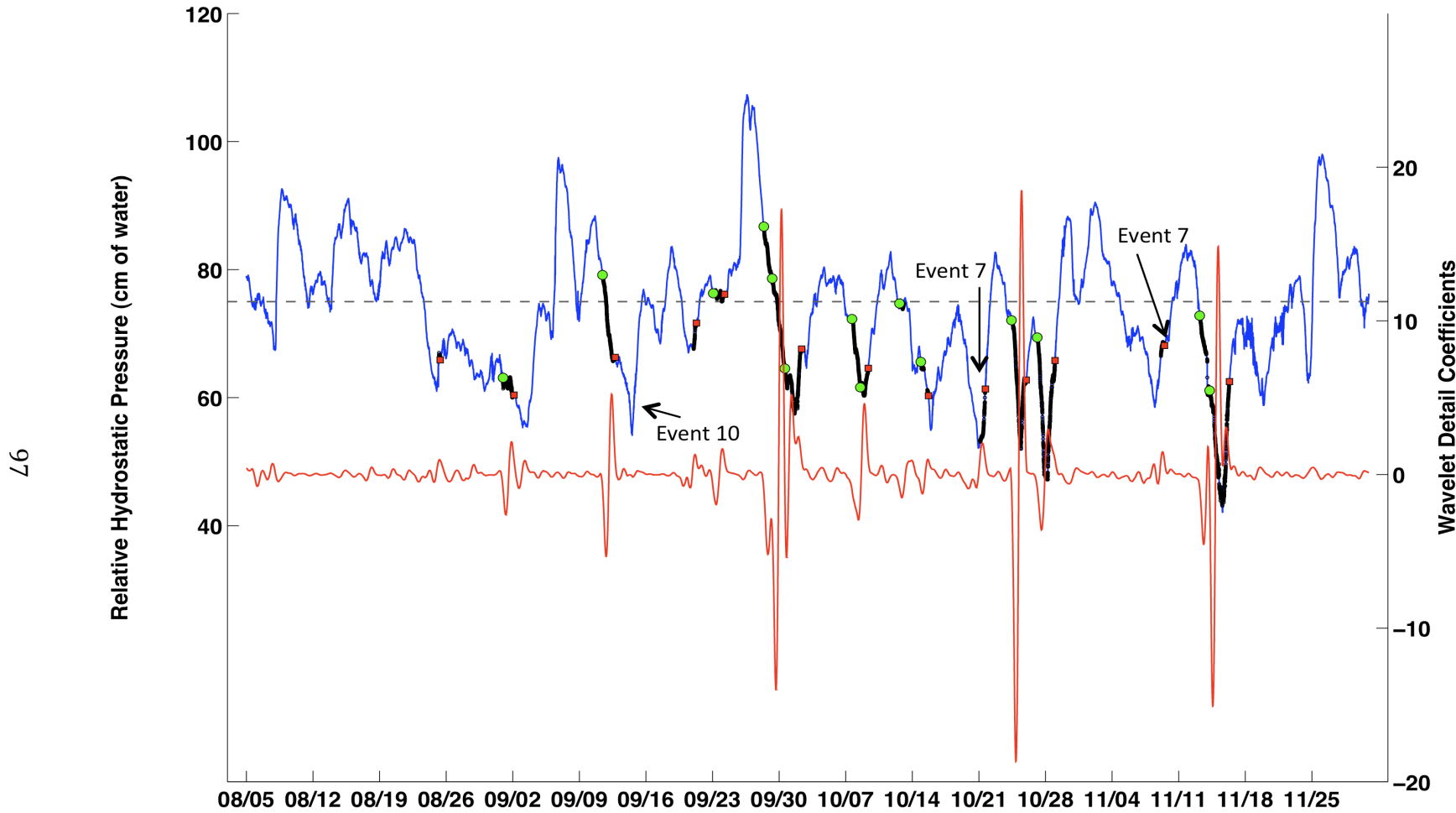


Figure 12(a) Wavelet details at scale 8 (11.6 hour) at the 9m(A) site plotted against hydrostatic pressure. The thick dark lines show hydrostatic pressures during bubbling events. The dashed line marks the threshold at which 70% of the bubbling events (at the 21.3 hour scale) are triggered. The green circles indicate the onset of bubbling events (i.e. unique events separated by more than 1 day), while the red squares mark the end of the event.

Wavelet details for 9m(A) trap (at 1.3 hour scale) and corresponding hydrostatic pressures

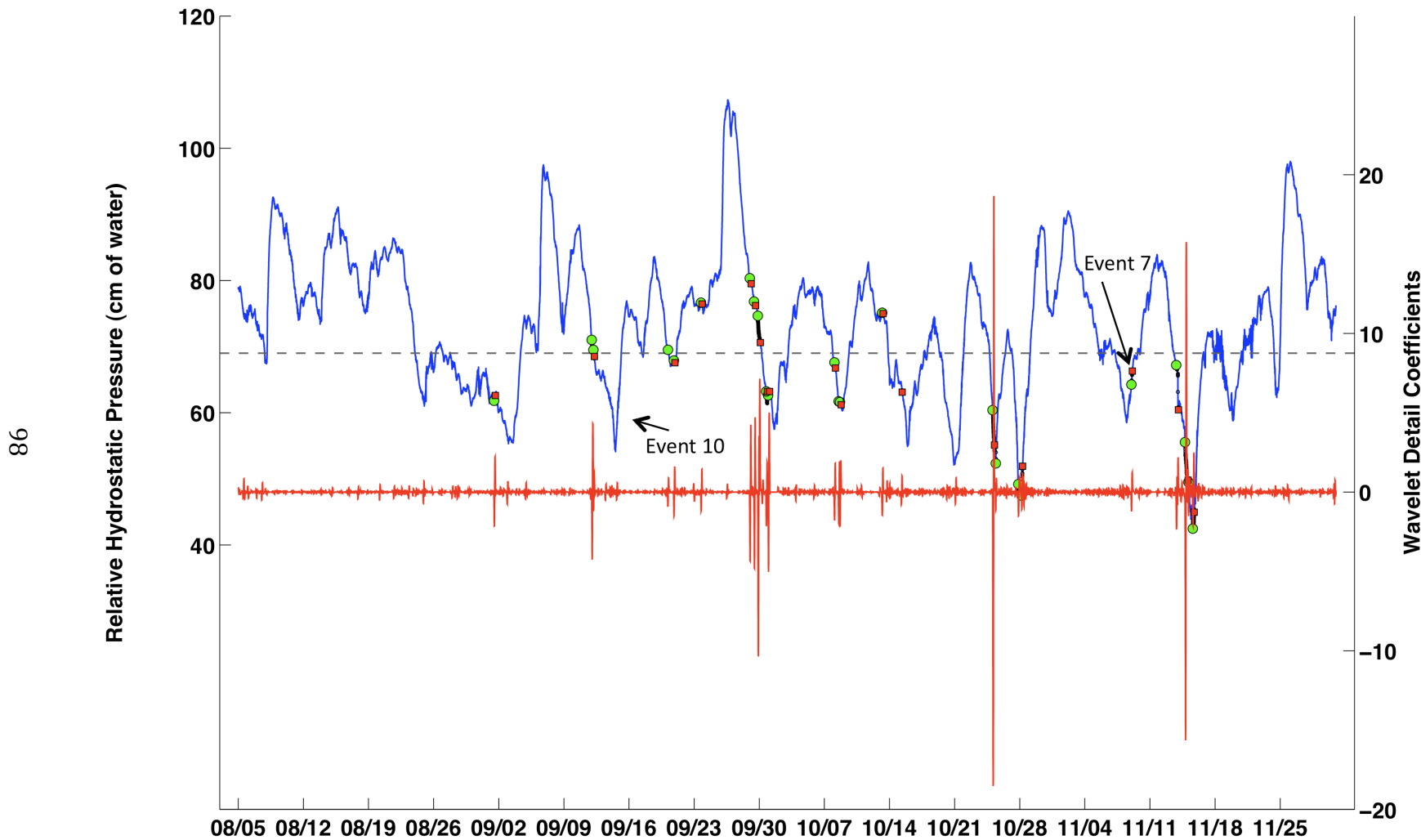


Figure 12(b) Wavelet details at scale 5 (1.3 hours) at the 9m(A) site plotted against hydrostatic pressure. See Figure 12(a) for information on plot symbols. The bubbling events indicated in Figure 12(a) comprise bubble bursts shown in this figure.

Wavelet details for 25m trap (at 11.6 hour scale) and corresponding hydrostatic pressures

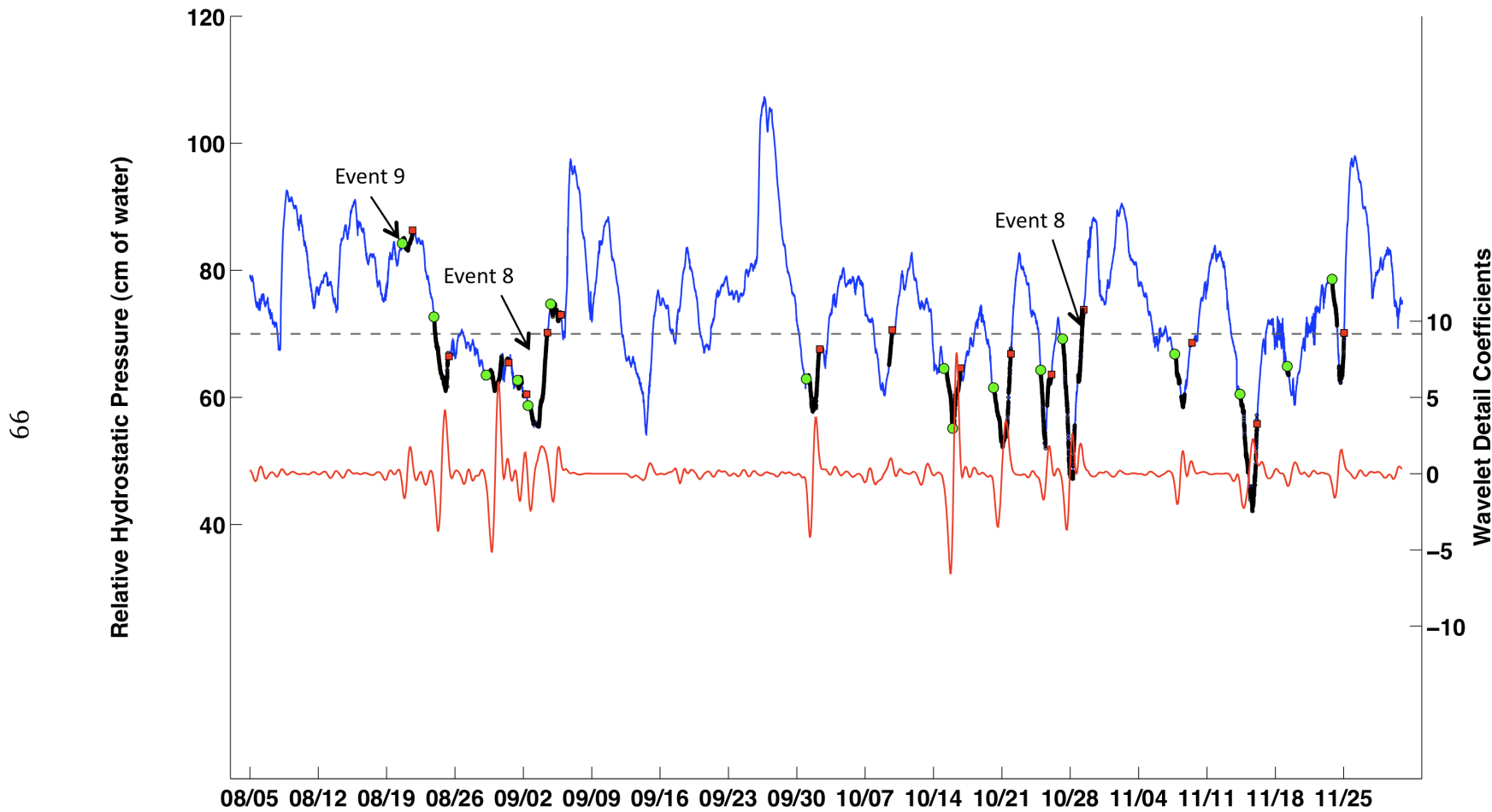


Figure 13(a) Wavelet details at scale 8 (11.6 hours) at the 25m site plotted against hydrostatic pressure. See Figure 12(a) for information on plot symbols.

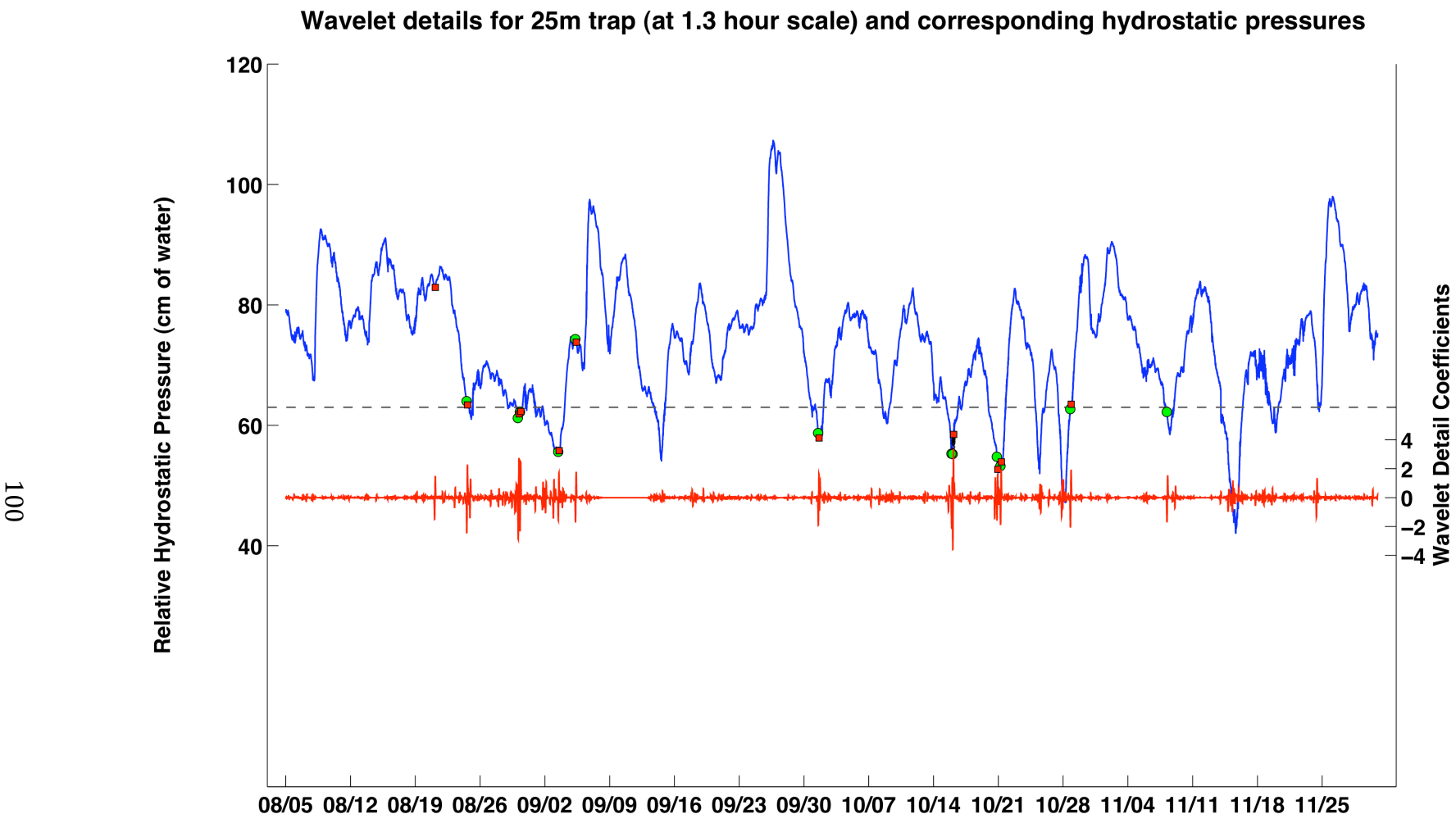


Figure 13(b) Wavelet details at scale 5 (1.3 hours) at the 25m site plotted against hydrostatic pressure. See Figure 12(a) for information on plot symbols. The bubbling events indicated in Figure 13(a) comprise bubble bursts shown in this figure.

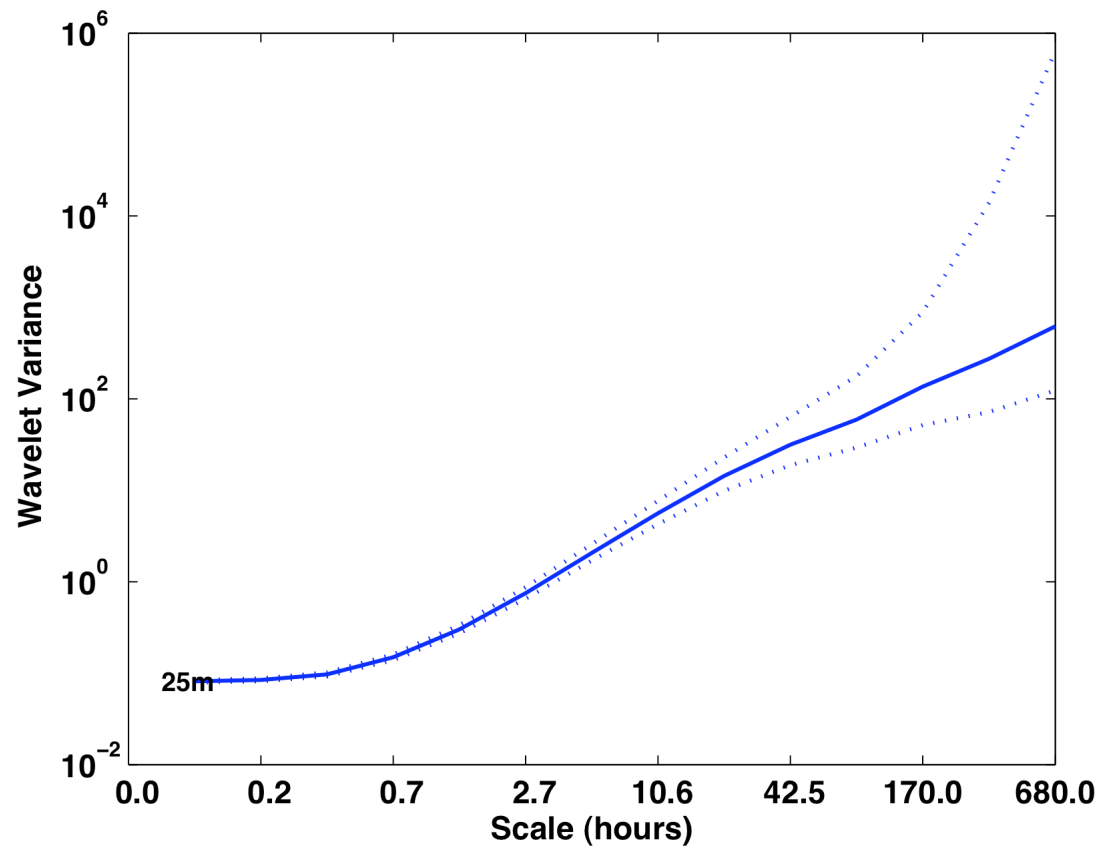


Figure 14 No periodicity could be identified from the wavelet variance of the 25m trap computed from scale 1 (5 minutes) to scale 14 (28 days). The dotted lines represent the confidence intervals for the variance.

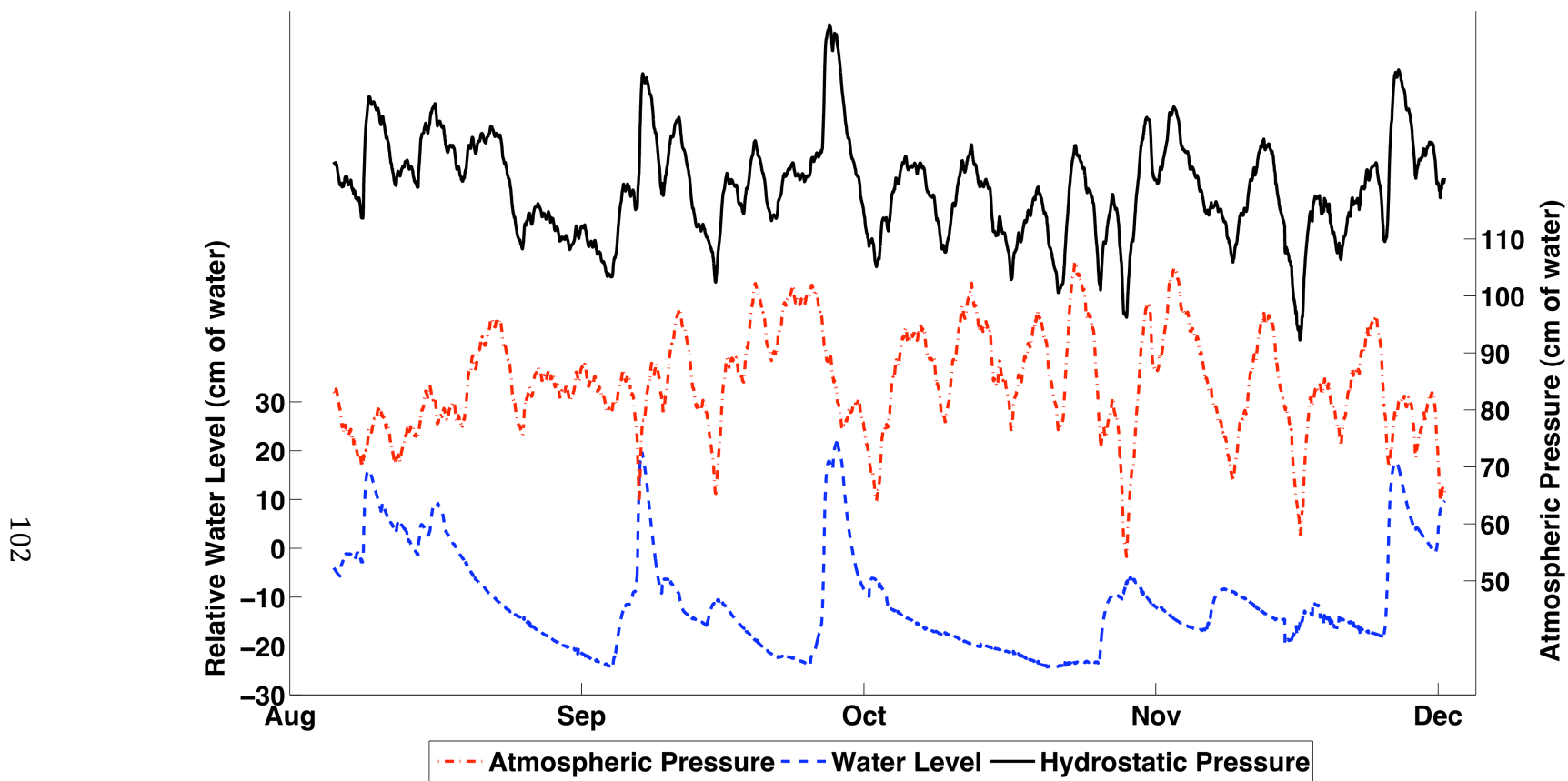


Figure 15 Atmospheric pressure, water level and their sum, i.e. hydrostatic pressure at the Upper Mystic lake

REFERENCES

1. Addison, P. S. 2002. The Illustrated Wavelet Transform Handbook: Applications in Science, Engineering, Medicine and Finance. Institute of Physics Publishing, Bristol, UK.
2. Aurilio, A. C., R. P. Mason and H. F. Hemond. 1994. Speciation and Fate of Arsenic in Three Lakes of the Aberjona Watershed. Environ. Sci. Technol. **28**: 577-585.
3. Bäckstrand, K., P. M. Crill, M. Mastepanov, T. R. Christensen and D. Bastviken. 2008. Total hydrocarbon flux dynamics at a subarctic mire in northern Sweden. J. Geophys. Res. **113**: G03026, doi:10.1029/2008JG000703.
4. Baldocchi, D., E. Falge and K. Wilson. 2001. A spectral analysis of biosphere-atmosphere trace gas flux densities and meteorological variables across hour to multi-year time scales. Agric. For. Meteorol. **107**: 1-27, doi:DOI: 10.1016/S0168-1923(00)00228-8.
5. Bastviken, D., J. Cole, M. Pace and L. Tranvik. 2004. Methane emissions from lakes: Dependence of lake characteristics, two regional assessments, and a global estimate. Global Biogeochem. Cycles. **18**: B4009.
6. Boles, J. R., J. F. Clark, I. Leifer and L. Washburn. 2001. Temporal variation in natural methane seep rate due to tides. Coal Oil Point area, California. J. Geophys. Res. **106 (C11)**: 27,077-27,086, doi:10.1029/2000JC000774.
7. Boudreau, B. P., C. Algar, B. D. Johnson, I. Croudace, A. Reed, Y. Furukawa, K. M. Dorgan, P. A. Jumars, A. S. Grader and B. S. Gardiner. 2005. Bubble growth and rise in soft sediments. Geology. **33**: 517-520, doi:10.1130/G21259.1.
8. Casper, P., S. C. Maberly, G. H. Hall and B. J. Finlay. 2000. Fluxes of methane and carbon dioxide from a small productive lake to the atmosphere. Biogeochemistry. **49**: 1-19.
9. Chanton, J. P., C. S. Martens and C. A. Kelley. 1989. Gas transport from methane-saturated, tidal freshwater and wetland sediments. Limnol. Oceanogr. **34**: 807-819.
10. Chanton, J. P. and C. S. Martens. 1988. Seasonal Variations In Ebullitive Flux And Carbon Isotopic Composition Of Methane In a Tidal Freshwater Estuary. Global Biogeochem. Cycles. **2**: 289-298.
11. Christensen, T. R., A. Ekberg, L. Ström, M. Mastepanov, N. Panikov, M. Öquist, B. H. Svensson, H. Nykänen, P. J. Martikainen and H. Oskarsson. 2003. Factors controlling large scale variations in methane emissions from wetlands. Geophys. Res. Lett. **30**: 1414, doi:10.1029/2002GL016848.
12. Coifman, R. R., and D. L. Donoho. 1995. Translation-Invariant De-Noising, p. 125-150. In Anonymous Lecture Notes in Statistics: Wavelets and Statistics. Springer-Verlag.
13. Crill, P. M., K. B. Bartlett, J. O. Wilson, D. I. Sebacher, R. C. Harriss, J. M. Melack, S. MacIntyre, L. Lesack and L. Smith-Morrill. 1988. Tropospheric methane from an Amazonian floodplain lake. J. Geophys. Res. **93**: 1564-1570, doi:10.1029/JD093iD02p01564.
14. Dise, N. B., E. Gorham and E. S. Verry. 1993. Environmental Factors Controlling Methane Emissions from Peatlands in Northern Minnesota. J. Geophys. Res. **98 (D6)**: 10,583-10,594.
15. Donoho, D. L. 1995. De-noising by soft thresholding. IEEE Transactions on Information Theory. **41**: 613-627.
16. Donoho, D. L., I. M. Johnstone, G. Kerkyacharian and D. Picard. 1995. Wavelet Shrinkage: Asymptopia? Journal of the Royal Statistical Society. Series B (Methodological). **57**: 301-369.
17. Eckert, W. and R. Conrad. 2007. Sulfide and methane evolution in the hypolimnion of a subtropical lake: a three-year study. Biogeochemistry. **82**: 67-76.

18. Engle, D. and J. M. Melack. 2000. Methane emissions from an Amazon floodplain lake: Enhanced release during episodic mixing and during falling water. *Biogeochemistry*. **51**: 71-90.
19. Fechner-Levy, E. J. and H. F. Hemond. 1996. Trapped methane volume and potential effects on methane ebullition in a northern peatland. *Limnol. Oceanogr.* **41**: 1375-1383.
20. Glaser, P. H., J. P. Chanton, P. Morin, D. O. Rosenberry, D. I. Siegel, O. Ruud, L. I. Chasar and A. S. Reeve. 2004. Surface deformations as indicators of deep ebullition fluxes in a large northern peatland. *Global Biogeochem. Cycles*. **18**: GB1003, doi:10.1029/2003GB002069.
21. Graps, A. 1995. An introduction to wavelets. *IEEE Computational Science & Engineering*. **2**: 50-61.
22. Greinert, J. 2008. Monitoring temporal variability of bubble release at seeps: The hydroacoustic swath system GasQuant. *J. Geophys. Res.* **113**: C07048, doi:10.1029/2007JC004704 ER.
23. Greinert, J. and B. Nützel. 2004. Hydroacoustic experiments to establish a method for the determination of methane bubble fluxes at cold seeps. *Geo-Mar. Lett.* **24**: 75-85, doi:10.1007/s00367-003-0165-7.
24. Grossmann, A. and J. Morlet. 1984. Decomposition of Hardy Functions into Square Integrable Wavelets of Constant Shape. *SIAM J. Math. Anal.* **15**: 723-736, doi:10.1137/0515056.
25. Guralnik, V., and J. Srivastava. 1999. Event detection from time series data. International Conference on Knowledge Discovery and Data Mining. 33-42.
26. Hajj, H. M., T. Q. Nguyen and R. T. Chin. 1995. On multi-scale feature detection using filter banks. Proc. Asilomar Conference on Signals, Systems and Computers. 70.
27. Jansen, M. 2001. Noise reduction by wavelet thresholding. Springer.
28. Joyce, J. and P. W. Jewell. 2003. Physical Controls on Methane Ebullition from Reservoirs and Lakes. *Environmental and Engineering Geoscience*. **9**: 167-178, doi:10.2113/9.2.167.
29. Kallache, M., H. W. Rust and J. Kropp. 2005. Trend assessment: applications for hydrology and climate research.
30. Keller, M. and R. F. Stallard. 1994. Methane emission by bubbling from Gatun Lake, Panama. *J. Geophys. Res.* **99 (D4)**: 8307-8319.
31. Kelly, C. A. and D. P. Chynoweth. 1981. The Contributions of Temperature and of the Input of Organic Matter in Controlling Rates of Sediment Methanogenesis. *Limnol. Oceanogr.* **26**: 891-897.
32. Kettunen, A., V. Kaitala, J. Alm, J. Silvola, H. Nykänen and P. J. Martikainen. 2000. Predicting variations in methane emissions from boreal peatlands through regression models. *Boreal Env. Res.* **5**: 115-131.
33. Kettunen, A., V. Kaitala, J. Alm, J. Silvola, H. Nykänen and P. J. Martikainen. 1996. Cross-Correlation Analysis of the Dynamics of Methane Emissions From a Boreal Peatland. *Global Biogeochem. Cycles*. **10**: 457-471.
34. Kumar, P. and E. Foufoula-Georgiou. 1997. Wavelet Analysis for Geophysical Applications. *Rev. Geophys.* **35**: 385-412.
35. Labat, D., R. Ababou and A. Mangin. 2000. Rainfall-runoff relations for karstic springs. Part II: continuous wavelet and discrete orthogonal multiresolution analyses. *238*: 149-178, doi: 10.1016/S0022-1694(00)00322-X.

36. Leifer, I., J. R. Boles, B. P. Luyendyk and J. F. Clark. 2004. Transient discharges from marine hydrocarbon seeps: spatial and temporal variability. *Environ. Geol.* **46**: 1038-1052, doi:10.1007/s00254-004-1091-3.
37. Liikanen, A., T. Murtoniemi, H. Tanskanen, T. Väisänen and P. J. Martikainen. 2002. Effects of temperature and oxygen availability on greenhouse gas and nutrient dynamics in sediment of a eutrophic mid-boreal lake. *Biogeochemistry*. **59**: 269-286.
38. Mallat, S. G. 1999. *A wavelet tour of signal processing / Stephane Mallat*. Academic Press.
39. Martens, C. S. and J. V. Klump. 1980. Biogeochemical cycling in an organic-rich coastal marine basin-I. Methane sediment-water exchange processes. *Geochim. Cosmochim. Acta*. **44**: 471-490.
40. Mass, C. F., W. J. Steenburgh and D. M. Schultz. 1991. Diurnal Surface-Pressure Variations over the Continental United States and the Influence of Sea Level Reduction. *Mon. Weather Rev.* **119**: 2814-2830.
41. Masteponov, M., C. Sigsgaard, E. J. Dlugokencky, S. Houweling, L. Ström, M. P. Tamstorf and T. R. Christensen. 2008. Large tundra methane burst during onset of freezing. *Nature*. **456**: 628-630, doi:10.1038/nature07464.
42. Mathworks. Signal Processing Toolbox Documentation - xcov. **2009**.
43. Mattson, M. D. and G. E. Likens. 1990. Air pressure and methane fluxes. *Nature*. **347**: 718-719.
44. McGinnis, D. F., J. Greinert, Y. Artemov, S. E. Beaubien and A. Wüest. 2006. Fate of rising methane bubbles in stratified waters: How much methane reaches the atmosphere? *J. Geophys. Res.* **111**: C09007, doi:10.1029/2005JC003183.
45. Nason, G. P. and B. W. Silverman. 1995. The stationary wavelet transform and some statistical applications. *Lect. Notes. Statist.* **103**: 281-300.
46. Ogata, Y. 1988. Statistical Models for Earthquake Occurrences and Residual Analysis for Point Processes. **83**: 9-27.
47. Orfanidis, S. J. 1995. *Introduction to Signal Processing*. Prentice Hall, Upper Saddle River, NJ.
48. Ostrovsky, I., D. F. McGinnis, L. Lapidus and W. Eckert. 2008. Quantifying gas ebullition with echosounder: The role of methane transport by bubbles in a medium-sized lake. *Limnol. Oceanogr. - Methods*. **6**: 105-118.
49. Percival, D. B., and A. T. Walden. 2000. *Wavelet methods for Time Series Analysis*. Cambridge Univ. Press, Cambridge, UK.
50. Percival, D. 2008. Analysis of Geophysical Time Series Using Discrete Wavelet Transforms: An Overview, p. 61-79. In R. V. Donner and S. M. Barbosa [eds.], *Nonlinear Time Series Analysis in the Geosciences*. Springer.
51. Peterson, E. J. R. 2005. Carbon and electron flow via methanogenesis, SO_4^{2-} , NO_3^- and Fe^{3+} reduction in the anoxic hypolimnia of Upper Mystic Lake. Master of Science thesis. Massachusetts Institute of Technology.
52. Priestley, M. B. 1992. *Spectral analysis and Time series*, Vol. 1. Academic Press.
53. Rudd, J. W. M., and C. D. Taylor. 1980. Methane cycling in aquatic environments, p. 77-150. In M. R. Droop, Jannasch, H.W. [ed.], *Advances in Aquatic Microbiology*. Academic Press.
54. Senn, D. B. 2001. Coupled arsenic, iron, and nitrogen cycling in arsenic-contaminated Upper Mystic Lake. Doctor of Philosophy thesis. Massachusetts Institute of Technology.

55. Smith, R. L. 1989. Extreme Value Analysis of Environmental Time Series: An Application to Trend Detection in Ground-Level Ozone. **4**: 367-377.
56. Spliethoff, H. M. 1995. Biotic and abiotic transformations of arsenic in the Upper Mystic Lake.
57. Stearns, D. S. 2002. Digital Signal Processing with Examples in MATLAB. CRC Press, Florida, US.
58. Torrence, C. and G. P. Compo. 1998. A Practical Guide to Wavelet Analysis. Bull. Amer. Meteor. Soc. **79**: 61-78.
59. Treat, C. C., J. L. Bubier, R. K. Varner and P. M. Crill. 2007. Timescale dependence of environmental and plant-mediated controls on CH₄ flux in a temperate fen. J. Geophys. Res. **112**: G01014, doi:10.1029/2006JG000210.
60. Walter, K. M., L. C. Smith and F. S. Chapin III. 2007. Methane bubbling from northern lakes: present and future contributions to the global methane budget. Philos. Trans. R. Soc. A. **365**: 1657-1676, doi:10.1098/rsta.2007.2036.
61. Walter, K. M., S. A. Zimov, J. P. Chanton, D. Verbyla and F. S. Chapin III. 2006. Methane bubbling from Siberian thaw lakes as a positive feedback to climate warming. Nature. **443**: 71-75, doi:10.1038/nature05040.
62. Wanner, H., S. Brönnimann, C. Casty, D. Gyalistras, J. Luterbacher, C. Schmutz, D. B. Stephenson and E. Xoplaki. 2001. North Atlantic Oscillation - Concepts And Studies. Surv. Geophys. **22**: 321-381.
63. Whitcher, B., P. Guttorp and D. B. Percival. 2000. Wavelet analysis of covariance with application to atmospheric time series. J. Geophys. Res. **105**: 14941-14962, doi:10.1029/2000JD900110

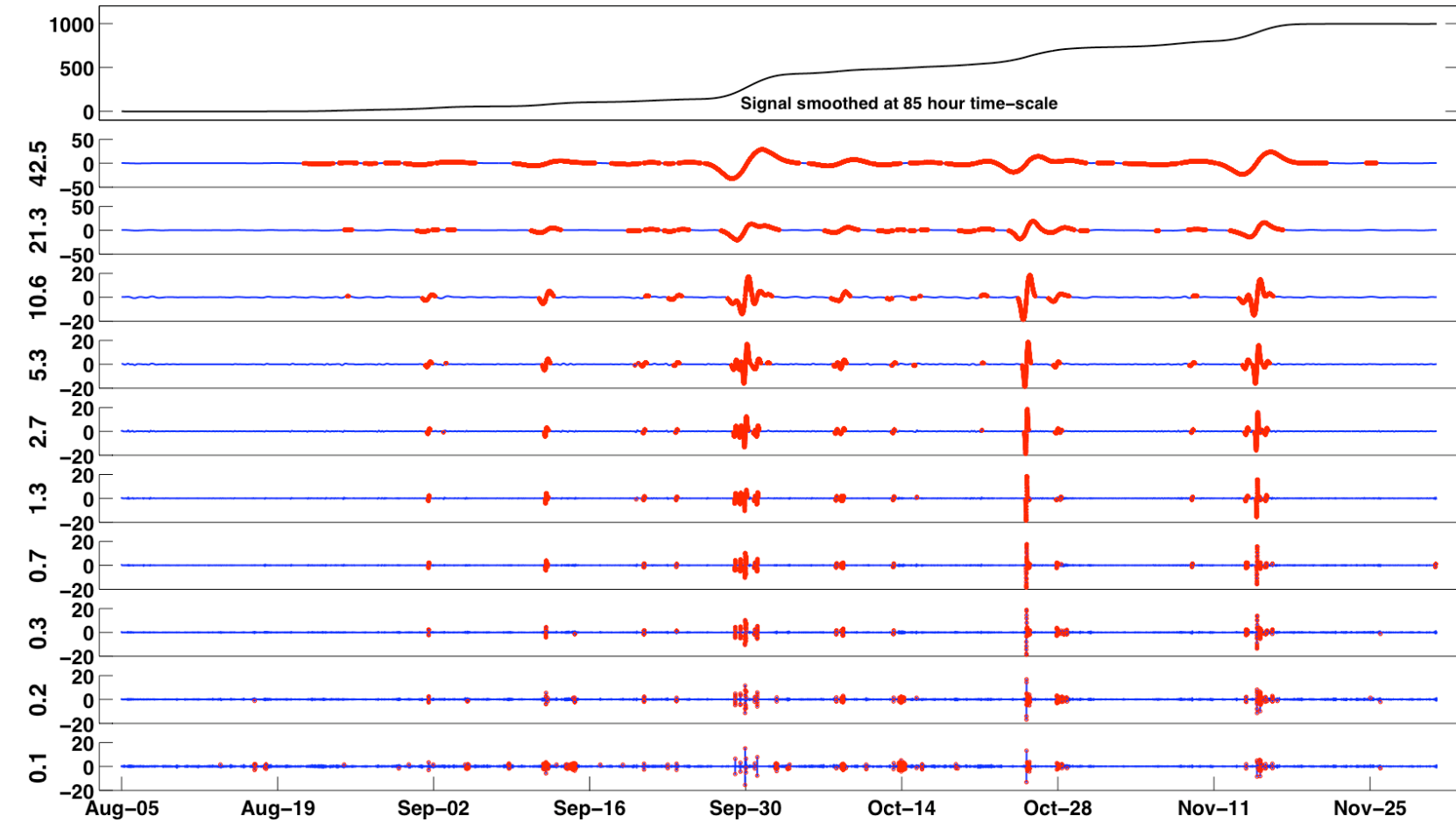
Appendix for Chapter 3

Figure 1 – Multi-resolution analysis of remaining traps (9m(A), 9m(B), 19m, 22m, 23m)

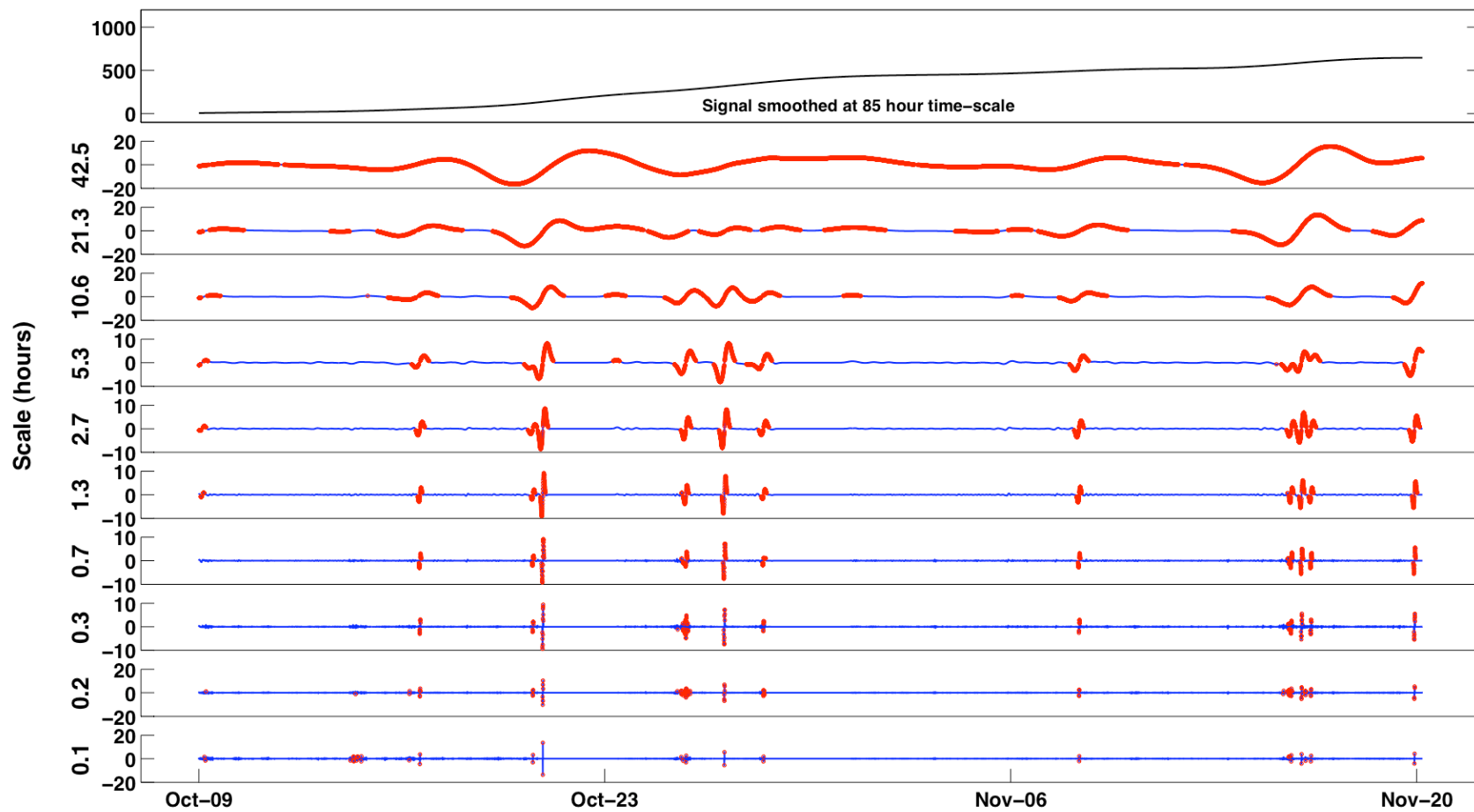
Figure 2 – Comparison of wavelet details at 11.6 hour and 1.3 hour scales against hydrostatic pressure for remaining traps (9m(B), 13m, 19m, 22m, 23m)

80I

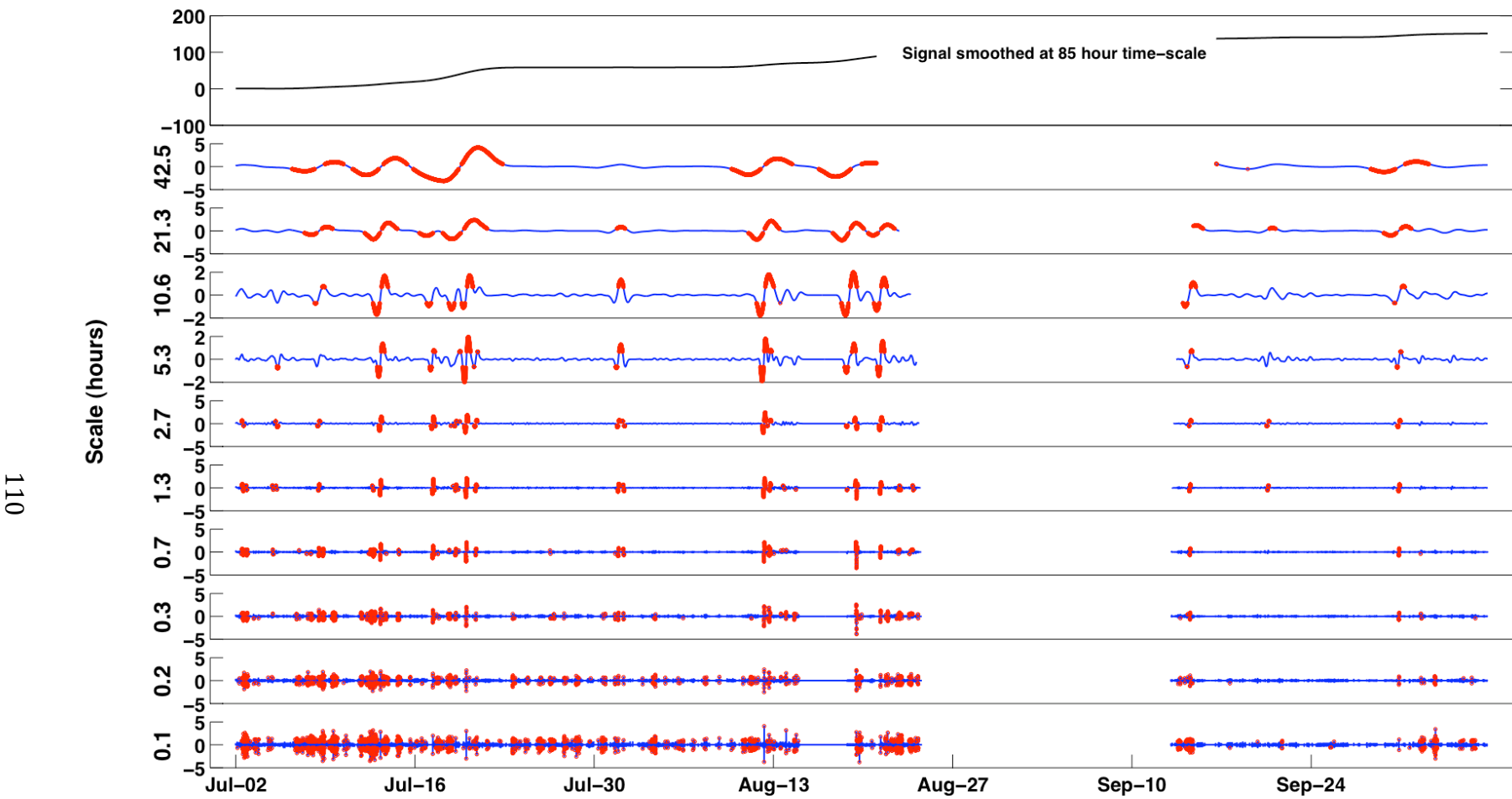
Multiresolution Analysis (9m(A) trap) – 10 level decomposition using the Haar wavelet



Multiresolution Analysis (9m(B) trap) – 10 level decomposition using the Haar wavelet

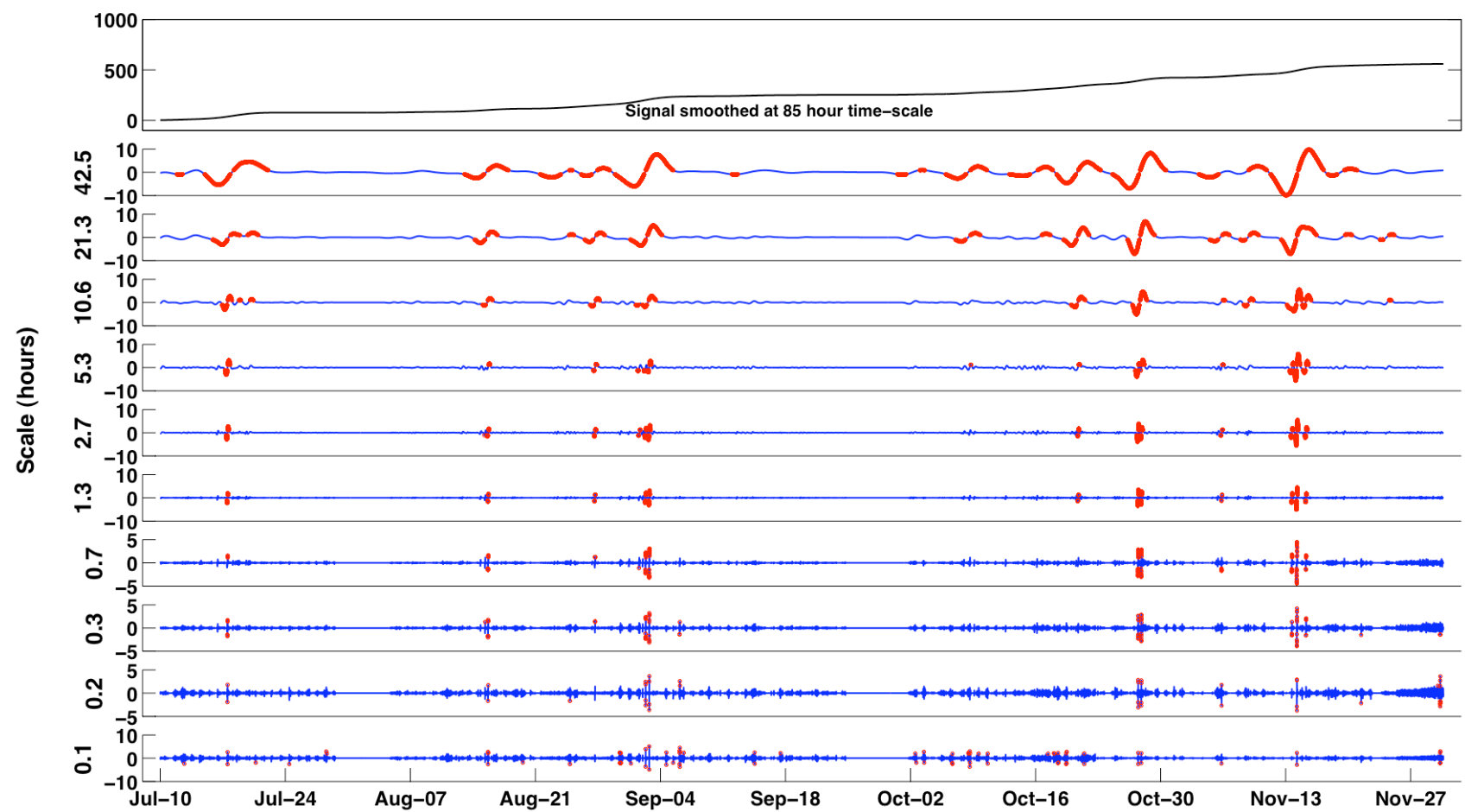


Multiresolution Analysis (19m trap) – 10 level decomposition using the Haar wavelet

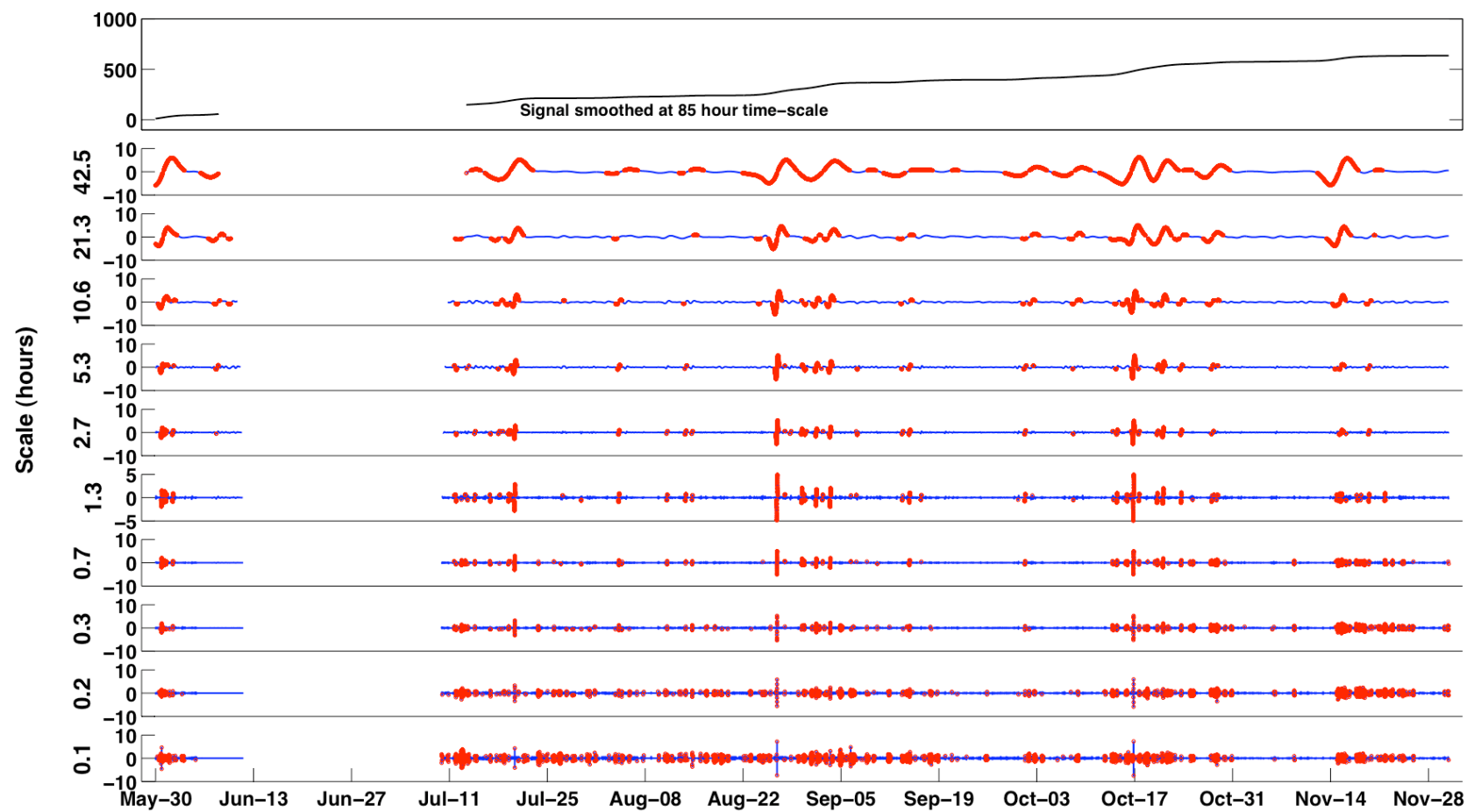


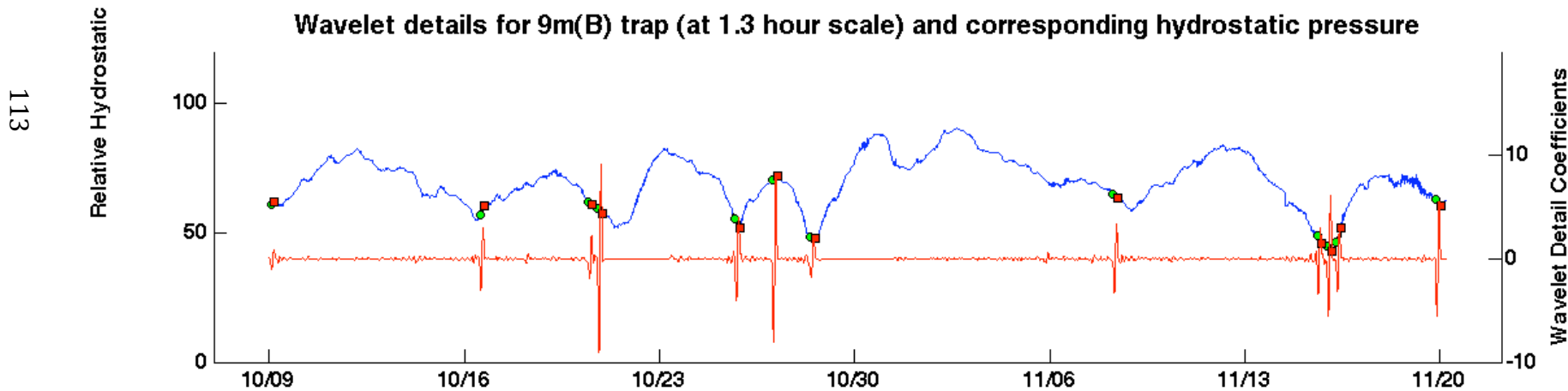
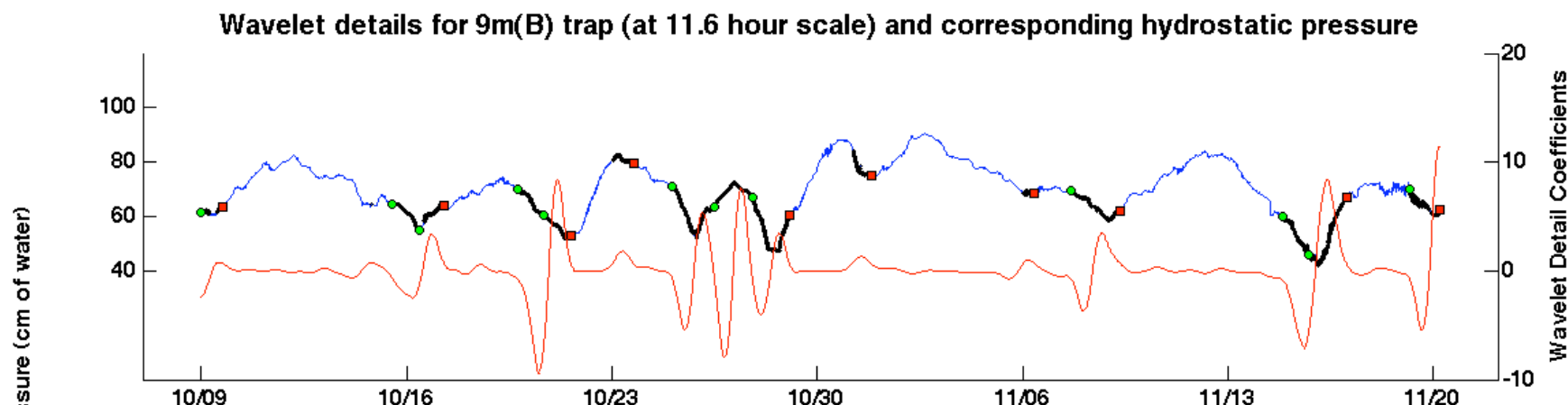
Multiresolution Analysis (22m trap) – 10 level decomposition using the Haar wavelet

III

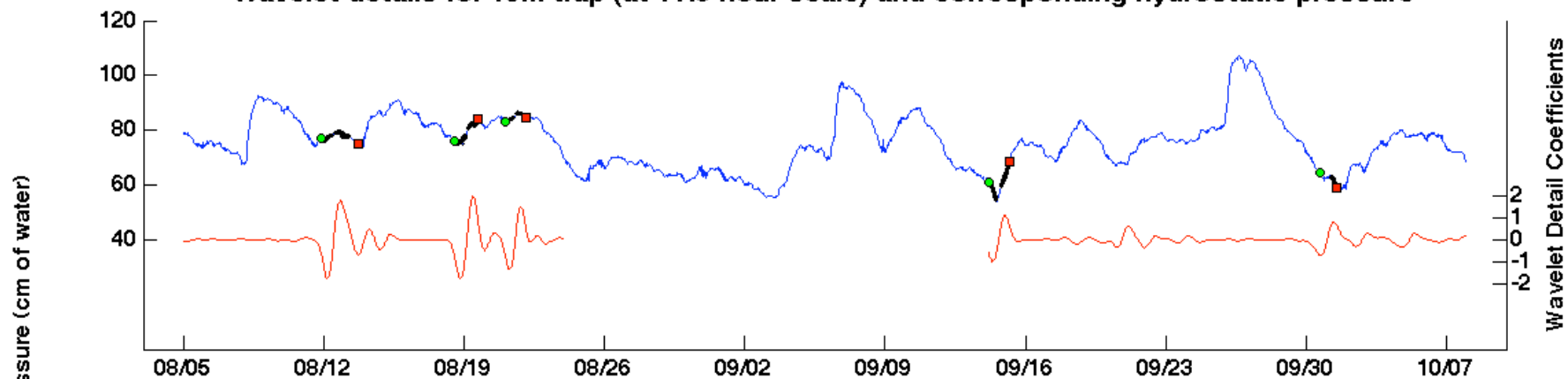


Multiresolution Analysis (23m trap) – 10 level decomposition using the Haar wavelet

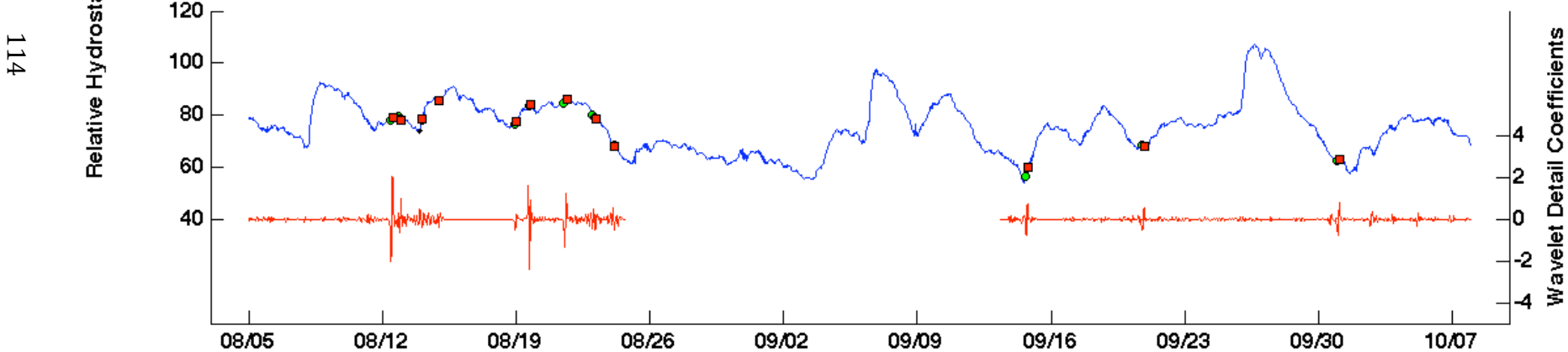


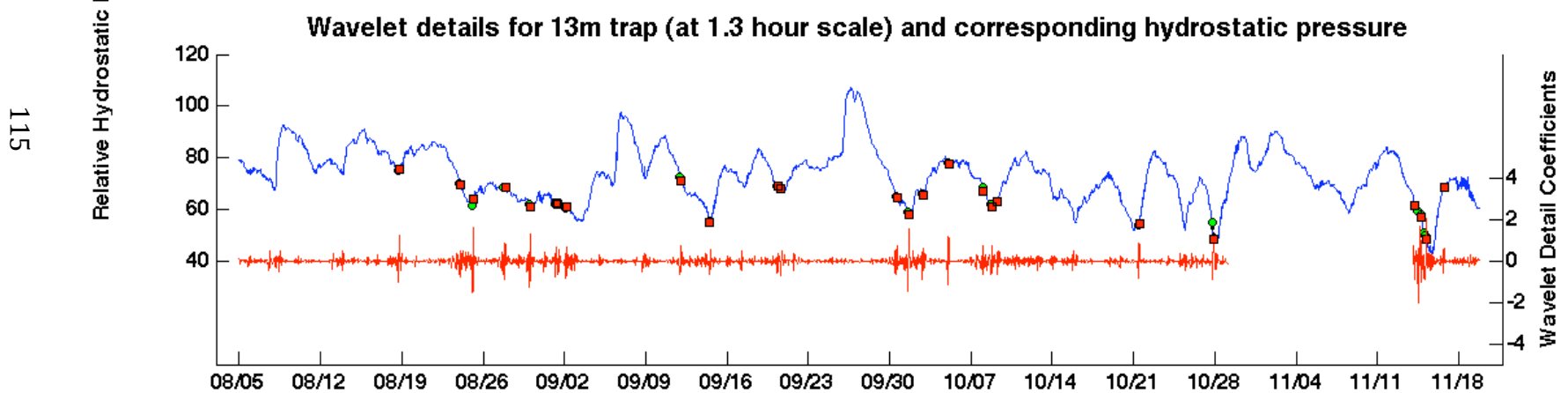
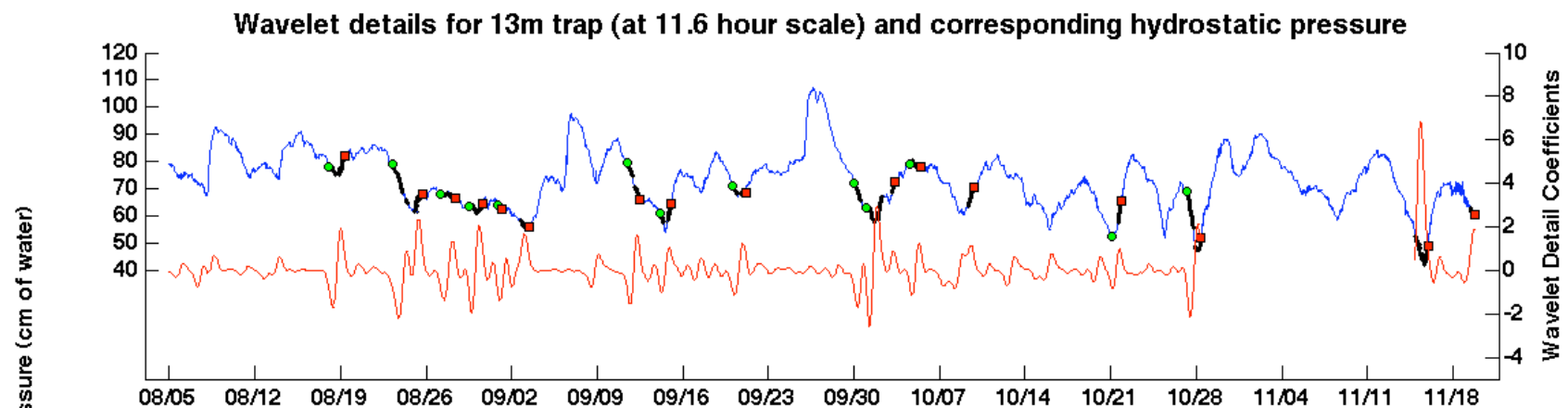


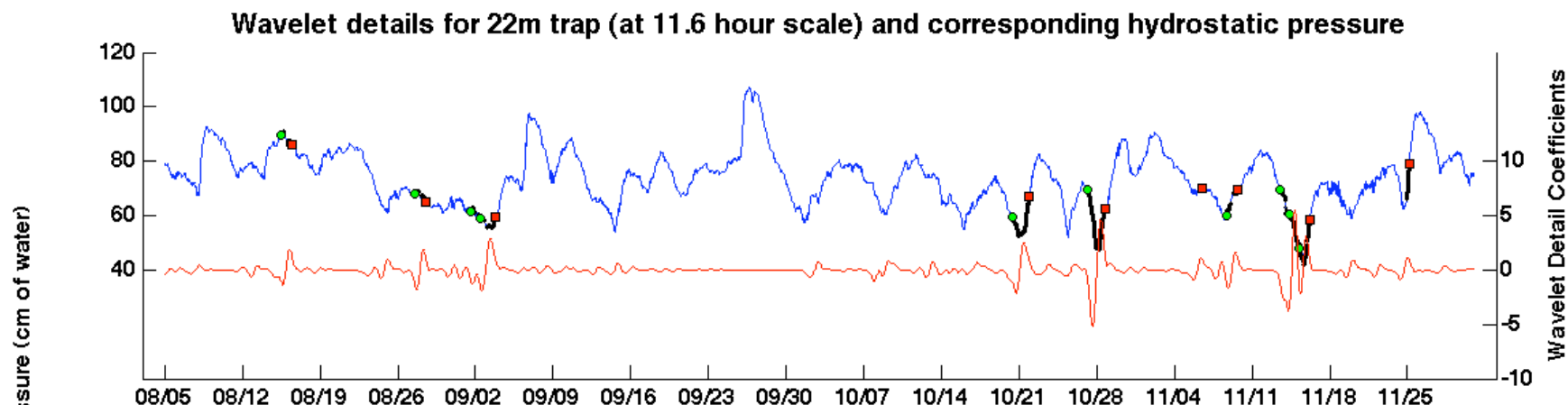
Wavelet details for 19m trap (at 11.6 hour scale) and corresponding hydrostatic pressure



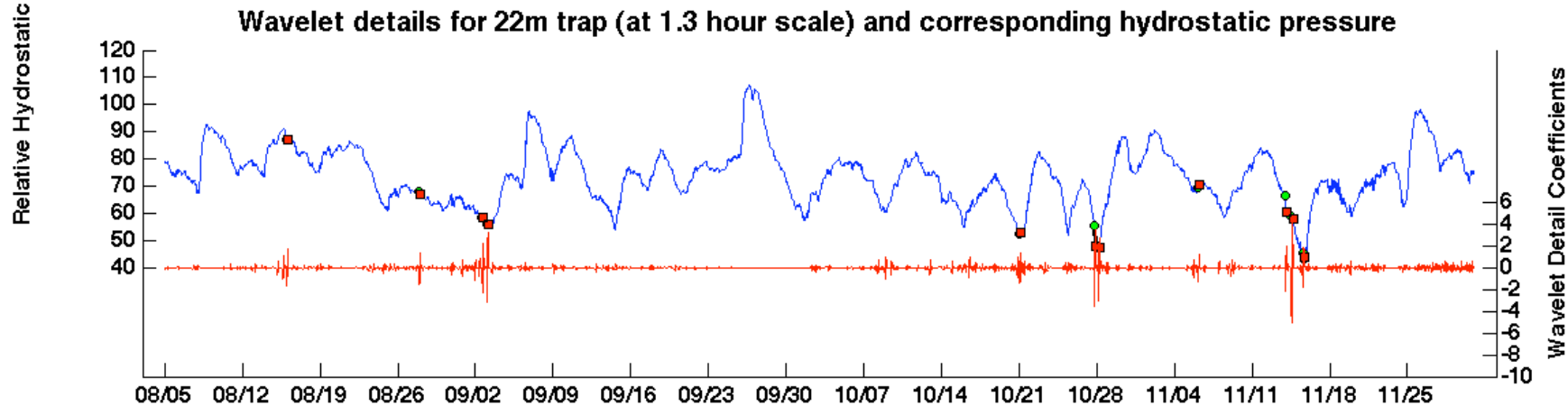
Wavelet details for 19m trap (at 1.3 hour scale) and corresponding hydrostatic pressure

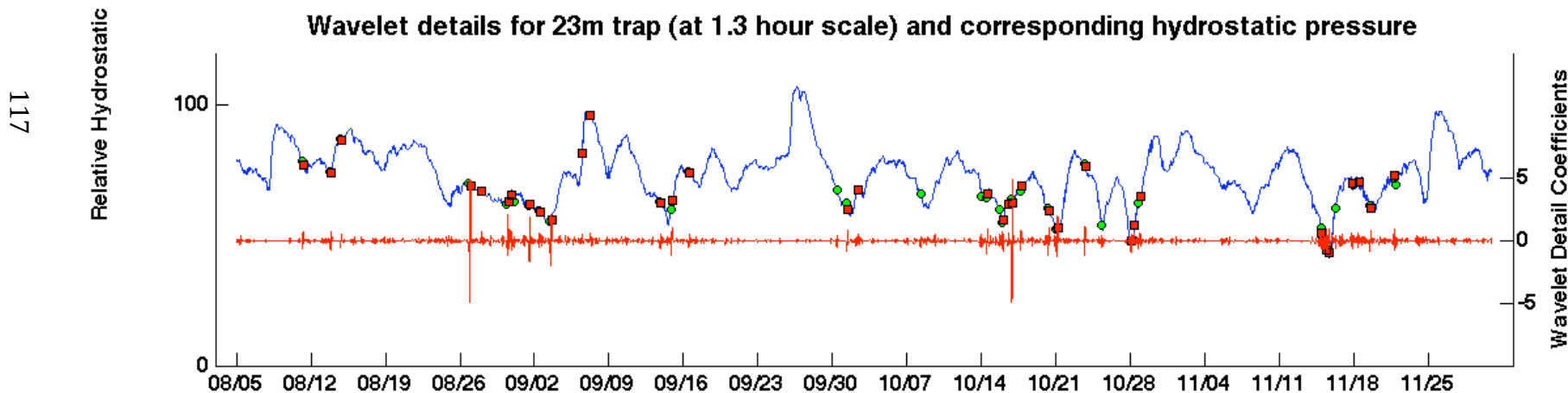
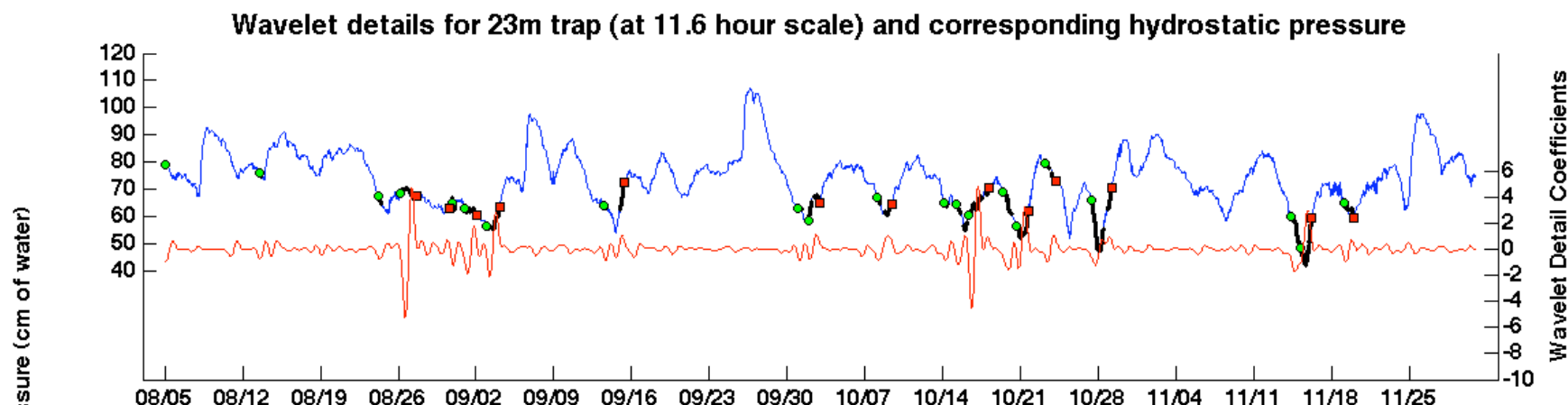






911





Chapter 4: Methane export from a eutrophic, temperate, freshwater lake

1. INTRODUCTION

Recent studies have found that atmospheric methane emissions from freshwater lakes have been underestimated in the past (Bastviken et al. 2004, Walter et al. 2007). Methane produced in lakes is released to the atmosphere through ebullition, diffusion through the air-water interface at the lake surface, and transport through emergent vegetation (Rudd and Taylor 1980). Of these, bubbling is typically the dominant pathway for export (e.g. Casper et al. 2000, Walter et al. 2006), but it has not been well quantified due to the difficulty in measuring its spatial and temporal heterogeneity. Prior estimates of methane bubbling from lakes have typically been based on a limited set of measurements conducted over short periods (e.g. Bastviken et al. 2004, Keller and Stallard 1994). Many studies that measured the sum of diffusive and ebullitive fluxes used floating chambers at the lake surface, and had to separate the fluxes by further analysis (e.g. Miller and Oremland 1988, Smith and Lewis 1992).

The main objective of this paper is to quantify methane emissions to the atmosphere from a small, seasonally stratified, eutrophic temperate lake situated in an urban watershed. Methane bubbling and air-water exchange were monitored for 13 months over two years at the Upper Mystic Lake in Woburn, Massachusetts. In particular, intensive measurements of ebullition were conducted in order to account for its temporal and spatial variation. This study did not consider efflux from emergent aquatic vegetation, which were a negligible part of the total lake surface.

2. METHODS

2.1 Study site

The Upper Mystic Lake (UML) is a eutrophic, dimictic, kettlehole lake situated in eastern Massachusetts, north of Boston. It has a total surface area of 0.58 km^2 , and a total volume of 6.8 million m^3 . The maximum depth at the center is 25 m; the average depth of the lake is 15 m, with sharp gradations present near the edges. A spillway at the southern end limits the maximum water level at the lake.

The lake typically stratifies into two layers in early summer around May, and this effect intensifies through the summer and fall (Figure 1). The temperatures near the sediments are at $\sim 4^\circ\text{C}$ for most of the year. Vertical turnover occurs around November or December, which typically results in a uniformly oxygenated isothermal water column (Aurilio et al. 1994, Spliethoff 1995). The lake freezes during the winter, when it stratifies again. Ice melt followed by spring overturn generally occurs between mid and late March.

High methane concentrations are typically present in the hypolimnion and sediments of the UML. The dissolved methane content in the hypolimnion was previously measured to increase steadily from $\sim 200 \text{ }\mu\text{M}$ in August to $\sim 700 \text{ }\mu\text{M}$ in November (Peterson 2005). The average porewater concentration of methane in a 1 m long freeze core collected on September 2008 from a site 20 m deep was $4\pm0.8 \text{ mM}$ (methods and results presented in Chapter 5).

The organic matter content of the top meter of the sediments is between 20 and 40% of dry weight (Spliethoff and Hemond 1996, Chapter 5). The lake is also nitrogen rich; nitrate concentrations of up to $150 \text{ }\mu\text{M}$ and ammonium concentrations of up to $400 \text{ }\mu\text{M}$ in the hypolimnion have been previously reported (Peterson 2005, Senn 2001).

2.2 Ebullition flux measurements

Bubbling fluxes were measured by means of submerged funnel traps, which are described in detail in Chapter 2. Briefly, a trap contains a 0.5 m diameter cone linked to a transparent PVC pipe that functions as a gas collection chamber. Gas can be withdrawn from the trap using syringes through a valve at the top of the pipe. The volume of gas can be manually measured by either reading the height of the gas column in the transparent pipe, which was marked in 1 cm intervals, or from the total volume of gas collected in the syringes. Both measurements were collected during field sampling, and the results were averaged. The traps were attached to floats and were suspended at depths of ~ 1 m from the water surface.

In 2007, eleven traps were deployed from mid July-November (Figure 2(a)). The traps were manually sampled once every 3 to 14 days until Nov 30th. Seven traps were left at the lake over the winter; however only two were found in position after ice-melt the following April, while the remaining five traps were found stranded on the shore. In 2008, weekly manual sampling was conducted from April to November. The locations of the traps were the same as in 2007, excepting for the 23 m and 25 m sites (Figure 2(b)). Two additional traps were deployed in September ~15 to 30 m from the original 9 m site.

From June to December 2008, several traps were equipped with pressure sensors that could automatically measure the volume of gas collected. With these devices, bubbling fluxes, along with hydrostatic pressure at the lake, were measured at a resolution of 5-10 minutes. The data recorded by the automated traps and their analyses using statistical and wavelet methods are presented in Chapter 3.

Volumetric trap fluxes ($\text{ml.m}^{-2}.\text{d}^{-1}$) were calculated by dividing the total volume of gas accumulated in the trap by the cone base area (0.2 m^2) and the sampling time interval. The lake

surface was divided into polygons that were graphically determined such that each point on the surface was represented by the trap closest to it. Total ebullition flux from the lake was calculated by multiplying individual trap fluxes by the fraction of the lake surface represented by their corresponding polygons. Six different polygon configurations were used to account for different trap deployment times over the two years (e.g. Figure 3, Appendix Table 2). However, there were times when some trap data were unavailable because the traps had been removed briefly for maintenance, or had moved due to possible storm or human activity, or because samples had been compromised during collection. These occasions occurred for 25 out of a total of 611 individual trap measurements; in these cases fluxes for the corresponding polygons were estimated using flux density data from the adjacent polygon that best matched their previous bubbling patterns.

2.3 Bubble gas concentration measurements

Gas samples collected in syringes were stored underwater, and analysis commenced within 24-48 hours of collection. Laboratory tests of samples and standards stored underwater in glass syringes showed ~1-3% leakage after 7 days. Methane content was measured using a flame ionization detector gas chromatograph (Perkin Elmer 3920B) fitted with a 6-foot long, 1/8" diameter molecular sieve 5A packed column. Helium was used as a carrier gas; from August 2008 experiments were done with a carrier flow rate of 20-25 ml/min and a column temperature of 120°C. Prior to August 2008, the carrier flow rate was ~30 or 35 ml/min at corresponding column temperatures of 90 or 60°C. Calibration was done independently for each experiment using 19.04% (from Aug 2008) and 100% CH₄ standards (Airgas). FID peak heights were recorded with a strip chart recorder (Perkin Elmer 056).

Methane, oxygen, nitrogen and carbon dioxide were also measured simultaneously using a thermal conductivity detector gas chromatograph (F&M Scientific Corporation, Avondale, PA) containing a 6-foot long, 1/8" diameter molecular sieve 5A and 5-foot long, 1/8" diameter Hayesep-C packed columns. Helium was used as a carrier at a flow rate of 15-20 ml/min for the former and 45-60 ml/min for the latter column; both columns were used at room temperatures. In 2007 peak heights were recorded using a chart recorder (Perkin Elmer 056), and in 2008 peak areas were quantified using an integrator (Hewlett-Packard, HP3394A). Oxygen and nitrogen were calibrated with ambient air, while CO₂ was calibrated using a 1% standard (Scotty Transportables). Starting Aug 2008, a 20.16% standard (Airgas) was also used for nitrogen calibration, and a 5% standard (Matheson Portables) was used for oxygen calibration. The additional standards were used to verify the accuracy of calibrations, and fit well to the previous instrument calibration curves. Calibrations were done independently for each experiment to account for the differences in experimental settings.

Only FID methane values were used due to their higher precision when compared with the methane measurements made on the TCD gas chromatograph. Nitrogen content was then determined by difference by assuming that bubbles only consisted of oxygen, nitrogen and methane; the TCD results were used as confirmatory evidence of the calculated nitrogen values.

2.4 Dissolved gas concentration measurements

Dissolved gas samples were collected approximately once a month using a slightly modified version of a sampling device described in Peterson (2005). The apparatus consisted of a 50 ml gas-tight glass syringe fitted with a plastic Luer-lok™ valve into which sample is drawn. This sampling system preserved anoxia and minimized losses caused due to depressurization of gases while bringing the sample to the surface. The syringe barrel was clamped to a second 50

ml syringe filled with water that was connected via tubing to a peristaltic pump operated from the boat, and served as a hydraulic operator.

Sample syringes were prefilled with 2-4 ml of milli-Q water to completely flush out air from the syringe tip and luer lock valve. This also served to wet the syringe plunger to ensure smooth motion during sample collection as well as prevent gas leakage. The luer lock valves were washed thoroughly and dried in a chemical hood for several days before sampling to purge methane that could possibly have been trapped in the valve. Samples were stored underwater in ice to limit losses caused due to leakage and methane oxidation. Samples were acidified to pH 2 for preservation immediately after return to the laboratory, and were analyzed within 24-48 hours of sampling.

The analysis was done using a routine headspace equilibration with helium (Swinnerton et al. 1962, Campbell and Vandegrift 1998). Methane partitioned into the headspace was analyzed with an FID gas chromatograph using the same procedure followed for bubble gas analysis. Standards of 100 ppm, 500 or 1000 ppm, and 1% or 4% methane (Scotty Transportables and Matheson Trigas Portables) were used to calibrate for different concentration ranges. Sample volumes were measured from the difference between the weights of sample syringes and empty syringes; volume readings from the syringe barrels were 1-2 ml lower than the volumes measured by weight. It was assumed that the weighed volumes were more accurate, since the 50 ml syringes only had 2 ml graduations. The difference between the two water volume measurements was also applied to headspace volumes.

Dissolved gas concentrations (C_w in μM) were calculated as:

$$C_w = P \left(\frac{V_a}{V_w RT} + K_H \right) * 10^6 \quad (1)$$

where P = Partial pressure of methane in syringe headspace (atm) as measured from the FID peak heights

V_a = Headspace volume (ml)

V_w = Sample volume (ml)

$R = 0.0821 \text{ L.atm.mol}^{-1}\text{K}^{-1}$

K_H = Henry's constant at 25°C = 0.00129 M.atm⁻¹ (Morel and Hering 1993)

T = Laboratory temperature (K)

The analysis errors in dissolved gas concentrations were calculated by including the standard errors from the multiple GC injections, errors in measurement of headspace and water volumes, as well as the standard errors of duplicate samples. In 2008, laboratory pressures and temperatures were measured at the time the experiments were conducted. Lab temperatures were not constant during the course of an experiment and could vary from anywhere between 21 and 25°C. All concentrations were calculated at 25°C; the error in concentrations that might result from assuming this temperature would be less than 2%. Measured atmospheric pressures were used to calculate concentrations in 2008. 2007 concentrations were calculated using 1 atm pressure; the possible error from using this value is approximately 1%.

2.5 Surface air-water gas exchange calculations

Air water exchange fluxes at the lake water surface ($F_{a/w}$) were calculated using the dissolved gas concentrations at the surface (C_{w0}) as:

$$F_{a/w} = k(C_{w0} - p_a K_H) \sim kC_{w0} \quad (2)$$

where p_a = concentration of methane in the atmosphere (1.8 ppm), and

k is a “piston velocity” that is calculated by combining equations from Jahne et al. (1987) and Kanwisher (1963) as:

$$k(cm/s) = \left(\frac{Sc(T)}{600}\right)^a k_{600} = \left(\frac{Sc(T)}{600}\right)^a (4 * 10^{-4} + 4 * 10^{-5} u_{10}^2) \quad (3)$$

where $Sc(T)$ is the Schmidt number for methane at surface water temperature T

u_{10} = wind speed (m/s) at 10 m above the lake surface

$a = -2/3$ for $u_{10} < 5$ m/s, $a = -1/2$ for $u_{10} \geq 5$ m/s

Daily averaged wind data for the two-year period was obtained from a weather station that was approximately a mile from the lake (Turkey Hill, Arlington Heights). The data was compared to wind speeds measured on 36 days in 2008 at 1 m above the lake surface using an anemometer (Model no. 034B, Met One Instruments) installed on a buoy attached to a datalogger (Campbell, CR 10). Wind speeds at the UML were estimated from the weather station data as ($R^2=0.7$):

$$u_{UML,1m}(m/s) = u_{station}(m/s) + 0.5 \quad (4)$$

Wind speed from the lake surface was converted to wind speed at 10 m using the following equation from Mackay and Yeun (1983).

$$u_{10} = \left(\frac{10.4}{\ln z + 8.1} \right) u_z \quad (5)$$

2.6 Other measurements

Particulate organic matter deposition was measured at five locations (9m(A), 12m, 13m, 22m, 23m sites) using sediment traps suspended near the lake bottom. The traps were constructed as described in Benoit and Hemond (1990). Briefly the traps consisted of a ~10 cm diameter PVC pipe attached to a funnel. The pipe was tightly filled with ~10 cm long plastic drinking straws that were held in place by friction. A 100 ml Nalgene bottle, which could be screwed on to a cap that was glued to the bottom of the funnel, was used to collect settling

organic matter. Particulate matter harvested from the trap was analyzed using the loss on ignition method. Samples were filtered onto a glass fiber filter (VWR Scientific), dried at 60°C for 24 hours and combusted at 375°C in the presence of air for 24 hours. POM content (as % dry weight) was calculated as the difference between the post-combustion weight and the dry weight.

Temperature, dissolved oxygen, pH and conductivity profiles of the lake were collected using submersible Hydrolab MiniSonde probes, as outlined in Chapter 5. The electrodes were calibrated using standard solutions within 24 hours prior to field measurement.

Hydrostatic pressure was calculated as the sum of average daily atmospheric pressures obtained from the Turkey Hill weather station and interpolated lake water levels (water level sampling interval ~ 3-14 days). Water depths at trap sites were measured in both years using an acoustic depth finder.

3. RESULTS

Considerable spatial and temporal variation in ebullition fluxes was observed, both in 2007 and in 2008 (Figure 4). Ebullition fluxes at different sites ranged from 0 to 228 ml.m⁻².d⁻¹ in 2007, and from 0 to 253 ml.m⁻².d⁻¹ in 2008 (Table 1, Appendix Table 3). Fluxes measured in 2008 were smaller than those in 2007 by about a factor of 2 (Figure 5). Long-term average fluxes at sites located very close to each other (9m(A), (B) and (C)) were similar for their common period of deployment (Sep-Dec 2008); however the timing of large bubble episodes varied considerably between the three sites (Table 2).

In 2007, more bubbling was seen in mid July-September than in October and November. However, this trend was not repeated in 2008, where fluxes peaked in October. Winter fluxes were only measured at three deep sites in 2007 and were small (1 to 6 ml.m⁻².d⁻¹). Flux errors

were calculated from the standard deviation (1σ) of volume readings obtained from the syringe and pipe measurements, and were small (0 to $10 \text{ ml.m}^{-2}.\text{d}^{-1}$).

The composition of collected varied spatially and temporally, with higher methane concentrations being present at locations having higher fluxes (Table 1, Figure 6). The bubbles mainly consisted of methane and nitrogen; a small amount of oxygen was also present, while carbon dioxide concentrations were below detection limits (<<1%) (Figure 7). The mixing ratio of methane in the trapped gas ranged from ~ 30% to 90% (Appendix Table 4). Calculated errors ranged from 1 to 3% methane, and include standard errors from syringe replicates as well as from multiple GC injections. Oxygen concentrations of most samples varied from 0.2 to ~ 5% (Appendix Table 5).

The measured gas concentrations are similar to previous observations of bubble gas content in freshwater lakes (e.g. Casper et al. 2000, Keller and Stallard 1994). In addition, the oxygen values were compared to the results obtained from the SiBu-GUI bubble dissolution model (Greinert and McGinnis 2009, McGinnis et al. 2006) that was used as described in Chapter 5 (Section 5.3) to estimate the extent of gas diffused across the air-water interface of a single bubble rising through the water column. The model was used for typical bubble radii of 1-5 mm, as is observed in other aquatic systems (Ostrovsky et al. 2008, Rehder et al. 2002). Other inputs to the model included an initial gas composition of 100% methane, a bubble release depth of 20 m, and the actual temperature and dissolved gas profiles from the UML in September 2008 (Figures 1(b) and 8(b)). The observed oxygen concentrations were generally consistent with the values predicted by the model (Table 3); however at times the observed concentrations were slightly lower (by ~1-2%) than the model results.

Volumetric bubbling fluxes were multiplied by the methane content of each sample for the corresponding time period to obtain an estimate for the methane bubbling flux density for each individual trap measurement (Appendix Table 6). This varied from 0 to 8.6 mmol CH₄.m⁻².d⁻¹ over the two years for the different sites (Table 1). The site-specific average gas content was used for dates when bubble composition data were not available, which includes 13 occasions where samples were compromised due to mishandling of the syringes or traps during field collection or transport. Methane concentrations measured on samples obtained when the traps were over-full were discarded due to the possibility of excessive methane diffusion into the water column. The oxygen content of the compromised and over-full samples was often high (~5-20%), indicating contamination by air. The gas content of samples less than 3 ml was also not used, since these samples could not be run on the TCD to measure the oxygen values to test for leakage. These substitutions would not have affected total flux estimates, which were found to be insensitive to small differences (at least 5%) in methane content. Syringes that had significantly higher oxygen values (by ~2% or more) as well as lower methane values (by ~5% or more) compared to replicates were presumed to have been subject to leakage and were discarded from analysis.

The total ebullition between sampling dates was calculated by multiplying the methane flux at each site by its representative polygon area and the length of the sampling interval. This was divided by the total period of measurement (134 days in 2007 and 229 days in 2008) to estimate season-long ebullition fluxes from the UML, which were 0.8±0.1 mmol CH₄.m⁻².d⁻¹ from mid-July to November 2007 and 0.5±0.02 mmol CH₄.m⁻².d⁻¹ from April to November 2008. This amounts to a lakewide ebullitive release of ~8 kg/d in 2007 and ~4.5 kg/d in 2008.

Calculated methane flux errors were usually between 0 and 0.2 mmol CH₄.m⁻².d⁻¹, and only included errors from volume readings and methane content measurements.

Methane concentrations in the hypolimnion steadily increased over the summer and fall (Figure 8, Tables 1 and 2 in Chapter 5). Epilimnion concentrations were one to two orders of magnitude smaller (inset, Figure 8), but were always supersaturated with respect to atmospheric concentrations. Concentrations in the upper mixed layer slowly increased from April to October but decreased in November. The average diffusive flux across the air-water interface was 0.3±0.1 mmol CH₄.m⁻².d⁻¹ for July-November 2007 and 0.2±0.1 mmol CH₄.m⁻².d⁻¹ for April-November 2008 (Table 4). It is unlikely that diffusive fluxes were higher than the calculated values during periods between sample collections prior to fall turnover, since surface concentrations changed slowly for the entire period of measurement and wind speeds were not highly variable. The average estimated wind speed at the UML was 1.5 ± 0.5 m/s (1 σ) from April to November 2008, and was 1.2 ± 0.4 m/s from July to November 2007.

4. DISCUSSION

4.1 Temporal variability in ebullition fluxes

Bubbling occurred in a highly episodic manner in both 2007 and 2008. The automated trap data collected from August to November 2008 showed that synchronous lake-wide ebullition episodes were triggered when hydrostatic pressures fell below a site-dependent threshold (Chapter 3). An examination of the low-resolution manual flux measurements shows that high ebullition fluxes also occurred during two periods of notably low hydrostatic pressure during 2007 (Figure 9(a)). No particular seasonal trend was detected for either year (Figure 9). Winter fluxes were low in 2007 for three sites (20 m, 22 m and 23 m) that had been

representative of the average bubbling at the lake during summer and fall. However, these fluxes could have been significantly underestimated as they were based on only one observation in each of three traps.

Ebullition fluxes in 2007 were about 2 times larger than in 2008. It is unlikely that the observed variation could be caused due to slight differences in mooring location between years or trap movement around the buoy watch circle (circle radius \approx lake depth at site), except possibly at the 23 m and 25 m sites that were at locations \sim 70 m apart over the two years. The spatial variation expected around a watch circle was tested using three traps at the 9 m location situated about 15-30 m apart from each other; these had similar average bubbling fluxes over three months (Table 2). Moreover, the spatial patterns of ebullition are similar across both years; sites that bubbled the most in 2007 also had high fluxes in 2008 and vice versa.

Lower lake water levels in 2007 might have caused the higher bubbling fluxes observed in that year, as compared to 2008 (Figure 10). Due to the loss of an absolute reference, there could have been as much as 10 cm uncertainty between the water levels measured in 2007 and 2008. However, even with this possible error, there were clearly two periods in 2007 (Aug 7th – Sep 9th, Sep 13th – Oct 13th), where the water level was low relative to the season average, as well as being \sim 10 to 20 cm lower than the lowest water levels of 2008. The Turkey Hill weather data also show that precipitation between August-October was \sim 7 times lower in 2007 than in 2008. Approximately 70% of the ebullition between July and November 2007 occurred during these periods (Figure 9(a)), which could account for the large difference in fluxes between the two years. Similar inter-annual variations in ebullition were observed when the level of L. Kinneret dropped by 1-2m (Eckert and Conrad 2007).

While changes in methanogenesis rates might also have caused bubbling fluxes to vary between the two years, it seems unlikely that this could cause a factor of 2 difference in bubbling. The bottom waters of the UML were at nearly constant temperature and were anoxic for most of the year. The organic matter content of the sediments was high, and hence methanogenesis would probably not have been limited by substrate availability. The extent of the sediment reservoir is estimated in Section 6.4 of Chapter 5; given the concentrations of methane measured in the top 1 m of the UML porewaters ($\sim 4\text{mM}$), it was found that it would take ~ 1000 to 3000 days to exhaust the reservoir. This indicates that the sediment storage in the UML is potentially large enough to support the observed factor of 2 differences in bubbling. The large year-to-year variability also highlights the need for continuous, long-term monitoring of ebullition fluxes at similar field sites.

4.2 Spatial variation in ebullition fluxes

The reasons for the observed spatial variations are unclear. Previous studies have found that fluxes could be correlated either positively or negatively with the depth of the water column at the trap site (e.g. Casper et al. 2000, Keller and Stallard 1994, Walter et al. 2006). No strong pattern emerged between bubbling fluxes and lake depth or particulate organic matter (POM) deposition rates at the UML trap locations (Appendix Figure 1). However, in general, the deep, central locations tended to bubble more than the shallow sites near the shore; the exceptions to this were the 9 m and 13 m sites that were located near the river inflow at the northern end of the lake. The lack of correlations with depth or POM fluxes might not be significant, given the limited number of bubble and sediment traps that were deployed. It is also possible that the observed spatial variation was a result of the differences in organic matter accumulation rates caused due to bathymetry and water currents. The sites with the lowest fluxes were typically

located near the shore, where the slope of the lake bottom was relatively high. Settling organic matter at these sites may have had a greater tendency to be resuspended and transported to deeper locations.

4.3 Variations in bubble gas content

Methane concentrations in trapped gas were strongly correlated with long-term average bubbling fluxes at the different locations (Figure 6). Thus, nitrogen concentrations were negatively correlated with average fluxes, since the bubbles mainly consisted of methane and nitrogen. Chanton et al. (1989) also observed an inverse relationship between the nitrogen content of bubbles and ebullition fluxes at the White Oak River estuary, North Carolina, and proposed that this was a result of bubble stripping of porewater nitrogen, assuming that the bubbles were at equilibrium with the sediment porewaters. However, seasonal variations in nitrogen concentrations were also observed at the White Oak River, and it was hypothesized that such changes occurred due to the replenishment of nitrogen in the sediments by molecular diffusion.

At the UML, trapped gas compositions appeared to vary temporally, and could significantly change within a few weeks (Figure 11). However, it is possible that some of this variation was caused due to leakage of air into the syringes. While the typical oxygen content of trap samples was around 0.5-2%, measured oxygen concentrations could at times be as high as 5-10%. If the oxygen in the sample were a result of air leakage, then the methane concentrations would be low due to the additional nitrogen present in the sample. Some gas might also have diffused across the air-water interface in between trap samplings (based on the leak test described in Section 3.4 in Chapter 2), and this possibility needs further investigation.

However, variations of ~10-40% methane occurred within a period of 1-2 weeks for several samples where the oxygen concentrations were < 1% (Figure 11). Based on the oxygen content, the maximum possible magnitude of error in the methane mixing ratio due to leakage in this subset of samples is less than 5%, and thus cannot wholly account for the observed variation in bubble methane concentrations. Another possible explanation is that the temporal changes in methane content of bubbles intercepted by the traps were actually caused due to trap movements in their watch circles. However, it seems unlikely that this would result in large differences in methane content, given that the long-term average concentrations at sites located close to each other (e.g. the 9m traps, and the deep traps) varied by ~5-20%.

It is also unlikely that short-term temporal variations in porewater nitrogen can occur at the relevant time scale of 1-2 weeks. The amount of nitrogen produced through denitrification is relatively small, given that observed nitrate concentrations in the UML were in the vicinity of 150 μM . Even if one assumes that all 150 μM of nitrate was involved in near-instantaneous denitrification, it would result in a negligible 0.1 atm increase in the partial pressure of nitrogen. Alternatively, if porewater nitrogen were to be replenished by sediment-water exchange, then it would take approximately 7-8 months for the nitrogen from the water column to diffuse through, for example, a path length of 20 cm in the sediments.

An alternate hypothesis is that short-term changes in gas content are caused due to variations in travel times of bubbles rising in the water, leading to different rates of methane dissolution into the water column. The SiBu-GUI model indicates that significant amounts of oxygen and nitrogen could actually be present in the bubbled gas, if bubble radii were less than 2 mm (Table 3). However, no measurements of bubble sizes at the UML were available to test this hypothesis.

The gas compositions over a sampling interval are only weakly related to the magnitude of ebullition observed during that time. The methane content of the bubbles was significantly correlated with the volumetric bubbling fluxes measured in 2008 in 6 out of 8 traps ($R^2=0.2$ to 0.5, $p<0.05$). However, none of the correlations were significant (i.e. $p>0.05$), when the fluxes were multiplied by the length of the sampling interval. It is possible that diffusive exchange between trapped gas and the water column, although small, is a contributing factor in the correlations. The relationship between bubble gas content and short-term fluxes needs to be further examined, based on the data from the automated traps.

4.4 Diffusive air-water exchange from the lake surface during fall and spring turnover

Concentrations of dissolved methane in the hypolimnion were much lower in April '08 than in November '07; this corresponds to a loss of ~400 kmol (6400 kg) of methane during the lake turnover. The fall and spring turnover periods have been previously shown to involve high rates of methane oxidation (e.g. Kankaala et al. 2007, Utsumi et al. 1998) or surface air-water exchange (Michmerhuizen et al. 1996, Phelps et al. 1998). At the UML, the lowest calculated rate of diffusive air-water exchange of methane for the entire measurement period was observed in November 2007 and 2008 during the approach to fall turnover. These values were small due to low methane concentrations in the surface water. Despite the rapid erosion of the thermocline and oxycline in the last 2 weeks of November 2007 (Figure 1), the surface water methane concentration measured on November 14th 2007 was only 0.2 μM , and was similar to that measured on November 30th 2007 (0.3 μM). The average wind speed in November 2007 (1.4 \pm 0.6 m/s) was close to the average wind speed for the rest of the measurement period.

A decrease of approximately 50 (± 30) kmol of methane occurred between November 14th and November 30th; however a significant amount of methane was still dissolved in the

hypolimnion on November 30th 2007 (~630 kmol, Figure 8(a)). The possibility that a large pulse of methane could have been released to the atmosphere after the last sampling date in 2007s, prior to freezing of the lake surface, cannot be ruled out. While ice cover probably prevented air-water exchange for ~3 months of the year following the fall turnover, some methane present in the hypolimnion could also have been released to the atmosphere during the period after ice melt during spring overturn.

5. SUMMARY AND CONCLUSIONS

The sum of diffusive and ebullitive fluxes at the UML was $1.1 \pm 0.1 \text{ mmol CH}_4.\text{m}^{-2}.\text{d}^{-1}$ in 2007 and $0.7 \pm 0.1 \text{ mmol CH}_4.\text{m}^{-2}.\text{d}^{-1}$ during the sampling period of 2008. Thus ~6 to 11 kg/d of methane was released to the atmosphere from the Upper Mystic Lake during the study periods of 2007 and 2008. Of this, approximately 70% of the methane escaped through ebullition (Table 5). By contrast, the decrease in methane storage in the water column during late fall and winter is about 2-3 times greater than the measured annual release through ebullition and diffusion across the air-water interface. Thus the fall and spring turnovers could potentially be important periods of additional methane export to the atmosphere, if the hypolimnetic methane was lost by diffusion across the lake surface. However, the surface water concentrations of methane did not increase in November, suggesting that oxidation within the lake could account for much of this decrease in methane storage.

The total methane fluxes from the UML appear to be modest in comparison to emissions from other freshwater lakes (Table 6). However, several of these studies either involved 24-hour deployments of flux chambers conducted during summer and fall, or deployed very few traps; hence there could be significant error in the estimates of ebullition from their field sites. For

example, peak fluxes at the UML ($\sim 3\text{-}5 \text{ mmol CH}_4\text{.m}^{-2}\text{.d}^{-1}$) are similar to those observed during the 24 hour deployments at L. Priest Pot or L. Gatun ($\sim 3\text{-}12 \text{ mmol CH}_4\text{.m}^{-2}\text{.d}^{-1}$) (Casper et al. 2000, Keller and Stallard 1994). However, average fluxes were about an order of magnitude smaller than the peak daily fluxes. It is thus critical to monitor fluxes with a long-term and spatially dense measurement scheme to improve estimates of methane emissions from freshwater lakes.

6. TABLES

Table 1 – Summary of bubbling 2007 and 2008 at the UML

Table 2 – Spatial and temporal variation in fluxes at three traps located close to each other (at the 9m locations)

Table 3 – Final gas concentrations in a pure methane bubble rising through a 20 m water column, as predicted by the SiBu-GUI model

Table 4 – Methane diffused across the air-water interface at the lake surface in 2007 and 2008

Table 5 – Comparison of methane bubbling and air-water diffusive fluxes at the UML

Table 6 – Methane export from other freshwater lakes

TABLE 1 (a) Summary of bubbling in 2007. The methane content errors shown are standard deviations from temporal variations, and are not analytical errors.

Trap Name	Depth at site (m)	Sampling Period (2007)	Average flux [Flux Range] (ml.m ⁻² .d ⁻¹)	Methane content (%)	Methane bubbled [Flux Range] (mmol CH ₄ .m ⁻² .d ⁻¹)
6m	6.7	Jul 19-Nov 30	9 [0 to 47]	39 ± 8	0.2 [0.0 to 0.7]
9m(A)	8.5	Jul 19-Nov 30	62 [0 to 210]	75 ± 15	2.0 [0.0 to 6.6]
10m	9.4	Aug 16-Nov 30	4 [0 to 35]	41 ± 0	0.0 [0.0 to 0.3]
12m	12.8	Aug 16-Nov 30	1 [0 to 1]	22 ± 0	0.0 [0.0 to 0.0]
13m	11.6	Jul 19-Nov 14	36 [0 to 133]	62 ± 6	0.9 [0.0 to 3.7]
15m	12.8	Jul 19-Nov 30	2 [0 to 19]	43 ± 6	0.0 [0.0 to 0.4]
19m	19.8	Aug 17-Nov 30	34 [0 to 122]	64 ± 9	1.0 [0.0 to 3.5]
20m	~20	Jul 19-Apr 5 '08	29 [0 to 201]	63 ± 9	0.8 [0.0 to 5.2]
22m	21.6	Jul 19- Apr 5 '08	54 [1 to 228]	66 ± 7	1.5 [0.0 to 6.3]
23m	23.2	Aug 16-Apr 5 '08	61 [5 to 210]	65 ± 21	1.8 [0.0 to 6.6]
25m	24.7	Aug 16-Nov 30	43 [1 to 149]	74 ± 6	1.4 [0.0 to 4.8]

TABLE 1 (b) Summary of bubbling in 2008.

Trap Name	Depth at site (m)	Sampling Period (2008)	Average flux [Flux Range] (ml.m ⁻² .d ⁻¹)	Methane content (%)	Methane released (mmol CH ₄ .m ⁻² .d ⁻¹)
6m	6.5	May 11-Jun 5 Aug 5-Nov 9	4 [0 to 21]	38 ± 7	0.1 [0.0 to 0.4]
9m(A)	8.8	May 11-Dec 1	28 [0 to 188]	69 ± 14	0.8 [0.0 to 5.4]
9m(B)	8.4	Sep 8-Dec 1	50 [6 to 167]	62 ± 16	1.5 [0.1 to 6.2]
9m(C)	6.9	Sep 8-Dec 1	39 [0 to 253]	81 ± 7	1.3 [0.0 to 8.6]
10m	7.1	Jul 2 – Nov 9	0 [0 to 3]	Non detect	0.0 [0.0 to 0.0]
12m	13.3	Jun 12-Nov 14	2 [0 to 11]	46 ± 1	0.0 [0.0 to 0.2]
13m	10.4	May 11-Dec 1	23 [0 to 71]	56 ± 9	0.6 [0.0 to 1.9]
15m	15.8	Jun 12-Nov 14	2 [0 to 10]	49 ± 7	0.0 [0.0 to 0.2]
19m	21.3	May 23-Nov 14	12 [1 to 53]	67 ± 11	0.4 [0.0 to 1.7]
20m	20.3	Winter-Apr 22 Jul 30-Nov 14	10 [0 to 42]	62 ± 7	0.3 [0.0 to 1.1]
22m	23.4	Winter-Apr 22 Jun 19-Dec 1	14 [0 to 67]	63 ± 15	0.4 [0.0 to 2.1]
23m	22.9	Winter-Dec 1	19 [0 to 89]	65 ± 12	0.6 [0.0 to 3.0]
25m	25.0	Apr 5-Dec 1	24 [0 to 118]	71 ± 8	0.7 [0.0 to 3.7]

Table 2 Average fluxes ($\text{ml.m}^{-2}.\text{d}^{-1}$) at 3 sites located $\sim 15\text{-}30 \text{ m}$ away from each other were similar over a 3 month period (in 2008), even though the timing of episodes varied across sites. Flux measurement errors are negligible and are not shown.

Trap Name	Sep 8	Sep 13	Sep 19	Sep 22	Sep 25	Oct 2	Oct 8	Oct 13	Oct 15	Oct 23	Oct 31	Nov 9	Nov 14	Dec 1	Average
9m(A)	5	42	11	43	15	188	25	30	40	39	108	37	30	48	47
9m(B)	6	17	8	167	38	33	13	22	30	124	123	44	12	59	50
9m(C)	2	41	253	23	0	87	60	34	9	9	11	18	0	4	39

Table 3 Predicted final gas compositions of a single pure methane bubble rising through 20 m of water, as predicted by the SiBu-GUI model. Temperature and dissolved gas conditions used were from September 2008 in the UML.

Bubble Radius	Methane (%)	Nitrogen (%)	Oxygen (%)
1 mm	5.1	81.9	12.1
2 mm	62.2	32.8	4.2
3 mm	80.3	16.9	2.3
4 mm	86.6	11.4	1.5
5 mm	90.2	8.3	1.1

Table 4 Methane flux diffused out of the air-water interface from the lake surface ($\text{mmol CH}_4 \cdot \text{m}^{-2} \cdot \text{d}^{-1}$) in (a) 2007 and (b) 2008. Flux errors shown were calculated from the analytical errors in concentration measurements.

(a) Air water exchange in 2007

	Average concentration (uM)	Average wind speed (m/s)	Average temperature (C)	Flux (mmol CH ₄ .m ⁻² .d ⁻¹)
Jul 2 - Aug 2	0.6 ± 0.2	1.6 ± 0.4	25.6	0.4 ± 0.1
Aug 2 - Aug 17	0.5 ± 0.1	1.5 ± 0.3	27.2	0.3 ± 0.1
Aug 17 - Sep 23	0.6 ± 0.2	1.8 ± 0.3	23.8	0.4 ± 0.1
Sep 23 - Oct 15	0.9 ± 0.2	1.6 ± 0.3	20.3	0.4 ± 0.1
Oct 15 - Nov 14	0.6 ± 0.6	1.8 ± 0.6	15.8	0.3 ± 0.3
Nov 14 - Nov 30	0.2 ± 0.1	1.8 ± 0.5	11.6	0.1 ± 0.0
AVERAGE (JUL-NOV)	0.6 ± 0.3	1.7 ± 0.4		0.3 ± 0.1

(b) Air water exchange in 2008

	Average concentration (uM)	Average wind speed at 1m (m/s)	Average temperature (C)	Flux (mmol CH ₄ .m ⁻² .d ⁻¹)
Apr 10 - Jun 12	0.3 ± 0.3	1.7 ± 0.4	17.1	0.1 ± 0.1
Jun 12 - Jul 16	0.5 ± 0.1	1.4 ± 0.4	27.2	0.3 ± 0.1
Jul 16 - Aug 13	0.5 ± 0.2	1.3 ± 0.2	26.2	0.3 ± 0.1
Aug 13 - Sep 13	0.6 ± 0.3	1.3 ± 0.3	23.6	0.3 ± 0.1
Sep 13 - Oct 13	0.6 ± 0.3	1.3 ± 0.3	19.2	0.2 ± 0.1
Oct 13 - Nov 9	0.3 ± 0.1	1.6 ± 0.5	13.6	0.1 ± 0.0
AVERAGE FLUX (APR-NOVEMBER)	0.5 ± 0.2	1.4 ± 0.2		0.2 ± 0.1

Table 5 Proportion of methane released from the UML through bubbling and diffusive air-water exchange from the lake surface.

Period (2007)	Air Water Exchange (%)	Bubbling (%)
Aug 2 - Aug 17	44	56
Aug 17 - Sep 23	20	80
Sep 23 - Oct 15	36	64
Oct 15 - Nov 14	55	45
Nov 14 - Nov 30	22	78
Aug-Nov	29	71

Period (2008)	Air Water Exchange (%)	Bubbling (%)
Apr 10 - Jun 12	20	80
Jun 12 - Jul 16	58	42
Jul 16 - Aug 13	46	54
Aug 13 - Sep 13	42	58
Sep 13 - Oct 13	38	62
Oct 13 - Nov 9	14	86
Apr-Nov	33	67

Table 6 Methane fluxes from other freshwater lakes.

Fsur refers to traps suspended underwater just below the water surface, Fsed to traps near the lake bottom just above the sediments and FC to floating flux chambers. * At location of sampling

Study	Lake Sites	Lake area (km ²)	Max Depth (m)	Sampling Dates	No. of stations	Trap Type	Sampling procedure	Ebullition (mmol CH ₄ .m ⁻² .d ⁻¹)	A/W fluxes (mmol CH ₄ .m ⁻² .d ⁻¹)
This study	Upper Mystic Lake, Massachusetts, US (eutrophic)	0.58	25m	Jul 19 2007-Nov 30 2008	6 to 13	Fsur	Continuous measurements once a week (3-14 days) till Nov. Winter fluxes measured w/ n=3 left for 4 months	0.5 to 0.8	0.2 to 0.3
Walter et al. (2006)	L. Tube Dispenser	0.11	16.5	Apr 26 2003-Jun 1 2004	11	Fsur	Year round. Continuous daily over summer, few hours over winter	4.45	0.21
	L. Shuchi	0.06	11		14			3.64	0.24
Bastviken et al. (2004)	11 lakes, Wisconsin, US			Jun-Aug 2001	2 to 15	FC	3-24h measurements. Total 242 chambers		
	L. Brown	0.33	5.5	1-2 times				0.33	0.43
	L. Crampton	0.26	15.2	1-2 times				0.19	0.19
	L. East Long	0.02		1-2 times				0.6	0.35
	L. Hummingbird	0.01	7.6	4-12 times				0.3	0.22
	L. Morris	0.06	6.7	1-2 times				3.7	0.64
	North gate bog	.003	8	1-2 times				0.2	0.23
	L. Paul	.002		4-12 times				0.6	0.93
	L. Peter	.003		4-12 times				1	0.6
	L. Roach	.45	10	1-2 times				0	0.15
	L. Tuesday	.009	15	1-2 times				0.3	0.87
	L. Ward	.003	8.2	1-2 times				2.3	0.55

Study	Lake Sites	Lake area (km ²)	Max Depth (m)	Sampling Dates	No. of stations	Trap Type	Sampling procedure	Ebullition (mmol CH ₄ .m ⁻² .d ⁻¹)	A/W fluxes (mmol CH ₄ .m ⁻² .d ⁻¹)
Huttunen et al. (2001), Huttunen et al. (2003)	L. Postilampi, Finland (eutrophic)	0.03	4	Jul-Oct 1996,	7 to 8	Fsed, Fsur		2.6±0.3	
	L. Kevaton, Finland (eutrophic)	4.1	10	1997, 1998	3	FC		0.28 to 12 (total)	
	L. Vehmasjarvi, Finland (eutrophic)	0.41	19	1997, 1998	2 to 3	FC		0.11 to 0.35 (total)	
Casper et al. (2000)	L. Priestpot, UK (hypereutrophic)	.01	3.5	Jun-Oct 1997	7	Fsed	Duplicate traps left in situ for 24 hours, once a week	12.4	0.34
Nakamura et al. (1999)	L. Kasumigaura, Japan (eutrophic)	168	4*	Jul 29-Aug 3, Aug 24-Sep 1 1993	1	Fsur	Every day	7.4±6.1	0.03 to 1.75
Addess and Effler (1996)	L. Onondaga, New York (alkaline, eutrophic)	12	19	Apr-Oct 1989	1	Fsed, Fsur	Triplicate cones on 16 occasions, once every 3 days	4	2.3
Keller and Stallard (1994)	L. Gatun, Panama	NA	10*	Feb-Oct 1988 at various sites	3 to 5	Fsur	15 periods (total 28 days) lasting 12 - 60 hrs	3	
Mattson (1989)	L. Mirror, New Hampshire	0.15	11	1987-88	11	Fsed	Continuously every 2-6 days (including some winter sites)	0.09 to .32	~ 0.1
Crill et al. (1988)	Lago Calado, Brazil	1-2*	7-9*	Jul-Sep 1985	1	FC	Continuous sampling with automated chamber	0.6 to 6	0 to 2.1
Strayer and Tiedje (1978)	L. Wintergreen, Michigan (eutrophic)	0.15	6	Jun-Oct 1972 & 1973	6	Fsed	Weekly	23±2	10 to 46

7. FIGURES

Figure 1 – State of lake stratification in the UML

Figure 2 – Trap deployment in 2007 and 2008

Figure 3 – Polygon areas for the traps deployed during August to November 2007

Figure 4 – Ebullition fluxes for 2007 and 2008

Figure 5 – Spatial and inter-annual variation in ebullition fluxes for 2007 and 2008

Figure 6 – Average flux vs. methane content of bubbled gas at different sites

Figure 7 – Bubbled gas composition in 2007 and 2008

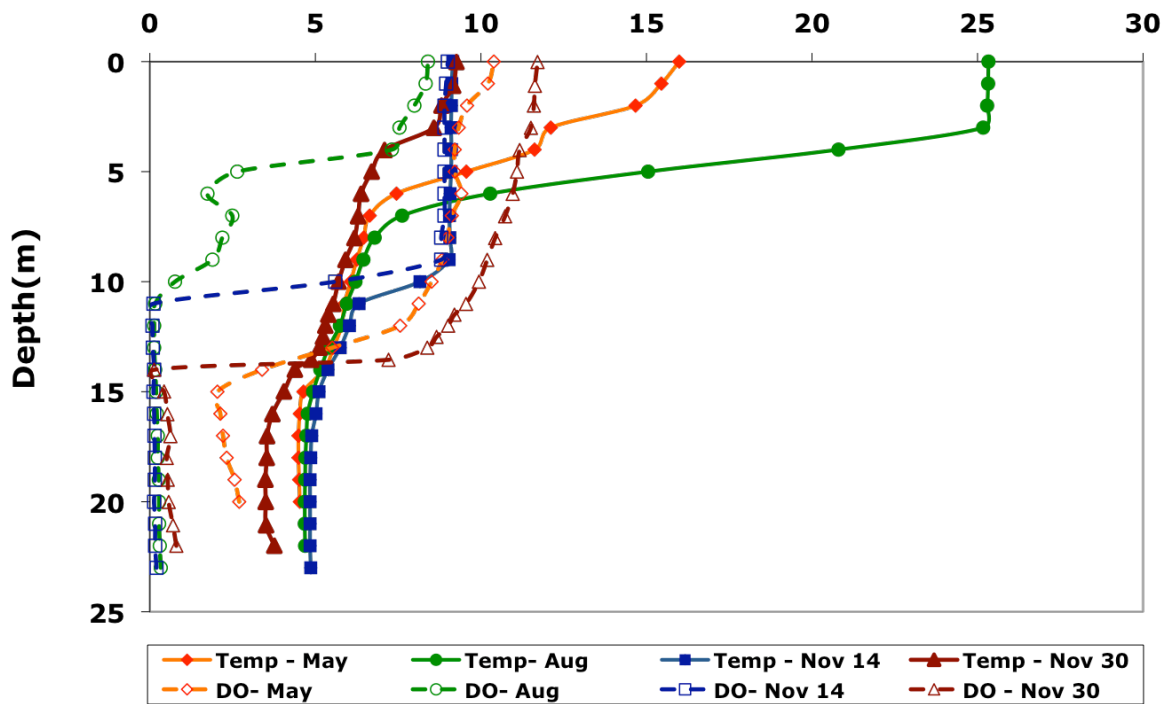
Figure 8 – Dissolved methane concentrations in 2007 and 2008

Figure 9 – Manual ebullition flux measurements versus hydrostatic pressure and water level

Figure 10 – Lake water levels in 2007 and 2008

Figure 11 – Temporal variations in methane content of bubbled gas

(a) 2007 - UML Temperature(C) / DO (mg/l)



(b) 2008 - UML Temperature(C) / DO (mg/l)

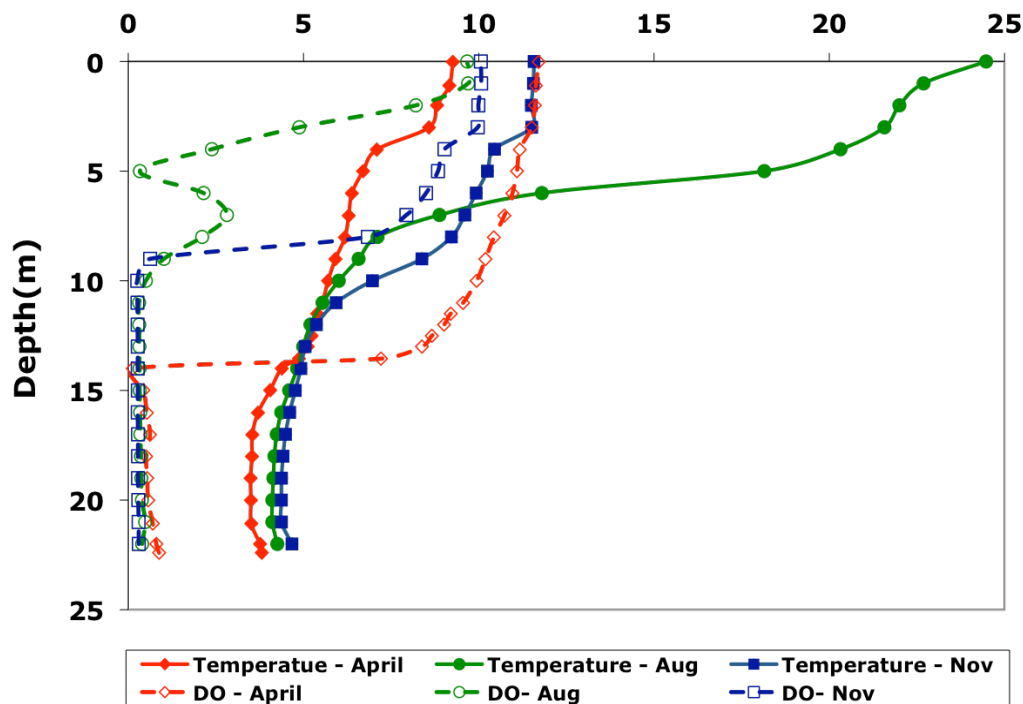


Figure 1 State of lake stratification in (a) 2007 and (b) 2008

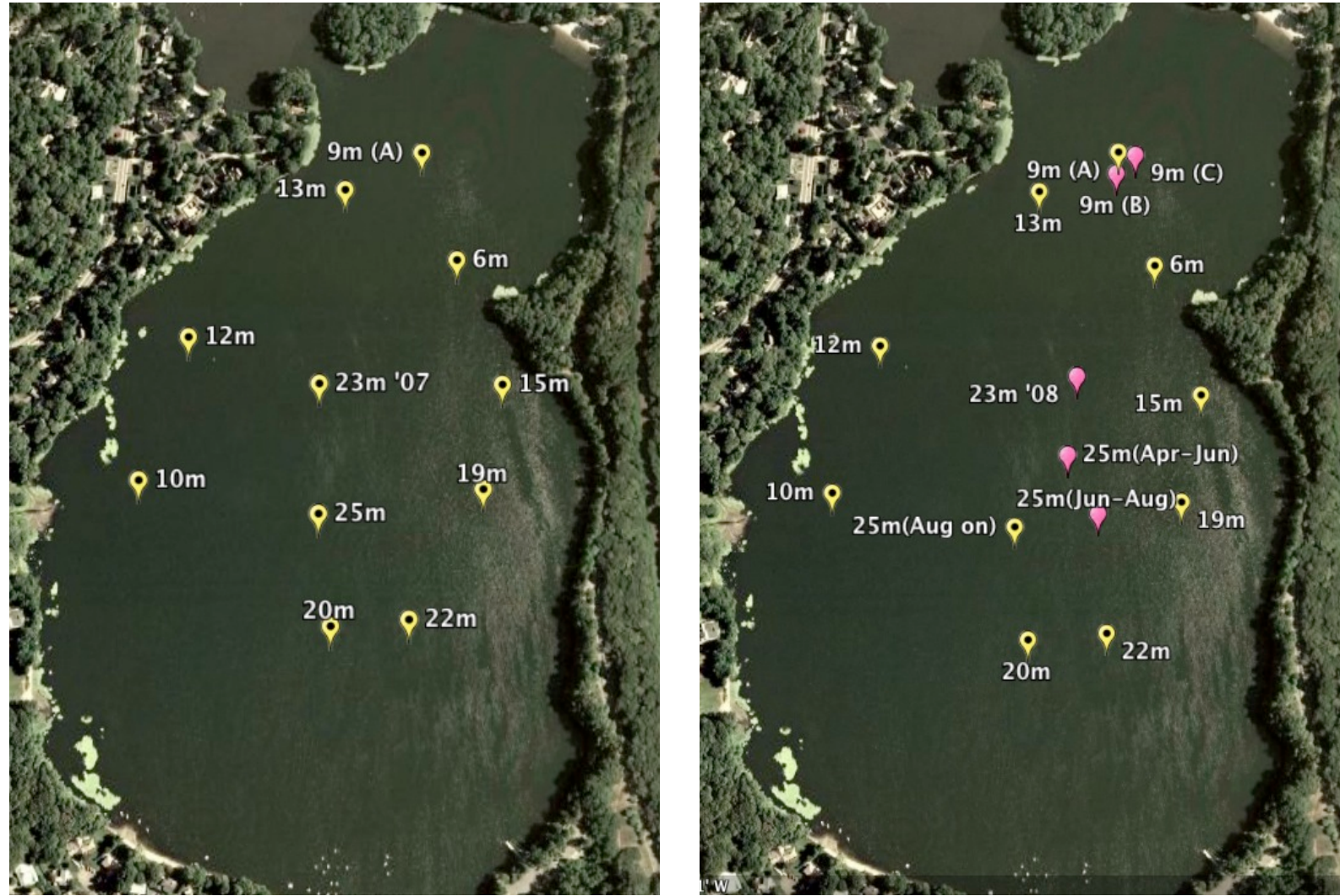


Figure 2 Trap deployment in (a) 2007 and (b) 2008. The locations were the same in both years except at the buoys without black dots (also colored pink). Trap names reflect the approximate depth of the water column at the deployment site.

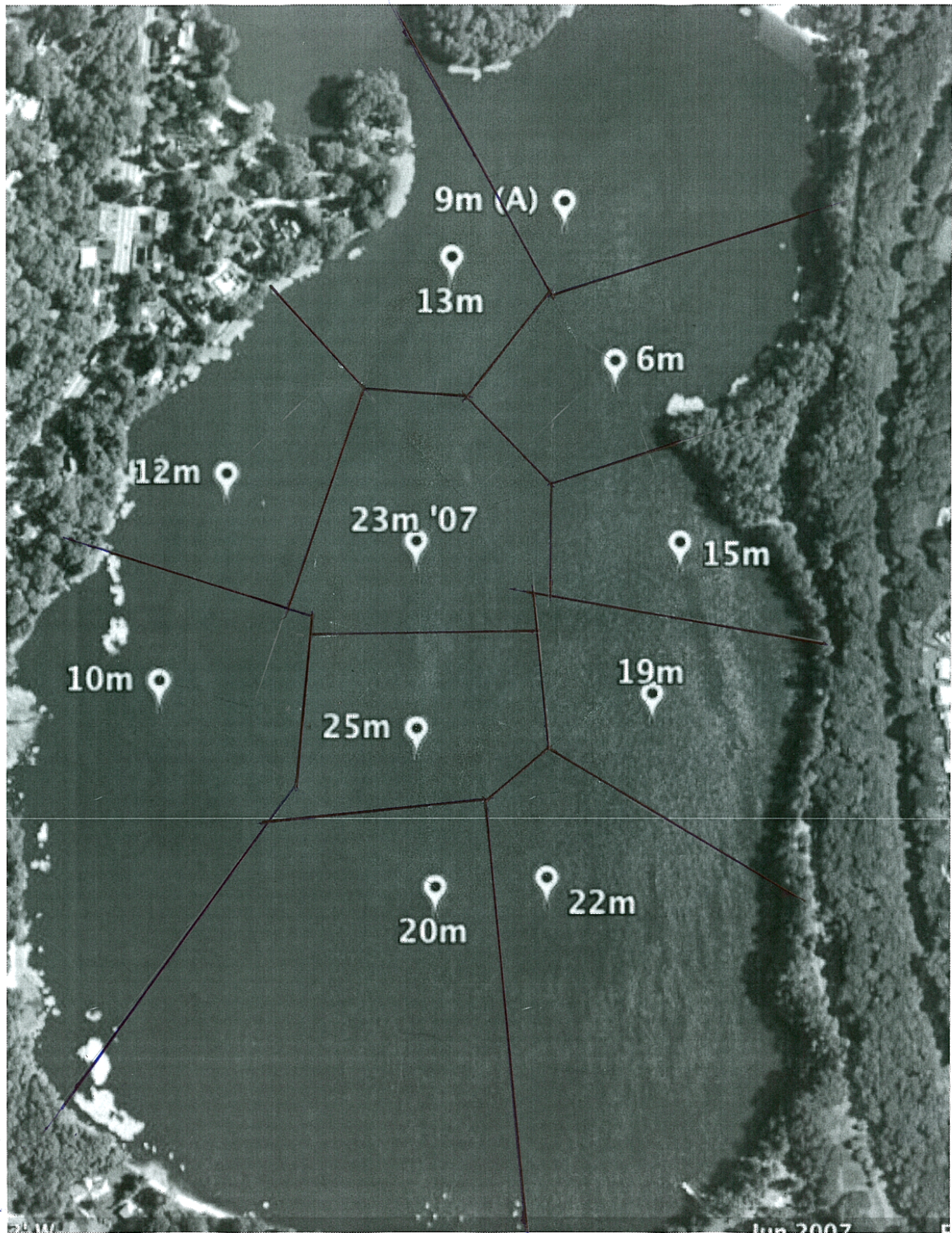


Figure 3 Polygons for calculation of ebullition fluxes from traps deployed between August and November 2007

(a) 2007 Bubbling fluxes in Upper Mystic Lake, MA

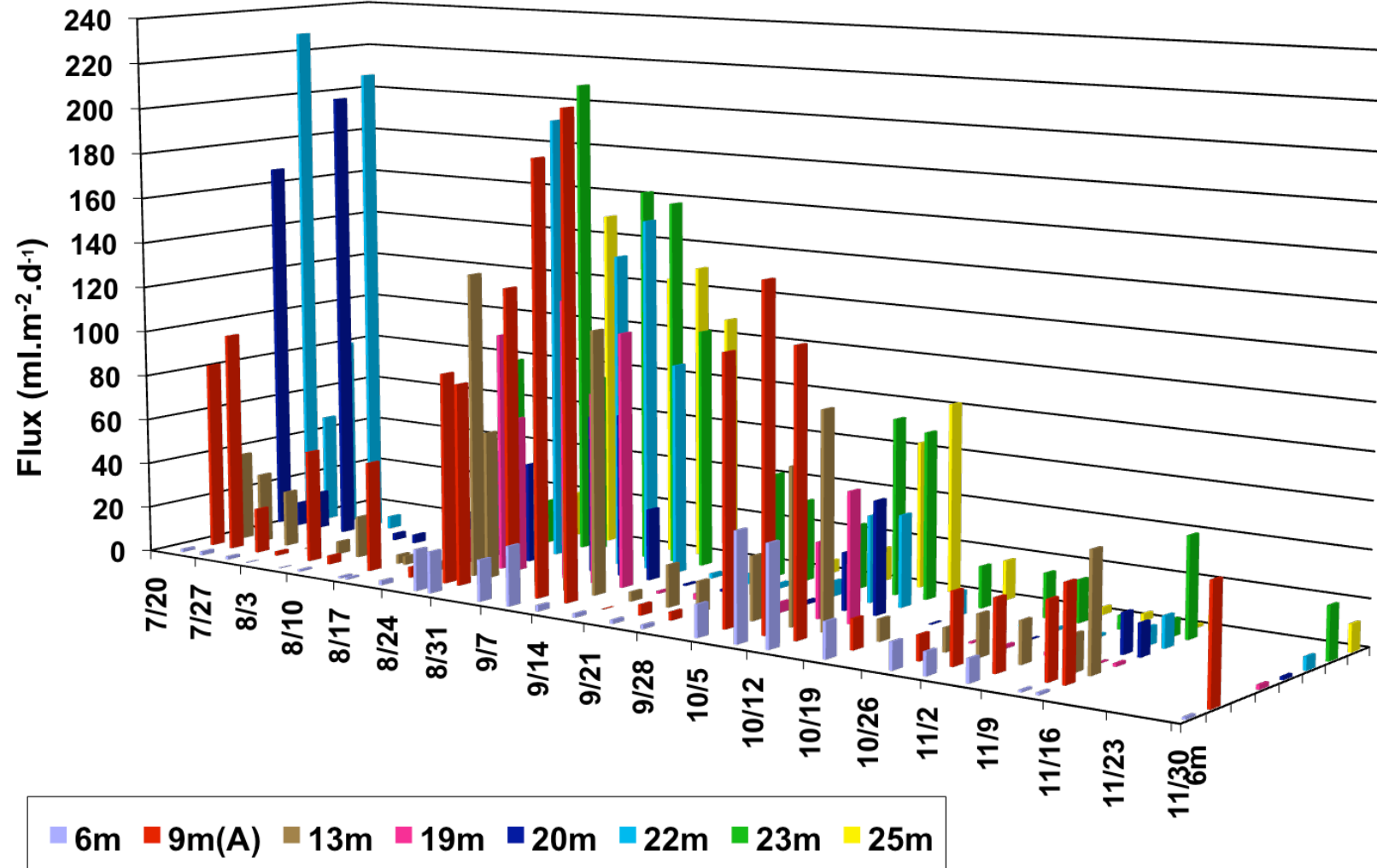


Figure 4 (a) Ebullition fluxes with sampled every 3-14 days in from mid July- November 2007

(b) 2008 Bubbling fluxes in Upper Mystic Lake, MA

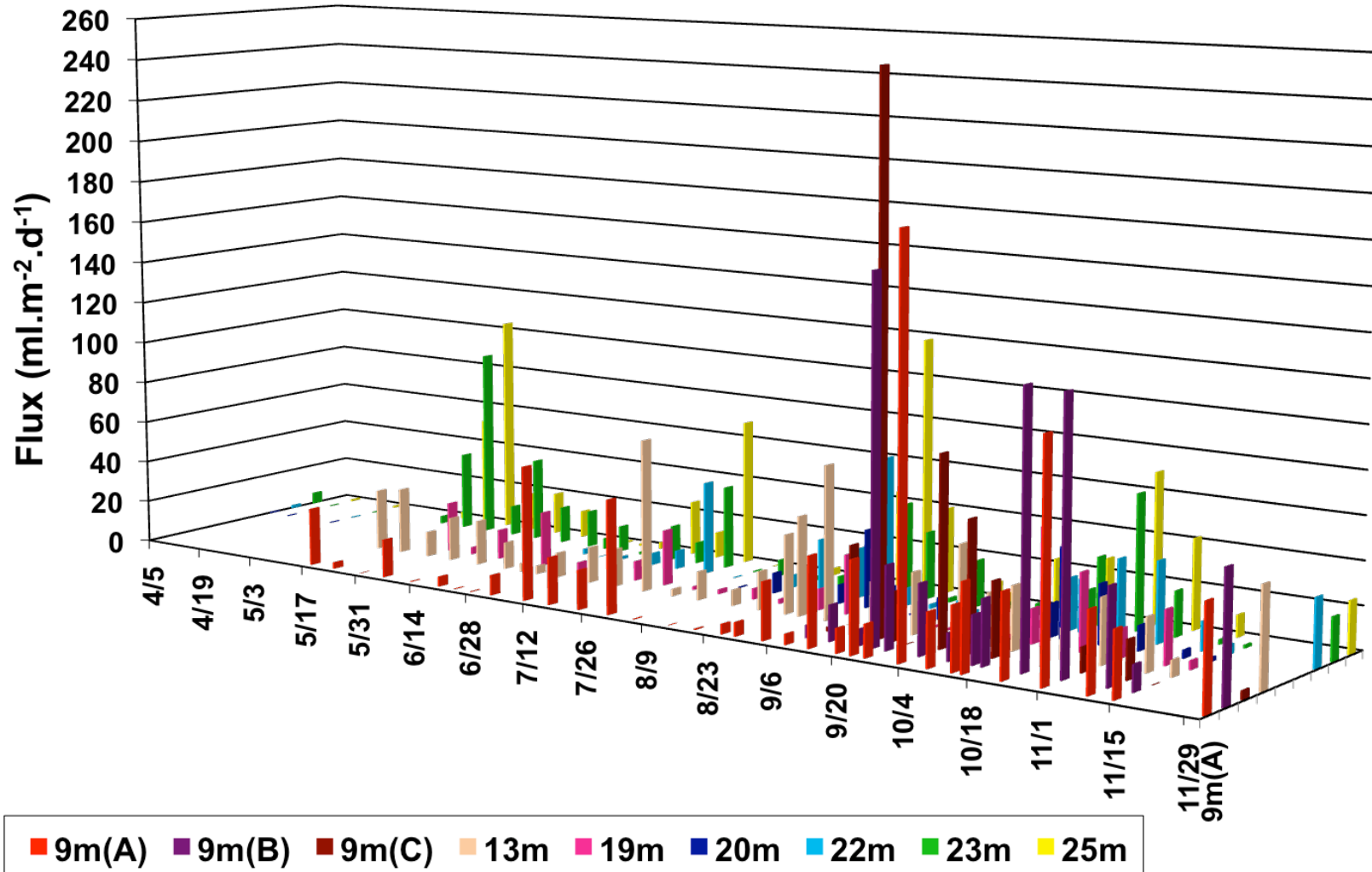


Figure 4 (b) Ebullition fluxes with sampled every 7-14 days in from April-November 2008

Spatial and inter-annual variation in average bubbling fluxes

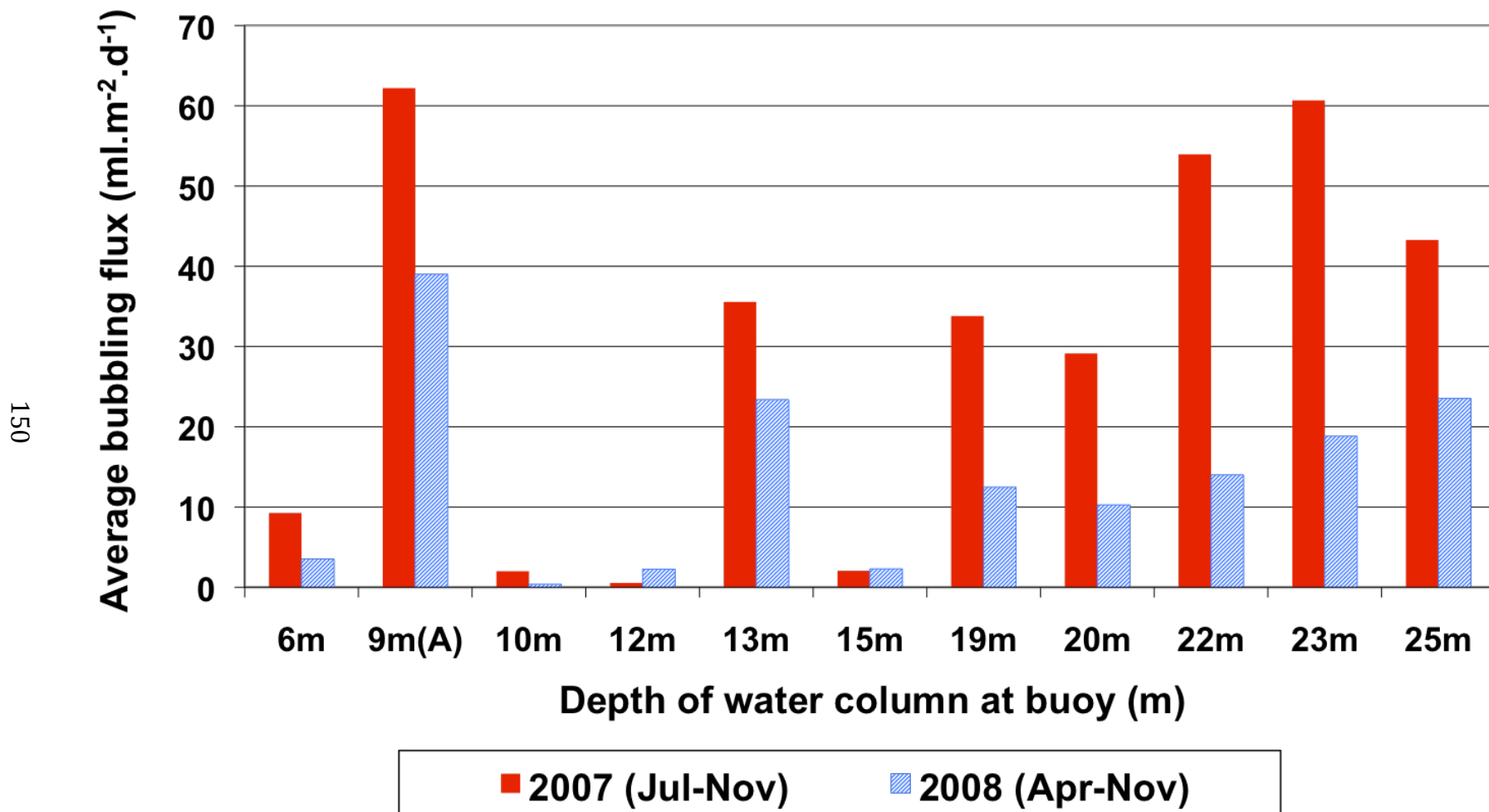


Figure 5 Average ebullition fluxes at various sites in 2007 and 2008. Fluxes in 2008 were approximately half the 2007 fluxes.

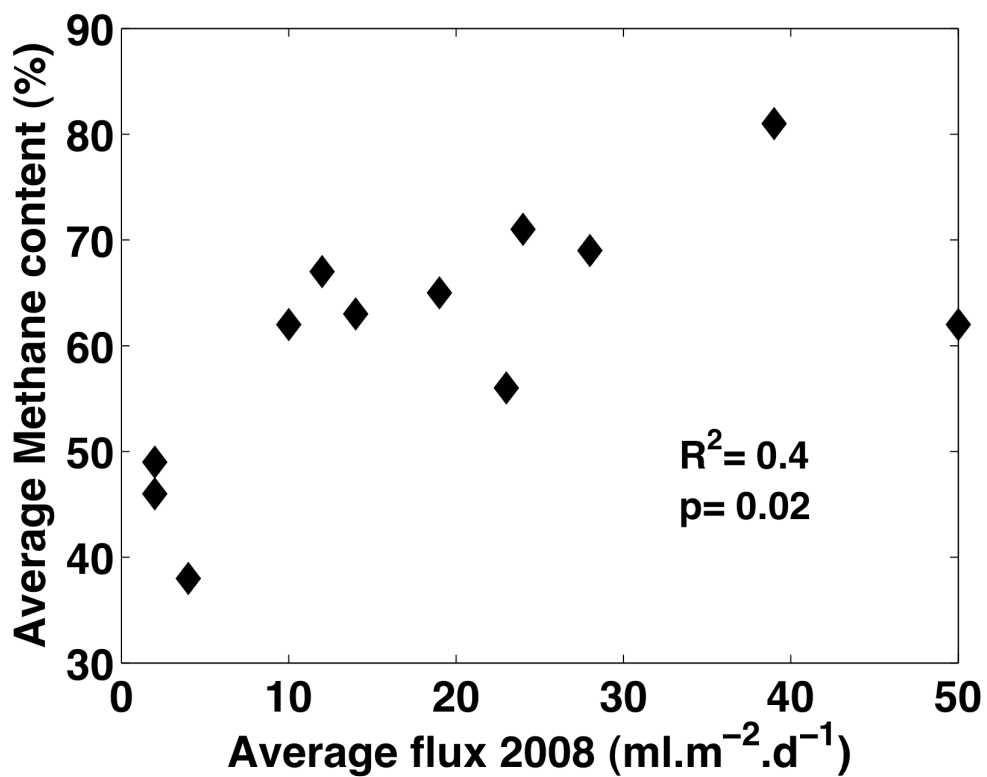
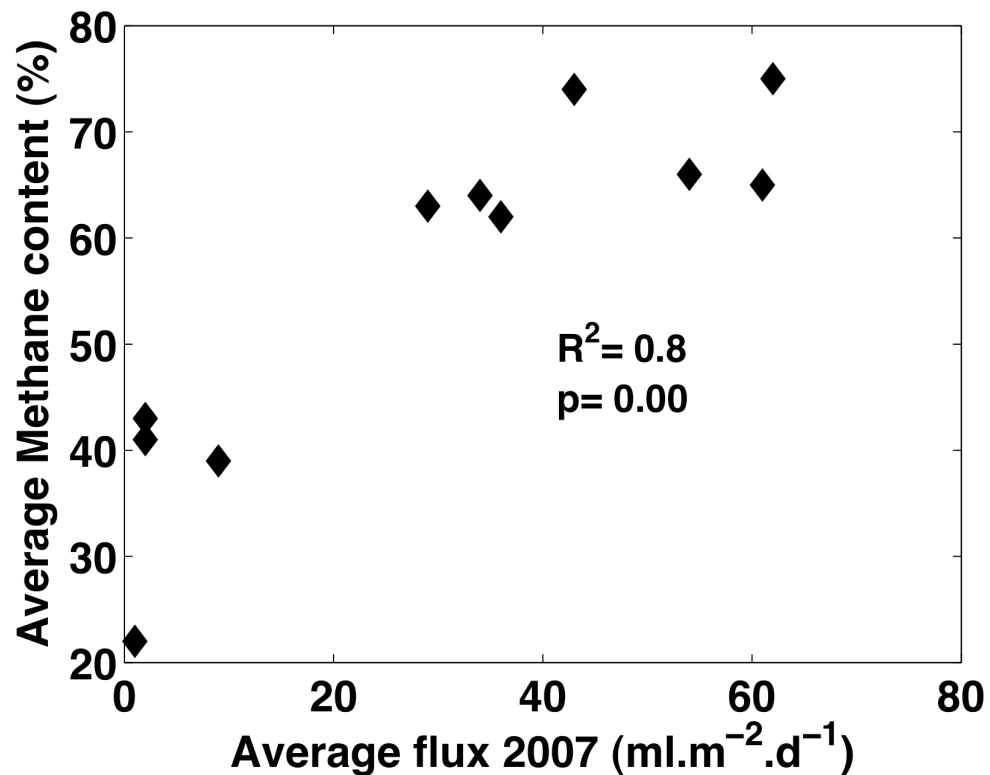


Figure 6 More methane was present in the bubbled gas at locations with higher fluxes in both 2007 (top) and 2008 (bottom). Fluxes and methane content shown are site averages.

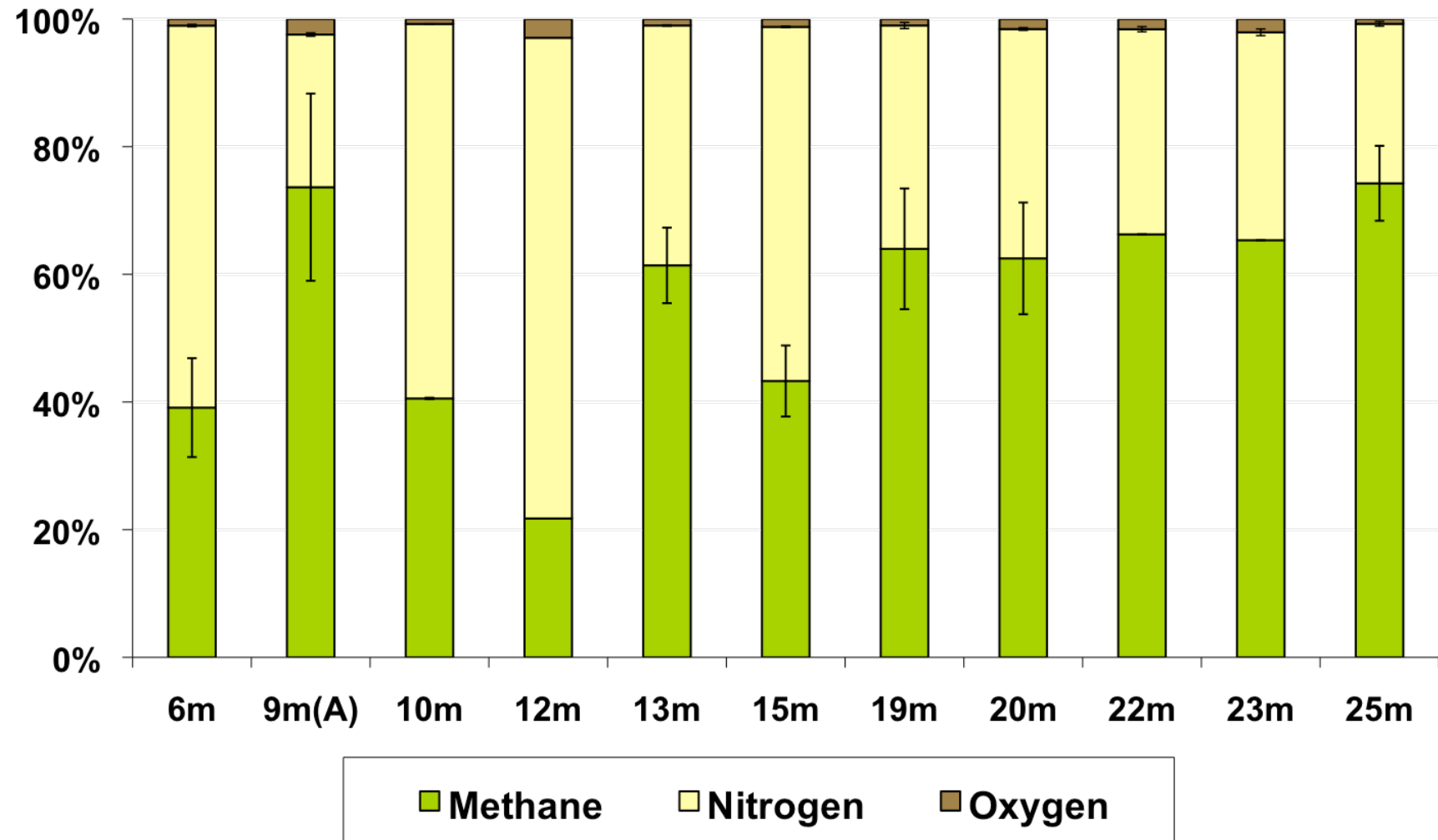


Figure 7(a) – Average gas bubble composition in 2007. Nitrogen values shown above were calculated by difference. The error bars reflect temporal variations in gas content; analytical errors are negligible in comparison

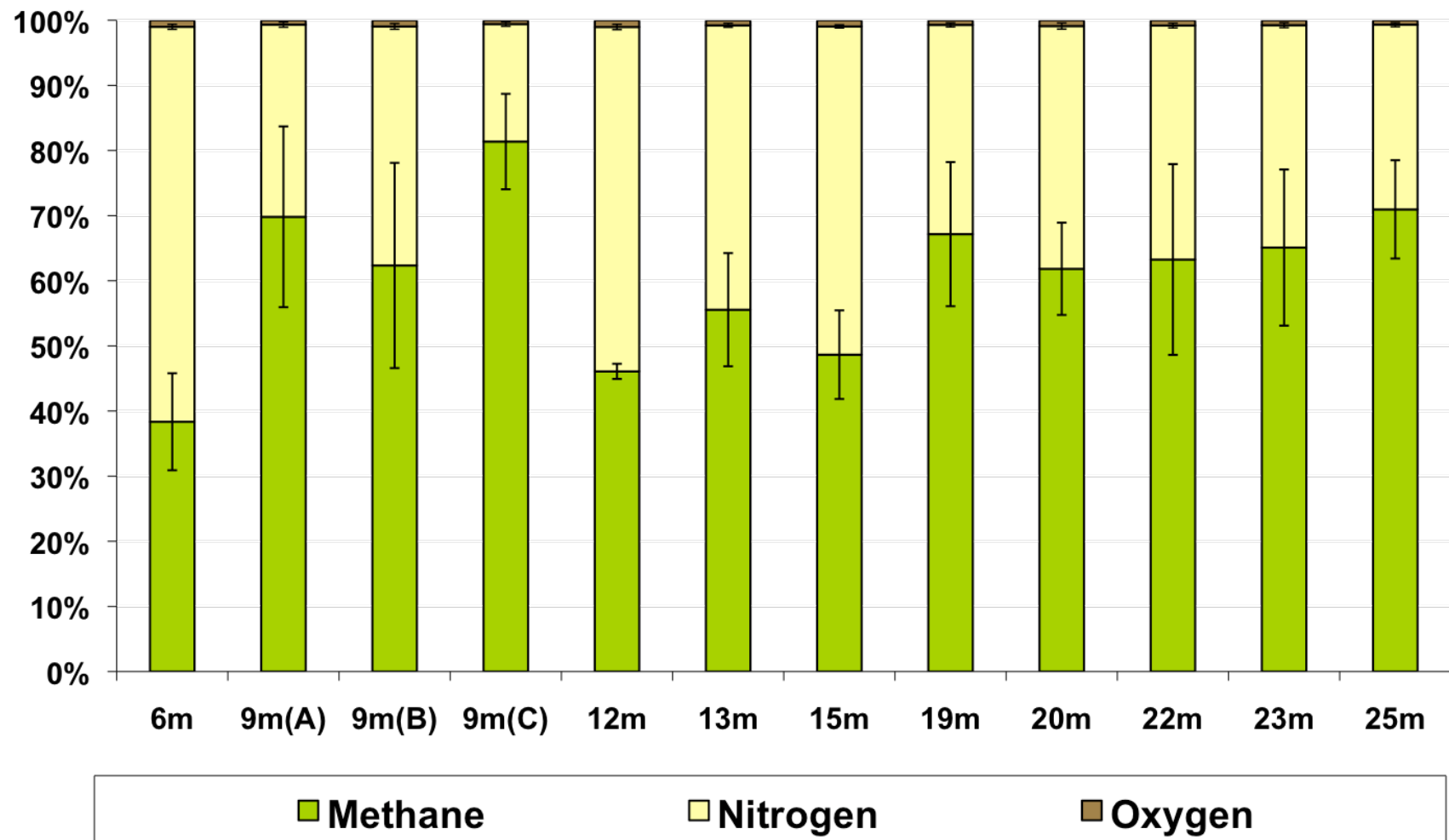


Figure 7(b) – Average gas bubble composition in 2008. Nitrogen values shown above were calculated by difference. The error bars reflect temporal variations in gas content; analytical errors are negligible in comparison

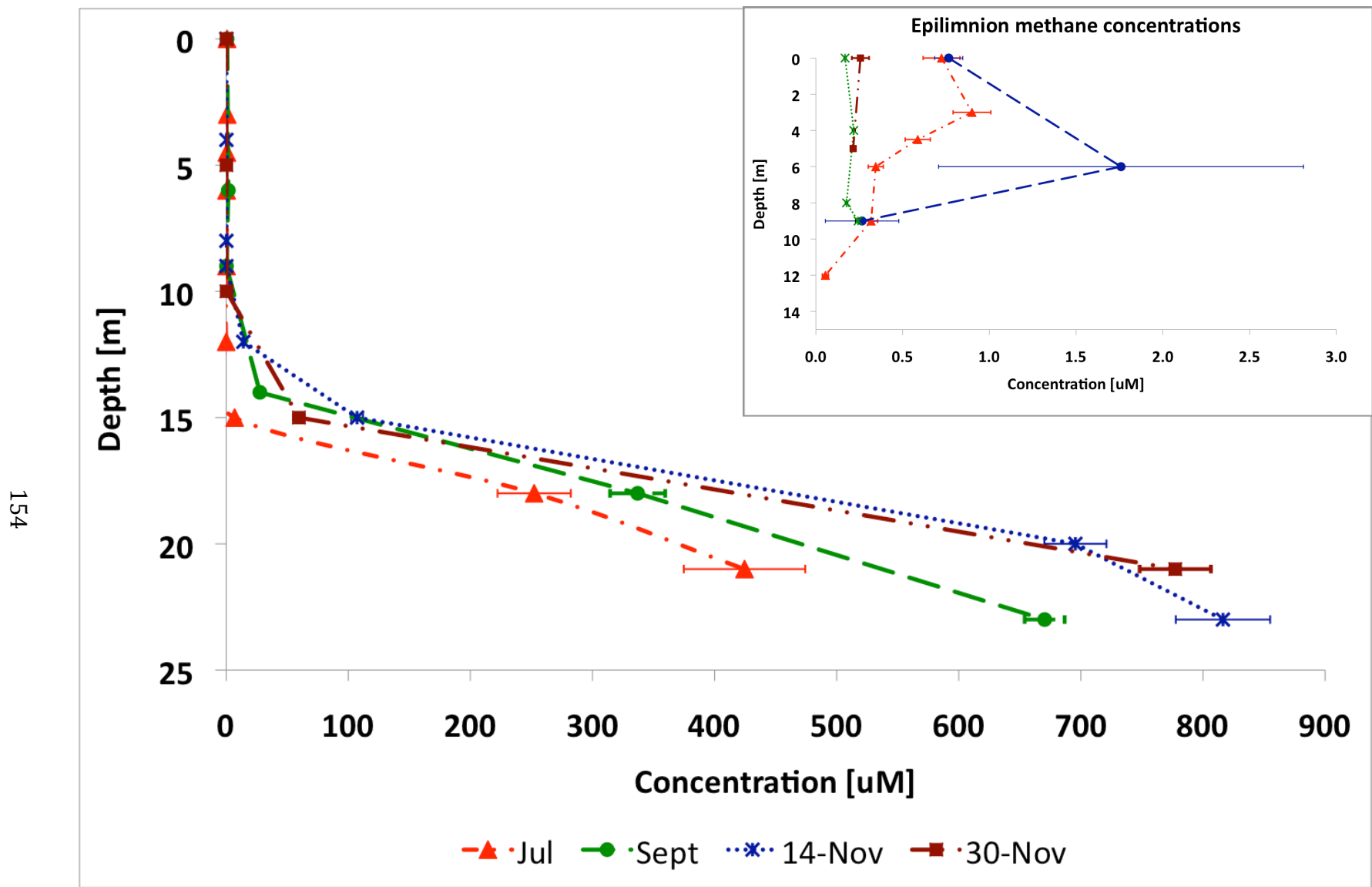


Figure 8 (a) Dissolved methane concentrations in the hypolimnion in 2007. Error bars include standard errors from duplicates and multiple GC injections.

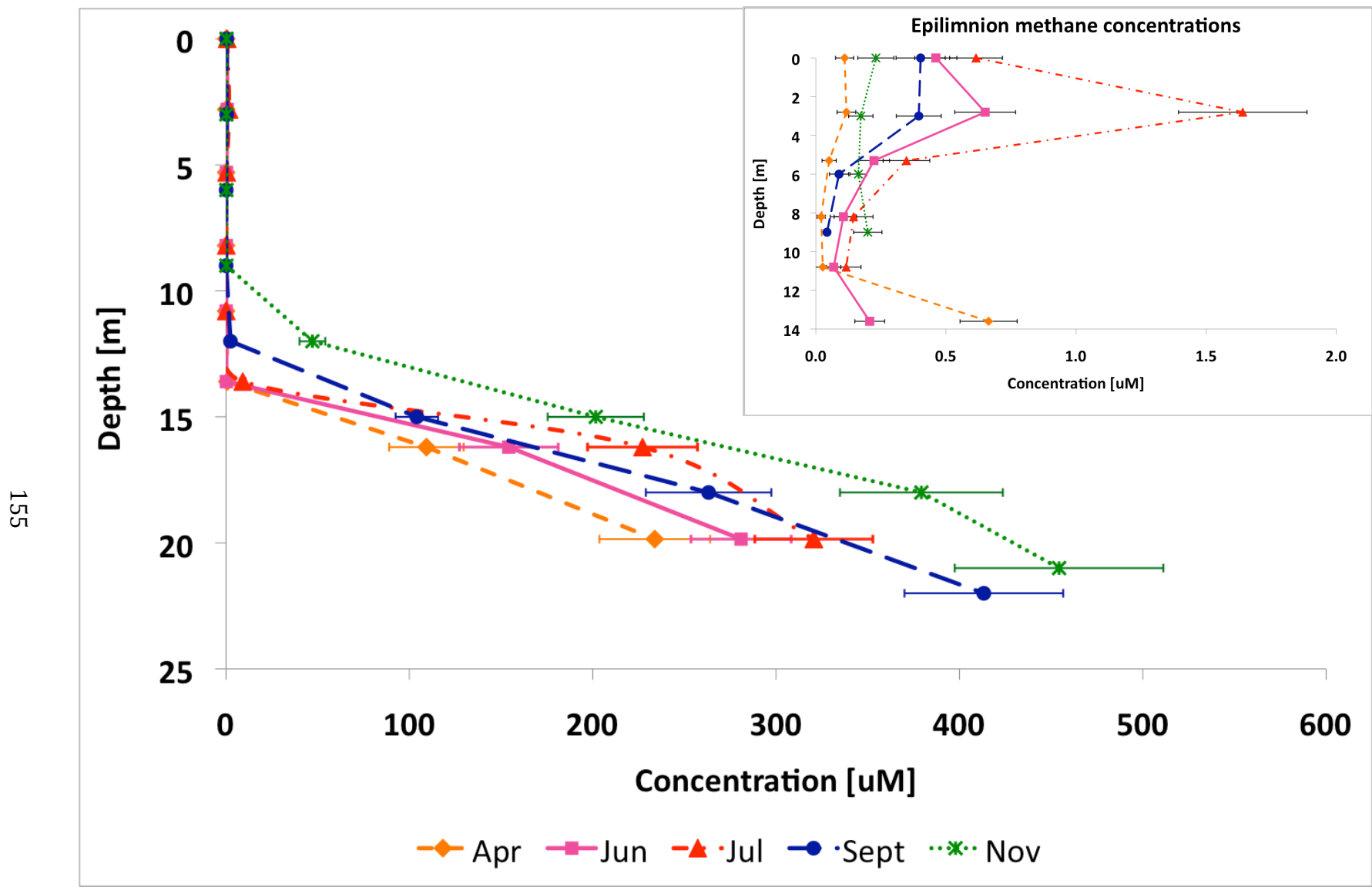


Figure 8 (b) Dissolved methane concentrations increased from April to November 2008 in the hypolimnion. Error bars include standard errors from duplicates and multiple GC injections

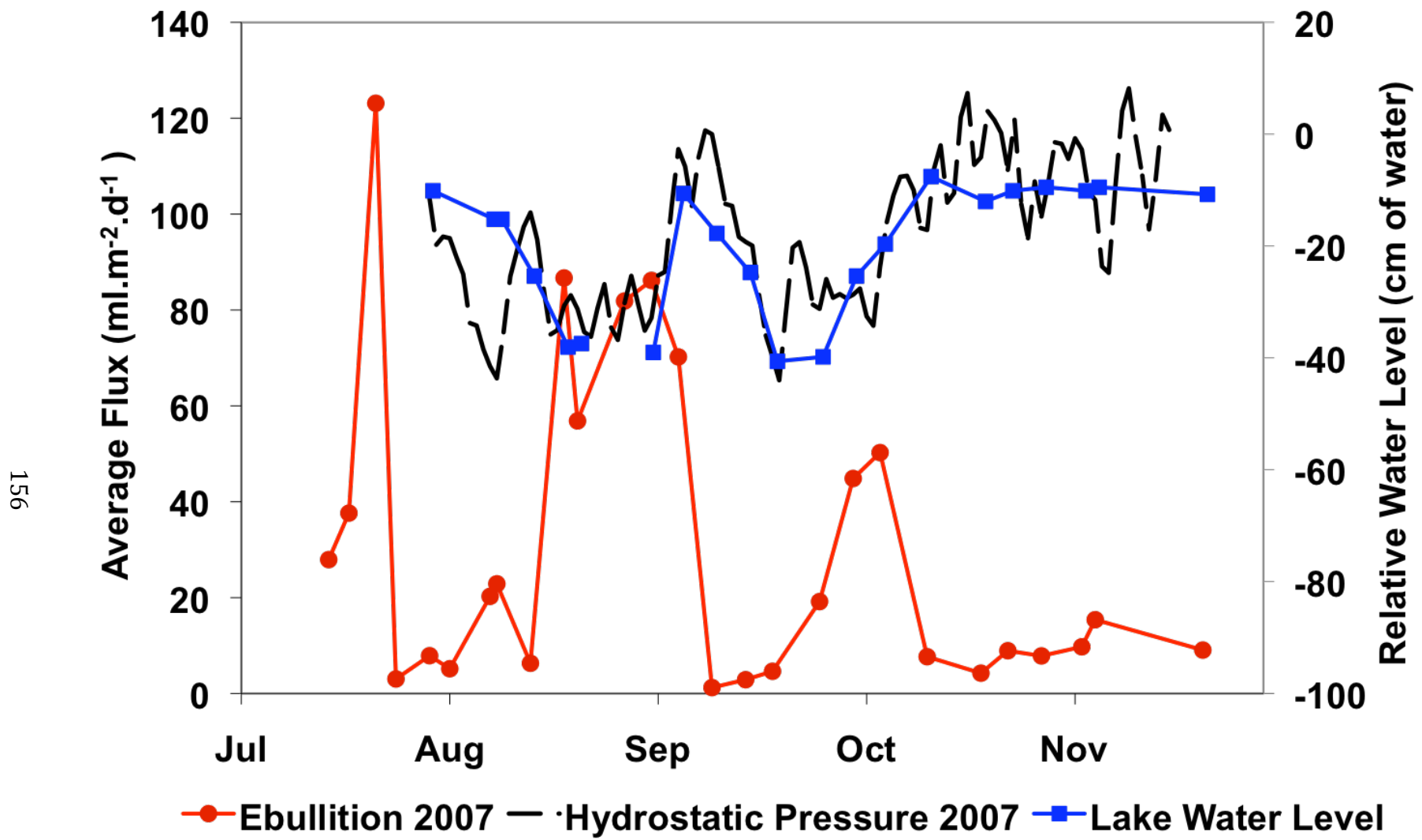


Figure 9(a) Ebullition is triggered during two periods of low hydrostatic pressure (and water level). No seasonal pattern was observed between July and November 2007.

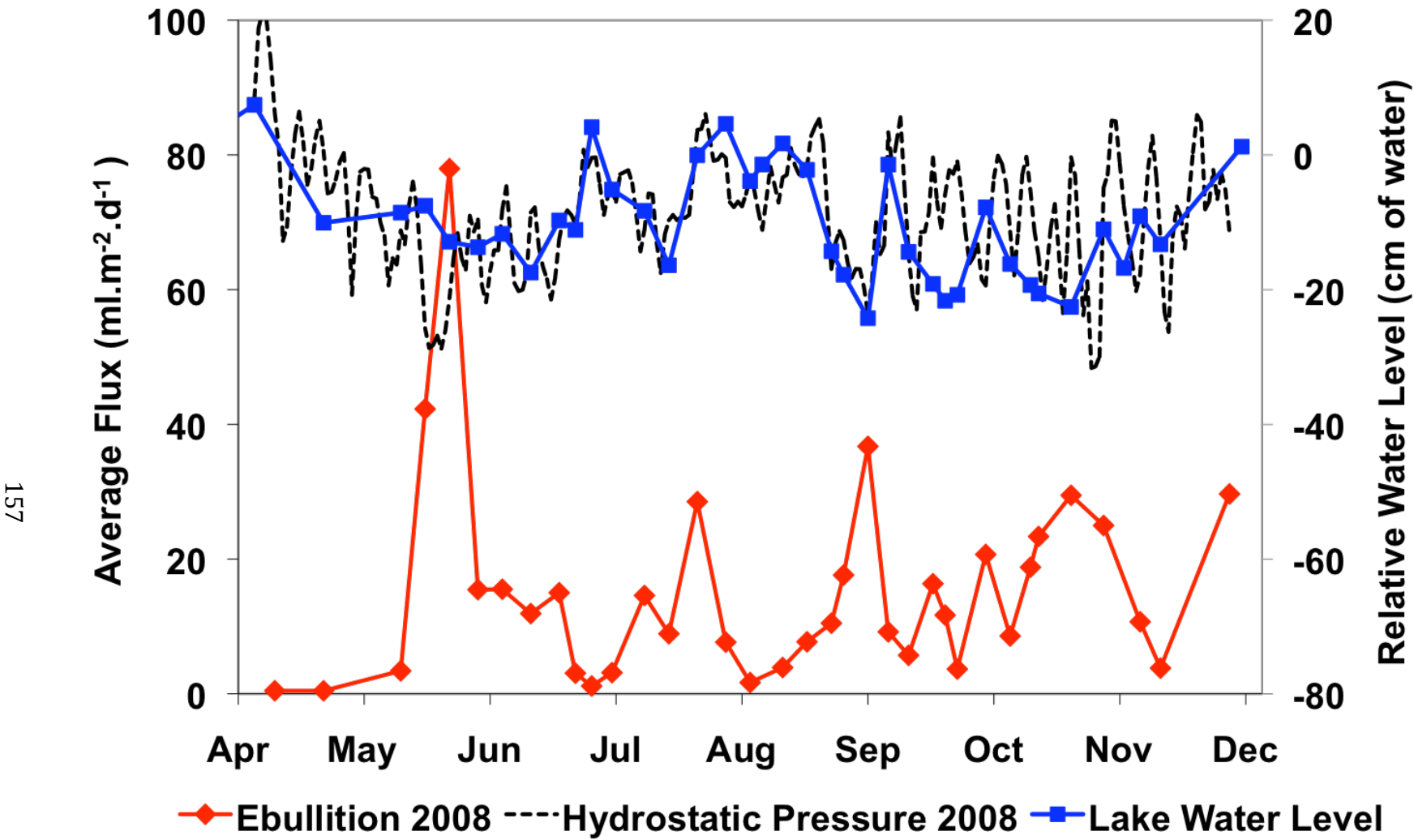


FIGURE 9 (b) – Ebullition is triggered during periods of low hydrostatic pressure. No seasonal pattern was observed between April and November 2008.

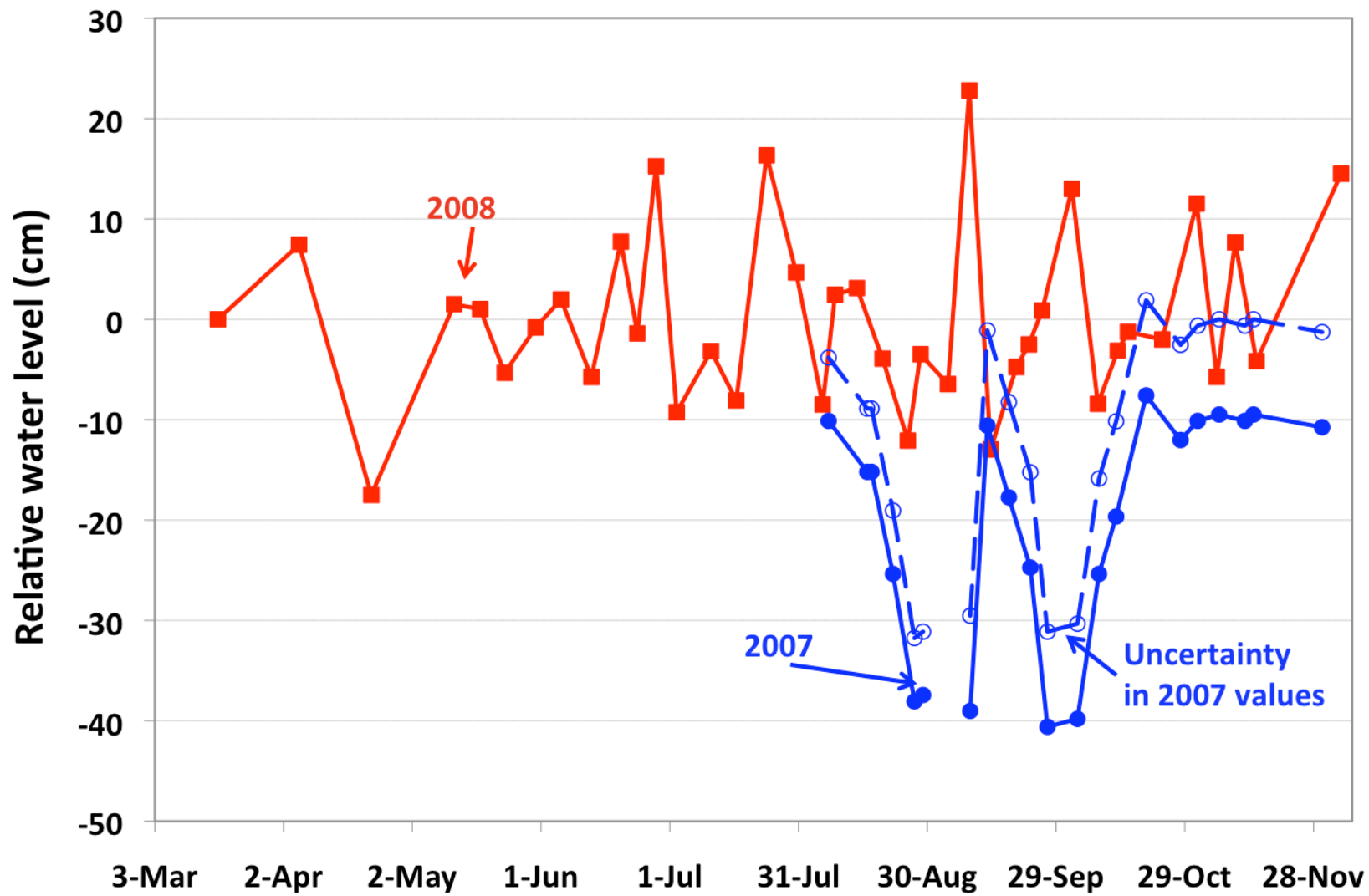


Figure 10 Lake water levels in 2007 vs. 2008. The uncertainty band in 2007 is due to the loss of an absolute reference.

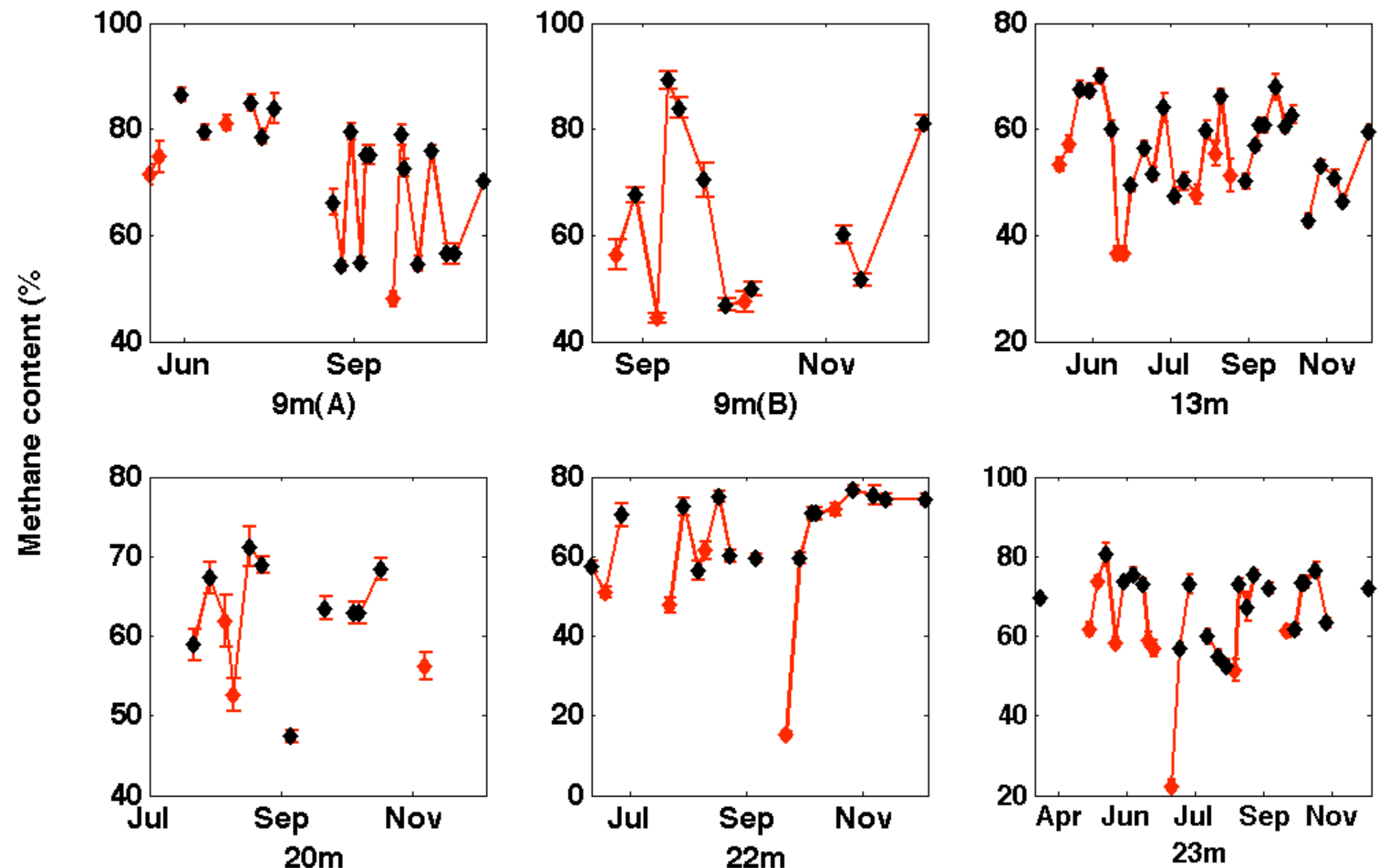


Figure 11 Variation in methane content at some sites in 2008. Errors bars shown only reflect analytical error and not possible leakage. The black dots represent the times at which the oxygen content in the sample was < 1%.

REFERENCES

1. Addess, J. M. and S. W. Effler. 1996. Summer Methane Fluxes and Fall Oxygen Resources of Onondaga Lake. *Lake Reserv. Manage.* **12:** 91.
2. Aurilio, A. C., R. P. Mason and H. F. Hemond. 1994. Speciation and Fate of Arsenic in Three Lakes of the Aberjona Watershed. *Environ. Sci. Technol.* **28:** 577-585.
3. Bastviken, D., J. Cole, M. Pace and L. Tranvik. 2004. Methane emissions from lakes: Dependence of lake characteristics, two regional assessments, and a global estimate. *Global Biogeochem. Cycles.* **18:** B4009.
4. Benoit, G. and H. F. Hemond. 1990. Polonium-210 and lead-210 remobilization from lake sediments in relation to iron and manganese cycling. *Environ. Sci. Technol.* **24:** 1224-1234.
5. Casper, P., S. C. Maberly, G. H. Hall and B. J. Finlay. 2000. Fluxes of methane and carbon dioxide from a small productive lake to the atmosphere. *Biogeochemistry.* **49:** 1-19.
6. Chanton, J. P., C. S. Martens and C. A. Kelley. 1989. Gas transport from methane-saturated, tidal freshwater and wetland sediments. *Limnol. Oceanogr.* **34:** 807-819.
7. Crill, P. M., K. B. Bartlett, J. O. Wilson, D. I. Sebacher, R. C. Harriss, J. M. Melack, S. MacIntyre, L. Lesack and L. Smith-Morrill. 1988. Tropospheric methane from an Amazonian floodplain lake. *J. Geophys. Res.* **93:** 1564-1570, doi:10.1029/JD093iD02p01564.
8. Eckert, W. and R. Conrad. 2007. Sulfide and methane evolution in the hypolimnion of a subtropical lake: a three-year study. *Biogeochemistry.* **82:** 67-76.
9. Greinert, J. and D. F. McGinnis. 2009. Single bubble dissolution model – The graphical user interface SiBu-GUI. *Environmental Modelling & Software.* **24:** 1012-1013, doi:DOI: 10.1016/j.envsoft.2008.12.011.
10. Huttunen, J. T., K. M. Lappalainen, E. Saarijärvi, T. Väisänen and P. J. Martikainen. 2001. A novel sediment gas sampler and a subsurface gas collector used for measurement of the ebullition of methane and carbon dioxide from a eutrophied lake. *Sci. Total Environ.* **266:** 153-158, doi:10.1016/S0048-9697(00)00749-X.
11. Huttunen, J. T., J. Alm, A. Liikanen, S. Juutinen, T. Larmola, T. Hammar, J. Silvola and P. J. Martikainen. 2003. Fluxes of methane, carbon dioxide and nitrous oxide in boreal lakes and potential anthropogenic effects on the aquatic greenhouse gas emissions. *Chemosphere.* **52:** 609-621, doi:DOI: 10.1016/S0045-6535(03)00243-1.
12. Jahne, B., K. O. Mannich, R. B. A. Dutzi, W. Huber and P. Libner. 1987. On the Parameters Influencing Air-Water Gas Exchange. *J. Geophys. Res.* **92 (C2):** 1937-1950.
13. Kankaala, P., S. Taipale, H. Nykänen and R. I. Jones. 2007. Oxidation, efflux, and isotopic fractionation of methane during autumnal turnover in a polyhumic, boreal lake. *J. Geophys. Res.* **112:** G02033.
14. Kanwisher. 1963. On the exchange of gases between the atmosphere and the sea. *Oceanographic research papers [0967-0637].* **10:** 195.
15. Keller, M. and R. F. Stallard. 1994. Methane emission by bubbling from Gatun Lake, Panama. *J. Geophys. Res.* **99 (D4):** 8307-8319.
16. Mackay, D. and A. T. K. Yeun. 1983. Mass transfer coefficient correlations for volatilization of organic solutes from water. *Environ. Sci. Technol.* **17:** 211-217.
17. Mattson, M. D. 1989. An electron budget for aerobic and anaerobic decomposition in oligotrophic lake sediments. Ph.D. thesis. Cornell University.

18. McGinnis, D. F., J. Greinert, Y. Artemov, S. E. Beaubien and A. Wüest. 2006. Fate of rising methane bubbles in stratified waters: How much methane reaches the atmosphere? *J. Geophys. Res.* **111**: C09007, doi:10.1029/2005JC003183.
19. Michmerhuizen, C. M., R. G. Striegl and M. E. McDonald. 1996. Potential methane emission from north-temperate lakes following ice melt. *Limnol. Oceanogr.* **41**: 985-991.
20. Miller, L. G. and R. S. Oremland. 1988. Methane efflux from the pelagic regions of four lakes. *Global Biogeochem. Cycles.* **2**: 269-277.
21. Morel, F., and J. G. Hering. 1993. Principles and applications of aquatic chemistry. Wiley.
22. Nakamura, T., Y. Nojiri, M. Utsumi, T. Nozawa and A. Otsuki. 1999. Methane emission to the atmosphere and cycling in a shallow eutrophic lake. *Arch. Hydrobiol.* **144**: 383-407.
23. Ostrovsky, I., D. F. McGinnis, L. Lapidus and W. Eckert. 2008. Quantifying gas ebullition with echosounder: The role of methane transport by bubbles in a medium-sized lake. *Limnol. Oceanogr. - Methods.* **6**: 105-118.
24. Peterson, E. J. R. 2005. Carbon and electron flow via methanogenesis, SO_4^{2-} , NO_3^- and Fe^{3+} reduction in the anoxic hypolimnia of Upper Mystic Lake. Master of Science thesis. Massachusetts Institute of Technology.
25. Phelps, A. R., K. M. Peterson and M. O. Jeffries. 1998. Methane efflux from high-latitude lakes during spring ice melt. *J. Geophys. Res.* **103**: 28913-29106.
26. Rehder, G., P. W. Brewer, E. T. Peltzer and G. Friederich. 2002. Enhanced lifetime of methane bubble streams within the deep ocean. *Geophys. Res. Lett.* **29**: 1731.
27. Rudd, J. W. M., and C. D. Taylor. 1980. Methane cycling in aquatic environments, p. 77-150. In M. R. Droop, Jannasch, H.W. [ed.], *Advances in Aquatic Microbiology*. Academic Press.
28. Senn, D. B. 2001. Coupled arsenic, iron, and nitrogen cycling in arsenic-contaminated Upper Mystic Lake. Doctor of Philosophy thesis. Massachusetts Institute of Technology.
29. Smith, L. K. and W. M. Lewis. 1992. Seasonality of Methane Emissions From Five Lakes and Associated Wetlands of the Colorado Rockies. *Global Biogeochem. Cycles.* **6**: 323-338.
30. Spliethoff, H. M. 1995. Biotic and abiotic transformations of arsenic in the Upper Mystic Lake.
31. Spliethoff, H. M. and H. F. Hemond. 1996. History of Toxic Metal Discharge to Surface Waters of the Aberjona Watershed. *Environ. Sci. Technol.* **30**: 121-128.
32. Strayer, R. F. and J. M. Tiedje. 1978. In Situ Methane Production in a Small, Hypereutrophic, Hard-Water Lake: Loss of Methane from Sediments by Vertical Diffusion and Ebullition. *Limnol. Oceanogr.* **23**: 1201-1206.
33. Utsumi, M., Y. Nojiri, T. Nakamura, T. Nozawa, A. Otsuki and H. Seki. 1998. Oxidation of dissolved methane in a eutrophic, shallow lake: Lake Kasumigaura, Japan. *Limnol. Oceanogr.* **43**: 471-480.
34. Walter, K. M., L. C. Smith and F. S. Chapin III. 2007. Methane bubbling from northern lakes: present and future contributions to the global methane budget. *Philos. Trans. R. Soc. A.* **365**: 1657-1676, doi:10.1098/rsta.2007.2036.
35. Walter, K. M., S. A. Zimov, J. P. Chanton, D. Verbyla and F. S. Chapin III. 2006. Methane bubbling from Siberian thaw lakes as a positive feedback to climate warming. *Nature.* **443**: 71-75, doi:10.1038/nature05040.

Appendix for Chapter 4

Table 1 - Buoy locations

Table 2 - Trap polygon areas in 2007 and 2008

Table 3 - Total volumetric ebullition fluxes in (a) 2007 (b) 2008

Table 4 - Bubble methane content in (a) 2007 (b) 2008

Table 5 - Bubble oxygen content in (a) 2007 (b) 2008

Table 6 - Methane released through ebullition (a) 2007 (b) 2008

Figure 1 - POM fluxes vs. depth

Figure 2 - Wind buoy

Table 1 Bubble trap names and locations in 2007 and 2008.

Trap Name	Approximate trap location
6m	42 26.240N, 71 08.880W
10m	42 26.103N, 71 09.150W
9m, 9m(A)	42 26.307N, 71 08.908W
9m(B)	42 26.294N, 71 09.910W
9m(C)	42 26.305N, 71 08.894W
13m	42 26.284N, 71 08.974W
12m	42 26.192N, 71 09.105W
15m	42 26.158N, 71 08.844W
20m	42 26.011N, 71 08.991W
19m	42 26.093N, 71 08.862W
22m	42 26.014N, 71 08.926W
23m	42 26.161N, 71 08.998W (2007) 42 26.171N, 71 09.946W (2008)
25m	42 26.083N, 71 08.996W (2007) 42 26 090, 71 08.955W (4/5/08-6/5/08) 42 26.095N, 71 08.917W (6/5/08-8/5/08) 42 26.080, 71 09 000W (8/5/08-end)

Table 2(a) Polygon areas, as a fraction of the lake surface, for the different traps in 2007

Jul 19 – Aug 16

Buoy name	Fraction Area
6m	0.08
9m	0.11
13m	0.13
15m	0.11
20m	0.38
22m	0.20

Aug 16 – Nov 30

Buoy name	Fraction Area
6m	0.07
9m	0.11
10m	0.13
12m	0.06
13m	0.05
15m	0.04
23m	0.06
25m	0.05

Table 2(b) Polygon areas, as a fraction of the lake surface, for the different traps in 2008. Fluxes measured prior to May 11 were averaged for extrapolation to the entire lake (i.e. assuming that each trap represented an equal fraction of the lake area)

191

**May 11 - May 23,
Jun 12 - Jun 19**

Buoy Name	Fraction Area
6m	0.08
9m	0.11
13m	0.08
23m	0.10
25m	0.64

**May 30 - Jun 12,
Nov 14 - Dec 1**

Buoy Name	Fraction Area
6m	0.08
9m	0.11
13m	0.08
19m	0.27
23m	0.10
25m	0.37

Jun 19 - Jul 30

Buoy Name	Fraction Area
9m	0.14
10m	0.19
12m	0.07
13m	0.06
15m	0.05
19m	0.06
22m	0.31
23m	0.07
25m	0.05

Jul 30 - Nov 14

Buoy Name	Fraction Area
6m	0.06
9m	0.11
10m	0.13
12m	0.07
13m	0.06
15m	0.04
19m	0.07
20m	0.20
22m	0.16
23m	0.06
25m	0.06

Table 3 (a) Volumetric ebullition fluxes ($\text{ml.m}^{-2}.\text{d}^{-1}$) with measurement errors in 2007. The total volume of gas collected in the traps was used to calculate these fluxes (COMP = Compromised samples).

Trap	Jul-20	Jul-23	Jul-26	Jul-30	Aug-02	Aug-07	Aug-10	Aug-16	Aug-17	Aug-22	Aug-27
6m		1 ± 1	2 ± 1	1 ± 1	0 ± 1	0 ± 1	1 ± 1	1 ± 0	1 ± 0	2 ± 2	18 ± 2
9m(A)		83 ± 1	97 ± 4	20 ± 1	2 ± 1	49 ± 1	4 ± 1	48 ± 1		5 ± 5	92 ± 7
10m									0 ± 0	0 ± 0	COMP
12m									1 ± 0	1 ± 0	0 ± 0
13m		39 ± 4	31 ± 2	25 ± 2	0 ± 1	6 ± 1	18 ± 1	4 ± 4	4 ± 4	4 ± 4	133 ± 6
15m		4 ± 1	2 ± 1	3 ± 1	4 ± 1	1 ± 1	2 ± 1	0 ± 1	0 ± 0	0 ± 0	0 ± 0
19m										15 ± 1	104 ± 1
20m	166 ± 8	11 ± 3	17 ± 1	201 ± 4	4 ± 1	3 ± 1	4 ± 1	30 ± 2	17 ± 17	8 ± 6	44 ± 2
22m	228 ± 8	48 ± 3	84 ± 3	210 ± 4	5 ± 1			16 ± 1	42 ± 5	3 ± 1	196 ± 1
23m									82 ± 6	19 ± 1	210 ± 1
25m										19 ± 1	149 ± 4

Trap	Aug-29	Sep-05	Sep-09	Sep-13	Sep-18	Sep-23	Sep-27	Oct-04	Oct-09	Oct-13	Oct-20
6m	18 ± 2	18 ± 4	26 ± 2	3 ± 1	2 ± 5	2 ± 5	2 ± 5	14 ± 5	47 ± 2	44 ± 3	15 ± 1
9m(A)	88 ± 4	132 ± 0	188 ± 4	210 ± 4	0 ± 1	5 ± 5	4 ± 3	115 ± 1	146 ± 5	121 ± 8	13 ± 1
10m	0 ± 0	0 ± 0	0 ± 1	0 ± 0	0 ± 0	0 ± 0	0 ± 0	0 ± 0	0 ± 0	1 ± 1	1 ± 1
12m	0 ± 0	0 ± 0	1 ± 1	0 ± 0	0 ± 0	0 ± 0	0 ± 0	0 ± 0	0 ± 0	1 ± 0	1 ± 0
13m	64 ± 4	96 ± 1	44 ± 3	114 ± 10	4 ± 1	18 ± 1	13 ± 2	27 ± 1	67 ± 7	93 ± 2	9 ± 1
15m	0 ± 0	0 ± 0	0 ± 0	0 ± 0	0 ± 0	1 ± 1	1 ± 1	1 ± 1	19 ± 6	2 ± 0	2 ± 0
19m	68 ± 4	122 ± 17	83 ± 2	111 ± 4	1 ± 1	2 ± 2	2 ± 2	4 ± 4	33 ± 2	56 ± 5	MOVED
20m	COMP	69 ± 1	71 ± 2	31 ± 2	1 ± 1	1 ± 0	2 ± 4	2 ± 4	25 ± 1	49 ± 3	0 ± 0
22m	COMP	137 ± 1	154 ± 8	92 ± 5	2 ± 1	5 ± 5	2 ± 3	7 ± 1	37 ± 2	40 ± 4	10 ± 1
23m	78 ± 4	164 ± 1	160 ± 2	105 ± 10	5 ± 5	45 ± 3	35 ± 2	28 ± 2	76 ± 1	72 ± 5	18 ± 1
25m	81 ± 4	124 ± 1	130 ± 6	108 ± 8	1 ± 1	1 ± 1	5 ± 5	14 ± 4	63 ± 4	82 ± 5	17 ± 1

Trap	Oct-28	Nov-01	Nov-06	Nov-12	Nov-14	Nov-30	AVERAGE
6m	12 ± 1	10 ± 1	10 ± 1	1 ± 0	1 ± 0	1 ± 0	9
9m(A)	11 ± 1	30 ± 2	30 ± 2	33 ± 2	41 ± 4	50 ± 2	62
10m	1 ± 1	18 ± 1	16 ± 3	0 ± 0	0 ± 1	0 ± 0	4
12m	1 ± 0	1 ± 0	1 ± 0	1 ± 0		0 ± 0	1
13m	10 ± 1	18 ± 0	18 ± 0	16 ± 1	50 ± 2	COMP	36
15m	1 ± 0	1 ± 0	1 ± 0	0 ± 0	2 ± 1	4 ± 0	2
19m	1 ± 0	1 ± 0	1 ± 0	0 ± 0	1 ± 1	2 ± 0	34
20m	0 ± 0	0 ± 0	0 ± 0	17 ± 2	14 ± 1	1 ± 0	29
22m	1 ± 0	1 ± 0	1 ± 0	8 ± 1	13 ± 1	6 ± 0	54
23m	19 ± 1	18 ± 2	6 ± 2	7 ± 1	43 ± 3	23 ± 1	61
25m	2 ± 0	3 ± 0	3 ± 0	1 ± 0	7 ± 1	12 ± 1	43

Table 3 (b) Volumetric ebullition fluxes ($\text{ml.m}^{-2}.\text{d}^{-1}$) with measurement errors in 2008. (COMP = Compromised samples).

Trap	Winter (Apr-05)	Apr-10	Apr-22	May-11	May-17	May-23	May-30	Jun-05	Jun-12	Jun-19	Jun-23	Jun-27
6m					0 ± 0	0 ± 0	0 ± 0	0 ± 0				
9m(A)					27 ± 1	3 ± 0	0 ± 0	18 ± 2	0 ± 0	5 ± 0	0 ± 0	0 ± 1
9m(B)												
9m(C)												
10m												
12m										1 ± 0	0 ± 0	0 ± 1
13m					29 ± 2	31 ± 2	12 ± 1	21 ± 1	21 ± 1	13 ± 1	4 ± 1	4 ± 1
15m										9 ± 2	2 ± 1	0 ± 1
19m							24 ± 2	3 ± 0	14 ± 1		26 ± 1	
20m	1 ± 1	0 ± 0	0 ± 0									
22m	2 ± 2	0 ± 0	0 ± 0								3 ± 1	0 ± 1
23m	6 ± 2	0 ± 0	0 ± 0	4 ± 0	37 ± 3	89 ± 3	14 ± 2	39 ± 1	17 ± 1	17 ± 1	5 ± 1	12 ± 1
25m		1 ± 0	1 ± 0	3 ± 0	52 ± 3	104 ± 4	18 ± 1	20 ± 2	13 ± 1	COMP	1 ± 1	1 ± 1

Trap	Jul-02	Jul-10	Jul-16	Jul-23	Jul-30	Aug-05	Aug-13	Aug-19	Aug-25	Aug-28	Sep-03	Sep-08	Sep-13
6m							0 ± 0	0 ± 0	0 ± 0	0 ± 1	0 ± 0	3 ± 0	2 ± 1
9m(A)	9 ± 1	63 ± 1	22 ± 0	19 ± 1	53 ± 1	0 ± 0	0 ± 0	0 ± 0	5 ± 0	7 ± 1	27 ± 2	5 ± 1	42 ± 3
9m(B)												6 ± 0	17 ± 1
9m(C)												2 ± 0	41 ± 2
10m		0 ± 0	0 ± 0	0 ± 0	0 ± 0	0 ± 0	0 ± 0	0 ± 0	0 ± 0	0 ± 1	0 ± 0	0 ± 1	0 ± 0
12m	1 ± 1	0 ± 0	0 ± 0	0 ± 0	0 ± 0	2 ± 0	0 ± 0	0 ± 0	1 ± 0	7 ± 1	0 ± 0	1 ± 1	0 ± 0
13m	12 ± 1	17 ± 1	18 ± 1	71 ± 1	3 ± 0	13 ± 1	7 ± 1	18 ± 1	37 ± 1	46 ± 3	71 ± 2	0 ± 1	21 ± 1
15m	2 ± 1	10 ± 1	4 ± 0	1 ± 0	0 ± 0	1 ± 0	0 ± 0	0 ± 0	5 ± 0	4 ± 1	2 ± 0	1 ± 0	1 ± 1
19m	4 ± 1	4 ± 0	9 ± 2	26 ± 1	2 ± 0	2 ± 0	5 ± 0	2 ± 0	14 ± 1	10 ± 1	28 ± 1	COMP	2 ± 0
20m						0 ± 0	10 ± 1	12 ± 1	8 ± 0	9 ± 1	36 ± 2	11 ± 1	1 ± 1
22m	1 ± 1	6 ± 1	9 ± 2	44 ± 1	0 ± 0	0 ± 0	6 ± 1	25 ± 1	10 ± 1	23 ± 2	67 ± 1	8 ± 2	2 ± 1
23m	1 ± 1	16 ± 1	10 ± 1	39 ± 2	0 ± 0	8 ± 1	2 ± 0	4 ± 0	7 ± 1	77 ± 2	43 ± 2	31 ± 2	2 ± 1
25m	3 ± 1	26 ± 2	12 ± 1	68 ± 2	0 ± 0	0 ± 0	3 ± 0	1 ± 0	50 ± 1	45 ± 2	118 ± 1	40 ± 1	1 ± 1

Trap	Sep-19	Sep-22	Sep-25	Oct-02	Oct-08	Oct-13	Oct-15	Oct-23	Oct-31	Nov-09	Nov-14	Dec-01	AVERAGE
6m	0 ± 0	0 ± 0	0 ± 1	0 ± 0	4 ± 0	21 ± 1	21 ± 1	11 ± 1	11 ± 1	0 ± 0			4
9m(A)	11 ± 1	43 ± 4	15 ± 1	188 ± 3	25 ± 1	30 ± 2	40 ± 2	39 ± 1	108 ± 3	37 ± 1	30 ± 2	48 ± 2	28
9m(B)	8 ± 1	167 ± 4	38 ± 1	33 ± 1	13 ± 1	22 ± 1	30 ± 5	124 ± 2	123 ± 2	44 ± 3	12 ± 1	59 ± 2	50
9m(C)	253 ± 2	23 ± 2	0 ± 1	87 ± 2	60 ± 1	34 ± 2	9 ± 1	9 ± 1	11 ± 1	18 ± 1	0 ± 2	4 ± 1	39
10m	0 ± 0	3 ± 0	3 ± 1	0 ± 0	0 ± 0	1 ± 0	1 ± 0	1 ± 0	0 ± 0	1 ± 0			0
12m	1 ± 0	3 ± 0	3 ± 1	0 ± 0	7 ± 1	11 ± 1	11 ± 1	0 ± 0	11 ± 1	2 ± 0	0 ± 1		2
13m	24 ± 2	28 ± 4	7 ± 1	44 ± 1	25 ± 1	29 ± 2	COMP	14 ± 1	30 ± 7	25 ± 1	8 ± 1	46 ± 1	23
15m	0 ± 0	1 ± 0	1 ± 1	0 ± 0	1 ± 0	COMP	COMP	4 ± 0	4 ± 0	3 ± 0	1 ± 1		2
19m	5 ± 0	1 ± 0	1 ± 1	6 ± 0	2 ± 0	16 ± 2	53 ± 2	36 ± 2	13 ± 1	25 ± 2	4 ± 1		12
20m	10 ± 1	2 ± 1	0 ± 1	13 ± 1	1 ± 0	15 ± 2	42 ± 5	28 ± 1	12 ± 1	4 ± 0	2 ± 0		10
22m	6 ± 0	2 ± 0	2 ± 1	15 ± 1	7 ± 1	24 ± 1	24 ± 1	36 ± 1	37 ± 3	13 ± 1	4 ± 4	31 ± 0	14
23m	21 ± 1	3 ± 0	3 ± 1	6 ± 0	13 ± 1	16 ± 2	31 ± 2	63 ± 2	21 ± 1	2 ± 0	1 ± 0	20 ± 5	19
25m	8 ± 1	4 ± 0	4 ± 1	24 ± 1	10 ± 1	27 ± 1	15 ± 2	70 ± 2	42 ± 1	10 ± 1	4 ± 4	24 ± 1	24

Table 4 (a) Percent methane in bubbles with analytical errors in 2007.
(COMP = Compromised samples, FULL= Overfull traps).

Trap	Aug-22	Aug-27	Aug-29	Sep-05	Sep-09	Sep-13	Sep-18	Sep-23	Sep-27	Oct-04	Oct-09
6m	48 ± 0	48 ± 0	48 ± 0	48 ± 0	48 ± 0		37 ± 1	37 ± 1	37 ± 1	37 ± 1	48 ± 0
9m(A)	91 ± 0	91 ± 0	88 ± 2	FULL	FULL	FULL		FULL	FULL	FULL	91 ± 0
10m		COMP									
12m											
13m	67 ± 0	67 ± 0	64 ± 1	FULL	62 ± 0	75 ± 1		51 ± 2	58 ± 1	58 ± 1	67 ± 0
15m								46 ± 1	46 ± 1	46 ± 1	
19m	65 ± 0	73 ± 1	68 ± 1	FULL	70 ± 0	76 ± 1		51 ± 1	51 ± 1	51 ± 1	65 ± 0
20m	77 ± 1	65 ± 1	COMP	68 ± 1	71 ± 1	65 ± 1			52 ± 1	52 ± 1	77 ± 1
22m		70 ± 1	COMP	FULL	77 ± 1	73 ± 2		56 ± 1	56 ± 1	57 ± 2	
23m	76 ± 1	76 ± 1	78 ± 0	FULL	81 ± 1	83 ± 1	13 ± 0	13 ± 0	69 ± 1	70 ± 1	76 ± 1
25m	75 ± 2	78 ± 1	81 ± 1	80 ± 1	79 ± 1	84 ± 1			69 ± 1	69 ± 1	75 ± 2

Trap	Oct-13	Oct-20	Oct-28	Nov-01	Nov-06	Nov-12	Nov-14	Nov-30	AVERAGE
6m	30 ± 0	39 ± 1	37 ± 0	45 ± 0		37 ± 0		25 ± 1	25 ± 1
9m(A)	87 ± 1	83 ± 2	72 ± 1	52 ± 1		68 ± 0	62 ± 1	56 ± 0	FULL
10m		41 ± 0	41 ± 0	41 ± 0		41 ± 0			
12m		22 ± 0	22 ± 0	22 ± 0		22 ± 0	22 ± 0		
13m	63 ± 2	66 ± 1	56 ± 0	55 ± 1		62 ± 1	60 ± 1	58 ± 0	
15m	46 ± 1	35 ± 2	35 ± 2	42 ± 0		42 ± 0			53 ± 1
19m	63 ± 2	72 ± 1	MOVED						
20m	65 ± 1	68 ± 2					54 ± 0	COMP	50 ± 1
22m	71 ± 1	70 ± 2	66 ± 2				COMP	63 ± 0	68 ± 2
23m	68 ± 1	71 ± 1	69 ± 0	71 ± 2		COMP	72 ± 0	67 ± 1	72 ± 2
25m	72 ± 0	76 ± 2	72 ± 1	63 ± 1		67 ± 0			74 ± 1

Table 4 (b) Percent methane in bubbles with analytical errors in 2008. (COMP = Compromised samples)

Trap	Winter (Apr-05)	Apr-10	Apr-22	May-11	May-17	May-23	May-30	Jun-05	Jun-12	Jun-19	Jun-23	Jun-27
6m												
9m(A)					71 ± 2	75 ± 3		86 ± 1		79 ± 2		
9m(B)												
9m(C)												
10m												
12m												
13m					53 ± 1	57 ± 2	68 ± 1	67 ± 1	70 ± 1	60 ± 1	37 ± 1	37 ± 1
15m										56 ± 1		
19m							79 ± 2	71 ± 1	69 ± 1		68 ± 1	
20m	51 ± 1											
22m	67 ± 1											
23m	70 ± 1			62 ± 2	74 ± 1	81 ± 3	58 ± 1	74 ± 1	76 ± 1	73 ± 1	59 ± 2	57 ± 2
25m				56 ± 2	75 ± 2	77 ± 2	78 ± 2	78 ± 1	74 ± 1	COMP		

Trap	Jul-02	Jul-10	Jul-16	Jul-23	Jul-30	Aug-05	Aug-13	Aug-19	Aug-25	Aug-28	Sep-03	Sep-08	Sep-13
6m													
9m(A)	81 ± 1	33 ± 1	85 ± 2	79 ± 2	84 ± 3						66 ± 2	54 ± 1	79 ± 2
9m(B)											56 ± 3	68 ± 1	
9m(C)													74 ± 1
10m													
12m													
13m	49 ± 1	56 ± 1	52 ± 1	64 ± 3	47 ± 1	50 ± 2	48 ± 2	60 ± 2	55 ± 2	66 ± 1	51 ± 3		50 ± 1
15m		50 ± 2	39 ± 1								47 ± 1		
19m	53 ± 1	33 ± 1	50 ± 2	70 ± 1			56 ± 2		67 ± 3	73 ± 2	68 ± 5	COMP	
20m							59 ± 2	67 ± 2	62 ± 3	53 ± 2	71 ± 3	69 ± 1	
22m		58 ± 1	51 ± 1	71 ± 3			48 ± 2	72 ± 2	56 ± 2	62 ± 2	75 ± 1	60 ± 2	
23m		22 ± 1	57 ± 1	73 ± 2		60 ± 2	55 ± 2	53 ± 2	51 ± 3	73 ± 2	67 ± 4	75 ± 1	
25m			60 ± 2	76 ± 3			48 ± 2		66 ± 2	72 ± 2	75 ± 2	75 ± 1	

Trap	Sep-19	Sep-22	Sep-25	Oct-02	Oct-08	Oct-13	Oct-15	Oct-23	Oct-31	Nov-09	Nov-14	Dec-01	AVERAGE
6m					27 ± 1	44 ± 1	44 ± 1	41 ± 1	34 ± 1				38 ± 7
9m(A)	55 ± 1	75 ± 2	75 ± 2	FULL	48 ± 1	79 ± 2	73 ± 2	55 ± 1	76 ± 1	56 ± 2	56 ± 2	70 ± 1	69 ± 14
9m(B)	44 ± 1	89 ± 2	84 ± 2	70 ± 3	47 ± 1	47 ± 2	50 ± 1	FULL	FULL	60 ± 2	52 ± 1	81 ± 2	62 ± 16
9m(C)	FULL	67 ± 1		88 ± 2	86 ± 2	76 ± 2	76 ± 2	86 ± 2	87 ± 2	86 ± 2	86 ± 2		81 ± 7
10m													0 ± 0
12m					46 ± 1	47 ± 1	47 ± 1		45 ± 1	45 ± 1			46 ± 1
13m	57 ± 1	61 ± 1	61 ± 1	68 ± 2	61 ± 1	63 ± 2	COMP	43 ± 1	53 ± 1	51 ± 1	47 ± 1	59 ± 1	56 ± 9
15m						COMP	COMP	45 ± 1	56 ± 1				49 ± 7
19m	71 ± 1			70 ± 2		76 ± 2	76 ± 2	72 ± 4	75 ± 1	72 ± 2	70 ± 1		67 ± 11
20m	47 ± 1			64 ± 1		63 ± 1	63 ± 1	68 ± 1	COMP	56 ± 2			62 ± 7
22m	60 ± 1			15 ± 1	60 ± 1	71 ± 2	71 ± 2	72 ± 1	77 ± 1	75 ± 2	74 ± 1	74 ± 1	63 ± 15
23m	72 ± 1			61 ± 2	62 ± 1	74 ± 2	74 ± 2	77 ± 2	63 ± 1	COMP		72 ± 1	65 ± 12
25m	68 ± 1			74 ± 2	66 ± 2	75 ± 2	75 ± 2	75 ± 1	76 ± 1	72 ± 2	71 ± 1	71 ± 1	71 ± 8

Table 5 (a) Percent oxygen in bubbles with analytical errors in 2007.

Trap	Aug-22	Aug-27	Aug-29	Sep-05	Sep-09	Sep-13	Sep-18	Sep-23	Sep-27	Oct-04	Oct-09
6m	0.8 ± 0.3	0.8 ± 0.3	0.8 ± 0.3	0.8 ± 0.3	0.8 ± 0.3		1.3 ± 0.5	1.3 ± 0.5	1.3 ± 0.5	1.3 ± 0.5	2.3 ± 0.4
9m(A)	0.4 ± 0.5	0.4 ± 0.5	0.8 ± 0.5	13.8 ± 0.3	1.4 ± 0.3	2.5 ± 0.2		4.6 ± 0.6	4.6 ± 0.6	4.6 ± 0.6	0.7 ± 0.5
10m		18.5 ± 0.9									
12m											
13m	0.8 ± 0.5	0.8 ± 0.5	0.9 ± 0.3	5.8 ± 0.2	0.7 ± 0.2	0.5 ± 0.2		0.8 ± 0.4	0.7 ± 0.3	0.7 ± 0.3	0.7 ± 0.3
15m								1.0 ± 0.4	1.0 ± 0.4	1.0 ± 0.4	1.0 ± 0.4
19m	0.6 ± 0.3	0.5 ± 0.5	1.5 ± 0.3	1.8 ± 0.2	0.6 ± 0.2	0.5 ± 0.2		1.3 ± 0.5	1.3 ± 0.5	1.3 ± 0.5	1.3 ± 0.7
20m	0.6 ± 0.3	0.6 ± 0.4	17.0 ± 0.5	0.6 ± 0.2	0.5 ± 0.3	0.5 ± 0.3			3.2 ± 0.9	3.2 ± 0.9	0.7 ± 0.4
22m		1.4 ± 0.3	15.4 ± 1.7	1.0 ± 0.0	0.5 ± 0.4	0.4 ± 0.2		4.1 ± 0.4	4.1 ± 0.4	0.8 ± 0.4	0.8 ± 0.3
23m	0.6 ± 0.3	2.1 ± 0.2	1.4 ± 0.2	1.7 ± 0.1	0.4 ± 0.2	0.4 ± 0.2	10.3 ± 0.3	10.3 ± 0.3	0.7 ± 0.4	1.7 ± 1.1	0.7 ± 0.3
25m	0.4 ± 0.3	0.9 ± 0.3	0.8 ± 0.2	0.5 ± 0.1	0.5 ± 0.2	0.3 ± 0.2			0.9 ± 0.4	0.9 ± 0.4	0.7 ± 0.3

Trap	Oct-13	Oct-20	Oct-28	Nov-01	Nov-06	Nov-12	Nov-14	Nov-30	AVERAGE
6m	0.9 ± 0.4	0.8 ± 0.3	0.9 ± 0.2		0.9 ± 0.2		0.9 ± 0.2	0.9 ± 0.2	1.0 ± 0.2
9m(A)	0.6 ± 0.2	0.8 ± 0.3	0.9 ± 0.2		0.6 ± 0.2	0.7 ± 0.2	0.6 ± 0.2	6.2 ± 0.2	2.5 ± 0.3
10m	0.8 ± 0.2	0.8 ± 0.2	0.8 ± 0.2		0.8 ± 0.2				0.8 ± 0.0
12m	2.9 ± 0.2	2.9 ± 0.2	2.9 ± 0.2		2.9 ± 0.2	2.9 ± 0.2			2.9 ± 0.0
13m	0.7 ± 0.3	0.7 ± 0.3	0.8 ± 0.2		0.6 ± 0.2	0.7 ± 0.2	0.9 ± 0.2		1.0 ± 0.1
15m	2.5 ± 0.3	2.5 ± 0.3	0.9 ± 0.2		0.9 ± 0.2			0.7 ± 0.2	1.2 ± 0.1
19m	0.5 ± 0.3	MOVED							1.0 ± 0.5
20m	1.1 ± 0.6					5.4 ± 0.3	14.5 ± 0.5	0.9 ± 0.2	1.6 ± 0.2
22m	0.4 ± 0.3	1.4 ± 0.3				7.6 ± 0.0	1.3 ± 0.2	0.9 ± 0.3	1.4 ± 0.4
23m	0.6 ± 0.3	0.5 ± 0.3	0.4 ± 0.1		3.1 ± 0.2	0.6 ± 0.2	1.7 ± 0.3	0.5 ± 0.1	2.1 ± 0.5
25m	0.5 ± 0.2	1.1 ± 0.3	1.9 ± 0.2		0.7 ± 0.2			0.6 ± 0.2	0.8 ± 0.4

Table 5 (b) Percent oxygen in bubbles with analytical errors in 2008.

Trap	Winter (Apr-05)	Apr-10	Apr-22	May-11	May-17	May-23	May-30	Jun-05	Jun-12	Jun-19	Jun-23	Jun-27
6m												
9m(A)					3.8 ± 0.3	3.4 ± 0.0		0.4 ± 0.0		1.0 ± 0.0		
9m(B)												
9m(C)												
10m												
12m												
13m					2.1 ± 0.1	1.8 ± 0.2	0.8 ± 0.0	0.6 ± 0.0	0.5 ± 0.0	0.6 ± 0.0	1.3 ± 0.1	1.3 ± 0.1
15m										1.1 ± 0.0		
19m							0.5 ± 0.0	0.7 ± 0.0	0.7 ± 0.0		0.6 ± 0.0	
20m	0.5 ± 0.0											
22m	0.4 ± 0.0											
23m	0.4 ± 1.1			1.1 ± 0.0	1.1 ± 0.1	0.5 ± 0.0	3.2 ± 0.3	0.7 ± 0.0	0.6 ± 0.0	0.9 ± 0.1	2.9 ± 0.1	2.2 ± 0.1
25m				0.8 ± 0.0	0.9 ± 0.0	0.8 ± 0.1	0.6 ± 0.2	0.5 ± 0.0	0.7 ± 0.0	14.1 ± 0.9		

172

Trap	Jul-02	Jul-10	Jul-16	Jul-23	Jul-30	Aug-05	Aug-13	Aug-19	Aug-25	Aug-28	Sep-03	Sep-08
6m												
9m(A)	1.2 ± 0.0	11.4 ± 1.4	0.6 ± 0.0	0.4 ± 0.0	0.8 ± 0.0						1.0 ± 0.1	0.5 ± 0.0
9m(B)												1.3 ± 0.1
9m(C)												
10m												
12m												
13m	1.0 ± 0.0	0.6 ± 0.0	0.7 ± 0.0	0.7 ± 0.1	0.8 ± 0.0	0.8 ± 0.0	1.1 ± 0.0	0.6 ± 0.1	2.0 ± 0.1	0.7 ± 0.1	1.1 ± 0.6	
15m		1.3 ± 0.1	0.8 ± 0.0								0.9 ± 0.0	
19m	1.5 ± 0.0	2.2 ± 0.1	2.0 ± 0.1	0.7 ± 0.0			2.1 ± 0.0			1.1 ± 0.1	0.5 ± 0.0	0.6 ± 0.0
20m							0.8 ± 0.0	0.8 ± 0.0	1.6 ± 0.0	1.7 ± 0.0	0.6 ± 0.1	0.5 ± 0.0
22m		0.7 ± 0.1	1.9 ± 0.1	1.0 ± 0.4			2.2 ± 0.0	0.5 ± 0.0	0.9 ± 0.0	1.2 ± 0.1	0.8 ± 0.1	0.9 ± 0.1
23m		1.9 ± 0.2	1.0 ± 0.1	0.6 ± 0.0		0.7 ± 0.0	0.7 ± 0.0	0.7 ± 0.0	1.7 ± 0.0	0.6 ± 0.0	0.9 ± 0.4	0.4 ± 0.1
25m			1.3 ± 0.1	0.9 ± 0.2			1.8 ± 0.0			0.7 ± 0.2	0.9 ± 0.3	0.6 ± 0.1

Trap	Sep-13	Sep-19	Sep-22	Sep-25	Oct-02	Oct-08	Oct-13	Oct-15	Oct-23	Oct-31
6m						1.7 ± 0.2	0.9 ± 0.0	0.9 ± 0.1	0.7 ± 0.1	0.8 ± 0.0
9m(A)	0.4 ± 0.0	0.6 ± 0.0	0.4 ± 0.0	0.4 ± 0.0	2.3 ± 0.2	4.6 ± 0.4	0.4 ± 0.1	0.4 ± 0.1	0.7 ± 0.1	0.3 ± 0.1
9m(B)	0.9 ± 0.1	1.5 ± 0.0	0.6 ± 0.3	0.4 ± 0.0	0.7 ± 0.1	0.7 ± 0.1	1.3 ± 0.7	0.8 ± 0.1	1.4 ± 0.2	1.8 ± 0.0
9m(C)	0.5 ± 0.0	8.1 ± 0.1	0.7 ± 0.0		1.2 ± 0.1	1.0 ± 0.2	0.7 ± 0.0	0.7 ± 0.1	0.3 ± 0.0	0.2 ± 0.0
10m										
12m						1.1 ± 0.1	0.7 ± 0.0	0.7 ± 0.1		0.8 ± 0.0
13m	0.6 ± 0.0	0.6 ± 0.0	0.5 ± 0.0	0.5 ± 0.0	0.6 ± 0.0	0.5 ± 0.1	0.5 ± 0.0	17.7 ± 1.7	0.9 ± 0.1	0.8 ± 0.0
15m								17.5 ± 1.6	17.5 ± 1.6	0.9 ± 0.1
19m		0.5 ± 0.0			0.4 ± 0.0		0.4 ± 0.0	0.4 ± 0.1	0.7 ± 0.2	0.5 ± 0.0
20m		0.8 ± 0.0			0.6 ± 0.1		0.5 ± 0.0	0.5 ± 0.1	0.5 ± 0.1	6.4 ± 0.1
22m		0.5 ± 0.0			1.1 ± 0.1	0.6 ± 0.1	0.7 ± 0.0	0.7 ± 0.1	1.1 ± 0.6	0.4 ± 0.0
23m		0.5 ± 0.0			1.1 ± 0.1	0.6 ± 0.1	0.4 ± 0.0	0.4 ± 0.1	0.5 ± 0.1	0.5 ± 0.0
25m		0.4 ± 0.0			0.5 ± 0.0	0.7 ± 0.1	0.5 ± 0.1	0.5 ± 0.1	0.5 ± 0.2	0.5 ± 0.0

Trap	Nov-09	Nov-14	Dec-01	AVERAGE
6m				1.0 ± 0.4
9m(A)	0.7 ± 0.1	0.7 ± 0.1	0.5 ± 0.0	0.7 ± 0.4
9m(B)	0.6 ± 0.1	0.6 ± 0.0	0.6 ± 0.1	0.9 ± 0.4
9m(C)	0.2 ± 0.0	0.2 ± 0.0		0.6 ± 0.3
10m				
12m	1.7 ± 0.0			1.0 ± 0.4
13m	0.7 ± 0.0	0.7 ± 0.0	0.6 ± 0.1	0.8 ± 0.3
15m				0.9 ± 0.2
19m	1.3 ± 0.0	0.8 ± 0.0		0.7 ± 0.3
20m	1.6 ± 0.0			0.9 ± 0.5
22m	0.6 ± 0.0	0.5 ± 0.0	0.5 ± 0.0	0.8 ± 0.4
23m			0.4 ± 0.0	0.8 ± 0.4
25m	0.4 ± 0.0	0.5 ± 0.0	0.5 ± 0.0	0.7 ± 0.3

Table 6 (a) Methane bubbling fluxes ($\text{mmol CH}_4 \cdot \text{m}^{-2} \cdot \text{d}^{-1}$) from the UML in 2007. Volumetric fluxes were multiplied by the methane content for the corresponding time period to calculate these fluxes.

Trap	Jul-20	Jul-23	Jul-26	Jul-30	Aug-02	Aug-07	Aug-10	Aug-16	Aug-17	Aug-22	Aug-27
6m		0.0 ± 0.0	0.4 ± 0.1								
9m(A)		2.6 ± 0.5	3.0 ± 0.6	0.6 ± 0.1	0.1 ± 0.0	1.5 ± 0.3	0.1 ± 0.0	1.5 ± 0.3		0.2 ± 0.2	3.5 ± 0.7
10m									0.0 ± 0.0	0.0 ± 0.0	
12m									0.0 ± 0.0	0.0 ± 0.0	0.0 ± 0.0
13m		1.0 ± 0.1	0.8 ± 0.1	0.6 ± 0.1	0.0 ± 0.0	0.1 ± 0.0	0.5 ± 0.0	0.1 ± 0.1	0.1 ± 0.1	0.1 ± 0.1	3.7 ± 0.4
15m		0.1 ± 0.0	0.0 ± 0.0	0.1 ± 0.0	0.1 ± 0.0	0.0 ± 0.0					
19m										0.4 ± 0.1	3.2 ± 0.5
20m	4.3 ± 0.6	0.3 ± 0.1	0.4 ± 0.1	5.2 ± 0.7	0.1 ± 0.0	0.1 ± 0.0	0.1 ± 0.0	0.8 ± 0.1	0.4 ± 0.4	0.3 ± 0.2	1.2 ± 0.2
22m	6.3 ± 0.7	1.3 ± 0.2	2.3 ± 0.3	5.8 ± 0.6	0.2 ± 0.0			0.4 ± 0.1	1.2 ± 0.2	0.1 ± 0.0	5.7 ± 0.6
23m									2.2 ± 0.7	0.6 ± 0.2	6.6 ± 2.1
25m									0.6 ± 0.1	4.8 ± 0.4	
Lake total		0.8 ± 0.1	1.1 ± 0.1	3.3 ± 0.3	0.1 ± 0.0	0.2 ± 0.0	0.1 ± 0.0	0.6 ± 0.1	0.6 ± 0.1	0.2 ± 0.0	2.6 ± 0.2

174

Trap	Aug-29	Sep-05	Sep-09	Sep-13	Sep-18	Sep-23	Sep-27	Oct-04	Oct-09	Oct-13	Oct-20
6m	0.4 ± 0.1	0.4 ± 0.1	0.5 ± 0.1	0.0 ± 0.0	0.0 ± 0.1	0.0 ± 0.1	0.0 ± 0.1	0.2 ± 0.1	0.6 ± 0.1	0.7 ± 0.1	0.2 ± 0.0
9m(A)	3.2 ± 0.7	4.1 ± 0.8	5.9 ± 1.2	6.6 ± 1.3	0.0 ± 0.0	0.1 ± 0.1	0.1 ± 0.1	3.6 ± 0.7	5.3 ± 1.1	4.2 ± 0.9	0.4 ± 0.1
10m	0.0 ± 0.0										
12m	0.0 ± 0.0										
13m	1.7 ± 0.2	2.5 ± 0.2	1.1 ± 0.1	3.6 ± 0.5	0.1 ± 0.0	0.4 ± 0.0	0.3 ± 0.1	0.7 ± 0.1	1.8 ± 0.3	2.5 ± 0.2	0.2 ± 0.0
15m	0.0 ± 0.0	0.4 ± 0.1	0.0 ± 0.0	0.0 ± 0.0							
19m	1.9 ± 0.3	3.3 ± 0.7	2.4 ± 0.4	3.5 ± 0.5	0.0 ± 0.0	0.1 ± 0.1	0.1 ± 0.1	0.1 ± 0.1	0.9 ± 0.1	1.7 ± 0.3	
20m		1.9 ± 0.3	2.1 ± 0.3	0.8 ± 0.1	0.0 ± 0.0	0.0 ± 0.0	0.0 ± 0.1	0.0 ± 0.1	0.7 ± 0.1	1.4 ± 0.2	0.0 ± 0.0
22m		3.8 ± 0.4	5.0 ± 0.6	2.8 ± 0.3	0.1 ± 0.0	0.1 ± 0.1	0.1 ± 0.1	0.2 ± 0.0	1.1 ± 0.1	1.1 ± 0.2	0.3 ± 0.0
23m	2.5 ± 0.8	4.5 ± 1.4	5.4 ± 1.7	3.6 ± 1.2	0.0 ± 0.0	0.2 ± 0.1	1.0 ± 0.3	0.8 ± 0.3	2.2 ± 0.7	2.1 ± 0.7	0.5 ± 0.2
25m	2.8 ± 0.3	4.1 ± 0.3	4.2 ± 0.4	3.8 ± 0.4	0.0 ± 0.0	0.0 ± 0.0	0.2 ± 0.2	0.4 ± 0.1	1.9 ± 0.2	2.6 ± 0.3	0.5 ± 0.0
Lake total	1.9 ± 0.2	2.3 ± 0.2	2.7 ± 0.2	2.2 ± 0.2	0.0 ± 0.0	0.1 ± 0.0	0.1 ± 0.0	0.6 ± 0.1	1.3 ± 0.1	1.5 ± 0.1	0.2 ± 0.0

Trap	Oct-28	Nov-01	Nov-06	Nov-12	Nov-14	Nov-30	AVERAGE
6m	0.2 ± 0.0	0.2 ± 0.0	0.2 ± 0.0	0.0 ± 0.0	0.0 ± 0.0	0.0 ± 0.0	0.2
9m(A)	0.2 ± 0.1	1.0 ± 0.2	0.9 ± 0.2	0.8 ± 0.2	0.9 ± 0.2	1.6 ± 0.3	2.0
10m	0.0 ± 0.0	0.3 ± 0.0	0.3 ± 0.1	0.0 ± 0.0	0.0 ± 0.0	0.0 ± 0.0	0.0
12m	0.0 ± 0.0	0.0 ± 0.0	0.0 ± 0.0	0.0 ± 0.0		0.0 ± 0.0	0.0
13m	0.2 ± 0.0	0.5 ± 0.0	0.5 ± 0.0	0.4 ± 0.0	1.2 ± 0.1		0.9
15m	0.0 ± 0.0	0.0 ± 0.0	0.0 ± 0.0	0.0 ± 0.0	0.0 ± 0.0	0.1 ± 0.0	0.0
19m	0.0 ± 0.0	0.0 ± 0.0	0.0 ± 0.0	0.0 ± 0.0	0.0 ± 0.0	0.0 ± 0.0	1.0
20m	0.0 ± 0.0	0.0 ± 0.0	0.0 ± 0.0	0.4 ± 0.1	0.4 ± 0.1	0.0 ± 0.0	0.8
22m	0.0 ± 0.0	0.0 ± 0.0	0.0 ± 0.0	0.2 ± 0.0	0.4 ± 0.1	0.2 ± 0.0	1.5
23m	0.6 ± 0.2	0.5 ± 0.2	0.2 ± 0.1	0.2 ± 0.1	1.2 ± 0.4	0.7 ± 0.2	1.8
25m	0.1 ± 0.0	0.1 ± 0.0	0.1 ± 0.0	0.0 ± 0.0	0.2 ± 0.0	0.4 ± 0.0	1.4
Lake total	0.1 ± 0.0	0.2 ± 0.0	0.2 ± 0.0	0.2 ± 0.0	0.4 ± 0.0	0.3 ± 0.0	

Table 6 (b) Methane bubbling fluxes (mmol CH₄.m⁻².d⁻¹) from the UML in 2008.

Trap	Winter (Apr-05)	Apr-10	Apr-22	May-11	May-17	May-23	May-30	Jun-05	Jun-12	Jun-19	Jun-23	Jun-27
6m					0.0 ± 0.0	0.0 ± 0.0	0.0 ± 0.0	0.0 ± 0.0				
9m(A)					0.8 ± 0.0	0.1 ± 0.0	0.0 ± 0.0	0.7 ± 0.1	0.0 ± 0.0	0.2 ± 0.0	0.0 ± 0.0	0.0 ± 0.0
9m(B)												
9m(C)												
10m												
12m										0.0 ± 0.0	0.0 ± 0.0	0.0 ± 0.0
13m					0.6 ± 0.0	0.7 ± 0.0	0.3 ± 0.0	0.6 ± 0.0	0.6 ± 0.0	0.3 ± 0.0	0.1 ± 0.0	0.1 ± 0.0
15m										0.2 ± 0.0	0.0 ± 0.0	0.0 ± 0.0
19m							0.8 ± 0.1	0.1 ± 0.0	0.4 ± 0.0		0.7 ± 0.0	
20m	0.0 ± 0.0	0.0 ± 0.0	0.0 ± 0.0									
22m	0.0 ± 0.1	0.0 ± 0.0	0.0 ± 0.0								0.1 ± 0.0	0.0 ± 0.0
23m	0.2 ± 0.0	0.0 ± 0.0	0.0 ± 0.0	0.1 ± 0.0	1.1 ± 0.1	3.0 ± 0.2	0.3 ± 0.0	1.2 ± 0.0	0.5 ± 0.0	0.5 ± 0.0	0.1 ± 0.0	0.3 ± 0.0
25m		0.0 ± 0.0	0.0 ± 0.0	0.1 ± 0.0	1.6 ± 0.1	3.3 ± 0.2	0.6 ± 0.0	0.6 ± 0.1	0.4 ± 0.0		0.0 ± 0.0	0.0 ± 0.0
Total		0.0 ± 0.0	0.0 ± 0.0	0.1 ± 0.0	1.3 ± 0.1	2.5 ± 0.1	0.5 ± 0.0	0.5 ± 0.0	0.4 ± 0.0	0.4 ± 0.0	0.1 ± 0.0	0.0 ± 0.0

Trap	Jul-02	Jul-10	Jul-16	Jul-23	Jul-30	Aug-05	Aug-13	Aug-19	Aug-25	Aug-28	Sep-03	Sep-08	Sep-13
6m							0.0 ± 0.0	0.0 ± 0.0	0.0 ± 0.0	0.0 ± 0.0	0.0 ± 0.0	0.1 ± 0.0	0.0 ± 0.0
9m(A)	0.3 ± 0.0	0.9 ± 0.0	0.8 ± 0.0	0.6 ± 0.0	1.9 ± 0.1	0.0 ± 0.0	0.0 ± 0.0	0.0 ± 0.0	0.1 ± 0.0	0.2 ± 0.0	0.7 ± 0.1	0.1 ± 0.0	1.4 ± 0.1
9m(B)												0.1 ± 0.0	0.5 ± 0.0
9m(C)												0.1 ± 0.0	1.2 ± 0.1
10m		0.0 ± 0.0	0.0 ± 0.0	0.0 ± 0.0	0.0 ± 0.0	0.0 ± 0.0	0.0 ± 0.0	0.0 ± 0.0	0.0 ± 0.0	0.0 ± 0.0	0.0 ± 0.0	0.0 ± 0.0	0.0 ± 0.0
12m	0.0 ± 0.0	0.0 ± 0.0	0.0 ± 0.0	0.0 ± 0.0	0.0 ± 0.0	0.0 ± 0.0	0.0 ± 0.0	0.0 ± 0.0	0.0 ± 0.0	0.1 ± 0.0	0.0 ± 0.0	0.0 ± 0.0	0.0 ± 0.0
13m	0.2 ± 0.0	0.4 ± 0.0	0.4 ± 0.0	1.9 ± 0.1	0.1 ± 0.0	0.3 ± 0.0	0.1 ± 0.0	0.4 ± 0.0	0.9 ± 0.0	1.3 ± 0.1	1.5 ± 0.1	0.0 ± 0.0	0.4 ± 0.0
15m	0.0 ± 0.0	0.2 ± 0.0	0.1 ± 0.0	0.0 ± 0.0	0.0 ± 0.0	0.0 ± 0.0	0.0 ± 0.0	0.0 ± 0.0	0.1 ± 0.0	0.1 ± 0.0	0.0 ± 0.0	0.0 ± 0.0	0.0 ± 0.0
19m	0.1 ± 0.0	0.1 ± 0.0	0.2 ± 0.0	0.8 ± 0.0	0.0 ± 0.0	0.1 ± 0.0	0.1 ± 0.0	0.1 ± 0.0	0.4 ± 0.0	0.3 ± 0.0	0.8 ± 0.1		0.1 ± 0.0
20m						0.0 ± 0.0	0.2 ± 0.0	0.3 ± 0.0	0.2 ± 0.0	0.2 ± 0.0	1.1 ± 0.1	0.3 ± 0.0	0.0 ± 0.0
22m	0.0 ± 0.0	0.1 ± 0.0	0.2 ± 0.0	1.3 ± 0.1	0.0 ± 0.0	0.0 ± 0.0	0.1 ± 0.0	0.7 ± 0.0	0.2 ± 0.0	0.6 ± 0.0	2.1 ± 0.0	0.2 ± 0.0	0.1 ± 0.0
23m	0.0 ± 0.0	0.2 ± 0.0	0.2 ± 0.0	1.2 ± 0.1	0.0 ± 0.0	0.2 ± 0.0	0.0 ± 0.0	0.1 ± 0.0	0.1 ± 0.0	2.3 ± 0.1	1.2 ± 0.1	1.0 ± 0.1	0.1 ± 0.0
25m	0.1 ± 0.0	0.8 ± 0.1	0.3 ± 0.0	2.2 ± 0.1	0.0 ± 0.0	0.0 ± 0.0	0.1 ± 0.0	0.0 ± 0.0	1.4 ± 0.1	1.3 ± 0.1	3.7 ± 0.1	1.2 ± 0.0	0.0 ± 0.0
Total	0.1 ± 0.0	0.3 ± 0.0	0.2 ± 0.0	0.8 ± 0.0	0.3 ± 0.0	0.0 ± 0.0	0.1 ± 0.0	0.2 ± 0.0	0.3 ± 0.0	0.5 ± 0.0	1.1 ± 0.0	0.3 ± 0.0	0.2 ± 0.0

Trap	Sep-19	Sep-22	Sep-25	Oct-02	Oct-08	Oct-13	Oct-15	Oct-23	Oct-31	Nov-09	Nov-14	Dec-01	AVG.
6m	0.0 ± 0.0	0.0 ± 0.0	0.0 ± 0.0	0.0 ± 0.0	0.0 ± 0.0	0.4 ± 0.0	0.4 ± 0.0	0.2 ± 0.0	0.2 ± 0.0	0.0 ± 0.0			1
9m(A)	0.3 ± 0.0	1.3 ± 0.1	0.5 ± 0.0	5.4 ± 1.1	0.5 ± 0.0	1.0 ± 0.1	1.2 ± 0.1	0.9 ± 0.0	3.4 ± 0.1	0.9 ± 0.0	0.7 ± 0.1	1.4 ± 0.1	19
9m(B)	0.1 ± 0.0	6.2 ± 0.2	1.3 ± 0.0	1.0 ± 0.1	0.3 ± 0.0	0.4 ± 0.0	0.6 ± 0.1	3.2 ± 0.8	3.2 ± 0.8	1.1 ± 0.1	0.3 ± 0.0	2.0 ± 0.1	35
9m(C)	8.6 ± 0.8	0.6 ± 0.1	0.0 ± 0.0	3.2 ± 0.1	2.2 ± 0.1	1.1 ± 0.1	0.3 ± 0.0	0.3 ± 0.0	0.4 ± 0.0	0.6 ± 0.0	0.0 ± 0.0	0.1 ± 0.0	32
10m	0.0 ± 0.0	0.0 ± 0.0	0.0 ± 0.0	0.0 ± 0.0	0.0 ± 0.0	0.0 ± 0.0	0.0 ± 0.0	0.0 ± 0.0	0.0 ± 0.0	0.0 ± 0.0			0
12m	0.0 ± 0.0	0.0 ± 0.0	0.0 ± 0.0	0.0 ± 0.0	0.1 ± 0.0	0.2 ± 0.0	0.2 ± 0.0	0.0 ± 0.0	0.2 ± 0.0	0.0 ± 0.0	0.0 ± 0.0		1
13m	0.6 ± 0.0	0.7 ± 0.1	0.2 ± 0.0	1.3 ± 0.1	0.6 ± 0.0	0.8 ± 0.0		0.3 ± 0.0	0.7 ± 0.1	0.5 ± 0.0	0.1 ± 0.0	1.1 ± 0.0	14
15m	0.0 ± 0.0	0.0 ± 0.0	0.0 ± 0.0	0.0 ± 0.0	0.0 ± 0.0			0.1 ± 0.0	0.1 ± 0.0	0.1 ± 0.0	0.0 ± 0.0		1
19m	0.2 ± 0.0	0.0 ± 0.0	0.0 ± 0.0	0.2 ± 0.0	0.1 ± 0.0	0.5 ± 0.1	1.7 ± 0.1	1.1 ± 0.1	0.4 ± 0.0	0.7 ± 0.1	0.1 ± 0.0		9
20m	0.2 ± 0.0	0.0 ± 0.0	0.0 ± 0.0	0.3 ± 0.0	0.0 ± 0.0	0.4 ± 0.1	1.1 ± 0.1	0.8 ± 0.0		0.1 ± 0.0	0.1 ± 0.0		7
22m	0.1 ± 0.0	0.0 ± 0.0	0.0 ± 0.0	0.1 ± 0.0	0.2 ± 0.0	0.7 ± 0.0	0.7 ± 0.0	1.1 ± 0.0	1.2 ± 0.1	0.4 ± 0.0	0.1 ± 0.1	1.0 ± 0.0	10
23m	0.6 ± 0.0	0.1 ± 0.0	0.1 ± 0.0	0.1 ± 0.0	0.3 ± 0.0	0.5 ± 0.1	1.0 ± 0.1	2.0 ± 0.1	0.6 ± 0.0		0.0 ± 0.0	0.6 ± 0.1	14
25m	0.2 ± 0.0	0.1 ± 0.0	0.1 ± 0.0	0.7 ± 0.0	0.3 ± 0.0	0.8 ± 0.0	0.5 ± 0.1	2.2 ± 0.1	1.3 ± 0.0	0.3 ± 0.0	0.1 ± 0.1	0.7 ± 0.0	17
Total	0.5 ± 0.0	0.4 ± 0.0	0.1 ± 0.0	0.6 ± 0.0	0.2 ± 0.0	0.5 ± 0.0	0.6 ± 0.0	0.8 ± 0.0	0.9 ± 0.0	0.3 ± 0.0	0.1 ± 0.0	0.9 ± 0.0	

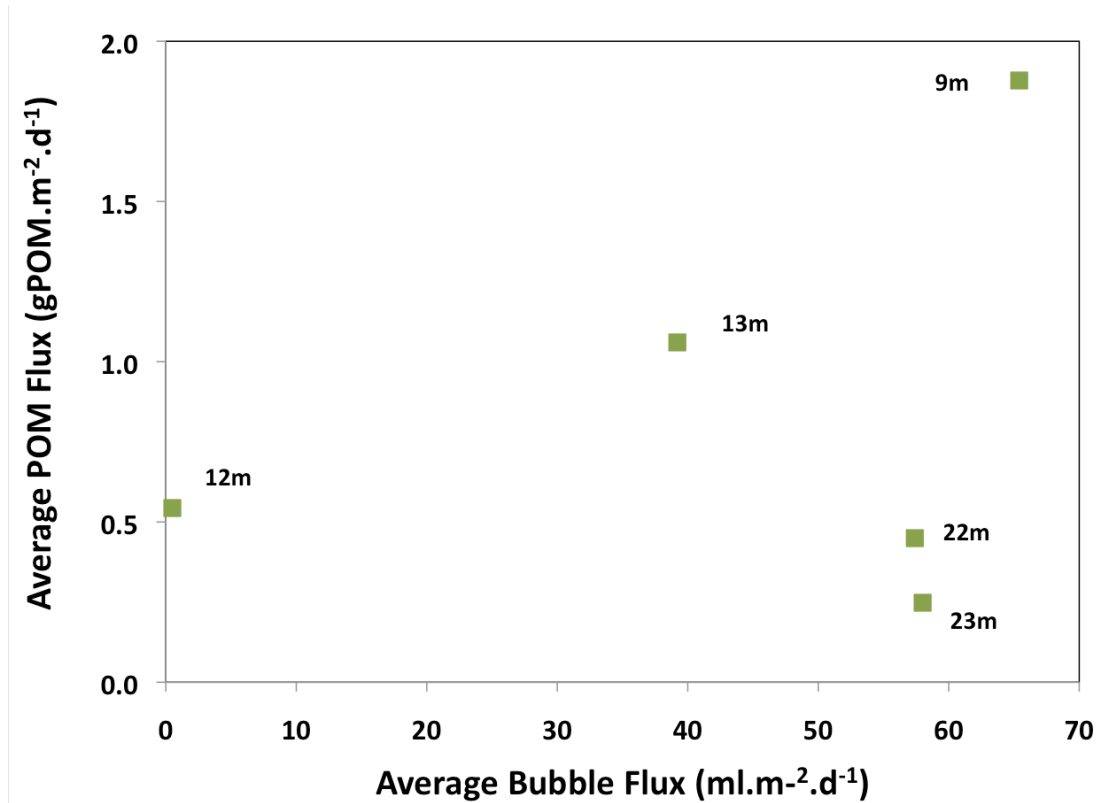


Figure 1 No strong relationship was observed between bubbling fluxes and particulate organic matter sedimentation rates. The sites at which POM fluxes were measured are shown in the figure.



Figure 2 A wind sensor was installed on a buoy in the middle of the lake.

Chapter 5: A mass balance of the methane cycle in the Upper Mystic Lake

1. INTRODUCTION

Significant quantities of methane are naturally produced in lakes, and some of this methane is released to the atmosphere. The methane cycle of a stratified lake consists of several processes such as ebullition, air-water exchange and oxidation (Figure 1). A mass balance of the methane cycle in a lake can help to estimate unknown quantities that are not directly measured, as well as to understand the relative importance of the various processes. For example, oxidation by methanotrophs has been previously determined to be an important sink of methane in stratified lakes (e.g. Fallon et al. 1980, Kankaala et al. 2006), and can decrease the amount of methane that is released to the atmosphere from a lake ecosystem. Previous studies have found that oxidation and air-water exchange can be especially important during the turnover periods, when mixing causes methane to be released from the hypolimnion into the upper mixed layer of a lake (e.g. Rudd and Hamilton 1978, Utsumi 1998). Another process that can reduce the amount of methane released to the atmosphere by ebullition is diffusion from the bubbles into the water column during bubble ascent.

Lake mass balances have been previously used to determine sources of methane emissions to the atmosphere (e.g. Bastviken et al. 2008), as well as to determine the significance of events such as the erosion of the pycnocline to the methane cycle (Scranton et al. 1993). This chapter presents a four-box model of the Upper Mystic Lake, where the different zones considered are an upper mixed layer, a transition zone, the anoxic water column in the bottom half of the lake, and the sediments.

2. BACKGROUND

2.1 Methane production

Methane is produced in lake sediments by microbially-mediated anaerobic decomposition of organic matter. This occurs through two main pathways – acetotrophic methanogenesis and hydrogenotrophic methanogenesis (Zinder 1993). In the first process, methanogenic bacteria convert acetate into methane and carbon dioxide.



In the latter pathway, methanogenic archaea reduce carbon dioxide and oxidize hydrogen to form methane.



Formate, carbon monoxide and other organic compounds such as alcohols can act as alternate electron donors for this process. Alternatively, some of the hydrogen and carbon dioxide can also be converted by homoacetogens into acetate, for subsequent conversion to methane via acetotrophic methanogenesis (Madigan and Martinko 2006). The amount of methane produced through each pathway depends on surrounding environmental variables such as temperature (Schulz and Conrad 1996), hydrogen, and the presence of other competitors such as sulfate-reducing bacteria (Conrad 2005, Winfrey and Zeikus 1979).

Methanogenesis rates have been found to vary with changing organic matter inputs, sediment temperatures and oxygen content (Kelly and Chynoweth 1981, Liikanen et al. 2002b). Maximum methanogenesis rates typically occur in the surface sediments (0-3 cm), as observed in incubation tests of slices collected from 10 to 20 cm long cores (e.g. Jones et al. 1982, Kelly and

Chynoweth 1980, Nüsslein et al. 2003). However these studies also observed methanogenesis in the deeper sediments, at rates that could at times be as high as in the surface sediments.

2.2 Methane release to the atmosphere

Ebullition is the dominant pathway for methane emissions to the atmosphere from freshwater lakes (e.g. Casper et al. 2000, Crill et al. 1988, Walter et al. 2006). Most of the methane present in bubbles is directly released to the atmosphere, causing energy and carbon to be lost from the lake ecosystem. However, some methane can be released into the water column through diffusion from rising bubbles.

Dissolved methane can also be released to the atmosphere through air-water exchange from the lake surface. Such export occurs during the open-water season and its rate varies according to surface concentrations of dissolved methane, wind speeds, and surface water temperatures. Loss by air-water exchange can be especially important during the fall or spring turnover when methane accumulated in the hypolimnion over the summer is mixed into the upper waters (e.g. Michmerhuizen et al. 1996, Rudd and Hamilton 1978).

Vascular plants containing hollow stems can act as conduits for methane export to the atmosphere. This process can be dominant in aquatic environments with substantial littoral vegetation such as shallow wetland lakes (Kankaala et al. 2004, Sebacher et al. 1985).

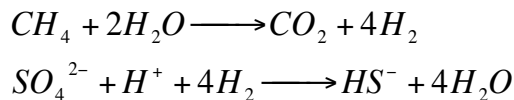
2.3 Aerobic methane oxidation

Dissolved methane can be oxidized by methanotrophs, which are strict aerobic bacteria that contain the enzyme methane monooxygenase (Madigan and Martinko 2006). In stratified lakes, maximum oxidation rates have been observed in narrow zones within the thermocline where methane and oxygen are present (e.g. Harrits and Hanson 1980, Rudd et al. 1974).

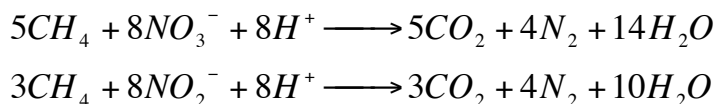
Methane oxidation has been previously measured using several techniques that include incubation tests that measure decreasing methane concentrations with time (e.g., Utsumi et al. 1998), radiotracer-based incubations (e.g. Rudd et al. 1974) and stable carbon isotopic fractionation (e.g. Eller et al. 2005, Kankaala et al. 2007). Independent whole-lake mass balances that account for turbulent diffusivities have also been used to obtain estimates of oxidation (Bastviken et al. 2002, Kankaala et al. 2006). High oxidation rates have been observed during the summer and fall, with maxima occurring during fall or spring turnovers (e.g. Harrits and Hanson 1980, Kankaala et al. 2006, Liikanen et al. 2002a).

2.4 Anaerobic methane oxidation

Microbially mediated anaerobic oxidation using sulfate as an electron acceptor is a major methane consumer in marine sediments (Barnes and Goldberg 1976, Reeburgh 1976). This phenomenon is thought to be caused by methanogens (ANME-1 and ANME-2 archaea) that run in reverse producing hydrogen and carbon dioxide, coupled with sulfate reducing bacteria that drive the net reaction by consuming hydrogen (DeLong 2000, Hallam et al. 2004).



Anaerobic oxidation is also thermodynamically favorable with nitrate as an electron acceptor.



Such a process has not been observed in any lake or ocean environments, though a recent study discovered the existence of organisms that can oxidize methane using nitrate in anoxic sediments of a freshwater canal with very high nitrate loading (~1mM) (Raghoebarsing et al. 2006). The

process is thought to occur very slowly, and hence might not compete successfully with other nitrate consumption mechanisms in natural waters.

The co-occurrence of sulphate-mediated AMO and aerobic oxidation has been observed in Lake Mendota and Lake Plusβee (Eller et al. 2005, Zehnder and Brock 1980). However, most studies have not found evidence of oxidation in samples collected from the anoxic hypolimnia of stratified freshwater lakes (e.g. Harrits and Hanson 1980, Kankaala et al. 2007, Rudd and Hamilton 1978).

3. METHODS

3.1 Water quality parameters

Temperature, dissolved oxygen, pH and conductivity profiles of the lake were collected using submersible Hydrolab MiniSonde probes, the depth being determined by a pressure transducer present within the same unit. All sensors, except for the temperature and depth sensors, were calibrated using standard solutions within 24 hours prior to field measurement. The depth sensor was calibrated to start at 0 m at the lake surface at the time of measurement. The temperature probe could only be calibrated by the manufacturer; thus surface water temperatures measured by the hydrolab instrument were cross-checked with an independent thermometer prior to sampling. Measurements were made every 0.5-1 m in 2007, and in April and October 2008. Near-continuous profiles (<10 cm depth intervals) were collected for the remaining months in 2008. Chlorophyll-a levels in 2007 were estimated using relative fluorescence data at 460 nm obtained with a SCUFA underwater fluorometer attached to one of the hydrolab probes. A Secchi disk was used to determine lake transparency

3.2 Ebullition, air-water exchange and dissolved gas concentrations

Ebullition fluxes were measured using the inverted funnel traps described in Chapter 2. The traps were deployed from Jul 19-Nov 30 2007 and Apr 5-Dec 1, 2008. Seven traps were left in the lake over the winter, of which four traps were lost due to icing. The details of trap field deployment and ebullition flux measurements are included in Chapters 3 and 4.

Air water exchange fluxes were estimated using dissolved methane concentrations at the surface, combined with wind and temperature records of the lake. Calculations for diffusive fluxes from the lake surface are described in Chapter 4. Dissolved methane profiles were also taken approximately once a month following the methodology outlined in Chapter 4. In 2007, profiles were mainly collected for oxidation tests, while the 2008 profiles were measured for purposes of mass balance estimates.

3.3 Oxidation tests

Incubation tests were used to measure the magnitude and rates of methane oxidation from July-October 2007. The tests were based on prior oxidation measurements (e.g. Bastviken et al. 2008, Utsumi et al. 1998) where water samples were taken at select depths and left to incubate in the laboratory under light and temperature conditions similar to those in the lake. Depths were chosen based on dissolved oxygen data collected simultaneously; several samples were taken near the oxic-anoxic interface where methane oxidation rates have been observed to be at their maximum. Since thermocline methane concentrations were usually very low (~0.1 μM), additional samples were collected at these depths and spiked with ~0.5 μM dissolved methane.

Sample syringes were prewashed in 1N nitric acid to remove trace metals, which are possible inhibitors of methanotrophs (Bedard et al. 1989), thoroughly cleaned with milli-Q water and sterilized at 121°C in an autoclave. Syringe samples in the field were collected at sites near

the lake center following the procedure previously outlined in Chapter 4 for dissolved gas measurements. The usage of gas tight sample syringes limits gas loss due to depressurization while bringing the sampler to the surface, and also prevents leakage during transport and incubation.

Samples for all measured depths were divided into three batches, each consisting of two syringes collected as duplicates. Duplicates were not taken for the July 2nd and August 2nd tests; instead samples were taken at additional depths to test for the possible presence of oxidation outside the zone between thermocline and oxycline. The first batch was used as a control; these samples were acidified immediately after collection to a pH of 2 to stop oxidation using ~ 200 µl of 1M nitric acid. A second batch was incubated underwater for ~12 (or 24) hours, while a third batch was incubated for ~24 (or 48) hours. The relatively short incubation time spans were selected to minimize bottle effects and changes in nutrient concentrations that typically affect long incubation experiments (>75 hours) (Rudd and Taylor 1980, Utsumi et al. 1998). Coolers containing ice baths were used to control incubation temperatures; the temperatures were based on field measurements at the depths the samples were collected from. Samples collected below the lake depth of 3 m were stored in the dark, while the shallower samples were stored underwater in an open tub.

Methane concentrations in the samples were measured using the FID gas chromatograph as described in Chapter 4. Both exponential fits (following first order kinetics) and linear fits (pseudo zero-order kinetics) of concentrations against time were examined. A p-value of 0.05 was used to identify statistically significant trends. Methane oxidation rates ($\text{mmol.m}^{-3}.\text{d}^{-1}$) at the sample depths were calculated by dividing the rate of methane loss over time by the corresponding lake cross-section area.

3.4 Sediment porewater methane measurements

Total methane present in sediment porewaters was measured in a 1 m-long freeze core taken on September 22nd, 2008. The core was collected near the lake center at a site where the water column depth was ~20 m following the method described in Spliethoff and Hemond (1996). Freeze coring was chosen as a means of preserving methane bubbles in the sediments, thus limiting gas loss due to bubbling or diffusion. Briefly, a 1.25 m x 7.6 cm x 7.6 cm hollow corer made of fiberglass reinforced resin, with an aluminum face on one side, was filled with a slurry of propanol and dry ice. The corer was dropped from a depth of ~5 m above the sediments and brought to the surface after ~20 min. Frozen sediments were broken into four slabs, wrapped in plastic and aluminum foil and transported to the laboratory in dry ice.

The core was stored overnight in a freezer at -80°C and laboratory analysis commenced within 24 hours of field sampling. The core was sliced into 16 pieces of lengths 5-8 cm in a cold room using an electrically heated tungsten wire attached to a hacksaw frame. Each piece was further sliced into smaller pieces that were immediately transferred as duplicates into gastight glass syringes with wetted barrels, fitted with 3-way Luer Lok™ valves. Air in the syringes was evacuated using a vacuum pump and the syringes were then filled with a headspace of ~35-45 ml of helium after being flushed three times. No visible melting of any of the sediment pieces was observed during this process.

The syringes were left to thaw completely in a tub filled with water at room temperature. Approximately 6 hours after initial preparation, the syringes were spiked with ~200µl of 3N propanoic acid to bring the pH of the mixture down to 2 in order to prevent bacterial activity that might have led to methanogenesis or methane oxidation. For 5 of the 14 pieces, a third replicate

syringe was spiked with 500 μ l of 2M bromo-ethane-sulfonic acid, a methanogenesis inhibitor (Gunsalus et al. 1976).

After thawing, the syringes were weighed and put on a wrist shaker for approximately a half hour for the sediment mixture to equilibrate fully with the headspace. Headspace gases were then analyzed using FID and TCD chromatography following the procedure outlined in Chapter 4. The volume of the porewater was calculated by multiplying the difference between the weights of the sample syringe and empty syringe with the water content of the sediment mixture. Concentrations in the porewater were calculated using equation (1) from Chapter 4. Calculated errors include the standard errors from multiple GC injections and from duplicate pieces, as well as errors in measurement of headspace and water volumes, and peak heights.

3.5 Other measurements

Sediment water content was calculated as the difference in wet and dry weights of sediments divided by the total weight of the wet mixture. The sediments were dried for 24 hours in an oven at 60°C. Sediment porosity was calculated as the water content multiplied by the mixture density, determined using mixture weights and volumes.

The organic matter content of the sediments was measured using the loss on ignition method. Dried sediments were combusted in an oven for 24 hours at 375°C in air. POM content (as % dry weight) was determined as the difference between the post-combustion weight and the dry weight.

Particulate organic matter settling fluxes were measured using five sediment traps from mid-August to December 2008. The trap construction, deployment and sample analysis are discussed in Chapter 4.

X-rays of sediment cores were taken prior to analysis in an attempt to visually observe any bubbles trapped. Cores were placed on an aluminum plate and exposed to a beryllium source for 20 seconds at a voltage of 160,000V and current of 3.8 mA.

4. RESULTS

4.1 Lake stratification

A strong temperature gradient was observed in the UML as early as spring (April/May) in both 2007 and 2008 (Figures 2(a) and 3(a)), and stratification intensified over the summer and fall. Anoxia was observed in the hypolimnion in both years (Figures (2(b) and 3(b)). In 2007, the onset of anoxia occurred around mid-June. In contrast, the water column below 14 m was already anoxic in April 2008.

The thermocline (depth of maximum temperature stratification) did not coincide with the oxycline (dissolved oxygen and methane boundary) except during the approach to fall turnover; at times the two boundaries differed by as much as 10 m. While the thermocline deepened from ~3 m in May to ~9-10 m in November, the oxycline exhibited an inverse trend and rose to a maximum depth of ~6 m in October. Rapid mixing and thermocline erosion were observed in the last 2 weeks of November 2007 during the approach to fall turnover. However, the water column remained stratified and anoxic below ~10-14 m on the last sampling dates of both years.

Dissolved methane concentrations in the hypolimnion increased over the summer and fall in 2007 and 2008 (Tables 1 and 2). High concentrations (200-800 μM depending on the period of observation) were measured near the sediments; concentrations decreased rapidly to ~10-30 μM at the oxycline. Methane minima (<0.1 μM) occurred in the zone between the thermocline and the oxycline (Figures 4 and 5). Concentrations in the upper mixed layer were low (~1 μM), but

supersaturated with respect to the atmosphere. Calculated errors include differences from duplicates, inaccuracies in measurement of sample volumes, headspace volumes and peak heights, as well as precision errors from multiple GC injections. Measurement errors typically ranged from 5-10% for concentrations $> 0.5 \mu\text{M}$; large errors (15-30%) were calculated for very small concentrations that were close to the GC detection limit of $\sim 0.05 \mu\text{M}$.

4.2 Methane loss to the atmosphere

The weekly measurements of ebullition fluxes and monthly surface air-water exchange estimates are summarized in Chapter 4. Average ebullition fluxes were $0.8 \pm 0.1 \text{ mmolCH}_4.\text{m}^{-2}.\text{d}^{-1}$ from June-November 2007 and $0.5 \pm 0.02 \text{ mmol CH}_4.\text{m}^{-2}.\text{d}^{-1}$ from April-November 2008. Average diffusive air-water fluxes from the lake surface were $0.3 \pm 0.1 \text{ mmol CH}_4.\text{m}^{-2}.\text{d}^{-1}$ in 2007 and $0.2 \pm 0.1 \text{ mmol CH}_4.\text{m}^{-2}.\text{d}^{-1}$ in 2008.

4.3 Methane oxidation tests

Methane oxidation was observed in two sets of samples, each of which was collected near the oxycline at the methane minimum, on July 2 (at $\sim 15 \text{ m}$) and October 15, 2007 (spiked sample at $\sim 7 \text{ m}$) (Appendix Figures 1-5). Concentrations decreased with a weak linear trend at a rate of $4.2 \text{ mmol.m}^{-3}.\text{d}^{-1}$ in June ($R^2=0.99$, $p=0.08$ after 24 hours incubation). Since duplicates were not collected in June, the calculated consumption rate must be viewed with caution since even small depth errors can cause significant concentration differences ($\sim 1-2 \mu\text{M}$) between duplicate samples collected near the oxycline (e.g. Appendix Figures 4 and 5). Both linear and exponential fits yielded a similar consumption rate of $0.3 \text{ mmol.m}^{-3}.\text{d}^{-1}$ in the October sample ($R^2=0.7$, $p=0.03$ after 48 hours incubation). However, it is possible that neither of these fits were significant, given the magnitude of errors in the concentration measurements.

4.4 Sediment core results

High concentrations of methane were present for at least 1 m of sediment depth in the UML porewater (Figure 6(a)). The shape of the profile is consistent with previous methane measurements in freshwater sediments (e.g. Chanton et al. 1989, Crill et al. 1988, Huttunen et al. 2006). Porewater concentrations increased with sediment depth from the surface up to 25 cm (Table 3). Concentrations were relatively uniform at sediment depths below 25 cm, and ranged from 3.7 to 5.1 mM (i.e. 60-85% saturation). 2.3 to 0.9 mM (i.e. 0.4-1.1 atm) of nitrogen had to be present in order for the porewater to be at saturation at these depths. For comparison, the concentration of dissolved nitrogen at equilibrium with air (0.78 atm) at 4°C is 0.7 mM.

The oxygen contents of the analyzed sediment mixtures were low but non-zero (2-5%) putting an upper bound on possible air contamination. The observed amount of oxygen, corresponding to ~1 ml of air, could also have entered the syringe while filling it with helium. Calculated nitrogen concentrations were discarded since this small amount of leakage (<1 ml) could result in very large errors.

The organic matter content of the core ranged from 20-30%, which is similar to previous observations in sediment cores taken at the UML (Spliethoff and Hemond 1996). The presence of bubbles was not observed in a preliminary examination of the X-ray negatives.

5. COMPONENTS OF THE MASS BALANCE MODEL

5.1 Overview

A four-box model was used to calculate the UML methane budget (Figure 7). The zones considered were:

- An upper mixed layer (Epilimnion) – Depths above the thermocline (depth of maximum temperature gradient). Temperatures and oxygen were relatively uniform in this zone, while methane concentrations were low ($\sim 1 \mu\text{M}$).
- A transition zone – This layer includes depths between the thermocline, but above the oxycline (depth where the highest gradient of dissolved oxygen was present). The steepest gradient of dissolved methane concentrations was also observed near the oxycline. Methane minima ($\sim 0.1 \mu\text{M}$) were present in this layer.
- Anoxic hypolimnion – In traditional lake literature, the hypolimnion is the lower stratum of the lake situated below the thermocline (Wetzel 1975). However, in this chapter, the term ‘hypolimnion’ is used to refer to the anoxic water column below the oxycline. High methane concentrations ($\sim 10\text{-}800 \mu\text{M}$) were observed at these depths; the concentrations gradually increased from April to November.
- Sediments

It was assumed that no methane enters or exits the lake via the groundwater. Plant mediated emissions were not considered in the model since the surface area covered by littoral vegetation is negligible compared to the open water.

The mass balance was done in monthly intervals based on the 2008 data; the period between April and June (e.g. Table 6) was treated as one interval since the concentration profile for May was not available. Changes in the volumes of the different zones were accounted for by considering the variations in the depths of the thermocline and oxycline. However, since the methane samples were only collected at 3 m depth intervals, the actual thermocline and oxycline depths measured from the hydrolab were not used to determine the different zones for each mass

balance period. Instead the thermocline and oxycline depths were approximated to a depth that was the nearest multiple of three of the actual values.

5.2 Methane buildup in the water column

Methane accumulation in the water column was calculated by multiplying the changes in concentration over time with the volumes of the corresponding depth intervals, and integrating over the lake depth. Volumes were obtained based on the cross-section areas listed in Appendix Table 1. Unknown concentrations and cross-section areas were estimated using linear interpolation (or linear extrapolation to the lake bottom).

Calculated errors include analytical errors in dissolved methane concentrations, and a (conservative) 5% bathymetric volume error that was estimated by comparing two independent maps of the lake. The error due to a possible 10 cm uncertainty in sampling depth was estimated using linear interpolation, and was found to be negligible (~2%). However, small variations in sampling depths can potentially be significant sources of error near the oxycline and thermocline boundaries, where concentration gradients are steepest. For the purpose of this study, it was assumed that the differences measured in duplicate samples accounted for variations in sampling depth, as well as analytical error. It was also assumed that the lake was mixed horizontally, and that a single profile collected at the lake center was representative of the entire water column.

5.3 Ebullition and diffusive air-water exchange to the atmosphere

The mass of methane bubbled between sampling periods was calculated as the sum of individual trap fluxes multiplied by the area represented by the traps (as described in Chapter 4) and the sampling interval. Total export of methane through diffusion across lake surface was obtained by multiplying air-water exchange fluxes with the lake surface area.

5.4 Dissolution from bubbles

The rate of mass exchange between a single bubble of radius r and the water column can be calculated as (McGinnis et al. 2006)

$$\frac{dM}{dz} = K_L \left(\frac{P}{K_H} - C_w \right) \frac{4\pi r^2}{v_b}$$

where z = depth of the bubble (m)

K_L = Gas transfer coefficient (m/s)

P = Concentration of methane in the bubble (atm)

K_H = Henry's constant (atm.m³.mol⁻¹)

C_w = Concentration of methane in the water (mol/m³)

v_b = Bubble velocity (m/s)

Both K_L and v_b are dependent on bubble size, which changes during bubble ascent due to gas exchange and decreasing hydrostatic pressure (Leifer and Patro 2002). The mass loss from a single bubble was computed using the SiBu-GUI model (Greinert and McGinnis 2009, McGinnis et al. 2006) assuming that bubble radii ranged from 1 to 5 mm, as is typically observed in aquatic environments (Ostrovsky et al. 2008, Rehder et al. 2002). The model accepts inputs for bubble diameter and initial gas composition, as well as lake temperature and gas concentration profiles. The output predicts a final bubble diameter and composition from which the amount of methane lost from a bubble is calculated.

The model was run for a pure methane bubble, assuming a bubble release depth of 20 m, using a lake temperature and gas composition profile from September 2008. Since the model was originally designed to calculate bubble dissolution through a hydrate stability zone, it requires an input parameter for a hydrate phase boundary depth. This input can be set to a large value (e.g.

100 m) in order to obtain the correct gas diffusion coefficients for a system where no hydrates are present (J. Greinert, personal comm.).

Gas dissolution at different water column depths was obtained from the model results to account for variations in the oxycline and thermocline (Table 4). The total number of moles diffusing from the bubbles was calculated by multiplying the measured surface ebullition fluxes with average estimates of methane diffusion from the model for bubbles of radii 1 to 5 mm. The amount of methane dissolving in the water column was mainly dependent on bubble size and almost insensitive (~5% change) to variations in environmental parameters and initial gas composition. Since actual bubble sizes were not measured in this study, the model results only represent order of magnitude estimates of bubble dissolution.

5.5 Eddy diffusion

Turbulent diffusivity K_z at the thermocline and oxycline boundaries were determined using a one-dimensional flux gradient model (Jassby and Powell 1975). This method uses heat as a conservative tracer and assumes that the colder water in the UML below a depth z can only receive heat through eddy diffusion. Temperature profiles measured at one location at the lake center were assumed to be representative of the entire water column. Solar radiant heat was not considered, as the Secchi disk readings indicated that lake transparency levels were low below 3 m (Appendix Table 2). Sediment heat exchange was also neglected in this calculation. K_z is estimated as (Schwarzenbach et al. 2003):

$$K_z = -\frac{\int_z^{z_{\max}} A(z') \frac{\partial T}{\partial t} dz'}{A(z) \frac{\partial T}{\partial z} \Big|_z}$$

where $A(z)$ = cross section area at depth z (m^2),

T = Temperature ($^{\circ}\text{C}$)

Lake profiles collected simultaneously from two Hydrolab temperature probes were compared to obtain estimates for temperature errors. Both the absolute and relative temperature profiles from the Hydrolab instruments differed by less than 0.1°C for most depths, except at the thermocline, where values could differ by as much as 0.3°C . On the basis of a $\pm 0.1^{\circ}\text{C}$ uncertainty, a $\pm 20\%$ error was estimated for K_z values at the oxycline, where temperature changes between sampling dates were on the order of 0.5°C . Errors due to temperature uncertainty were neglected at the thermocline, where spatial and temporal temperature changes were generally large ($>2^{\circ}\text{C}$). K_z values for the different measurement periods are presented in Table 5, and are consistent with a value of $0.17 \pm 0.09 \text{ m}^2/\text{d}$ previously estimated at a depth of 18 m at the UML (Senn 2001).

The temperatures measured by the Hydrolab probe in the hypolimnion on July 16th were slightly higher than the values from August (Appendix Table 3). No obvious source for the colder water in August could be identified; it was therefore assumed that the higher July temperatures were a result of sensor error and they were ignored from calculations of K_z . The readings from a second digital thermometer were $\sim 1.3^{\circ}\text{C}$ lower than the temperatures measured by the Hydrolab on both July 16th and August 16th, but the two thermometers differed by less than 0.5°C for three other dates during the measurement period. The possible inaccuracies in temperature measurements could significantly affect the estimated K_z values. However, it is also possible that a 1-dimensional mixing model might not be sufficient to calculate eddy diffusivities at the UML. Also, solar radiant heat at the thermocline might not have been negligible in April and May, when lake transparency levels were higher and the thermocline was shallower than the rest of the year. Thus the calculated K_z values should be only be considered as order of

magnitude estimates for mass balance purposes. The small negative value of K_z at the thermocline between May and June ($-0.03 \text{ m}^2/\text{d}$) was assumed to be an artifact of the error in temperature measurements; instead the K_z values from April to May was used for the entire mass balance interval of April-June.

5.6 Methane oxidation incubations

Possible methane oxidation was only observed at depths near the oxycline in two of the five incubation tests conducted between July and October. The July samples had higher oxidation rates ($4.2 \text{ mmol.m}^{-3}.\text{d}^{-1}$) than the October samples ($0.3 \text{ mmol.m}^{-3}.\text{d}^{-1}$), though duplicates were not taken for the former set, and relative errors were high for the latter. Even though the experimental evidence seems to suggest that methane oxidation rates were low, this interpretation is not consistent with the presence of a persistent methane minimum in the transition zone, where methane concentrations were 1-10 times smaller than the concentrations in the upper mixed layer. Oxygen at these depths was steadily consumed through the summer, which is consistent with (but does not necessarily require) the presence of methane oxidation in this zone.

Previous oxidation studies conducted in stratified lakes using radiotracer based incubations found rates ranging from 0 to $29 \text{ mmol.m}^{-3}.\text{d}^{-1}$, though the higher rates were mainly observed during lake turnovers, with little oxidation occurring during other times (as reviewed in Utsumi et al. 1998, Kankaala et al. 2006). The shape of the oxygen and methane profiles in these lakes was similar to those in the UML especially at the oxycline; however the absolute methane concentrations in the hypolimnia were lower ($\sim 10\text{-}100 \mu\text{M}$).

It is possible that oxidation rates measured from the incubation tests in this study were underestimated due to the sampling and experimental protocols followed. The coarse sampling

resolution (~1-2 m near the oxycline) was probably not sufficient to capture the depths at which maximum oxidation occurs. However, samples collected from the transition zone had very low methane concentrations, close to the GC detection limits, and it is likely that more instrument sensitivity was required in order to accurately measure decaying concentrations. The spike tests might not have been effective if oxidation followed Michaelis-Menton kinetics where, depending on the half-saturation constant, a substrate increase can cause reactions to move from first-order to zero-order rates. Longer incubation times might also have been needed. For example, Liikanen et al. (2002a) found that most of the oxidation occurred within 150 hours, following a day or two of low activity. However, longer tests can potentially be affected by bottle effects and leakage. Finally, temperatures in the lab incubations were not finely controlled, but were on average higher than lake conditions and could have resulted in increased oxidation (Harrits and Hanson 1980).

Thus the results from the oxidation experiments were treated as inconclusive, and the oxidation in the lake was estimated indirectly through the mass balance.

5.7 Diffusion from sediments

Outward flux from hypolimnetic sediments was calculated using the Fickian diffusion equation (Berner 1980):

$$J_s = \phi \frac{D_s}{\tau^2} \left(\frac{dc}{dx} \right)$$

where J_s = flux ($\text{mol}/\text{cm}^2/\text{s}$)

ϕ = porosity,

τ = tortuosity,

D_s = diffusion coefficient of methane in the sediments (cm^2/s)

$\frac{dc}{dx}$ = concentration gradient, dc (mol/cm³) across a diffusion path length dx (cm)

The measured porosity of the top 8.5 cm of the sediments was 0.9 to 0.97, which agrees with values reported in limnological literature (e.g. Huttunen et al. 2006). Tortuosity was calculated using two sets of empirical equations. The first is a logarithmic function for fine-grained unlithified sediments (Boudreau 1996)

$$\tau^2 = 1 - \ln \phi^2$$

which leads to a tortuosity of 1.12. The second method calculates tortuosity as (Iversen and Jorgensen 1993):

$$\tau^2 = 1 + n(1 - \phi)$$

where $n=3$ for clay sediments, giving a value of 1.18. The final value for tortuosity used in calculations was 1.15.

D_s was estimated to be $0.85*10^{-5}$ cm²/s, which is the molecular diffusion coefficient of methane in water at 4°C. This was calculated based on the temperature of water near hypolimnetic sediments at the UML and on previously reported values for molecular diffusion of methane in seawater ($=0.87\pm0.1*10^{-5}$ cm²/s from Iversen and Jorgensen 1993) and distilled water ($=0.84*10^{-5}$ cm²/s from Sahores and Witherspoon 1970) at 4°C. It was assumed that the sediments were at steady state; thus sorption of methane to sediments was not considered in the aqueous phase flux calculations.

The gradient $\frac{dc}{dx}$ was estimated by fitting a line through the porewater and near-sediment

water column concentrations (Figure 6(b)). The diffusive methane flux from the sediments of the UML is estimated to be $0.9*10^{-9}$ mmol.cm⁻².s⁻¹, i.e. 0.8 mmol.m⁻².d⁻¹. The flux error was

calculated using from the standard error of the residuals from the linear fit and was $\sim \pm 13\%$.

Methane concentrations in the porewaters of epilimnetic sediments were not measured.

6. MASS BALANCE DISCUSSION

6.1 Upper mixed layer mass balance

Quantitive estimates were made for the surface air water diffusive flux, diffusion across the thermocline, and gas dissolution from bubbles in the epilimnion mass balance. Since data were not available for methane diffused from epilimnetic sediments (D_{sed}) and oxidation in the water column, these processes were estimated from the mass balance (Figure 8). The two terms cannot be separated without further measurements; however their net sum can be estimated as:

$$Unknowns(D_{sed} - oxidation) = \frac{dM_E}{dt} + F_{a/w} A_{sur} + F_{th} A_{th} - \text{Gas diffused from bubbles}$$

where $\frac{dM_E}{dt}$ = Differential (not derivative) rate of upper mixed layer storage (mol/d)

$F_{a/w}$ = Surface air-water gas flux ($\text{mmol.m}^{-2}.\text{d}^{-1}$)

A_{sur} = Surface area of UML = $5.83 * 10^5 \text{ m}^2$

K_z = Eddy diffusion coefficient (m^2/d)

A_{th} = Lake cross-section area at thermocline depth

$\left. \frac{dc}{dz} \right|_{th}$ = Differential concentration gradient across the thermocline, normally

corresponding to a flux out of the upper mixed layer

Errors were calculated using a square sum propagation of uncertainty in each of the individual terms. Errors in the storage term could be large relative to the mean value ($\sim 20\text{-}50\%$

error), since the latter was calculated as the difference of concentrations over time, whereas the errors were summed.

Methane flux out of the upper mixed layer into the transition zone was positive or zero for most of the season (April-October); however all the terms in the mass balance were small when compared to air-water exchange from the lake surface (Table 6). Mixing in November caused the oxycline and thermocline to converge to the same depth, resulting in the disappearance of the transition zone. During this time, there was a large input of methane from the hypolimnion ($\sim 6 \pm 1$ kmol) into the upper mixed layer; the mass balance indicates that this methane was consumed internally within the water column by a sink.

Air-water exchange flux in November was estimated to be small during the approach to turnover, since the concentration of methane at the lake surface was low on November 9th 2008, and wind speeds were not much greater than the rest of the measurement period (from Chapter 4). The average residence time of methane in the upper mixed layer was on the order of 1 week to a month, depending on the depth of the epilimnion and the value of average concentrations used. However, the residence times were the lowest (~ 1 week) during April and May, when the epilimnion was shallow, and were higher (~ 25 to 30 days) in November, when the epilimnion depths were ~9-10 m. The residence time estimates suggest that a monthly sampling interval would probably have detected a significant increase in methane concentrations in the surface waters during November, if it had occurred.

The net sum of diffusion from epilimnion sediments and methane oxidation was positive from April-October, indicating that a source of methane was needed to balance efflux through air-water exchange from the lake surface (Table 6). Bubble dissolution as a source was relatively small compared to the net sum term. The net sum was positive for most of the sampling period,

except from October-November during the approach to fall turnover. One hypothesis that could explain these observations is that epilimnetic sediments release methane throughout the season at a rate that exceeds methane oxidation. According to this hypothesis, methane oxidation starts to become more significant relative to the sediment source in October and November, causing a decrease in the net sum term.

6.2 Transition zone mass balance

The transition zone (i.e. the oxic hypolimnion) in April was ~10 m deep; however this zone was steadily eroded over summer and fall, and completely disappeared by November, presumably due to mixing during the fall turnover. Diffusive fluxes across the thermocline and oxycline were sources to the transition zone because of the methane minima present at these depths. The quantities estimated from the mass balance in this zone were diffusion from sediments and methane oxidation (Figure 9).

$$D_{\text{sed}} - \text{oxidation} = \frac{dM_z}{dt} - K_{\text{th}} A_{\text{th}} \left. \frac{dc}{dz} \right|_{\text{th}} - K_{\text{ch}} A_{\text{ch}} \left. \frac{dc}{dz} \right|_{\text{ch}} - \text{Gas diffused from bubbles}$$

The mass balance indicates the presence of a methane sink through the sampling period up until the fall turnover (Table 7). Almost no methane was stored in this zone over the season; the average residence time calculated based on the storage and flux was on the order of a few days, which indicates that any methane input into this zone is consumed rapidly.

The period between July and August was the only period when a clear decrease in methane storage in the transition zone was observed. Interestingly, this followed a significant influx of methane from the thermocline and oxycline in the period between June and July. If methanotrophs were the major consumers of methane in this zone, then a possible theory is that

these organisms were stimulated by the pulse of methane in June/July and continued to be active at similar rates through August, thus causing the net decrease in methane concentrations.

6.3 Hypolimnion mass balance

Methane efflux from the sediments ($F_{sed/w}$) can be estimated from a hypolimnion mass balance as (Figure 10):

$$F_{sed/w} A_{sed} = \frac{dM_H}{dt} + K_z A_p \left. \frac{dc}{dz} \right|_{pycno} - \text{Gas diffused from bubbles}$$

where A_{sed} = Hypolimnion sediment area = $4.7 \times 10^5 \text{ m}^2$

$$\frac{dM_H}{dt} = \text{Hypolimnetic storage (mol/d)}$$

The mass balance estimate of sediment efflux can be compared against a theoretical value estimated on the basis of porewater concentration gradients (as measured in the freeze core), assuming molecular diffusion to be the main mode for sediment water exchange of methane. A hypolimnion sediment area of $4.7 \times 10^5 \text{ m}^2$ was estimated by representing the lake shape as the frustum of a cone (average hypolimnetic lake depth $\sim 12 \text{ m}$).

The month-to-month diffusive sediment fluxes calculated from the hypolimnion mass balance (Table 8) were not reliable estimates, since the errors propagated from the change in hypolimnion storage calculations were high (at least 40%). Instead a seasonal sediment flux was calculated from a linear fit of the hypolimnion storage values (Figure 11), and was found to be $\sim 1500 \text{ mol/d}$, i.e. $3.2 \text{ mmol.m}^{-2}.d^{-1}$. The seasonal sediment efflux thus calculated from the hypolimnion mass balance is about 4 times larger than the diffusive sediment flux calculated from freeze core concentrations ($0.8 \text{ mmol.m}^{-2}.d^{-1}$). Both values are consistent with previously reported values for sediment diffusive fluxes (Table 9). The difference between the two estimates could be due to inaccuracies in sediment area, as well as the extrapolation of a single core to the

whole lake basin for the entire season. However, at Cape Lookout Bight, Martens and Klump (1980) also measured benthic methane fluxes that were 1-3 times larger than the theoretical values calculated using molecular diffusion in sediments. Those authors proposed that the diffusive sediment water exchange might have been enhanced due to the presence of bubble tubes that had been observed in the sediments (porosity = 0.9-0.93). The mass balance indicates that most of the methane released from the sediments is stored within the water column at the anoxic hypolimnion until fall turnover.

6.4 Sediment mass balance

Change in porewater methane storage ($\frac{dS}{dt}$) can be estimated from the net release of gas

and the production rate as (Figure 12):

$$\frac{dS}{dt} = F_{prod} A_{sed} - F_{sed/w} A_{sed} - F_b A_{sur}$$

where A_{sed} = Sediment area (m^2)

F_{sed} = Diffusive flux from sediments to the water column ($mmol.m^{-2}.d^{-1}$)

F_b = Ebullition flux ($mmol.m^{-2}.d^{-1}$)

A_{sur} = Lake surface area (m^2)

The sum of sediment-water diffusive fluxes (0.8 to 3.2 $mmol.m^{-2}.d^{-1}$) and the bubbling fluxes (0.5 to 0.8 $mmol.m^{-2}.d^{-1}$) at the UML could be 1.3 to 4 $mmol.m^{-2}.d^{-1}$, depending on whether the freeze-core or mass balance estimate is used for the former value. This sum is presumably equal to the average methane production rate, assuming the sediments are at steady state in the long-term. For comparison, the production rate reported in three duplicate cores incubated at $4.5^\circ C$ from Lake Third Sister (Kelly and Chynoweth 1981) was 2.3 ± 1.4 $mmol.m^{-2}.d^{-1}$

¹. The authors also measured production rates in cores incubated at 9°C from Lake Frain's and Lake Third Sister, which ranged from 3.9 ± 2.3 to 4.7 ± 2.3 mmol.m⁻².d⁻¹.

Due to the constant temperature and anoxic conditions at the lake bottom, as well as the high amount of organic matter present in the sediments, the methane production rate probably did not change much from 2007 to 2008. This hypothesis is supported by the evidence that the hypolimnetic accumulation of methane occurred at a steady rate throughout the season (Figure 11). However, methanogenesis rates have been observed to vary in the short-term (order of weeks) with the input of fresh organic matter (Kelly and Chynoweth 1981). In a 3-year study, Eckert and Conrad 2007 observed that the rate of hypolimnetic accumulation in L. Kinneret increased with POM settling fluxes. The POM fluxes at the UML, as measured by a limited number of sediment traps, varied considerably from August-November, and were several times larger than the estimated methane production rate (Table 10). These fluxes only consider fine particulate organic matter and do not include large particles such as leaf litter than can further add to the organic matter content of the sediments. While it is possible that short-term methanogenesis rates near the top of the sediments varied with the POM fluxes; their effect on the overall methanogenesis rates were probably small, and did not measurably affect the total rate of change of storage. Furthermore, the sedimentation rates in the top layer of the UML sediments have been previously measured to be ~1 cm/yr (Spliethoff and Hemond 1996); it is unlikely that the organic matter accumulated in a very thin layer at the top of the sediments can dominate the overall methanogenesis rate.

The above hypothesis also indicates that the long-term temporal variability in bubble release from sediments is probably not an effect of changing methanogenesis rates. Given the average porewater concentration of the top 1 m of sediments (~4 mM) and total methane release

calculated above, one can estimate that it would take approximately 1000 to 3000 days to exhaust the sediment reservoir.

7. SUMMARY AND CONCLUSIONS

The mass balance shows that the seasonal water column storage of methane, which occurs primarily in the hypolimnion, is one of largest components of the methane cycle of the Upper Mystic Lake. At least 60% of total methane release from the sediments occurs through diffusion into the water column, if the flux estimate from the freeze core ($0.8 \text{ mmol.m}^{-2}.\text{d}^{-1}$) is compared with ebullition fluxes ($0.5 \text{ mmol.m}^{-2}.\text{d}^{-1}$). The mass balance however indicates that the proportion of methane diffused across the sediment-water interface can be about 4 times higher than the freeze core estimate, which means that the proportion of sediment-water exchange to bubbling can possibly be much larger than 60%. The amount of methane diffusing from bubbles into the water column was estimated to be a very small part of the storage term.

Small quantities of methane can diffuse from the hypolimnion into the upper lake depths. During stratification, this methane is evidently consumed internally within a transition zone that is present between spring and fall turnover. Due to the presence of the methane minimum in the transition zone, none of the methane diffused out of the lake surface, prior to turnover, originates in the hypolimnion. It thus appears as though the primary input of methane to the upper mixed layer (before the fall turnover) is release from epilimnetic sediments, and that most of this methane is emitted to the atmosphere through surface air-water exchange, and possibly consumed internally through oxidation. Further measurements are needed in order to separate the oxidation term from the epilimnetic sediment input into the lake.

A major question concerns the fate of the stored methane during the fall turnover when the thermocline erodes. Physically this corresponds to the transport of hypolimnetic water and solutes into the epilimnion. However, the concentrations measured in the upper mixed layer did not increase in November, despite this input of methane during the turnover; the mass balance indicates that an internal sink consumed most of this methane. It is hypothesized that this sink is methane oxidation, and that this process could play a major role in preventing hypolimnetic methane from being emitted to the atmosphere through air-water exchange. However, surface methane concentrations need to be sampled at higher temporal resolutions in order to rule out the possibility that a significant quantity of methane was released to the atmosphere during the fall turnover.

8. TABLES

Table 1 – Dissolved methane profiles, 2007

Table 2 – Dissolved methane profiles, 2008

Table 3 – Porewater concentrations from a freeze core collected on September 22nd, 2008

Table 4 – Results of bubble dissolution model for bubble sizes 1 to 5 mm

Table 5 – Turbulent diffusivities at the thermocline and oxycline

Table 6 – Upper mixed layer mass balance, 2008

Table 7 – Transition zone mass balance, 2008

Table 8 – Hypolimnion mass balance, 2008

Table 9 – Comparison of sediment water fluxes at different sites

Table 10 – Particulate organic matter fluxes from sediment traps

Table 1 Dissolved methane profiles (μM) in 2007

Depth (m)	July 2nd (Duplicates not taken)
0	0.7 \pm 0.1
3	0.9 \pm 0.1
4.5	0.6 \pm 0.1
6	0.3 \pm 0.0
9	0.3 \pm 0.0
12	0.1 \pm 0.0
15	7 \pm 1
18	252 \pm 30
21	425 \pm 50

Depth (m)	August 2nd (Duplicates not taken)
0	0.5 \pm 0.2
3	0.4 \pm 0.1
6	0.03 \pm 0.01
9	0.02 \pm 0.00
12	0.05 \pm 0.01
15	28 \pm 6
18	398 \pm 75
21	644 \pm 171

Depth (m)	August 17th
0	0.4 \pm 0.1
6	0.07 \pm 0.02
10	0.10 \pm 0.03
14	16.3 \pm 3.2
18	383 \pm 80
23	686 \pm 44*

* Collected on Aug 29

Depth (m)	Sept 23rd
0	0.8 \pm 0.1
6	1.8 \pm 1.1
9	0.3 \pm 0.2
14	28 \pm 3
18	337 \pm 23
23	670 \pm 16*

* Collected on Sept 9

Depth (m)	Oct 15th
0	1.0 \pm 0.2
6	0.4 \pm 0.1
7	0.07 \pm 0.02
9	1.2 \pm 1.0
14	31 \pm 3
22	718 \pm 73

Depth (m)	Nov 12th & 14th
0	0.2 \pm 0.0
4	0.2 \pm 0.0
8	0.2 \pm 0.0
9	0.2 \pm 0.0
12	14 \pm 1
15	107 \pm 5
20	696 \pm 25
23	816 \pm 39

Depth (m)	Nov 30th
0	0.3 \pm 0.0
5	0.2 \pm 0.0
10	0.3 \pm 0.1
15	60 \pm 4
21	777 \pm 29

Table 2 Dissolved methane profiles (μM) in 2008

Depth (m)	Apr 10	Jun 12	Jul 16
0	0.11 ± 0.03	0.5 ± 0.1	0.6 ± 0.1
2.8	0.12 ± 0.04	0.7 ± 0.1	1.6 ± 0.2
5.3	0.05 ± 0.03	0.22 ± 0.06	0.3 ± 0.1
8.2	0.02 ± 0.02	0.11 ± 0.05	0.15 ± 0.07
10.8	0.03 ± 0.04	0.07 ± 0.03	0.12 ± 0.06
13.6	0.7 ± 0.1	0.2 ± 0.1	9.1 ± 1.3
16.2	109.3 ± 20.3	154.2 ± 26.9	227.2 ± 30.0
19.85	233.8 ± 30.2	280.9 ± 27.3	320.6 ± 32.2

Depth (m)	Aug 13	Sep 13	Oct 13	Nov 9
0	0.4 ± 0.1	0.8 ± 0.1	0.3 ± 0.1	0.23 ± 0.07
3	0.4 ± 0.1	0.8 ± 0.2	0.8 ± 0.1	0.17 ± 0.05
6	0.09 ± 0.04	0.7 ± 0.1	0.12 ± 0.06	0.16 ± 0.03
9	0.04 ± 0.01	0.06 ± 0.02	0.9 ± 0.1	0.20 ± 0.05
12	2.4 ± 0.4	14.6 ± 1.8	12.1 ± 1.5	47.1 ± 7.0
15	104.1 ± 11.6	151.1 ± 19.3	162.5 ± 24.2	201.7 ± 26.2
18	263.2 ± 34.2	320.2 ± 37.4	326.9 ± 47.6	379.2 ± 44.4
20.5				454.3 ± 56.9
22	413.3 ± 43.3	446.1 ± 50.1	493.4 ± 62.2	

**Table 3 Methane porewater concentrations from a freeze core collected at 42°26'.
000N, 71°08.983W**

Depth from top of sediment (cm)	Methane (mmol/L porewater)	Methane (atm)	% Saturation [Methane (mM) /solubility (mM)]
0 to 8.5	1.55 ± 0.65	0.76 ± 0.32	25 ± 11
8.5 to 17.5	2.81 ± 0.16	1.38 ± 0.08	46 ± 3
17.5 to 24.5	3.71 ± 0.17	1.82 ± 0.08	61 ± 3
24.5 to 31	4.04 ± 0.19	1.98 ± 0.09	66 ± 3
31 to 36	4.51 ± 0.45	2.21 ± 0.22	74 ± 7
36 to 41	4.27 ± 0.27	2.10 ± 0.13	70 ± 4
41 to 46	4.00 ± 0.22	1.96 ± 0.11	65 ± 4
46 to 51	5.06 ± 0.28	2.49 ± 0.14	83 ± 5
51 to 58	3.99 ± 0.35	1.95 ± 0.17	65 ± 6
58 to 64.5	4.21 ± 0.25	2.07 ± 0.12	69 ± 4
64.5 to 71	4.35 ± 0.27	2.14 ± 0.13	71 ± 4
71 to 75	4.23 ± 0.11	2.08 ± 0.05	69 ± 2
75 to 81	3.99 ± 0.15	1.96 ± 0.07	65 ± 2
81 to 86.5	4.40 ± 0.11	2.16 ± 0.06	72 ± 2
86.5 to 91	4.43 ± 0.10	2.18 ± 0.05	73 ± 2
91 to 97	3.74 ± 0.27	1.84 ± 0.13	61 ± 4

Henry's constant at 4°C = 491 L.atm/mol (Calculated using $K_H=776$ L.atm/mol at 20°C from Stumm and Morgan)

Solubility of methane at 4°C and 3 atm pressure ~ 6 mM

Table 4 Fraction of methane lost from a single bubble released from a depth of 20m computed using the SiBu-GUI model (see text for model parameters). The average and standard deviations shown in this table were multiplied by ebullition fluxes to calculate the magnitude and error of bubble dissolution.

Bubble size (mm)	% CH ₄ lost at 15m	12m	9m	6m	3m	Surface
1	60	81	92	97	99	100
2	31	46	58	67	74	79
3	19	29	38	45	51	56
4	14	22	29	35	40	44
5	11	17	22	27	31	35
Average %	25	35	41	46	50	52
Standard deviation	19	26	30	32	34	35

Table 5 Estimate of turbulent diffusivity coefficients at the oxycline and thermocline. Temperature error in probe measurements were ~0.1°C resulting in a 20% error in K_z estimates.

Period (2008)	Approximate oxycline depth(m)	Kz at oxycline (m ² /d)	Approximate thermocline depth(m)	Kz at thermocline (m ² /d)
Apr 10 - May 15	14	0.06 ± 0.01	3	0.15
May 15-Jun 12	14	0.07 ± 0.01	3	-0.03
Jun 12 - Aug 13	12	0.16 ± 0.03	6	0.08
Aug 13 - Sep 13	9	0.04 ± 0.01	6	0.02
Sep 13 - Oct 13	9	0.01 ± 0.00	6	0.04
Oct 13 - Nov 9	9	0.07 ± 0.01	9	0.07

Table 6 Upper mixed layer mass balance for UML, 2008. The seasonal average values are shown in Figure 8.

Period (2008)	No. days	Approximate thermocline depth (m)	Upper mixed layer change of storage (kmol)	Air water exchange (kmol)	Flux across thermocline (kmol)	Diffusion from bubbles (kmol)	[D _{sed} - oxidation] (kmol)
Apr 10 - Jun 12	63	3m	0.6 ± 0.1	4.9 ± 4.3	0.4 ± 0.1	0.4 ± 0.2	5.5 ± 4.3
Jun 12 - Jul 16	34	3m	0.8 ± 0.2	6.0 ± 1.4	0.4 ± 0.3	0.1 ± 0.0	7.1 ± 1.5
Jul 16 - Aug 13	28	6m	-0.7 ± 0.2	4.3 ± 1.4	0.3 ± 0.2	0.3 ± 0.2	3.6 ± 1.4
Aug 13 - Sep 13	31	6m	1.2 ± 0.3	5.3 ± 2.6	0.0 ± 0.0	0.5 ± 0.2	6.1 ± 2.6
Sep 13 - Oct 13	30	6m	-0.6 ± 0.3	4.3 ± 2.6	0.0 ± 0.0	0.4 ± 0.2	3.2 ± 2.6
Oct 13 - Nov 9	27	9m	-0.7 ± 0.2	1.7 ± 0.5	-5.8 ± 1.1	1.1 ± 0.5	-6.0 ± 1.3
Total: Apr-Nov	213		0.5 ± 0.1	26.6 ± 6.0	-4.7 ± 1.2	2.8 ± 0.7	
Seasonal average (mol/d)	213		2 ± 0	125 ± 28	-22 ± 8	13 ± 3	

211

Table 7 Transition zone mass balance for the UML, 2008. The seasonal average values are shown in Figure 9.

Period (2008)	Approximate thermocline depth (m)	Approximate oxycline depth (m)	Transition zone change of storage (kmol)	Source: Flux across oxycline (kmol)	Source: Flux across thermocline (kmol)	Source: Diffusion from bubbles (kmol)	[D _{sed} - oxidation] (kmol)
Apr 10 - Jun 12	3m	14m	0.4 ± 0.1	0.1 ± 0.1	0.4 ± 0.1	4.9 ± 2.9	-5.0 ± 2.9
Jun 12 - Jul 16	3m	12m	0.6 ± 0.5	2.4 ± 1.0	0.4 ± 0.3	0.6 ± 0.3	-2.9 ± 1.2
Jul 16 - Aug 13	6m	9m	-1.3 ± 0.5	0.6 ± 0.5	0.3 ± 0.2	0.3 ± 0.1	-2.4 ± 0.7
Aug 13 - Sep 13	6m	9m	0.3 ± 0.1	1.1 ± 0.0	0.0 ± 0.0	0.4 ± 0.2	-1.2 ± 0.2
Sep 13 - Oct 13	6m	9m	0.1 ± 0.1	0.4 ± 0.0	0.0 ± 0.0	0.4 ± 0.1	-0.7 ± 0.2
Oct 13 - Nov 9	9m	9m	DID	NOT	EXIST		
Total: Apr-Oct			0.1 ± 0.1	4.6 ± 1.1	1.1 ± 0.4	6.5 ± 2.9	
Seasonal average (mol/d)			1 ± 0	22 ± 5	5 ± 2	30 ± 14	

Table 8 Hypolimnion mass balance for the UML, 2008. The seasonal average values are shown in Figure 10.

Period (2008)	Approximate oxycline depth (m)	Hypolimnion change of storage (10^5 mol)	Flux across oxycline (10^5 mol)	Diffusion from bubbles (10^5 mol)	Sediment efflux from mass balance (10^5 mol)
Apr 10 - Jun 12	14m	0.6 ± 0.3	0.0 ± 0.0	0.05 ± 0.04	0.6 ± 0.3
Jun 12 - Jul 16	12m	0.7 ± 0.3	0.0 ± 0.0	0.02 ± 0.01	0.7 ± 0.3
Jul 16 - Aug 13	9m	0.1 ± 0.3	0.0 ± 0.0	0.02 ± 0.02	0.0 ± 0.3
Aug 13 – Sep 13	9m	0.8 ± 0.3	0.0 ± 0.0	0.03 ± 0.02	0.8 ± 0.3
Sep 13 – Oct 13	9m	0.3 ± 0.4	0.0 ± 0.0	0.03 ± 0.02	0.3 ± 0.4
Oct 13 - Nov 9	9m	0.7 ± 0.4	0.1 ± 0.0	0.04 ± 0.03	0.7 ± 0.4
Total: Apr-Nov		3.2 ± 0.4	0.1 ± 0.0	0.12 ± 0.12	3.2 ± 0.4
Seasonal average (kmol/d)		1.5 ± 0.3	0.05 ± 0.01	0.06 ± 0.06	1.5 ± 0.3

* Estimated from a linear fit of monthly storage values (Figure 9)

Table 9 Comparison of sediment-water fluxes at different sites

Source	Location	Sediment diffusive flux (mmol.m⁻².d⁻¹)
Martens and Klump (1980)	Cape Lookout Bight, North Carolina	0.7±0.2 to 9.4±2.3
Molongoski and Klug (1980)	L. Wintergreen, Michigan	~22-30
Crill et al. (1988)	Lago Calado, Brazil	5.3-7.3
Adams and Naguib (1999)	L.Plusβee, Germany	2.3-6.9
Huttunen et al. (2006) (Lakes in Finland)	L. Tuusulanjrvi	4.5
	L. Postilampi	6.6
	L. Soiviojarvi	0.54
	L. Luiminkajarvi	1.7
	L. Ranuanjarvi	4.75
	L. Porttipahta	1.6
Data from Eckert and Conrad (2007), Ostrovsky et al. (2008)	L. Kinneret, Israel	12
Ostrovsky et al. (2008)	L. Kinneret, Israel	~10

**Table 10 POM fluxes (gPOM.m⁻².d⁻¹) in the UML as measured by five sediment traps.
Errors shown are standard deviations (1σ) from different traps, and not analysis errors.**

Period	9m(A)	12m	13m	22m	Lake center	Lake average POM flux (g POM.m⁻².d⁻¹)
Aug 13 - Sep 3		0.48	0.74	0.31	0.16	0.42 ± 0.25
Sep 3 - Sep 22	1.39	0.45	0.72	0.29	0.25	0.62 ± 0.47
Sep 22 - Oct 8	3.53	0.50	0.59	0.37	0.33	1.06 ± 1.38
Oct 8 - Oct 23	2.31	0.68	1.90	0.43	0.09	1.08 ± 0.97
Oct 23 - Nov 9	1.04	0.68	1.53	0.31	0.21	0.75 ± 0.55
Nov 9 - Dec 1	1.12	0.46	0.88	0.99	0.46	0.78 ± 0.31

9. FIGURES

Figure 1 – Sources and sinks of methane in a stratified lake

Figure 2 – UML temperature and dissolved oxygen stratification in 2007

Figure 3 – UML temperature and dissolved oxygen stratification in 2008

Figure 4 – UML epilimnion dissolved methane profiles in 2007

Figure 5 – UML epilimnion dissolved methane profiles in 2008

Figure 6(a) - UML porewater methane concentrations in a freeze core

Figure 6(b) - UML porewater methane concentrations vs. sediment depth

Figure 7 – Four box model for the Upper Mystic Lake mass balance

Figure 8 – Epilimnion mass balance

Figure 9 – Transition zone mass balance

Figure 10 – Hypolimnion mass balance

Figure 11 – Change in dissolved methane storage in the hypolimnion with time

Figure 12 – Sediment mass balance

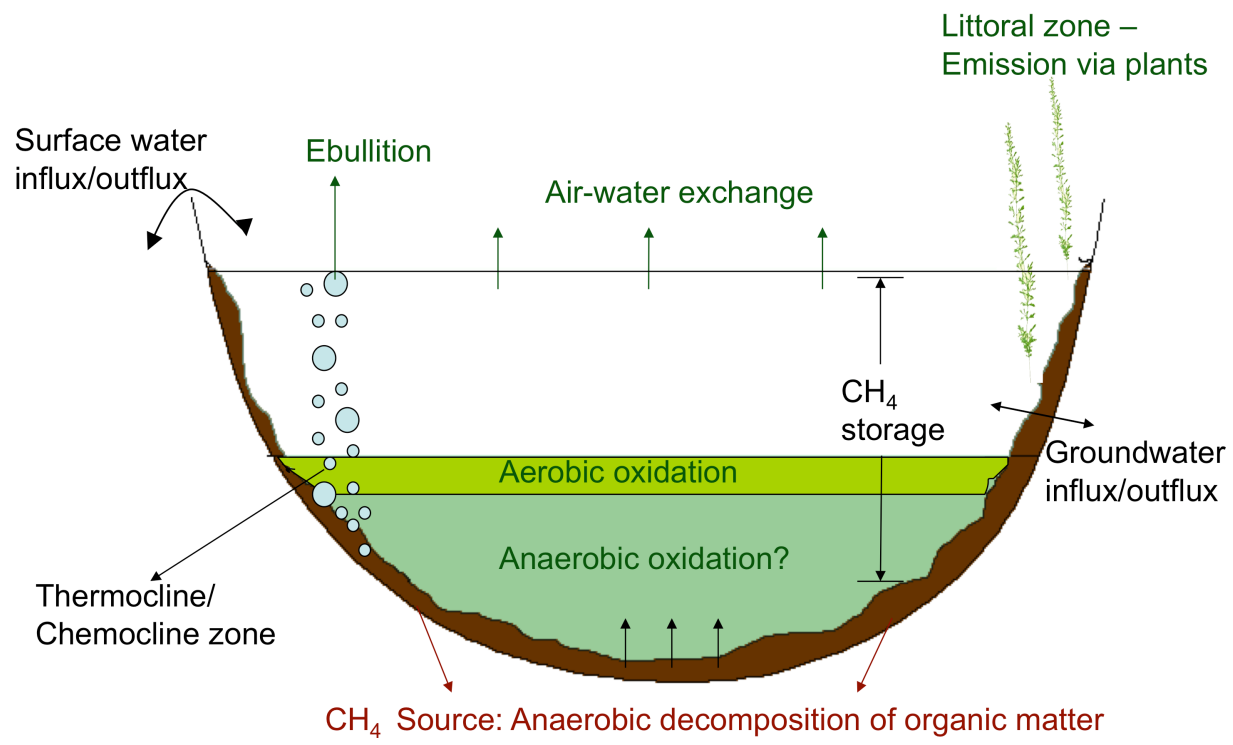
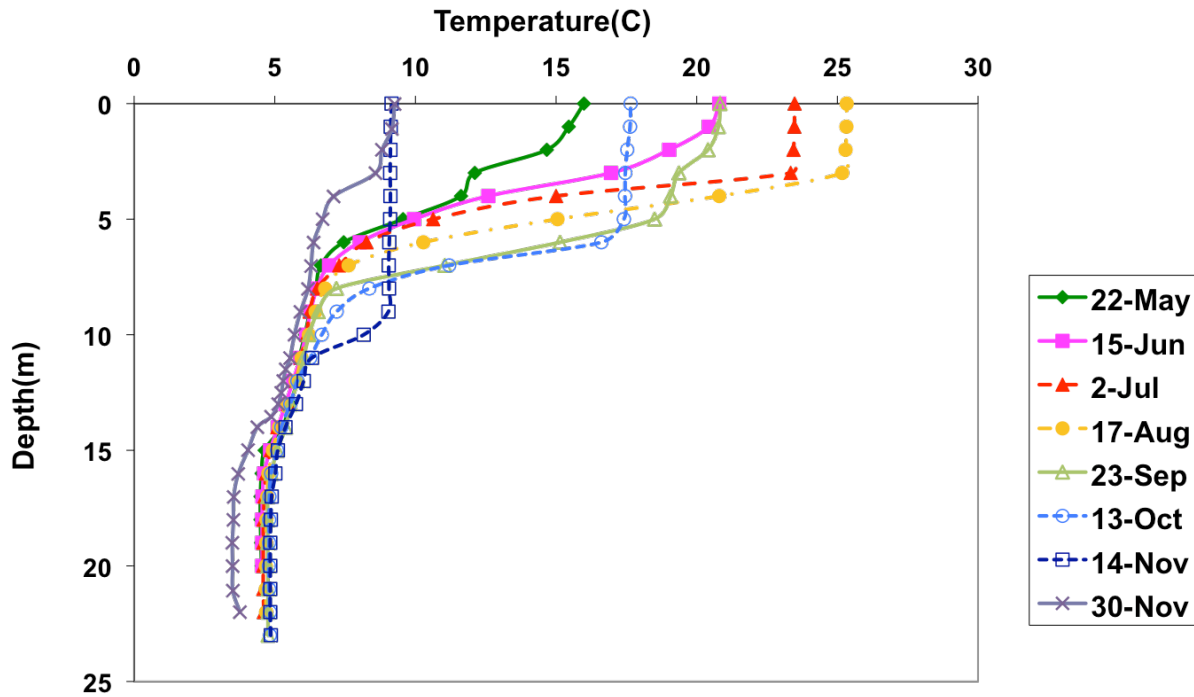


Figure 1 Potential sources and sinks of methane in a stratified lake

(a) UML Temperature Profiles - 2007



(b) UML Dissolved Oxygen Profiles - 2007

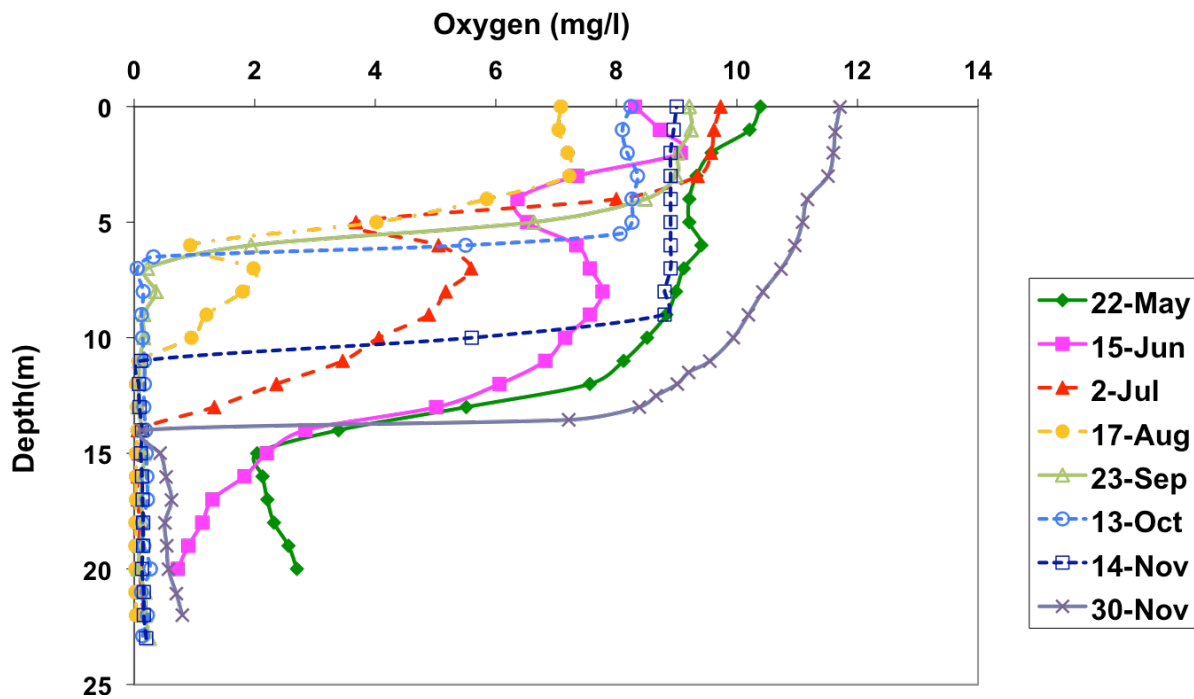
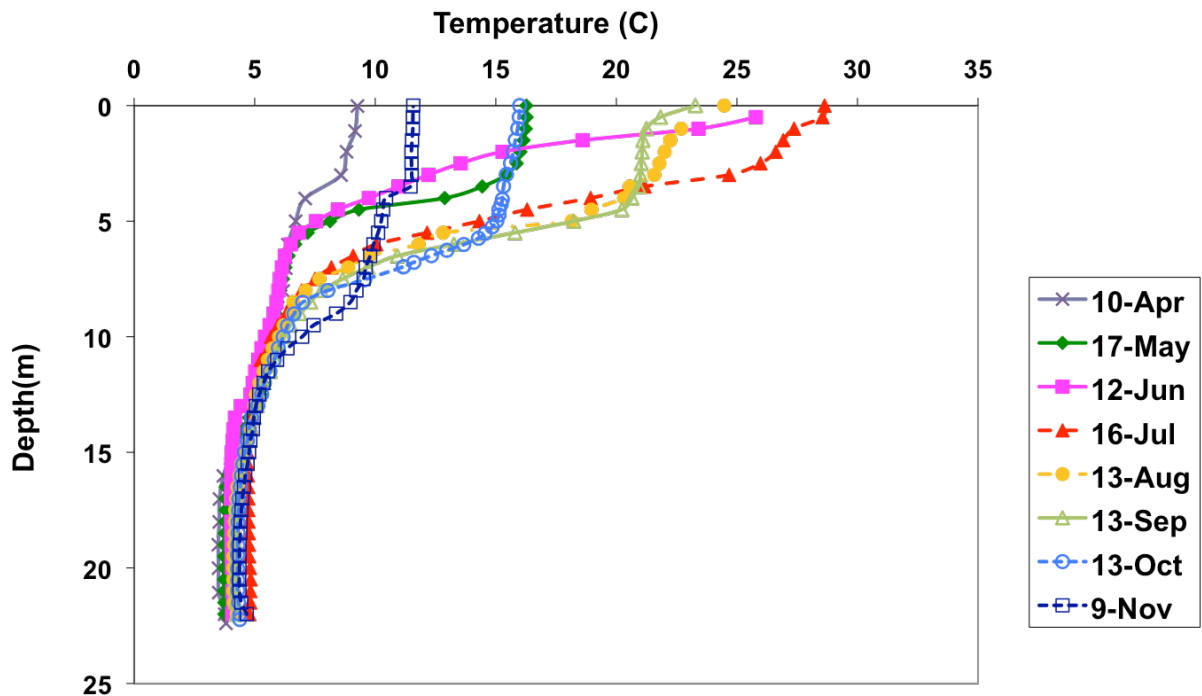


Figure 2 Stratification of (a) temperature and (b) oxygen intensified over the summer and fall of 2007. Fall overturn commenced around the end of September.

(a) UML Temperature Profiles - 2008



(b) UML Dissolved Oxygen Profiles - 2008

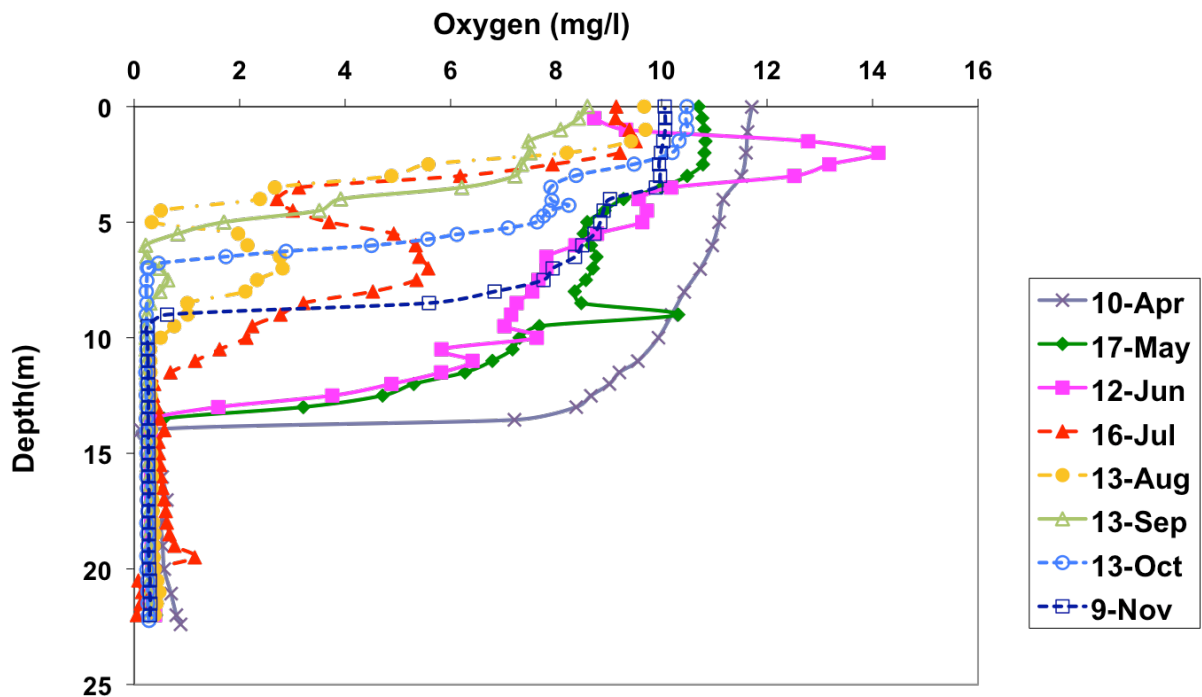


Figure 3 Stratification of (a) temperature and (b) oxygen intensified over the summer and fall of 2008. Fall overturn commenced around mid September.

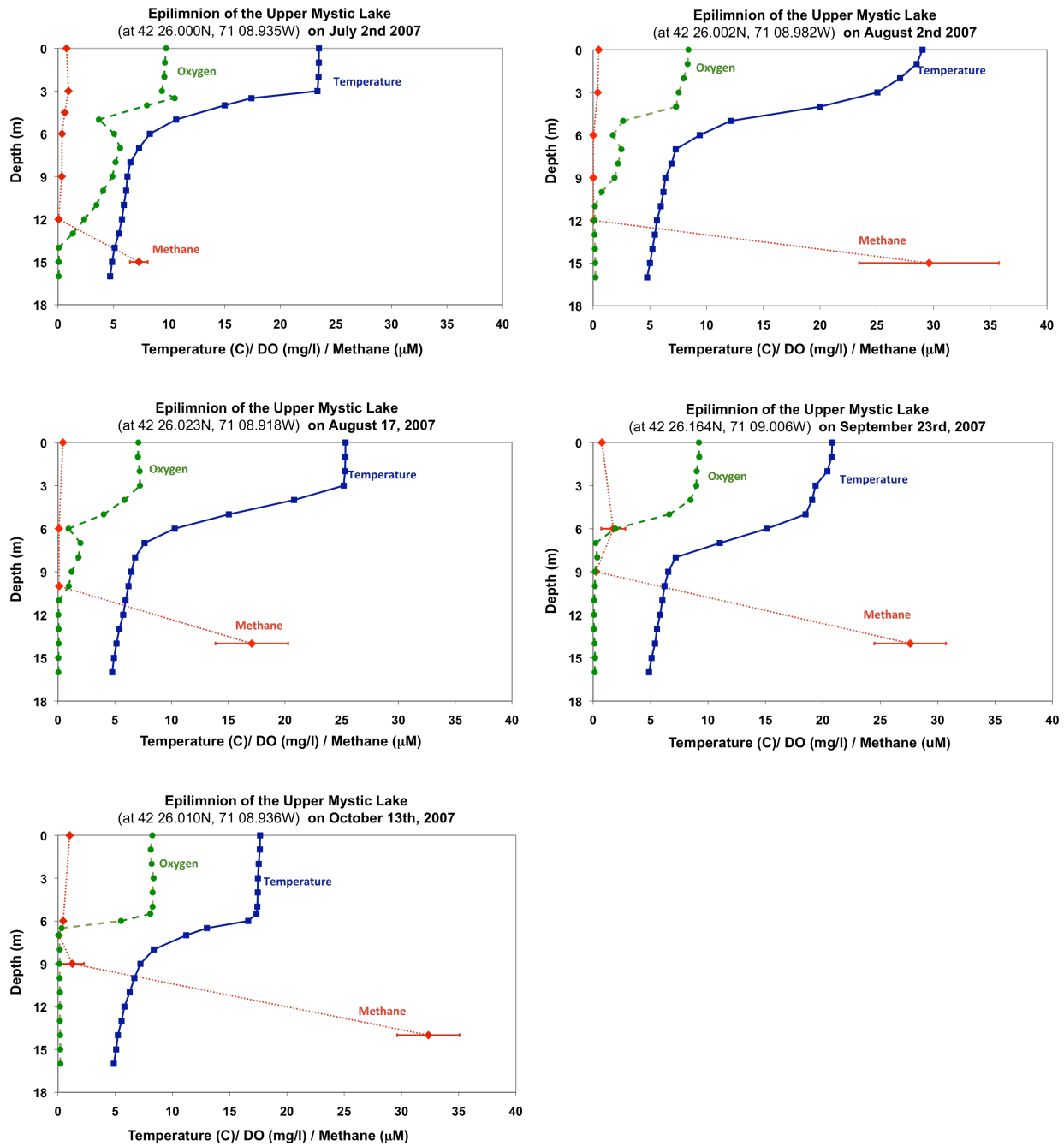


Figure 4 The UML was stratified into three layers – an upper mixed layer, a transition zone between the thermocline and the oxycline, and the hypolimnion (not shown in the above figures). Methane minima were observed in the transition zone on all sampling dates in 2007. (Markers: Temperature – blue squares, Oxygen – green circles, Methane – red diamonds)

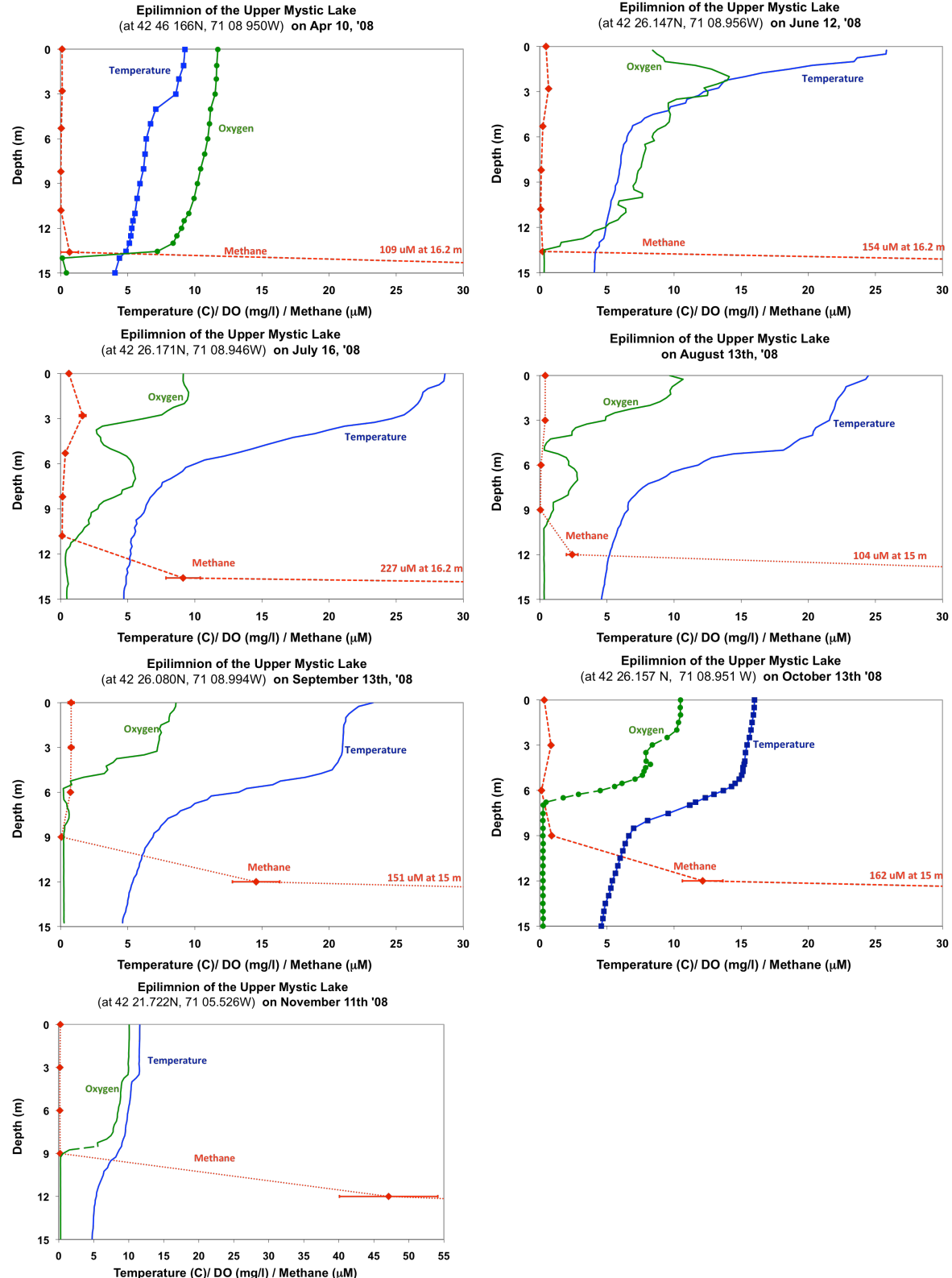


Figure 5 UML stratification in 2008. Temperature and dissolved oxygen profiles shown are averages over 25cm intervals for all dates except April and October.

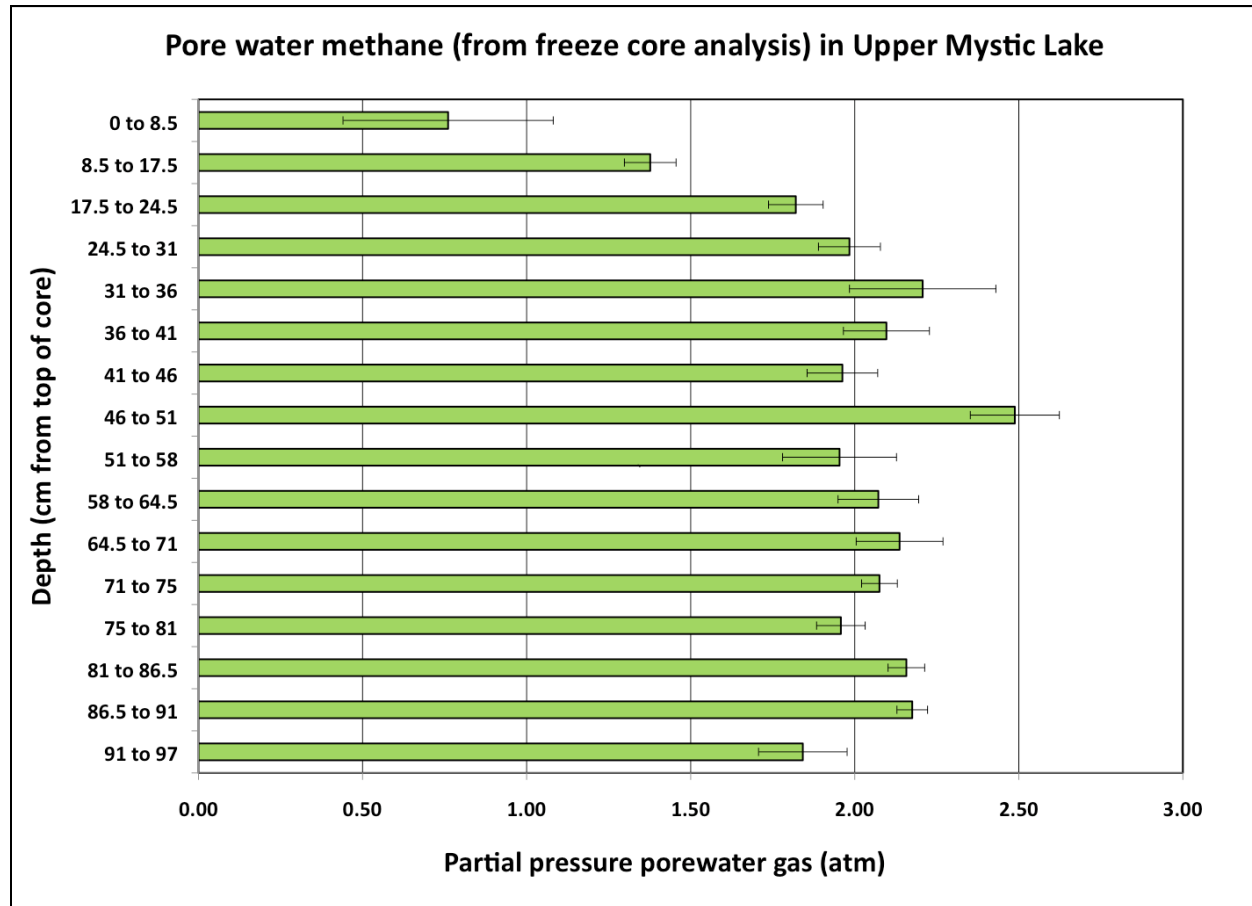


Figure 6(a) – Total porewater concentrations at a site ~ 20 m deep (saturation pressure ~ 3 atm).

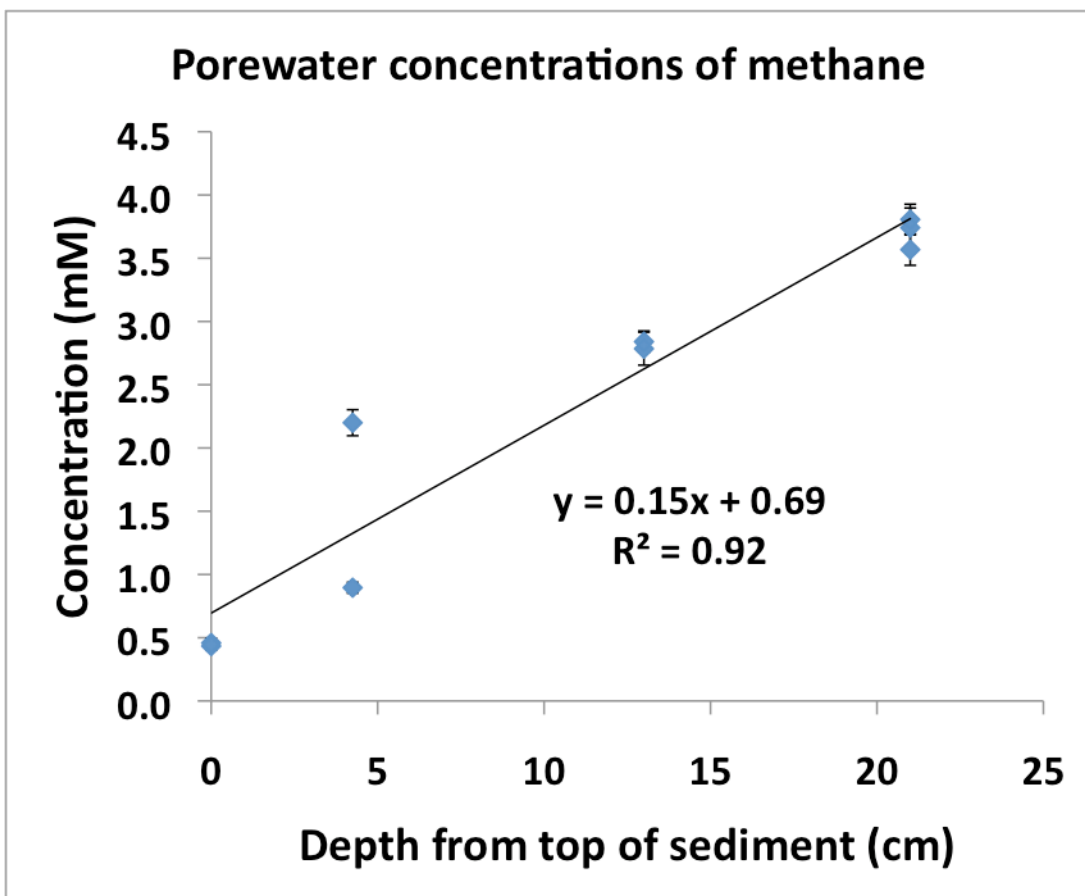


Figure 6(b) The concentration gradient in the sediments was estimated using a linear fit of porewater concentrations up to 25 cm depth, and a water column concentration of 0.45 mM near the sediments. The depths shown above are the sediment depths at the center of each core slice.

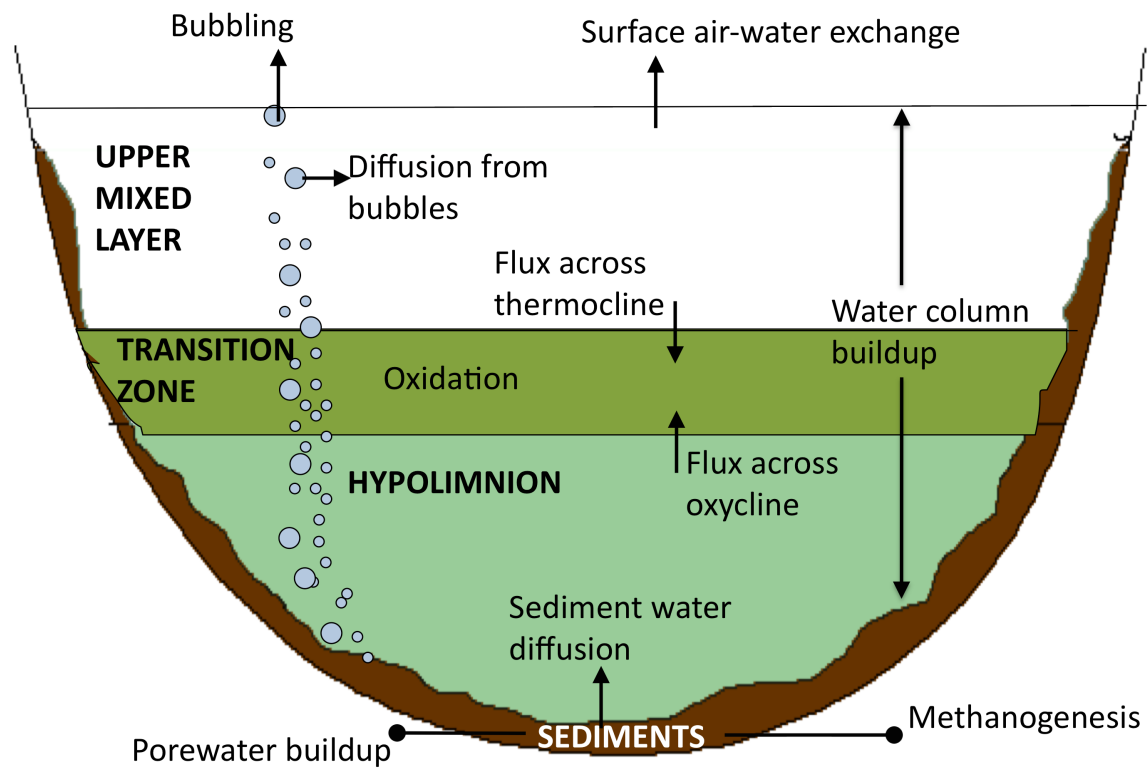
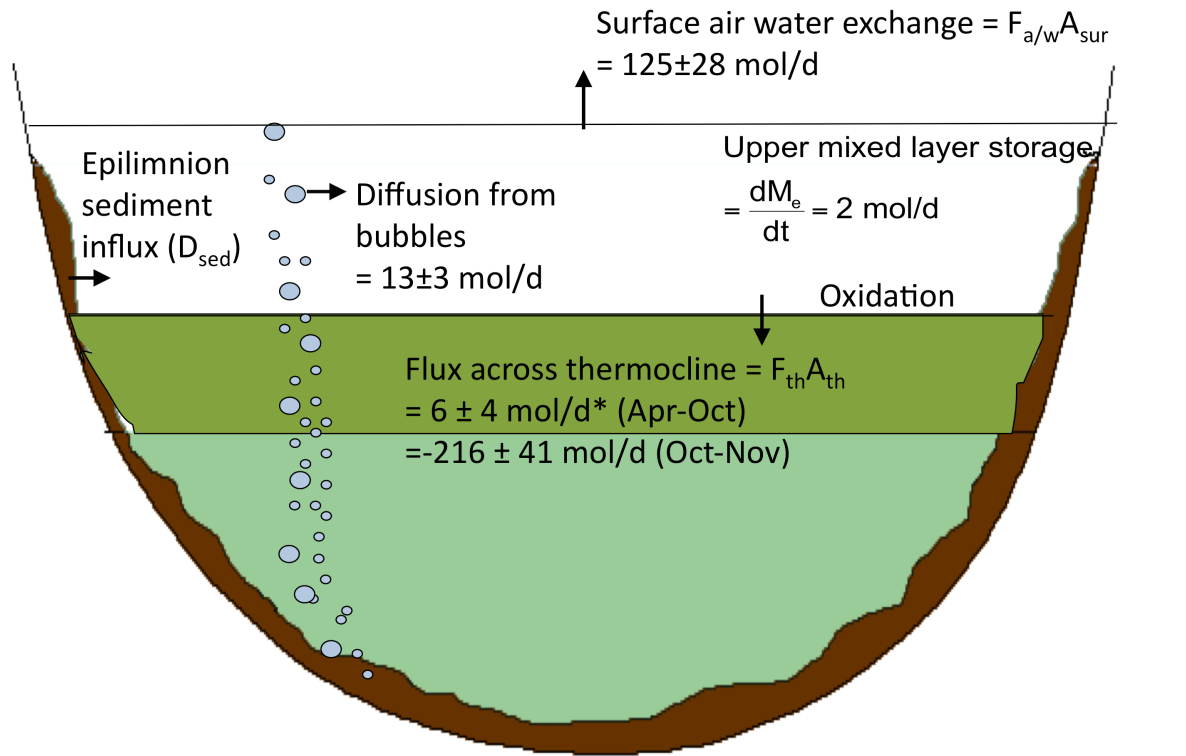


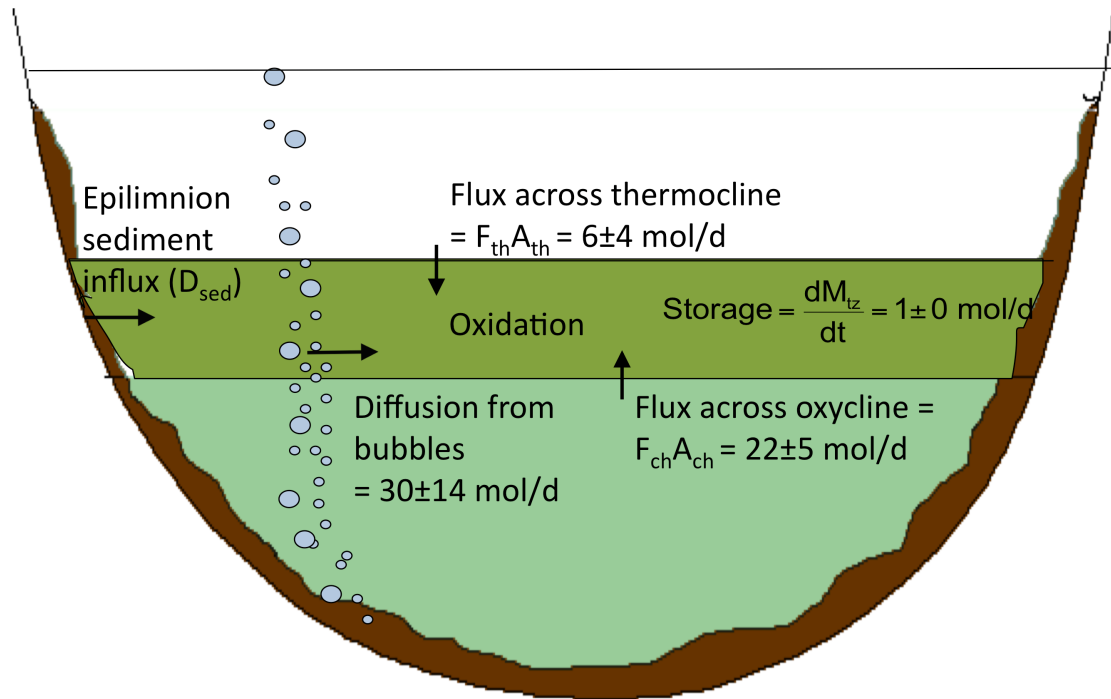
Figure 7 Components of the Upper Mystic Lake 4-box model



$$D_{sed} - oxidation = \frac{dM_E}{dt} + F_{aw} A_{sur} + K_{th} A_{th} \left. \frac{dc}{dz} \right|_{th} - \text{Gas diffused from bubbles}$$

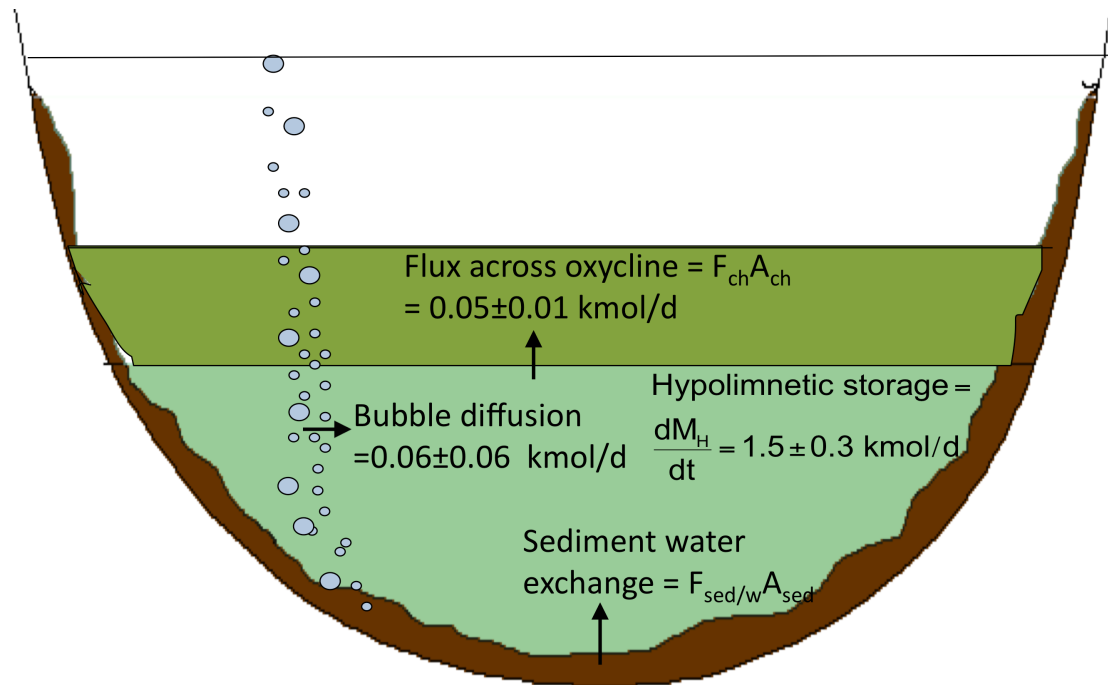
Figure 8 Mass balance for the upper mixed layer in the UML (see text for symbols). The numbers shown are seasonal (Apr-Nov) averages. Refer Table 6 for monthly values.

* Flux from the thermocline to the transition zone was positive or zero from April- mid October; however a large input of methane from the hypolimnion occurred during the turnover period, when the transition zone disappeared.



$$D_{sed} - oxidation = \frac{dM_{tz}}{dt} - K_{th}A_{th} \left. \frac{dc}{dz} \right|_{th} - K_{ch}A_{ch} \left. \frac{dc}{dz} \right|_{ch} - \text{Gas diffused from bubbles}$$

Figure 9 Mass balance for the transition zone (see text for symbols). The numbers shown are seasonal (Apr-Oct) averages. The transition zone did not exist in November. Refer Table 7 for monthly values.



$$F_{\text{sed/w}} A_{\text{sed}} = \frac{dM_H}{dt} + K_{\text{ch}} A_{\text{ch}} \left. \frac{dc}{dz} \right|_{\text{ch}} - \text{Gas diffused from bubbles}$$

Figure 10 Sediment fluxes into the water column were estimated using a hypolimnion mass balance (see text for symbols). The numbers shown are seasonal (Apr-Nov) averages. Refer Table 8 for monthly values. This estimate can be compared against the flux obtained from the concentration gradient in the top layer of sediments collected as a freeze core (see text).

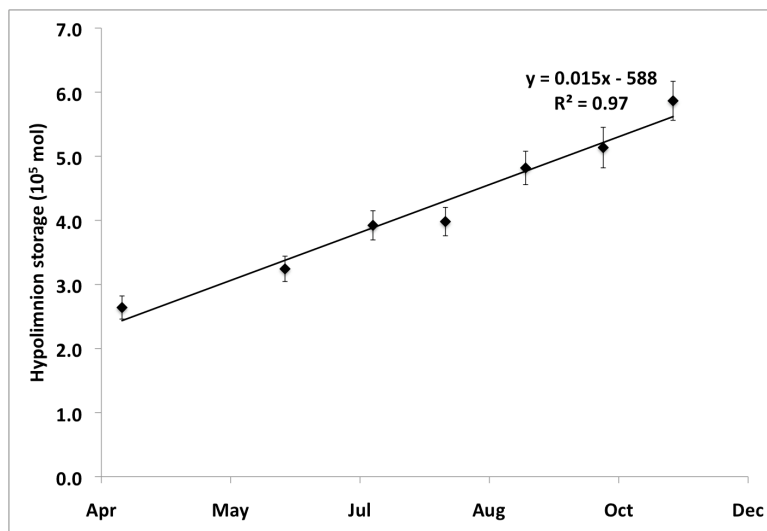


Figure 11 The change in hypolimnion storage with time from April to November 2008 was used to estimate diffusive sediment-water fluxes.

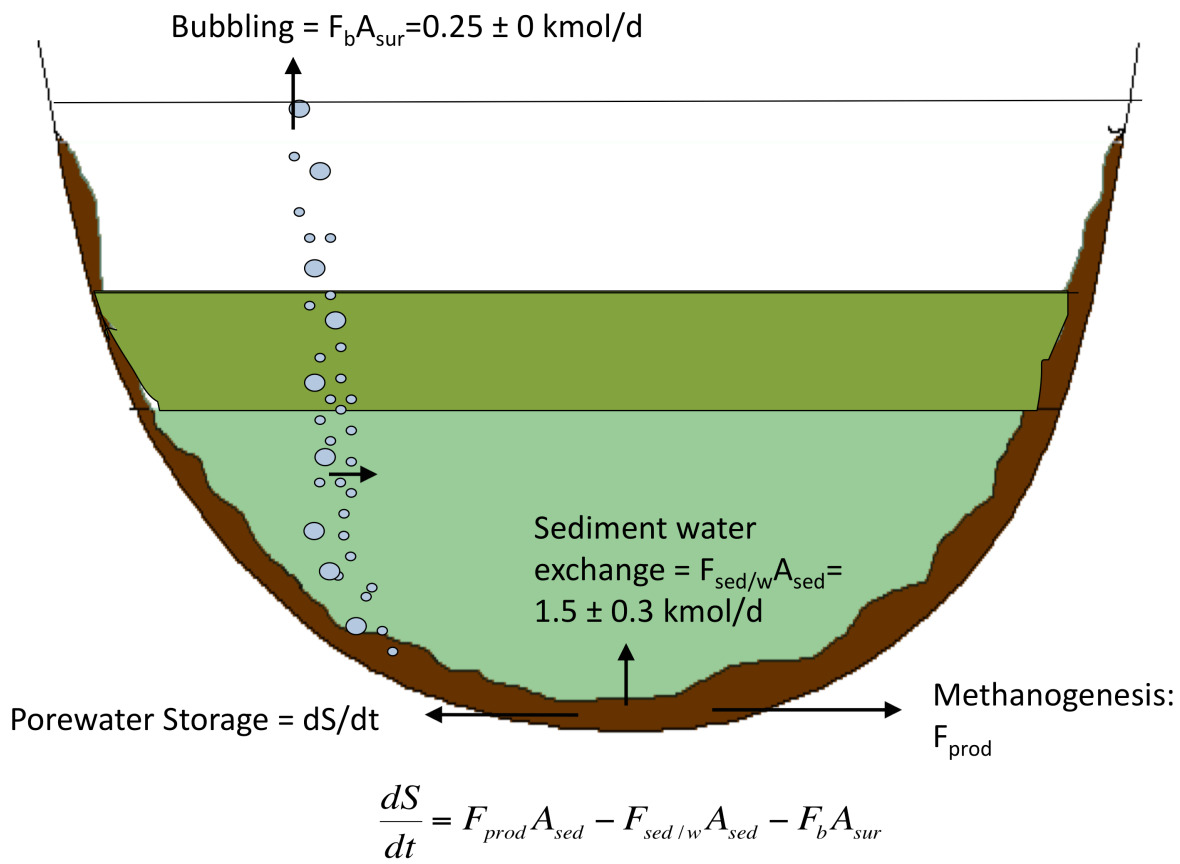


Figure 12 A methane production rate can be estimated using a sediment mass balance (see text for symbols). The numbers shown are seasonal (Apr-Nov) averages.

REFERENCES

1. Barnes, R. O. and E. D. Goldberg. 1976. Methane production and consumption in anoxic marine sediments. *Geology*. **4**: 297-300.
2. Bastviken, D., J. J. Cole, M. L. Pace and Van de Bogert, M. C. 2008. Fates of methane from different lake habitats: Connecting whole-lake budgets and CH₄ emissions. *J. Geophys. Res.* **113**: , doi:10.1029/2007JG000608.
3. Bastviken, D., J. Ejlersson and L. Tranvik. 2002. Measurement of Methane Oxidation in Lakes: A Comparison of Methods. *Environ. Sci. Technol.* **36**: 3354-3361.
4. Berner, R. A. 1980. Early diagenesis: A theoretical approach. Princeton University Press.
5. Boudreau, B. P. 1996. The diffusive tortuosity of fine-grained unlithified sediments. *Geochim. Cosmochim. Acta*. **60**: 3139-3142.
6. Casper, P., S. C. Maberly, G. H. Hall and B. J. Finlay. 2000. Fluxes of methane and carbon dioxide from a small productive lake to the atmosphere. *Biogeochemistry*. **49**: 1-19.
7. Chanton, J. P., C. S. Martens and C. A. Kelley. 1989. Gas transport from methane-saturated, tidal freshwater and wetland sediments. *Limnol. Oceanogr.* **34**: 807-819.
8. Conrad, R. 2005. Quantification of methanogenic pathways using stable carbon isotopic signatures: a review and a proposal. *Org. Geochem.* **36**: 739-752, doi:DOI: 10.1016/j.orggeochem.2004.09.006.
9. Crill, P. M., K. B. Bartlett, J. O. Wilson, D. I. Sebacher, R. C. Harriss, J. M. Melack, S. MacIntyre, L. Lesack and L. Smith-Morrill. 1988. Tropospheric methane from an Amazonian floodplain lake. *J. Geophys. Res.* **93**: 1564-1570, doi:10.1029/JD093iD02p01564.
10. DeLong, E. F. 2000. Microbiology: Resolving a methane mystery. *Nature*. **407**: 577-579.
11. Eckert, W. and R. Conrad. 2007. Sulfide and methane evolution in the hypolimnion of a subtropical lake: a three-year study. *Biogeochemistry*. **82**: 67-76.
12. Eller, G., L. Känel and M. Krüger. 2005. Cooccurrence of Aerobic and Anaerobic Methane Oxidation in the Water Column of Lake Plußsee. *Appl. Environ. Microbiol.* **71**: 8925-8928.
13. Fallon, R. D., S. Harrits, R. S. Hanson and T. D. Brock. 1980. The Role of Methane in Internal Carbon Cycling in Lake Mendota During Summer Stratification. *Limnol. Oceanogr.* **25**: 357-360.
14. Greinert, J. and D. F. McGinnis. 2009. Single bubble dissolution model – The graphical user interface SiBu-GUI. *Environmental Modelling & Software*. **24**: 1012-1013, doi:DOI: 10.1016/j.envsoft.2008.12.011.
15. Gunsalus, R., D. Eirich, J. Romesser, W. Balch, S. Shapiro, and R. S. Wolfe. 1976. Methyl-transfer and methane formation. Proceedings of Symposium on Microbial Production and Utilization of Gases (H₂, CO₂, CO). 191-198.
16. Hallam, S. J., N. Putnam, C. M. Preston, J. C. Detter, D. Rokhsar, P. M. Richardson and E. F. DeLong. 2004. Reverse Methanogenesis: Testing the Hypothesis with Environmental Genomics. *Science*. **305**: 1457-1462, doi:10.1126/science.1100025.
17. Harrits, S. M. and R. S. Hanson. 1980. Stratification of Aerobic Methane-Oxidizing Organisms in Lake Mendota, Madison, Wisconsin. *Limnol. Oceanogr.* **25**: 412-421.
18. Huttunen, J. T., T. S. Vaisanen, S. K. Hellsten and P. J. Martikainen. 2006. Methane fluxes at the sediment-water interface in some boreal lakes and reservoirs. *Boreal Environ. Res.* **11**: 27-34.
19. Iversen, N. and B. B. Jorgensen. 1993. Diffusion-Coefficients of Sulfate and Methane in Marine-Sediments - Influence of Porosity. *Geochim. Cosmochim. Acta*. **57**: 571-578.

20. Jassby, A. and T. Powell. 1975. Vertical Patterns of Eddy Diffusion During Stratification in Castle Lake, California. *Limnol. Oceanogr.* **20**: 530-543.
21. Jones, J. G., B. M. Simon and S. Garderner. 1982. Factors Affecting Methanogenesis and Associated Anaerobic Processes in the Sediments of a Stratified Eutrophic Lake. *J. Gen. Microbiol.* **128**: 1-11, doi:10.1099/00221287-128-1-1.
22. Kankaala, P., J. Huotari, E. Peltomaa, T. Saloranta and A. Ojala. 2006. Methanotrophic activity in relation to methane efflux and total heterotrophic bacterial production in a stratified, humic, boreal lake. *Limnol. Oceanogr.* **51**: 1195-1204.
23. Kankaala, P., A. Ojala and T. Käki. 2004. Temporal and spatial variation in methane emissions from a flooded transgression shore of a boreal lake. *Biogeochemistry*. **68**: 297-311.
24. Kankaala, P., S. Taipale, H. Nykänen and R. I. Jones. 2007. Oxidation, efflux, and isotopic fractionation of methane during autumnal turnover in a polyhumic, boreal lake. *J. Geophys. Res.* **112**: G02033.
25. Kelly, C. A. and D. P. Chynoweth. 1980. Comparison of In Situ and In Vitro Rates of Methane Release in Freshwater Sediments. *Appl. Environ. Microbiol.* **40**: 287-293.
26. Kelly, C. A. and D. P. Chynoweth. 1981. The Contributions of Temperature and of the Input of Organic Matter in Controlling Rates of Sediment Methanogenesis. *Limnol. Oceanogr.* **26**: 891-897.
27. Leifer, I. and R. K. Patro. 2002. The bubble mechanism for methane transport from the shallow sea bed to the surface: A review and sensitivity study. *Cont. Shelf Res.* **22**: 2409-2428, doi:DOI: 10.1016/S0278-4343(02)00065-1.
28. Liikanen, A., J. T. Huttunen, K. Valli and P. J. Martikainen. 2002a. Methane cycling in the sediment and water column of mid-boreal hyper-eutrophic Lake Kevaton, Finland. *Arch. Hydrobiol.* **154**: 585-603.
29. Liikanen, A., T. Murtoniemi, H. Tanskanen, T. Väisänen and P. J. Martikainen. 2002b. Effects of temperature and oxygen availability on greenhouse gas and nutrient dynamics in sediment of a eutrophic mid-boreal lake. *Biogeochemistry*. **59**: 269-286.
30. Madigan, T. M., and J. M. Martinko. 2006. Brock: Biology of Microorganisms, 11th ed. Pearson Prentice Hall, Upper Saddle River, New Jersey.
31. Martens, C. S. and J. V. Klump. 1980. Biogeochemical cycling in an organic-rich coastal marine basin-I. Methane sediment-water exchange processes. *Geochim. Cosmochim. Acta*. **44**: 471-490.
32. McGinnis, D. F., J. Greinert, Y. Artemov, S. E. Beaubien and A. Wüest. 2006. Fate of rising methane bubbles in stratified waters: How much methane reaches the atmosphere? *J. Geophys. Res.* **111**: C09007, doi:10.1029/2005JC003183.
33. Michmerhuizen, C. M., R. G. Striegl and M. E. McDonald. 1996. Potential methane emission from north-temperate lakes following ice melt. *Limnol. Oceanogr.* **41**: 985-991.
34. Molongoski, J. J. and M. J. Klug. 1980. Anaerobic metabolism of particulate organic matter in the sediments of a hypereutrophic lake*. *Freshwat. Biol.* **10**: 507-518, doi:10.1111/j.1365-2427.1980.tb01225.x.
35. Nüsslein, B., W. Eckert and R. Conrad. 2003. Stable Isotope Biogeochemistry of Methane Formation in Profundal Sediments of Lake Kinneret (Israel). *Limnol. Oceanogr.* **48**: 1439-1446.

36. Ostrovsky, I., D. F. McGinnis, L. Lapidus and W. Eckert. 2008. Quantifying gas ebullition with echosounder: The role of methane transport by bubbles in a medium-sized lake. Limnol. Oceanogr. - Methods. **6**: 105-118.
37. Raghoebarsing, A. A., A. Pol, K. T. van de Pas-Schoonen, A. J. P. Smolders, K. F. Ettwig, W. I. C. Rijpstra, S. Schouten, J. S. S. Damste, H. Camp and M. S. M. Jetten. 2006. A microbial consortium couples anaerobic methane oxidation to denitrification. Nature. **440**: 918-921.
38. Reeburgh, W. S. 1976. Methane consumption in Cariaco Trench waters and sediments. Earth Planet. Sci. Lett. **28**: .
39. Rehder, G., P. W. Brewer, E. T. Peltzer and G. Friederich. 2002. Enhanced lifetime of methane bubble streams within the deep ocean. Geophys. Res. Lett. **29**: 1731.
40. Rudd, J. W. M. and R. D. Hamilton. 1978. Methane Cycling in a Eutrophic Shield Lake and its Effects on Whole Lake Metabolism. Limnol. Oceanogr. **23**: 337-348.
41. Rudd, J. W. M., and C. D. Taylor. 1980. Methane cycling in aquatic environments, p. 77-150. In M. R. Droop, Jannasch, H.W. [ed.], Advances in Aquatic Microbiology. Academic Press.
42. Rudd, J. W. M., R. D. Hamilton and N. E. R. Campbell. 1974. Measurement of Microbial Oxidation of Methane in Lake Water. Limnol. Oceanogr. **19**: 519-524.
43. Sahores, J. and P. A. Witherspoon. 1970. Diffusion of light paraffin hydrocarbons in water from 2 to 80C.
44. Schulz, S. and R. Conrad. 1996. Influence of temperature on pathways to methane production in the permanently cold profundal sediment of Lake Constance. FEMS Microbiol. Ecol. **20**: 1-14, doi:10.1111/j.1574-6941.1996.tb00299.x.
45. Schwarzenbach, R. P., P. M. Gschwend, and D. M. Imboden. 2003. Environmental organic chemistry, 2nd ed. Wiley-InterScience.
46. Scranton, M. I., P. Crill, M. A. d. Angelis, P. L. Donaghay and J. M. Sieburth. 1993. The Importance of Episodic Events in Controlling the Flux of Methane From an Anoxic Basin. Global Biogeochem. Cycles. **7**: 491-507.
47. Sebacher, D. I., R. C. Harriss and K. B. Bartlett. 1985. Methane emissions to the atmosphere through aquatic plants. J. Environ. Qual. **14**: 40.
48. Senn, D. B. 2001. Coupled arsenic, iron, and nitrogen cycling in arsenic-contaminated Upper Mystic Lake. Doctor of Philosophy thesis. Massachusetts Institute of Technology.
49. Spliethoff, H. M. 1995. Biotic and abiotic transformations of arsenic in the Upper Mystic Lake.
50. Spliethoff, H. M. and H. F. Hemond. 1996. History of Toxic Metal Discharge to Surface Waters of the Aberjona Watershed. Environ. Sci. Technol. **30**: 121-128.
51. Utsumi, M. 1998. Dynamics of dissolved methane and methane oxidation in dimictic Lake Nojiri during winter. Limnol. Oceanogr. **43**: 10-17.
52. Utsumi, M., Y. Nojiri, T. Nakamura, T. Nozawa, A. Otsuki and H. Seki. 1998. Oxidation of dissolved methane in a eutrophic, shallow lake: Lake Kasumigaura, Japan. Limnol. Oceanogr. **43**: 471-480.
53. Walter, K. M., S. A. Zimov, J. P. Chanton, D. Verbyla and F. S. Chapin III. 2006. Methane bubbling from Siberian thaw lakes as a positive feedback to climate warming. Nature. **443**: 71-75, doi:10.1038/nature05040.
54. Wetzel, R. G. 1975. Limnology. Saunders.

55. Winfrey, M. R. and J. G. Zeikus. 1979. Microbial Methanogenesis and Acetate Metabolism in a Meromictic Lake. *Appl. Environ. Microbiol.* **37**: 213-221.
56. Zehnder, A. J. B. and T. D. Brock. 1980. Anaerobic Methane Oxidation: Occurrence and Ecology. *Appl. Environ. Microbiol.* **39**: 194-204.
57. Zinder, S. H. 1993. Physiological ecology of methanogens. In: *Methanogenesis: Ecology, Physiology, Biochemistry and Genetics*. Chapman and Hall.

Appendix for Chapter 5

Table 1 - Areas and volumes used for mass balance analysis

Table 2 - Lake transparency levels from the Secchi disk

Table 3 - Temperature profiles in 2008

Figures 1 to 5 - Methane oxidation test results

Table 1 – Upper Mystic Lake cross-sectional areas and volumes used in calculations (Senn 2001, Spliethoff 1995)

Table 1(a)

Depth (m)	Area (10^5 m^2)
0	5.83
3	4.19
6	3.67
9	3.19
12	2.7
15	2.06
18	1.62
21	1.2
24	0.7

Table 1(b)

Interval (m)	Volume (10^6 m^3)
0-3	1.53
3-6	1.2
6-9	1.04
9-12	0.9
12-15	0.73
15-18	0.56
18-21	0.43
21-24	0.28

Table 2 Lake transparency as determined by the Secchi disk

Date and time of sampling	Average Secchi disk reading (m)
22 May 2007, 3:30 PM	3.2
15 Jun 2007, 12:00 AM	2.3
2 Jul 2007, 6:00 PM	1.9
17 Aug 2007, 4:45 PM	2.3
23 Sep 2007, 1:50 PM	2.4
12 Jun 2008, 3:15 PM	3.0

Table 3 Temperature profiles (°C) in 2008

Depth	4/10/08	5/17/08	6/12/08	7/16/08	8/13/08	9/13/08	10/13/08	11/9/08
0	9.26	16.26	25.83	28.63	24.47	23.28	15.99	11.58
1	9.16	16.24	23.41	27.37	22.69	21.24	15.91	11.56
2	8.81	16.02	15.28	26.61	22.00	21.07	15.73	11.50
3	8.58	15.42	12.20	24.68	21.57	21.00	15.44	11.51
4	7.09	13.09	9.73	18.93	20.32	20.65	15.27	10.45
5	6.7	8.12	7.55	14.32	18.14	18.23	15.04	10.25
6	6.38	6.56	6.49	10.04	11.80	13.27	13.67	9.93
7	6.29	6.25	6.13	8.18	8.88	9.69	11.18	9.60
8	6.18	6.06	5.98	6.95	7.11	7.76	8.03	9.22
9	5.91	5.86	5.79	6.31	6.57	6.88	6.63	8.38
10	5.7	5.71	5.43	5.68	6.01	6.22	6.18	6.97
11	5.54	5.51	5.15	5.26	5.54	5.84	5.81	5.93
12	5.3	5.32	4.92	5.24	5.20	5.38	5.40	5.37
13	5.12	5.10	4.43	4.94	4.99	5.07	5.13	5.05
14	4.38	4.50	4.11	4.88	4.82	4.85	4.77	4.92
15	4.05	4.15	4.05	4.71	4.59	4.58	4.58	4.77
16	3.7	3.94	4.02	4.72	4.37	4.41	4.44	4.61
17	3.54	3.79	4.01	4.74	4.24	4.31	4.34	4.49
18	3.53	3.77	4.02	4.75	4.17	4.26	4.31	4.42
19	3.49	3.73	4.04	4.76	4.14	4.24	4.30	4.37
20	3.5	3.73	4.06	4.80	4.11	4.23	4.29	4.37
21	3.51	3.73	4.07	4.82	4.11	4.22	4.30	4.37
22	3.76	3.74	4.06	4.78	4.25	4.22	4.39	4.67
23		3.82				4.41		

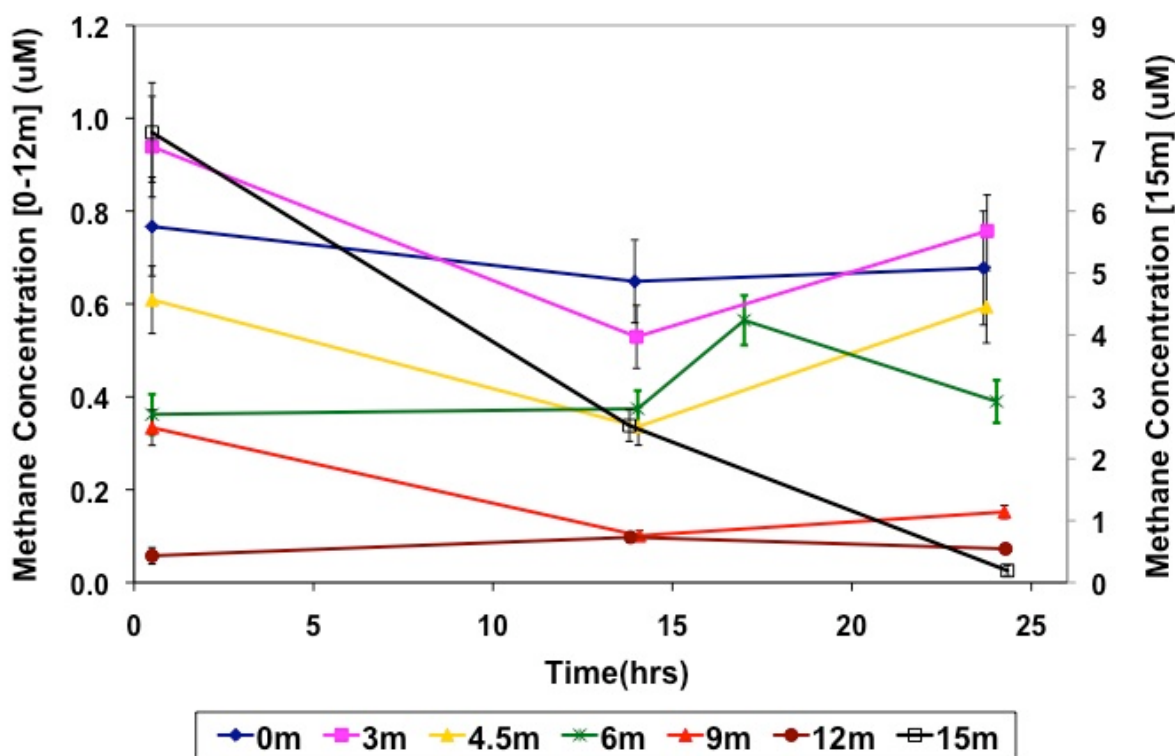


Figure 1 Incubation tests for Jul. 2, 2007. Only the 15m samples (black, open squares) had significant methane oxidation. Duplicates were not collected for any of the samples.

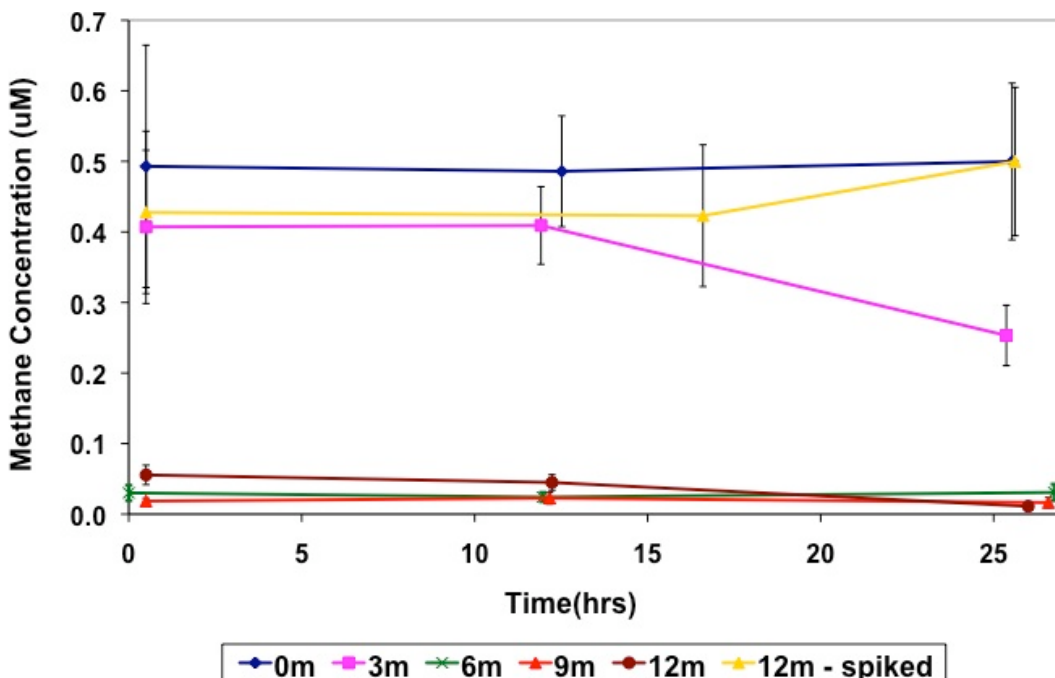


Figure 2 Incubation tests for Aug. 2, 2007. No significant methane oxidation rates were detected. Duplicates were not collected for any of the samples.

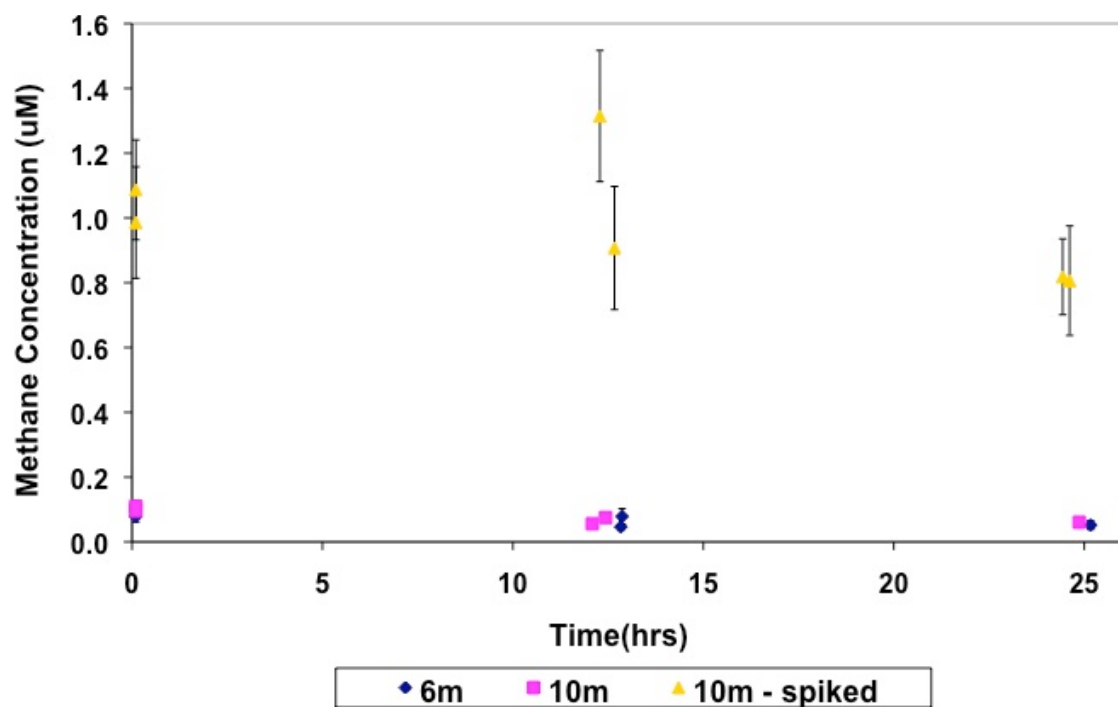


Figure 3 Incubation tests for Aug. 17, 2007. No significant methane oxidation rates were detected.

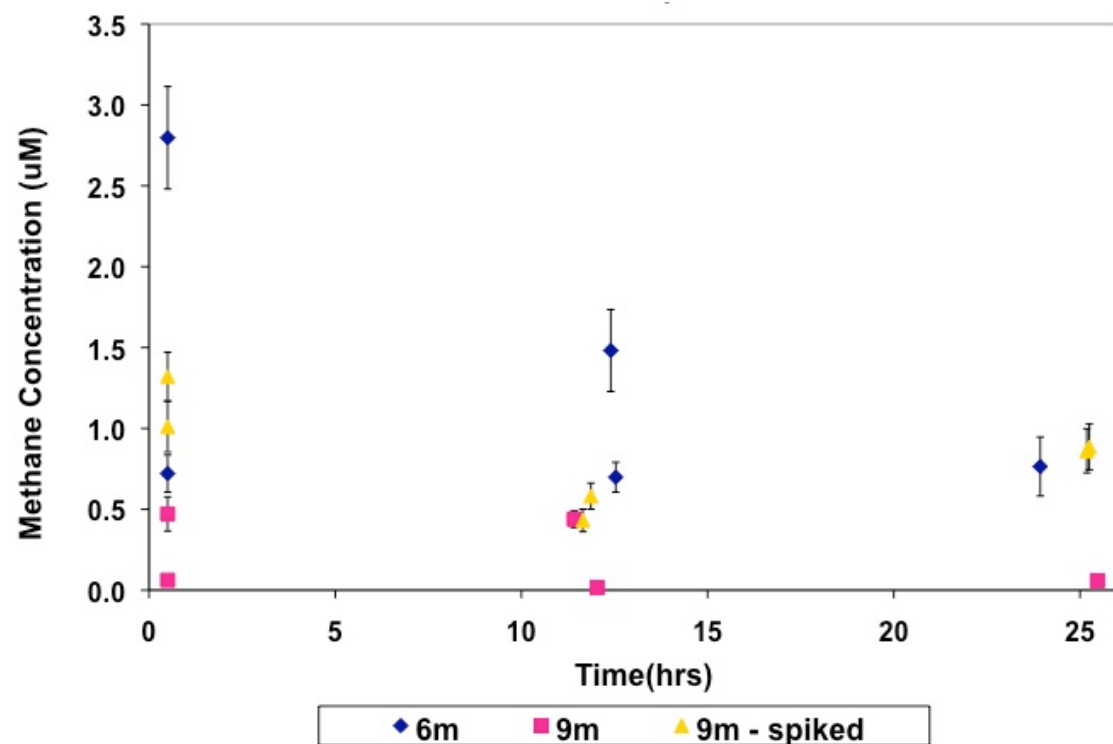


FIGURE 4 Incubation tests for Sep. 23, 2007. No significant oxidation rates were detected.

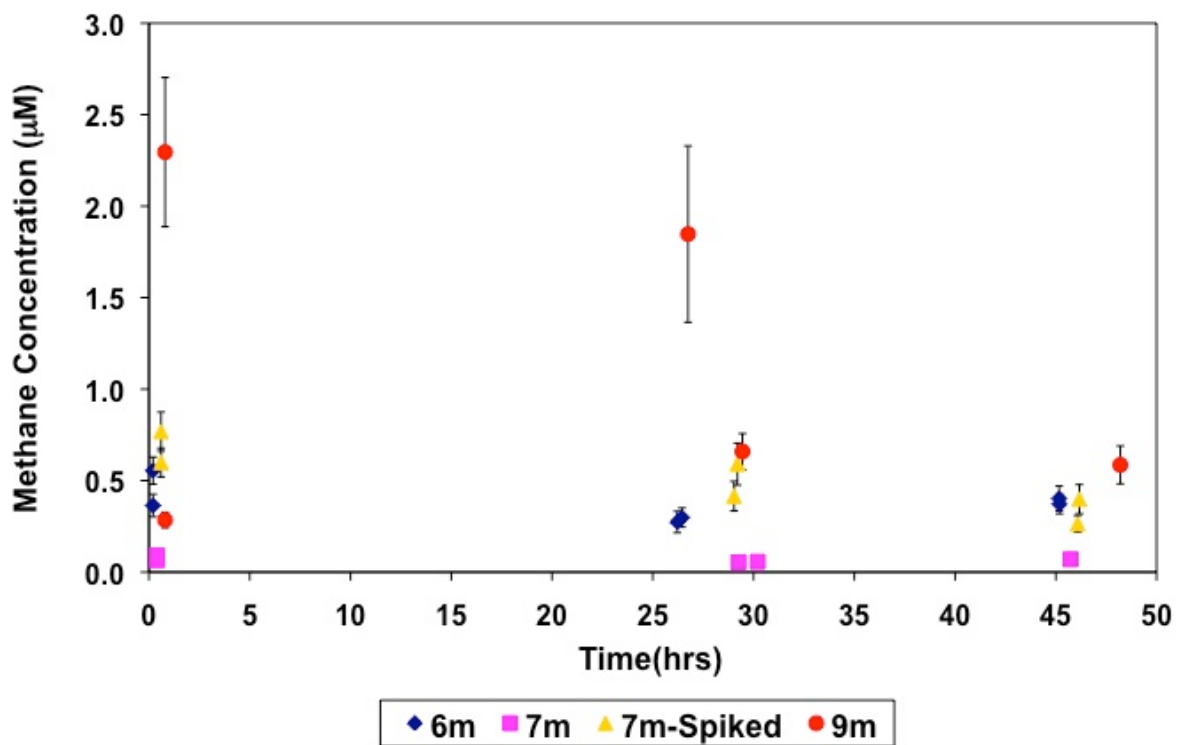


Figure 5 Incubation tests for Oct. 15, 2007. Only the 7m spiked sample (triangles) had significant oxidation rates.

Chapter 6: Summary and Future work

1. SUMMARY

This thesis is the result of a two-year study of methane biogeochemistry at the Upper Mystic Lake. As part of this effort, several traditional limnological methods were used to collect data on methane emissions to the atmosphere, transport within the water column and quantities present in the sediments. Additionally, the use of sensor hardware to obtain high-resolution measurements and software for event detection based on wavelet analysis add important elements of methodology to environmental research.

In particular, intensive measurements of ebullition were conducted. Bubbling has been recognized to be the dominant mode of methane emissions to the atmosphere from lakes, but is a complicated process to quantify due to its spatial and temporal heterogeneity. Most prior ebullition studies in lakes have involved manual, infrequent measurements that can lead to inaccurate estimates of the magnitude and variations in fluxes.

The automated bubble trap developed for this project can be used to measure ebullition fluxes from lakes, as well as from some other aquatic habitats such as wetlands and estuaries. The trap is easy to build, consumes little power, and is a cost-effective means of collecting long-term, high-temporal-resolution bubbling data. Moreover, the device consists of several components that are individually useful in their own right. The circuit can be easily adapted to detect a large range of pressure differentials in many systems. For example, we used the same instrumentation to measure the lake water level, which matched measurements from a commercial sensor within 1%. The custom-made waterproof housing, as well as the vacuum leak test, can be employed in a broad range of underwater studies.

A unique dataset was collected from the automated chambers; to our knowledge there is no other study that has measured bubbling fluxes over a comparable period (4-6 months) with such high temporal resolution (5-10 minutes) in a deep freshwater setting. The data revealed insights into the processes that can control ebullition in the short-term. Synchronous lake-wide bubbling episodes were triggered when total hydrostatic pressure (sum of atmospheric pressure plus water column depth) fell below a site-dependent threshold. The bubbling episodes occurred about 5-10% of the time, during which most of the total bubbled gas for the season was released (30-70% depending on the site). The wavelet analysis showed that some of these episodes, which could last for several days, actually consisted of several short 5-20 minute bubble bursts.

The Upper Mystic Lake emits significant amounts of methane to the atmosphere. The average lake-wide ebullition flux was $0.8 \pm 0.1 \text{ mmol.m}^{-2}.\text{d}^{-1}$ from mid-July to November 2007, and $0.5 \pm 0.02 \text{ mmol.m}^{-2}.\text{d}^{-1}$ from April to November 2008. Considerable spatial variation was observed, and short-term fluxes could vary by as much as a factor of 20 between stations that were only 15-30 m apart. However the spatial patterns of bubbling were similar in both years; sites that bubbled more in 2007 also had higher fluxes in 2008 and were located either in the deep, central portion or in a relatively shallow zone near the north-eastern part of the lake. The mixing ratio of methane present in the collected gas ranged from 30% to 90%, and was generally higher at locations that bubbled more. The diffusive methane flux through air-water exchange from the lake surface was $0.3 \pm 0.1 \text{ mmol.m}^{-2}.\text{d}^{-1}$ ($\sim 3\text{kg CH}_4/\text{d}$) in 2007 and $0.2 \pm 0.1 \text{ mmol.m}^{-2}.\text{d}^{-1}$ ($\sim 2 \text{ kg CH}_4 / \text{d}$) in 2008. Ebullition comprised about 70% of total methane emissions over the two years.

Dissolved methane concentrations ranged from ~ 200 - $800 \mu\text{M}$ near the lake bottom over the study period; a gradual hypolimnetic accumulation of methane over the summer and fall was

observed in both years. However, a significant amount of methane (\sim 400 kmol) was lost from the lake hypolimnion between December 2007 and April 2008, during which time the fall and spring turnovers occurred. Concentrations in the upper mixed layer were low for the entire sampling period (\sim 1 μ M), and a methane minimum was found at the mid-depths of the lake throughout the period of warm season stratification.

Porewater methane concentrations measured in the upper 1 m of lake sediments were high (\sim 4 mM). A theoretical sediment-water diffusive flux of \sim 0.8 mmol.m $^{-2}$.d $^{-1}$ was calculated based on the profile of porewater methane measurements. However, this estimate was four times smaller than the flux calculated from a hypolimnion mass balance (3.2 mmol.m $^{-2}$.d $^{-1}$).

Mass balance calculations showed that most of the methane released from the hypolimnetic sediments accumulated within the anoxic layer of the hypolimnion. Based on the absence of an increase in epilimnetic concentrations during the fall, we hypothesize that some of the hypolimnetic methane may have been primarily lost to oxidation during the fall turnover. In fact, the data suggest that methane released to the atmosphere through diffusive air-water exchange from the lake surface originated primarily in the epilimnetic sediments. Bubble dissolution was determined to not be a major source of methane to the water column.

2. FUTURE WORK

Measuring methane fate and transport with adequate spatial-temporal density is a difficult problem that lies at the intersection of physical, chemical, and biological sciences as well as engineering. The work from this thesis can spawn future work in several directions. These include improving estimates of the various methane cycle processes measured as part of this

study, as well as obtaining measurements with different instrumentation to measure unknown quantities.

Achieving better spatial resolution of bubbling fluxes is necessary to get better estimates of the magnitude of ebullition; one prior study found that hotspots could contribute as much as 95% of the bubbling in a lake, when compared to randomly placed background traps (Walter et al. 2006). While the bubble traps in this study provide a preliminary estimate of the extent of spatial variation at the UML, they have very limited areal coverage. At times, traps located about 15-30m apart could have very different fluxes. Seismic and sonar imaging of the lake bottom can qualitatively identify potential ‘hot spots’; automated bubble traps can then be placed at these locations to measure fluxes in the long-term. A preliminary seismic survey of the UML in June 2009 suggests the presence of pockmarks and free gas pockets in shallow sediments (Figure 1) (C. Ruppel, personal comm.). Quantitative estimates of gas storage in the sediments can potentially account for the variations in the magnitude of fluxes during bubbling episodes.

Other acoustic instruments such as the echosounder (Ostrovsky et al. 2008) are capable of identifying bubbling in-situ with high spatial resolution over long ranges (~100s of meters). These instruments can also be used to measure bubble size, which is an important factor in determining how much methane is lost as a bubble rises through the water column. The method might thus be able to identify smaller bubbles that dissolve within the water column, which are not measured by surface bubble traps, as well as test for the possible existence of upwelling flows caused by bubble entrainment.

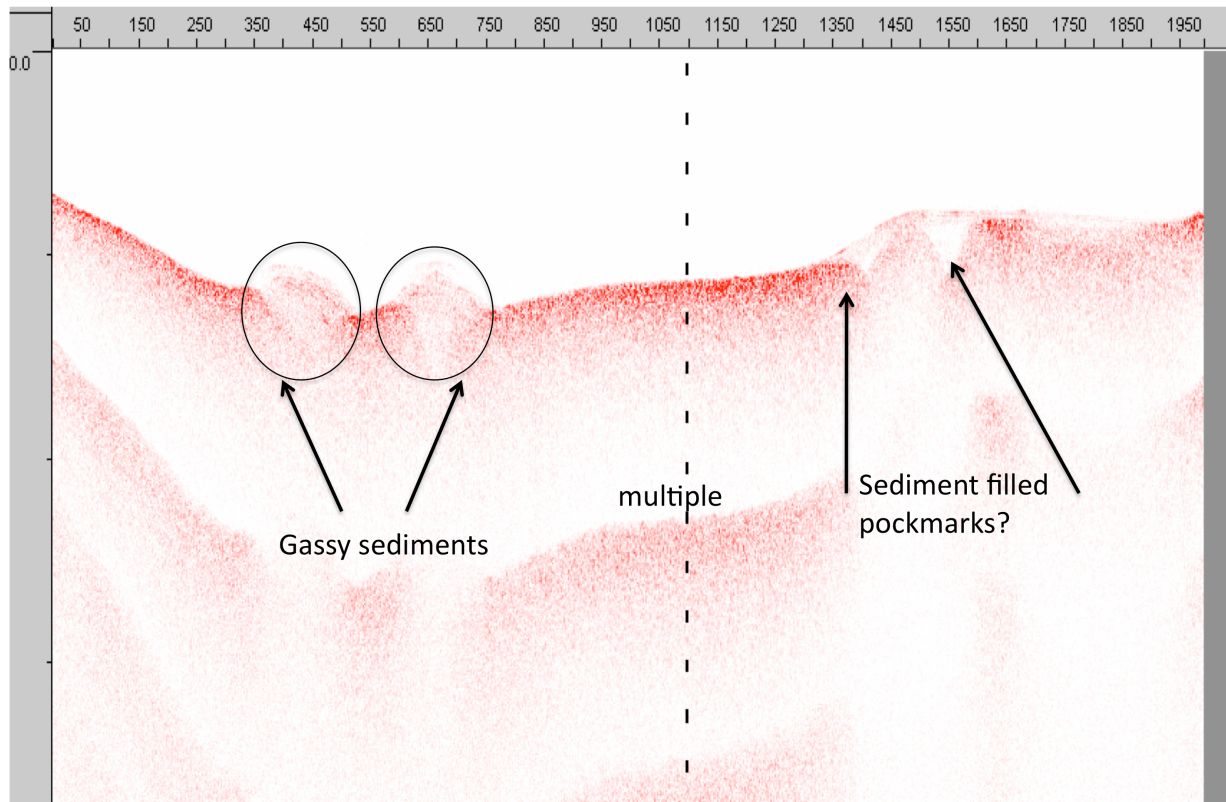


Figure 1 Trace from a seismic imaging survey at the UML in summer 2009

The lake mass balance indicates that water column buildup plays an important role in the methane cycle. A large quantity of methane is stored in the hypolimnion by the end of fall; though the limited data suggest that this methane is oxidized during the fall and spring turnovers between December and April, it is not conclusively shown that there is no appreciable release to the atmosphere during this period. Thus the lake turnovers can thus be critical, both from a perspective of atmospheric methane emissions, as well as for gaining insight into microbiological processes. Furthermore, the mass of methane present in the water column was calculated using a single profile from the center of the lake; measurements of spatial variation across the lake from instrumentation such as the Nereus, an automated underwater robot

equipped with a mass spectrometer, (Hemond et al. 2008) can improve whole-lake estimates of dissolved methane.

3. BROADER IMPACTS

Better estimation of methane from natural sources such as lakes can lead to improved modeling of climate change and can contribute to the prioritization of emission reduction schemes for methane. Its short atmospheric life span of 9-15 years in the atmosphere (Houghton et al. 2001) has prompted the establishment of control strategies relevant in the intermediate term. However, such measures might prove to be ineffective if methane from natural sources were found to greatly dominate over anthropogenic sources.

The study of bubbling is not only relevant for methane emissions in lakes, but can also contribute to understanding other processes that affect both lake and ocean waters. For example, bubble plumes can induce artificial vertical mixing in lake waters. Also, excess methane production, undetected due to bubble loss, can potentially balance the redox budget by accounting for seemingly excessive carbon dioxide levels detected in some lakes. Excessive ebullition from lakes can, in some rare instances, have other catastrophic effects (besides climate change) such as the 1986 incident in Lake Nyos, Cameroon where hundreds of people died from an eruption of carbon dioxide bubbles. (Kling et al. 1987). A study of bubbling processes could yield knowledge that would help prevent such disasters in the future.

From a different point of view, methane has recently received considerable attention as an alternative source of energy, and studies have been performed about the possibility of harvesting methane from systems such as landfills (Rather September 13, 2008), ocean hydrates (Ruppel 2007), and certain lake beds, e.g., Lake Kivu in central Africa (Halbwachs 2003, Jones

2003). So far, the large amounts of methane produced in lakes are either lost to the atmosphere or are lying untapped in the water column. A good comprehension of methane sinks would help determine the feasibility of harvesting this fuel to power surrounding communities without damage to the ecosystem. For example, a significant amount of methane (~6400 kg) was lost from the hypolimnion of the Upper Mystic Lake during December to April. If this methane were not lost prior to icing, then it could be potentially be tapped from under the ice-cover during the winter. Developing other means of collecting methane from lakes could open up new possibilities, particularly in certain locations in Asia and Africa, where there are many areas lacking power infrastructure but where tropical lakes can contain large quantities of methane.

REFERENCES

1. Halbwachs, M. 2003. The exploitation of methane in Lake Kivu.
2. Hemond, H. F., A. V. Mueller and M. Hemond. 2008. Field Testing of Lake Water Chemistry with a Portable and an AUV-based Mass Spectrometer. *J. Am. Soc. Mass Spectrom.* **19:** 1403-1410, doi:DOI: 10.1016/j.jasms.2008.04.019.
3. Houghton, J. T., Y. Ding, D. J. Griggs, M. Noguer, P. J. van der Linden, X. Dai, K. Maskell and C. A. Johnson. 2001. IPCC, 2001: Climate Change 2001: The Scientific Basis. Contribution of Working Group I to the Third Assessment Report of the Intergovernmental Panel on Climate Change.
4. Jones, N. 2003. Chock-full of methane, Lake Kivu stores enough energy to power all of Rwanda. *New Scientist.* **177:** 17.
5. Kling, G. W., M. A. Clark, G. N. Wagner, H. R. Compton, A. M. Humphrey, J. D. Devine, W. C. Evans, J. P. Lockwood, M. L. Tuttle and E. J. Koenigsberg. 1987. The 1986 Lake Nyos Gas Disaster in Cameroon, West Africa. *Science.* **236:** 169-175.
6. Ostrovsky, I., D. F. McGinnis, L. Lapidus and W. Eckert. 2008. Quantifying gas ebullition with echosounder: The role of methane transport by bubbles in a medium-sized lake. *Limnol. Oceanogr. - Methods.* **6:** 105-118.
7. Rather, J. September 13, 2008. Tapping power from trash. *The New York Times.* NJ3, New York Edition.
8. Ruppel, C. 2007. Tapping Methane Hydrates for Unconventional Natural Gas. *Elements.* **3:** 193-199, doi:10.2113/gselements.3.3.193.
9. Walter, K. M., S. A. Zimov, J. P. Chanton, D. Verbyla and F. S. Chapin III. 2006. Methane bubbling from Siberian thaw lakes as a positive feedback to climate warming. *Nature.* **443:** 71-75, doi:10.1038/nature05040.